Exploring the Immunostimulatory Properties of GAS Pili

Risa Takahashi

A thesis submitted in fulfilment of the requirements for the degree of
Doctor of Philosophy in

Department of Molecular Medicine and Pathology
The University of Auckland
2023

Abstract

The global burden of *Streptococcus pyogenes* (Group A Streptococcus, GAS) infection related diseases has resulted in widespread investigation into the virulence factors of the bacterium, in an effort to produce a prophylactic vaccine. One vaccine candidate is the GAS pilus, which is a long, filamentous cell surface anchored structure. GAS pili have been demonstrated to elicit adaptive immune response but little is known about the innate immune response to the structure.

This study thus aimed to elucidate the interaction between GAS pili and components of the innate immune system, using recombinant pilus proteins and whole assembled pili expressed on the surrogate *L. lactis* bacterium to explore the immunomodulatory properties of the complex. Pili interaction with toll-like receptors (TLRs) and their ability to activate immune cells was explored *in vitro* with immunoassays, flow cytometry and reporter cell lines. The inflammatory response elicited by the structure was also modelled using wax moth larvae and the adjuvanting capacity of the pilus proteins was assessed using a mice intranasal immunisation model.

Assays using TLR reporter cell lines depicted proteins physically interacting with and activating TLR2, an attribute further consolidated in competition assays using a TLR2 antagonist. Furthermore, specificity of the pilus proteins for TLR2 in the TLR2/6 heterodimeric form was revealed. Pilus proteins were also illustrated activating macrophages and inducing upregulation of proteins and pro-inflammatory cytokines associated with the enhanced ability of these cells to modulate the adaptive immune system. The wax moth larvae model indicated that this pili mediated stimulation of innate immunity did not appear to be a contributor to disease pathogenesis. Furthermore, immunisation of mice with pilus proteins conjugated to the low immunogenicity influenza antigen M2e resulted in enhanced M2e specific antibody production.

These results uncovered the previously undiscovered characteristics of GAS pilus proteins being TLR2 agonists with the ability to prime innate immune cells to enhance adaptive immune responses, without exerting deleterious effects on the recipient. This emphasises the suitability of GAS pili as a vaccine candidate and highlights its potential as a vaccine adjuvant.

Acknowledgements

I would like to thank everyone who made my PhD journey a fun ride and pushed me towards the finish line through all of the challenges and COVID disruptions.

Firstly, a big thank you to my main supervisor Dr Catherine Tsai who has supported me from the pre-PhD honours year right to the end of my thesis write up. Thank you so much for your guidance both in and out of the lab, providing me with numerous opportunities and answering all of my late night emails. Your mentorship has played a big part in shaping my PhD experience into an enjoyable one and I am grateful to have found such an encouraging supervisor.

Thank you to my co-supervisor Prof Thomas Proft for giving me the opportunity to thrive in the group and giving me insightful advice to improve and expand on the assays in this project. Thank you also to my second co-supervisor Assoc. Prof Nikki Moreland for providing a different perspective to the project when I was getting too sucked into the small details. Thank you to Dr Fiona Radcliff, Dr Ries Langley, Dr Natalie Lorenz and Fiona Clow for providing your expertise which allowed me to complete assays within this project. I would also like to extend my thanks to Dr Fujihashi and his team at Chiba University Hospital for giving me the opportunity to learn new skills and gain experience in their lab.

To all of the other past and present members of the Proft group and I&I: Dr Jacelyn Loh, Adrina Khemlani, Tiger, Lauren, Alana, Bassie, Reuben, Lewis, Carlos, Farina, Sravya, Francis and many more. Thank you all for listening to my random rants, answering all of my silly questions and the countless hangs and laughs. You all made my PhD years full of banter and good times and I never got bored during assay incubations. Special thanks to Adrina for always helping me out around the lab and ensuring I was equipped to run all my experiments. Thank you also to my friends and support group outside of the lab for keeping me grounded and chirpy throughout these past couple of years.

Last but not least, thank you to my Dad and Mum who have given me the unequivocal backing and love that has gotten me here today. Thank you for being my support system in all aspects of my life.

Table of Contents

List of Figures

List of Tables

List of Abbreviations

C°	Degree Celsius	LTA	Lipoteichoic acid
AP1	Ancillary pilin 1	mAb	Monoclonal antibody
AP2	Ancillary pilin 2	MCAC	Metal affinity chromatography
APC	Antigen presenting cells	MFI	Mean fluorescence intensity
APSGN	Acute post-streptococcal glomerulonephritis	MHC	Major histocompatibility complex
		MTT	3-(4,5-dimethylthiazol-2-yl)-2,5-diphenyltetrazolium bromide
ARF	Acute rheumatic fever	MyD88	Myeloid differentiation primary response 88
BAL	Bronchoalveolar lavage	NFκB	Nuclear factor kappa B
bp	Base pair	NLR	Nucleotide-binding oligomerisation domain like receptors
BP	Backbone pilin	NW	Nasal wash
CFU	Colony-forming unit	PBMC	Peripheral blood mononuclear cell
CLR	C-type lectin receptor	PBS	Phosphate buffer saline
ConA	Concanavalin A	PCR	Polymerase chain reaction
CV	Column volume	PoRB	*Neisseria meningitides* porin B
CWSS	Cell wall sorting signal	PRR	Pattern recognition receptor
DAMP	Danger associated molecular pattern	RHD	Rheumatic heart disease
DC	Dendritic cell	rpm	Revolutions per minute
DMSO	Dimethyl sulfoxide	RT	Room temperature
DOL	Degree of labelling	s	Seconds(s)
ELISA	Enzyme-linked immunosorbent assay	SAgs	Superantigens
FACS	Fluorescence activated cell sorter	S.D	Standard deviation
FCT	Fibronectin- and collagen-binding T-antigen region	SDS-PAGE	Sodium dodecyl sulphate polyacrylamide gel electrophoresis
FR1	Upstream flanking region	SEAP	Secreted alkaline phosphatase
FR2	Downstream flanking region	SEC	Size exclusion chromatography
GAS	Group A streptococcus	SPR	Surface plasmon resonance
GSH	Glutathione	SrtA	Sortase A
GST	Glutathione-S-transferase	SSL3	Staphylococcal superantigen-like 3
h	Hour	TBS	Tris buffered saline
His	6×Histidine tag	TCR	T-cell receptor
HRP	Horseradish peroxidase	TLR	Toll-like receptor
Ig	Immunoglobulin	WT	Wild type
IPTG	Isopropyl β-D-thiogalactopyranoside		
kDa	Kilodalton		
L/ml/µl	Litre/Millilitre/Microliter		
LB	Luria-Bertani broth		
LPS	Lipopolysaccharide		

Chapter 1: Introduction

1.1   *Streptococcus pyogenes*-an important human pathogen

Streptococcus pyogenes, or Group A Streptococcus (GAS), is a Gram positive, β-haemolytic bacterial pathogen, which exclusively infects humans. This bacterium causes a wide spectrum of diseases, ranging from self-limiting, superficial infections to severe invasive disease and immune sequelae, as summarised in Table 1.1.

GAS has posed a persistent disease burden on the global population for centuries, with literature describing GAS associated diseases spanning as far back as 1553 (1). GAS remains a highly prevalent bacterium today, with the global incidence rates of GAS pharyngeal infections estimated to be about 600 million per year and GAS infections attributed to about 600,000 deaths annually (2). Despite the global impact of this bacterium, there is currently no vaccines available, with the highly variable nature of GAS strains proving to be an obstacle in producing a vaccine with broad protection (3).

Table 1.1. Overview of major GAS associated diseases.

Disease	Sign/Symptom
Superficial Infections	
• Throat infections (e.g. pharyngitis)	Acute sore throat, fever (4)
• Skin infection (e.g. impetigo)	Skin pustules which enlarge and break down into scabs (5,6)
Invasive Infections	
• Necrotising fasciitis	Fever, toxemia, tissue destruction (7)
• Toxic shock syndrome	Diffuse tissue damage, thrombosis and multi-organ dysfunction (8)
Post Infection Sequelae	
• Acute rheumatic fever (ARF)	Polyarthritis, carditis, rapid and jerky movements, rash (9–11)
• Rheumatic heart disease (RHD)	Chronic damage to heart valves, stroke, infective carditis (9–11)
• Acute post-streptococcal glomerulonephritis (APSGN)	Renal dysfunction, edema, hypertension and urinary sediment abnormalities (18–21)(6,11)

1.1.1   Disease burden

Although superficial infections are generally self-limiting, with annual global case numbers of pharyngitis alone exceeding 600 million, they still cause major healthcare expenditure and

illness burden. Pharyngitis for example, is estimated to be acquired by 15% of schoolchildren and 4-10% of adults in developed countries annually. Incidence rates are even greater in developing nations, with the number of affected individuals being 5 to 10-fold higher (12). More pressing is the burden of the severe GAS associated diseases, such as immune sequelae and invasive GAS infections, which affect roughly 18.1 million people globally. Focusing on the most well documented, rheumatic heart disease (RHD), conservative estimates indicate that about 300,000 deaths per year are attributable to the condition, and the total global population of individuals with RHD may be as high as 19.6 million. Furthermore, RHD is the most common pediatric heart disease, with over 2.4 million children between the ages of 5 and 14 affected (2,4).

The bulk of GAS diseases occur in low resource settings where poor sanitation, reduced access to antibiotics, high rates of poverty and household crowding catalyse the spread of infection and increase the prevalence of repeated infections (13,14). In fact, an estimated 95% of cases of serious GAS diseases occur in low resource settings and in the case of acute post-streptococcal glomerulonephritis (APSGN), incidence rates are 4 fold in such environments, compared to affluent settings. This pattern is echoed when studying the rate of invasive GAS diseases, where incidence was 1.5 per 100,000 in high income countries but in lower resource settings such as Kenya, incidence was 13 per 100,000 (15).

Low resource settings with increased disease incidence are not restricted to developing countries and may be found in pockets of socio-economically disadvantaged groups within a developed country. This phenomenon is especially prominent in New Zealand, where a disproportionate number of Māori and Pacific Islander populations are affected by GAS infections, resulting in the country experiencing 3 fold greater rate of GAS diseases than other developed countries (16). In fact, rates of invasive GAS are 5 times higher in Māori peoples and 17 times higher in Pacific Islanders, compared to Europeans/Asians. Furthermore, these communities have some of the highest rates of ARF in the world, second to sub-Saharan Africa. While the rates of ARF declined by 71% in non-Māori/Pacific children between 1993 and 2009, there was a 79% and 73% increase seen in Māori and Pacific children respectively, an outcome which appears to be fueled by socio-economic deprivation (17–19). ARF poses a particularly large health burden in New Zealand due to the possibility of disease progression to RHD, which can evoke permanent injury and mortality. The cumulative annual costs of ARF and RHD are

upwards of NZD$12 million, translating to a prominent strain on the New Zealand healthcare system (20).

1.1.2 Molecular Epidemiology

GAS consists of a plethora of genetically diverse strains, which are indexed in a number of different systems. Categorising strains is very important for a bacterium with great diversity such as GAS, as elucidating the correlation between clinical outcomes and strain types may assist in identifying patients likely to become severely affected by their GAS infection. Furthermore, it can inform vaccine development, highlighting which strains require particular focus. Identification of the most commonly circulating GAS strains can supplement this process and help engineer a vaccine that provides protection against the GAS strains most likely to be encountered by an individual. Grouping of related GAS strains can also assist in streamlining vaccines to achieve broad coverage without including all strains (21,22).

The first typing scheme developed was M typing, a serological method utilising antibodies raised against the M protein, an antiphagocytic virulence factor extending from the cell surface. M proteins present as an alpha- helical coiled coil dimer with a surface exposed hypervariable N-terminus region. The sequence variation of these proteins at the N terminus dictates antigenic specificity, and this is detected using M-protein specific antisera (23). More than 80 different M serotypes have been identified thus far and in most cases, immunity against GAS infections is specific to M types (23,24). In addition to M proteins, the T antigen is also used as a serological marker to group GAS strains. This grouping system involves agglutination of trypsin treated GAS cells with T-antigen specific antisera. Around 22 distinct T types have been defined, most of which can be correlated to M types. However, specificity is lower, with multiple M types sharing the same T type (25,26).

More recently, M protein serotyping has been replaced with *emm* typing, a molecular typing system based around the M protein gene sequence. The first 30 codons of the hypervariable amino terminus of the protein is examined and *emm* types are classified as unique when they have <92% nucleotide identity across this region, compared to other *emm* types. Currently, over 200 *emm* types have been determined and surveillance reports have demonstrated a correlation with specific clinical presentations (Table 1.2) (27–29). These *emm* types can be further grouped by *emm* pattern typing, which clusters *emm* types into three groups (A-C, D

and E) based on the presence and arrangement of *emm* or *emm*-like genes. This grouping system correlates with tissue tropism; pattern A-C strains are mainly isolated from oropharyngeal infections and thus referred to as the "throat specialists", pattern D strains are usually associated with superficial skin infections ("skin specialists") and pattern E strains are commonly found at both sites of infection ("generalists") (21). Analysis at the *emm* pattern level can reveal disease associations as well as provide insight into pathogenesis. For instance, it was found that the majority of GAS strains isolated from ARF patients in New Zealand was pattern D strains (skin tropism), suggesting a role of skin infections in disease progression (30).

Table 1.2. Example of specific clinical presentations and associated M types. Table adapted from (29,31,32).

Clinical Presentation	M type of associated strains
Pharyngitis	M1, M3, M5, M6, M12, M14, M17, M19, M24
Impetigo	M33, M41, M42, M52, M53, M70
Acute rheumatic fever	M1, M3, M5, M6, M11, M12, M14, M17, M18, M19, M24, M27,M28, M29, M30, M32, M41
Acute post-streptococcal glomerulonephritis	M1, M4, M12, M49, M55, M57, M60
Necrotising Fasciitis	M1, M3, M28
Streptococcal toxic shock syndrome	M1, M3

1.2   GAS pathogenesis

GAS infection is initiated by adherence to host cells facilitating bacterial colonisation. It has been hypothesised that adherence is a two stage process. Reversible, hydrophobic interactions between bacterial surface components and the host cell extracellular matrix counteract the electrostatic repulsion between bacteria and host cells in order to establish initial contact. This is followed by irreversible, high affinity binding between GAS adhesion proteins and specific host cell receptors (33,34). Lipoteichoic acid (LTA) is an example of an adhesion factor postulated to contribute to the first stage of adherence, whilst M protein is an adhesin implicated in the second stage of adherence (35,36). There is also a wide array of molecules that bind to host fibronectin, a ubiquitous glycoprotein found in extra cellular matrix and as a soluble protein in plasma (33). GAS pili are a recently identified surface bound virulence factor critical

for the binding and colonisation of host cells. Observations of the pili mediating adhesion to various cell lines and primary tissue cells have indicated their role in the host tissue specific adherence of GAS (37–39).

Once infection is established, GAS bacteria must undergo cellular invasion and dissemination. Fibronectin binding proteins can encourage invasion by inducing a phagocytosis like uptake into endothelial cells (40). Secreted virulence factors are also heavily involved in the spread of GAS to deeper tissue. One such protein group is the secreted streptolysin toxins, which oligomerise within the cytoplasmic host cell membrane to form transmembrane pores which facilitate cell lysis and expedite the movement of GAS into deeper tissue (41). Another virulence factor associated with invasion is streptococcal pyrogenic exotoxin B (SpeB), a cysteine protease that aids the spread of GAS by degrading a variety of proteins such as components of the extracellular matrix and complement factors (42,43).

GAS bacteria must evade the host immune system to maintain survival in the host. Streptolysin can be deployed again at this stage, forming pores on the host cell membrane to promote necrosis or apoptosis (44). SpeB also drives immune evasion by hydrolysing individual immune proteins such as complement components, cytokines, chemokines, anti-microbial peptides and immunoglobulins (45,46). Fibronectin binding proteins and M protein can also contirbute to immune evasion, by halting the process of C3b mediated opsonophagocytosis and reducing C3b deposition respectively (47–49). In addition to the aforementioned proteins, there are a multitude of virulence factors which facilitate GAS surival through processes such as adhesion, internalisation, invasion, dissemination and anti-phagocytic activity (50).

Subsequent to infiltration and immune evasion, GAS may trigger toxic shock syndrome (TSS), a severe systemic inflammation which can result in shock and multi-organ failure. The pyrogenic exotoxins responsible for this phenomenon are referred to as superantigens (SAgs), and these molecules are able to directly bind to MHC II molecules on antigen presenting cells (APCs) and the variable Vbeta region of T cell receptors, away from peptide-specific recognition sites (51). This simultaneous attachment to both structures results in low specificity, excessive T cell activation, and the uncontrollable release of pro-inflammatory cytokines, referred to as a "cytokine storm"(51,52).

1.3   GAS Pili

Pili (*sing.* pilus) refer to the polymeric, non-flagellar organelles extending from the bacterial cell surface. These appendages were first discovered in the 1950s on Gram-negative pathogens and were extensively characterised over the following five decades. Pili were subsequently observed in Gram-positive bacteria, starting with *Corynebacterium* species and followed by *Streptococcus* species, but their properties are still comparatively poorly understood (53).

Pili found in Gram negative bacteria are typically assembled via non-covalent polymerisation of pili subunits, and based on their pathways of biosynthesis, have been grouped into 5 different classes (54). On the other hand, Gram positive pili are covalently linked structures which can be separated into two separate categories based on size. Some species of Gram positive bacteria have short, rod-like pili between 70 and 500 nm in length attached to the cell surface, whilst other bacteria have longer, hair-like pili extending up to 3 µm (53,55).

Pili were identified on GAS in 2005, joining *Streptococcus pneumoniae* and *Streptococcus agalactiae* as the streptococcal pathogens reported to possess pili. The discovery of pili on GAS was preceded by studies describing the presence of covalently linked pili on *Streptococcus agalactiae* and *C. diphtheria*. Both organisms utilise a sortase enzyme to catalyse the linkage between surface proteins possessing conserved pilin motifs and containing a cell wall sorting signal (56). Based on this information, complete GAS genomes and GAS sequences were searched for genes coding proteins containing the LPXTG motif and genes coding sortase enzymes closely linked together. Sequences matching this description were found within a pathogenicity island referred to as the Fibronectin-binding, Collagen-binding T-antigen (FCT) region (25,56). This suggested the presence of GAS pili encoded by the FCT region. Further confirmation was provided using immunoblots for cell wall components of 4 GAS strains with antisera specific for LPXTG containing proteins. The immunoblots resulted in a ladder of bands with high molecular mass, mirroring the immunoblots of linked pilin components of *C. diphtheria* and *Streptococcus agalactiae*. Furthermore, immunogold electron microscopy of these strains with LPXTG protein antisera uncovered pili-like structures protruding from the surface of the bacteria (56).

1.3.1 The Fibronectin-binding Collagen-binding T-antigen region

The FCT region is a pathogenicity island approximately 11-16 kb in length, flanked by highly conserved sequences (57). Each GAS strain possesses one FCT region and to date, nine different FCT types have been identified (Figure 1.1). These regions can be highly diverse across different GAS strains, with sequence similarity of particular genes between different FCT regions as low as 20%. However, there are common characteristics found across the range of FCT types. One example is the region containing sequences for either one or two transcriptional regulators. One of these is always a regulator either part of the *nra* or *rofA* lineage and is positioned upstream of the FCT region. There are also genes encoding one or two fibronectin binding proteins and sortase enzymes within the island. Finally the region contains the sequences for the protein subunits that make up the GAS pili (26,58). There are three structural pilus proteins (pilins); the major subunit which is known as the backbone pilin (BP) and the two minor subunits, ancillary pilin 1 (AP1) and ancillary pilin 2 (AP2). The BP is in fact the T-antigen, the surface protein which had been extensively used as a serological marker long before the pili were identified in GAS. In line with T typing having lower specificity than M typing, the same BP variant appears to be shared by strains of different M types (26,57).
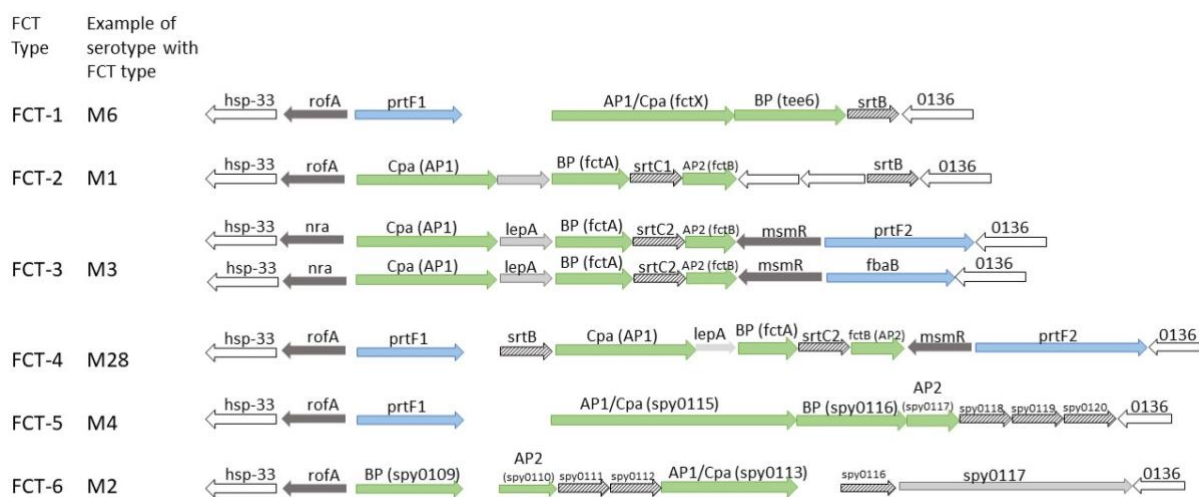
Figure 1.1. Gene organisation of the antigenically different FCT regions identified thus far. Dark gray arrows are transcriptional regulator genes, blue arrows are fibronectin-binding protein genes, green arrows are previously reported or inferred surface-expressed pilus protein genes, hatched gray arrows are sortase genes or putative genes encoding sortase and light gray arrows are other open reading frames. Adapted from (57).

Falugi et. al. surveyed the FCT region of 57 GAS strains and revealed a total of 15, 14 and 5 sequence variants of the genes encoding for BP, AP1 and AP2 subunits respectively. While BP variants found within FCT-3 and FCT-4 showed up to 81% sequence similarity, the BPs from the remaining FCT regions shared less than 30% sequence similarity when comparisons were made between BPs from any other FCT region. This pattern was mirrored when investigating AP1; variants of AP1 in FCT-3 and FCT-4 were closely related while there was significantly less similarities when contrasting AP1 variants from other sets of FCT regions. There is evidence of interstrain recombination within this section of the pathogenicity island, most apparent when comparing FCT-3 and FCT-4. For example, two M44 strains bearing FCT-3 and FCT-4 respectively shared the same BP variant but had differing AP1 variants. Conversely, M11 and M28 both harbored FCT-4 but had differing BP variants associated to the same AP1 variant. This gives an indication that pilus components have been exchanged between FCT regions. In contrast to BP and AP1, AP2 is relatively conserved within each FCT region, irrespective of strain or M type carried. It has been suggested that this lack of variability is correlated to the fact that AP2 is less exposed on the surface of the bacteria (26,56).
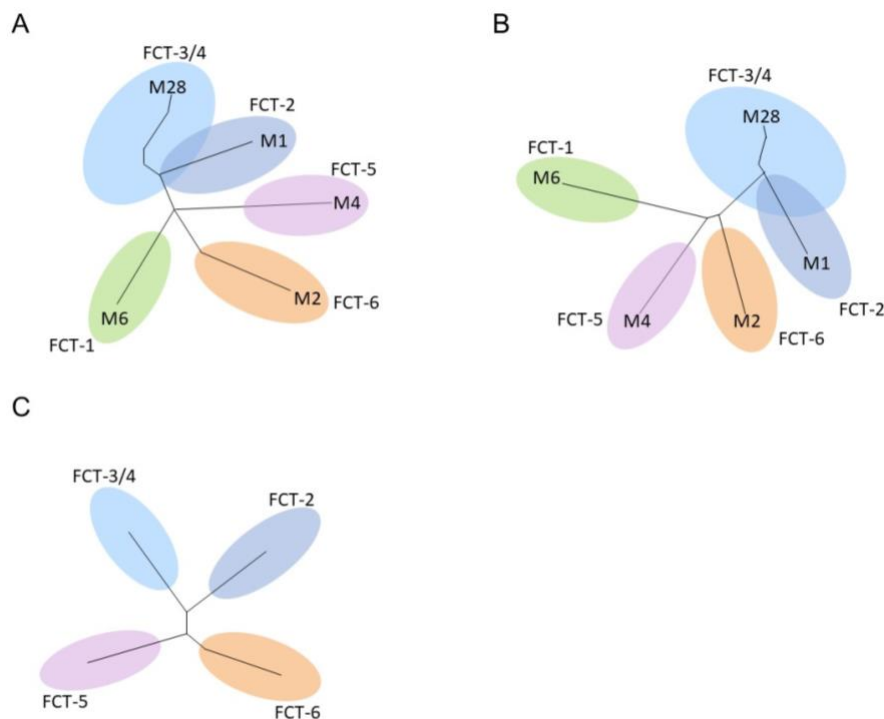
Figure 1.2. Variation in GAS pilus subunit types. Phylogenetic trees based on (A) backbone pilin-BP, (B) collagen-binding protein of Group A streptococci-AP1 (C) and ancillary pilin 2-AP2 gene sequences. Different variant groups are represented by different colours and an example of M serotype associated is given. Adapted from (26).

The variability of the FCT regions also include the pili expression regulatory factors encoded in the pilus locus. As mentioned above, all FCT regions regardless of type possess one of the regulators from the global regulatory RALP family, either *nra* or *rofA* (59). However, these regulators demonstrated heterogeneity in its effects on pilus expression across different strains (59,60). Divergence is also seen in regulatory mechanisms situated outside of the FCT locus. For example FasX, a small regulatory RNA which post transcriptionally inhibits pilus expression by reducing the stability of pilus operon mRNA, targets BP genes in some GAS strains and AP in other strains (61,62).

The response to changes in the environment has also been found to differ between strains. For example, strains with FCT-2, 3 or 4 demonstrated pH dependent pilus expression, with production only occurring in acidic conditions, whilst FCT-1 strains expressed the complex irrespective of pH (63). In addition, bistable expression levels of the structure can occur in some strains, where genes are not expressed in a uniform matter, resulting in subpopulations with differing levels of protein production (58).

1.3.2 Structure

The construction of GAS pili is facilitated by sortase enzymes, which are membrane associated cysteine transpeptidases. These enzymes recognise proteins that possess a cell wall sorting signal (CWSS) at the C terminus; consisting of one variant of the LPXTG-like sortase recognition motif followed by a block of hydrophobic residues and a positively charged tail. (37, 38).

The backbone chain of the pilus consists of 10-100 BP subunits covalently linked together (66). Crystal structures of the protein have revealed that BP consists of 2 or 3 domains made entirely of β sheets. Attachment of each BP monomer to its successive subunit was found to occur via linkage between a C terminal CWSS cleavage site and a conserved lysine residue. Sortase enzymes cleave between the peptide bond of threonine and glycine in the recognition motif found within the CWSS to form an acyl-enzyme intermediate. Nucleophilic attack of the pilin motif lysine residue of the adjacent subunit then facilitates the formation of an amide bond between the new cleaved C terminus CWSS and that lysine residue (67,68). The importance of the lysine residue was demonstrated with expression of a mutant BP where the lysine residue

was replaced with arginine. This resulted in the subunit solely being produced in a monomeric form, indicating the loss of polymerisation (69).

Whilst the BP spans the majority of the structure, the base subunit and tip subunit of the pili consist of the minor pilins AP2 and AP1, respectively (Figure 1.3) (68). Although the minor pilins make up a very small proportion of the pilus, they are fundamental for correct pili structure and localisation, as demonstrated by strains with mutations in these subunits. Studies utilising GAS minor pilin deletion mutants revealed that in a mutant M1 strain CSF370 devoid of AP2, the expressed pili were found in the supernatant of the bacterial culture, as opposed to being attached to the bacterial cell wall. In comparison, pili of the AP1 deletion M1_CSF370 strain still localised to the cell wall. This exhibited the role of AP2 in linking pili to the cell wall (70). Studies in several different FCT type strains have indicated that the process of anchorage to the cell wall via AP2 requires the "housekeeping sortase" Sortase A (SrtA). It has been shown that the housekeeping sortase cleaves between threonine and glycine of the sortase recognition motif to form an acyl enzyme intermediate, which is subsequently linked to free amino acids on the cell wall peptidoglycan (64,70,71).
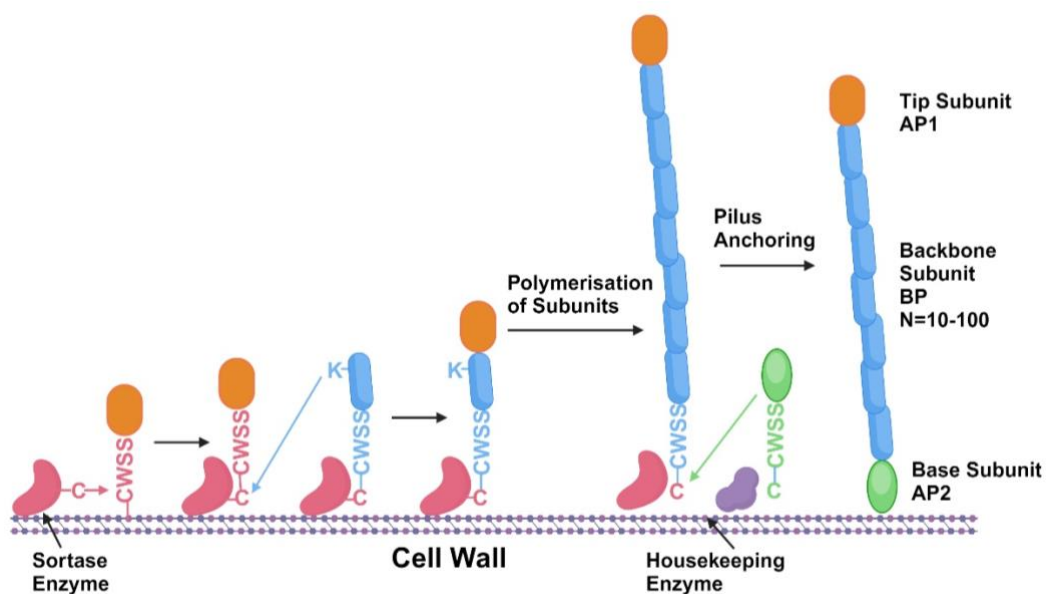
Figure 1.3. Schematic diagram of pilus from GAS M1 strain SF370. The pilus consists of AP1 tip subunit (in orange otherwise referred to as Spy0125), up to 100 copies of BP backbone subunit (in blue otherwise referred to as Spy0128) and AP2 base subunit (in green otherwise referred to as Spy0130) which anchors the structure to the cell wall. Diagram created with biorender.com.

Whilst AP2 anchors the pili to the cell wall, AP1 is confined to the tip of the pilus. In an engineered M1_SF370 strain, where the lysine residue in BP used for polymerisation was replaced with alanine, not only was BP found as a monomer, AP1 was unable to attach to this modified BP monomer. This illustrates that AP1 attaches to BP via the same lysine residue covalently linking BP monomers together. AP1 could only attach to BP at this particular lysine, thus the subunit inhibits pili elongation by preventing further linage of BP subunits. This is supported by electron microscopy of antibody labelled AP1 and BP indicating that AP1 is always found capping a chain of BP subunits (69,70).

1.3.3 Function

Genetically modified versions of the pili and GAS strains with pilus gene deletions have been extensively utilised in the identification of the complex as a virulence factor. Compared to wild type M1_SF370 strain, mutants with deletions of the pilus sortase or backbone pilin displayed five-fold reduction in adherence to human pharyngeal cell lines (39). A five-fold decrease in adherence was also seen when wild type M6 GAS and AP1 deletion M6 GAS were tested for association to a human epithelial cell line (37). Similarly, in M1T1 serotype the isogenic pilus gene deletion strain showed a 87% reduction in keratinocyte adhesion compared to the wild type bacteria (72). In addition to changes in adhesion to immortalised cell lines, pili deletion mutants demonstrated decreased binding to primary keratinocytes and tonsil epithelium (38). These studies demonstrate the ability of pili to facilitate binding of GAS to host cells present in principle sites of infection and strongly suggest its role in colonisation during the early phase of infection. Of note, the target protein for pili mediated adhesion to host cells was variable between GAS strains and FCT types. Whilst pili in M1 (FCT-2), M3 (FCT-3) and M6 (FCT-1) strains bound to the salivary glycoprotein gp340, the type 1 collagen has been reported to be the binding partner of pili in the M12 (FCT-4) strain (73,74).

Pilus- mediated cellular adhesion also appears to have the ability to subsequently contribute to the process of invasion, with deletion of pilus from M2 GAS ensuing in diminished bacterial internalisation into cell lines (75). Furthermore, both M4 and M53 GAS demonstrated that the presence of pili was instrumental for progression of invasive infections (76,77). These results echoed observations of the closely related Group B Streptococcus pili facilitating invasion of the blood brain barrier following attachment to host cells (78).

Not only do GAS pili possess the ability to bind to host cells, they also appear to facilitate the formation of biofilms. Upon incubation of wild type M1_SF370 GAS with epithelial cells, the formation of multilayered microcolonies was recorded (39). This phenomenon was not seen when the BP deletion M1_SF370 strain was incubated in the presence of epithelial cells. On polystyrene, wild type GAS had six-fold more efficient biofilm formation compared to the pili deletion counterpart (39). Similar trends were observed when clinical strains were isolated, corresponding pilus deletion strains were constructed, and the rate of biofilm formation was compared (79). Although many GAS strains shared the capability to deploy pili to form biofilms, the progression of this process was incongruous. Whilst the FCT-2 pilus from the M1 strain appeared to promote this phenomenon via auto aggregation, the FCT-1 pilus from the M6 strain contributed to the initial attachment to cells required in the early stages of biofilm growth (79,80). Furthermore, it has been observed that in GAS with certain FCT types, biofilm formation was augmented at lower pH and was directly correlated to increased pilus expression in more acidic environments. On the other hand, GAS strains possessing FCT-1 had high pilus expression levels regardless of changes in pH and had stronger biofilm formation than bacteria with other FCT types (63,81).

There is mounting evidence for the AP1 subunit's role as the adhesive determinant in a variety of GAS strains. In conditions where wild type GAS bound to tonsil cells in abundance, the corresponding AP1 deletion mutant was functionally defective, despite forming detectable cell surface pili (38). When M6 (FCT-1) pili were expressed on surrogate *Lactococcus lactis*, cell binding was preserved in bacteria expressing both AP1 and BP but attenuated in *L. lactis* only expressing BP (37). In line with these results, when purified pili subunit proteins were incubated with a pharyngeal cell line, binding activity was not observed for BP but AP1 demonstrated dose dependent binding (39). Moreover, AP1 was demonstrated to bind to type-1 collagen and displayed sequence homology to collagen and fibronectin binding proteins (73). AP1 appears to also be responsible for the role of pili in biofilm formation, with biofilm formation unaffected by the addition of BP antibodies to wild type GAS, while the addition of AP1 antibodies resulted in abolition of biofilms (37). Despite the AP1 subunit primarily contributing to pili mediated adhesion in the aforementioned GAS strains, the BP subunit appears to be the key component of pili adhesive properties in other strains, re-iterating the narrative of pili variability. This was seen in the pilus from serotype M2 GAS, with significantly reduced bacterial binding to HaCaT cells observed following addition of BP

12

specific antibodies but not antibodies binding to AP1 (75). The BP of M4 GAS was also depicted to have substantial influence on pili adhesion to cell lines, with deletion of the subunit abrogating bacterial binding to HaCaT cells (76).

Another facet of GAS pili function is the immune evasion conferred by the pilus structure. In both M4 GAS and M2 GAS, the presence of pili enhanced the survival of bacteria in both whole blood and cell lines (75,76). Pilus deletion in the M53 strain also resulted in decreased bacterial fitness in a mouse infection model and attenuated survival in whole blood due to increased phagocytosis, further alluding to the structure assisting in immune evasion to prolong bacterial clearance from the host (82). As GAS have been demonstrated to avoid the host immune killing mechanisms by surviving intracellularly in host cells, pilus-mediated cellular uptake may be one process through which the complex assists in immune evasion (83). Exclusively in M4 GAS, BP has been depicted to bind to the host acute phase protein haptoglobin. This appeared to result in protection against anti-microbial peptides, likely due to increased steric hindrance on the bacterial surface (76).

As most studies on GAS pili thus far have been centered on the adhesive properties of GAS, there has been less focus on elucidating the pili's interaction with the different components of the host immune system. As pili are exposed structures expressed on the cell surface in abundance, it is expected that the complex can directly interact with immune cells.

1.3.4 Prospects in Vaccine Development

The global health burden posed by GAS infections is indicative of the need to produce a vaccine to provide prophylactic protection and there is a variety of candidates being surveyed currently. One such GAS component is the M protein, where an experimental vaccine consisting of recombinant peptides from different M proteins fused together has reached phase II clinical trials (84). Such M protein based vaccines face problems surrounding coverage, due to the widely variable nature of M protein (85). This is exacerbated by vast regional differences, with low resource settings displaying a different profile of serotypes and greater serotype variation compared to high resource settings (85). Methods such as serological identification of antigens and proteomic analysis of cell wall extracts is also being used to identify potential conserved non-M protein GAS vaccine (86–88). Despite the majority of these candidates conferring protection against GAS in animal models, they often fail to fulfil the requirement of providing

broad coverage against the large array of currently circulating strains. Thus, a general trend observed within this space is the extension of coverage by using a combination of antigens derived from different proteins (88,89). Examples include the fibronectin based FSB vaccine, which contains a fibronectin binding domain, the M protein C terminus and motifs from streptolysin and SpeB. Another potential combination vaccine employs streptococcal CXC protease co-administered with a conserved M protein peptide (90). Of note, many non-protein M vaccines are poorly immunogenic and require additional components such as Alum and cholera toxin B to ensure a protective immune response is evoked (91,92).

The GAS pili have shown promise circumventing problems related to vaccine coverage and immunogenicity seen in the aforementioned GAS components. The main function of GAS pili in adherence means that the corresponding antibodies produced against the pili would likely provide both neutralising and opsonising activities (93). The complex was confirmed to be a protective antigen in a study where mice were immunised with components of the GAS pili and subsequently given a dose of the bacteria calculated to kill 90% of mock immunised negative control mice. The mice administered with the combination of pilus proteins had survival rates higher than 70%, similar to the levels of protection achieved with the M protein (56). Furthermore, pilus proteins were found to induce protective antibodies in mouse models without the addition of adjuvants. This implied the structure possessing immunostimulatory characteristics, a property lacking in many other GAS vaccine candidate proteins (56).

An examination of the GAS strains currently circulating Europe and the US illustrates the presence of 27 predominant M types. Sequence analysis of pilin genes suggest that an amalgamation of backbone pilins (or BP proteins) from 12 pilus types would be sufficient to confer protection against 90% of these M types (26). This suggests that a pilus-based vaccine would require less antigens than an M based vaccine targeting the same panel (94). Not only does the pilus exhibit less variation compared to the M protein, it has been shown to be a temporally conserved complex. A recent study comparing historical and contemporary GAS infection samples from New Zealand indicated that there was very little variation within single *tee* genes, with <2 nucleotide differences between the same *tee* types across the two time periods (94). The stability of the sequence over time suggests that pilus-based vaccines would be effective in providing long term immunity against GAS, as the phenotypes of circulating pili would not stray over time from the antigens contained within the vaccine. The pili's

characteristics of relatively broad coverage and stability of alleles across time make this complex a highly promising GAS vaccine candidate.

Our lab has delved into investigations on the vaccine potential of the pili, either as a vaccine target for GAS disease or as a vaccine delivery system for broader infectious diseases. TeeVax is a multivalent recombinant protein vaccine consisting of 3 recombinant proteins, each containing 5-7 domains from a range of T antigens hybridised together. Immunisation of rabbits with TeeVax induced the production of specific and cross-reactive anti-T antigen IgG and IgA antibodies, which were demonstrated to possess the ability to mediate killing of GAS bacterium. While TeeVax is delivered as a set of recombinant proteins, GASPEL uses *Lactococcus lactis* as a delivery and expression platform for the pilus. *L. lactis* is a non-pathogenic food grade bacterium with immunostimulatory properties, making it a safe delivery vehicle which can be administered without the addition of toxic adjuvants (66). Preceding studies have used *L. lactis* to express Group B Streptococcus pili and these bacterium were found to confer protection against challenge with GBS isolates (95). GASPEL applies a similar approach, with *L. lactis* used to express fully assembled pili from the 6 different FCT types. When this bacterium was delivered mucosally to rabbits, they elicited the production of specific IgG and IgA antibodies against each pilus subunit, which were cross reactive between some pilus types including some more distantly related pili. Moreover, these antibodies were functional, possessing the capacity to reduce or neutralise adhesion of GAS to a keratinocyte cell line and facilitate opsonophagosytosis (66). In contrast to TeeVax and GASPEL, which are purposed to protect against GAS specifically, PilVax is a novel application of the pilus structure, where it is expressed in *L. lactis* and used as a peptide antigen delivery platform. Studies demonstrated the feasibility of inserting antigens, such as epitopes from *S. aureus* and *Mycobacterium tuberculosis* proteins, into selected loop regions within the BP structure. Immunisation with these recombinant *L. lactis* strains in mice resulted in enhanced immunogenicity and the generation of antigen specific antibodies (96,97). These results supported the rationale of utilising GAS pili to stabilise and amplify otherwise poorly immunogenic peptides for subunit vaccine development.

Although many vaccine candidates have been derived from GAS, there is particular interest in pilus due to its potential to provide broad coverage against GAS strains and induce an immune response without the need for assistance from additional immune potentiators. This

characteristic has also been incorporated into the use of the structure as a vehicle for delivery of non-GAS antigens. However, there is a lack of information surrounding the innate immune response to the pili. Investigation into this avenue will provide a complete picture of the pili's immunological features and potentially expand the usage of this component against infections.

1.4   Bacterial Sensing and Initiation of Immune Responses

Following a bacterial infection, two immune defence networks are sequentially activated in order to eliminate the microbial organism. The innate immune system acts as the first line of defence, offering immediate and broad protection, and is followed by the adaptive immune system, which provides a more specific and prolonged immune response (98).

Activation of the innate immune system is mainly mediated by conserved molecular structures specific to foreign bacteria, known as pathogen associated molecular patterns (PAMPs). These structures are recognised by pattern recognition receptors (PRRs), which can be grouped into soluble and cell bound PRRs. Soluble PRRs have the capacity to bind to various microbial proteins to mediate the direct elimination of bacteria (99). On the other hand, cell bound PRRs are expressed primarily on antigen presenting cells (APCs) such as macrophages and dendritic cells (DCs). These receptors recognise PAMPs and activate processes to directly kill bacteria, as well as upregulate pathways involved in priming the adaptive immune response to clear infection (100,101).

The most significant soluble PRRs are the components of the complement system, an amalgamation of plasma proteins made in the liver and by immune cells, that can be activated by pathogens to trigger a cascade of reactions to defend against initial infection (99,102). There are three pathways towards complement activation; the classical pathway, which can be initiated mainly via binding of IgG or IgM to antigens on the pathogen surface, followed by binding of complement proteins to the antibody Fc region; the mannose binding-lectin pathway, which is put into motion via collectin or ficolin protein binding to poly-mannose components of microbial cell walls; and the alternative pathway, which utilises spontaneously occurring complement component, which is inactivated in the absence of pathogen surfaces to bind to (103,104). The pathways merge at the generation of C3 convertase, an enzyme that produces C3b, which binds to bacteria to promote their uptake and destruction by phagocytic cells (105). Complement components may also assemble into membrane-attack complexes on the

microbial outer membrane to promote cell lysis (106). Another family of soluble PRRs are the pentraxins, characterised by their cyclic pentameric structures (99). These molecules can bind to mannose on bacterial cell walls and act as opsonins, as well as activating the classical complement pathway by binding to initial components of the reaction cascade (107).

An important family of cell bound PRRs is the dimeric, membrane spanning toll like receptors (TLRs), which are found on various cells of the innate immune system such as DCs and macrophages. These PRRs are composed of N-terminus leucine rich repeats that interact with PAMPs, a transmembrane region, and an intracellular toll-interleukin-1 receptor (TIR) domain responsible for transducing downstream signaling (108). There are 10 TLRs in the human immune system, which can be divided into two subgroups based on whether they are located on the cell surface or embedded in intracellular vesicles. The former interacts with surface associated components of extracellular pathogens, whereas the latter recognises pathogen nucleic acid (109). Upon ligand binding, TLRs undergo conformational changes to recruit adaptor molecules to the intracellular TIR domain. MyD88 is the most prolific of these adaptor molecules, interacting with all TLRs aside from TLR3. Through phosphorylation, MyD88 initiates a signaling cascade resulting in the nuclear translocation of the transcription factor NFκB, a family of inducible transcription factors responsible for regulation of genes associated with a multitude of different immune and inflammatory processes (110).

Although TLRs are the most prominent and extensively studied transmembrane PRRs, bacteria can also be sensed by members of the C-type lectin receptors (CLRs). Each CLR contains at least one carbohydrate recognition domain, allowing the complex to interact with bacteria through glucan, fucose and mannose structures (111). The recognition of such highly conserved features allows receptors to interact with a broad range of pathogens and activated receptors can trigger the cascade of reactions resulting in NFκB signaling (112,113).

As expression of the aforementioned PRRs is restricted to the cell surface and the lumen of lysosomal vesicle membranes, they are unable to recognise pathogens that have invaded the cytosol (114). This recognition is accomplished by an array of cytosolic PRRs, broadly grouped into retinoid acid-inducible gene I like receptors (RLRs) and nucleotide-binding oligomerisation domain like receptors (NLRs) (100). Whilst RLRs interact with viral RNA, NLRs are key sensors of microbial cell wall peptidoglycan. In a process akin to TLRs, the C-

terminal potion of the NLR binds to bacterial components such as muramyl dipeptide, to initiate receptor oligomerisation and N terminal signaling. This in turn activates the signaling pathways such as NFκB, inducing a multitude of immune processes (115).

NFκB has aptly been dubbed as the master regulator of innate immune responses due to the range of pathways it is downstream and upstream of. For starters, upon stimulation they can provide early defence against bacterial infection through upregulation of cationic NFκB defensins. These molecules induce membrane permeabilisation and propel the upregulation of reactive oxidase species, which are toxic to a broad range of microbes and also encourage the activity of anti-microbial peptides (116,117). Furthermore, the transcription factor elicits the process of phagocytosis against invading pathogens, providing another layer of immediate defence (118). NFκB can also direct the maturation of APCs, giving cells the ability to uptake and process bacteria recognised via their PRR and subsequently present antigenic peptides to lymphocytes of the adaptive immune system (110,118,119). This presents the opportunity for adaptive immune cells to produce protective antibodies specific to the displayed antigen (120,121). Adhesion factors assisting in the process of cell recruitment, such as vascular cell adhesion molecule-1, are also upregulated by NFκB, inducing infiltration of further immune cells to mount a defence against infection (122). Another major aspect of immune response coordinated through NFκB is the secretion of pro-inflammatory cytokines which provide signals to activate immune cells in an endocrine, paracrine or autocrine manner (118). These molecules can act on immune cells that have not yet interacted with the bacteria to prime them for PAMP recognition. For example, the cytokine TNF is able to enhance vascular endothelial permeability and recruit neutrophils and monocytes to the site of infection, which can then be activated via signaling through cytokine receptors (109,123). Cytokines also play a key role in the cross talk between innate and adaptive immune cells by further inducing APC maturation, enhancing their ability to interact with lymphocytes, and directly stimulating adaptive immune cells. This in turn can activate lymphocyte production of protective antibodies or mobilise cytotoxic cells (109,124,125).
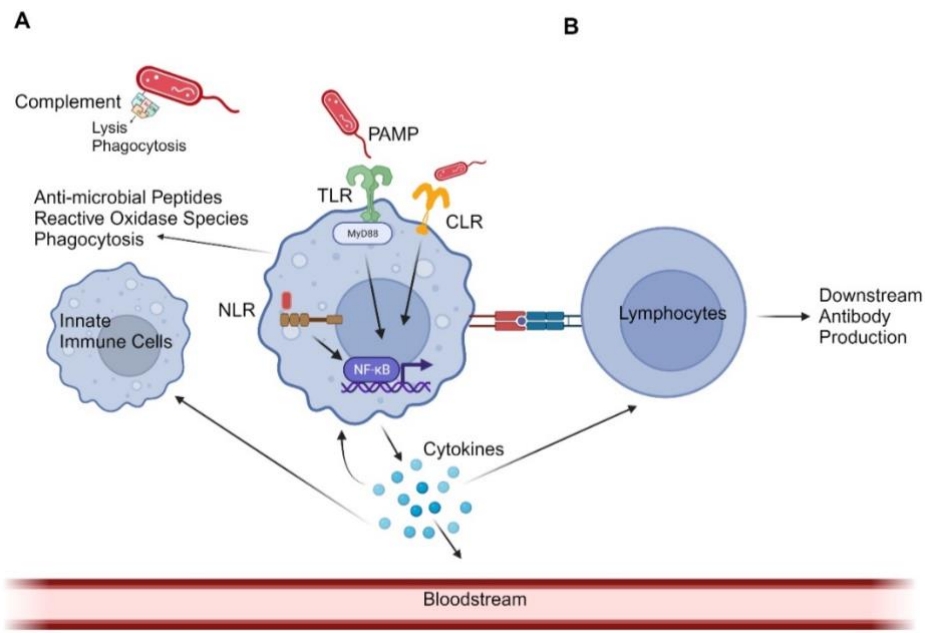
Figure 1.4. Schematic representation of downstream effects of PRR activation. (A) PAMPs on pathogen are recognised by soluble PRR propelling elimination of bacteria. PAMPs interact with cell bound PRRs such as TLR coupled to MyD88, CLR and NLR, inducing downstream activation and nuclear translocation of NFκB, resulting in transcription of an array of pro-inflammatory genes. This results in upregulation of defence mechanisms against pathogens, increased receptor expression and cytokine secretion. These cytokines signal in an autocrine, paracrine and endocrine manner (B) PRR mediated APC activation triggers the presentation of pathogenic antigens to lymphocytes. Coupled with co-stimulatory molecules and cytokine signalling, this can activate downstream antibody production. Diagram created with biorender.com.

Another key player in the transition from the initial indiscriminate defence to a highly specific adaptive immune response is the TLRs. Out of the cell bound PRRs, these receptors induce the broadest range of responses in innate immune cells associated with modulating adaptive immune cells. Furthermore, unlike the other PRRs, TLRs are also extensively expressed on adaptive immune cells and possess the ability to directly regulate their activity (126–130).

One of the first steps in antibody production is the presentation of antigens on APCs to T cells. APCs such as DCs can phagocytosis apoptotic bodies as well as pathogens, and the differences in response to these two molecules appears to be dictated by the engagement of TLRs. Studies using macrophages have indicated that cells containing cargo which engaged with TLRs underwent induced phagosome maturation not observed in cells interacting with apoptotic host cells. This maturation was triggered by pathways downstream of TLRs such as MyD88 signaling and resulted in presentation of bacterial antigens on MHC class II molecules on the

cell surface (Figure 1.5A) (131). Thus, it appears that TLR signals are assisting in the process of distinguishing whether ingested cargo contained self or non-self-antigens.

TLR activation is also implicated in the upregulation of co-stimulatory factors which interact with lymphocytes in parallel with the process of antigen presentation. Intermediate signaling proteins produced downstream of TLR activation, such as MyD88, as well as TLR induced cytokines, such as TNF, promote the upregulation of co-stimulatory molecules such as CD40 and CD80 on APCs (132,133). In concert with antigens presented on MHC class II, these molecules interact with T helper cells to facilitate their activation and expansion. In fact, studies using CD40$^{-/-}$ mice indicated that T helper cell proliferation and activation was dependent on expression of this co-stimulatory molecule on dendritic cells (133). B cells then present antigen to these activated T helper cells, stimulating their capacity to secrete signalling cytokines, which in turn induce the B cells to produce antibodies. Thus the activation of TLRs indirectly affects the process of antibody production via its control over co-stimulatory molecule expression (Figure 1.5B). Recent studies have also indicated that CD40 expression on dendritic cells may contribute to increased B cell survival (134). Co-stimulatory molecule upregulation is thus another avenue of innate immunity which can be augmented by TLR ligands.

The plethora of pro-inflammatory mediators released following TLR activation can contribute to the recruitment and migration of immune cells. For example, many cytokines released downstream of TLRs such as CCL2 and IL-8 act as chemoattractants for immune cells. Cell adhesion molecules, such as adhesion molecule-1, and vasodilators are also upregulated to expedite the process of cell migration (135). Studies in mice found that co-administration of antigens with TLR4 agonists resulted in a localised release of cytokines which increased recruitment of dendritic and monocytic cells. Subsequent trafficking of antigens by these cells to lymph nodes, which act as antibody production sites, was also heightened (Figure 1.5C) (136). Therefore, TLR ligands can enhance the amount of innate immune cells uptaking and transporting antigens to adaptive immune cells. Furthermore, cytokines upregulated by TLR induction can direct the polarization of the T helper cell (Th) response towards distinct T helper cell subsets (Figure 1.5D). Cytokines such as IL-12 and IFNγ have been observed to promote T cell differentiation into Th1 effector cells, which can activate cytotoxic T cells and opsonising antibody production. This results in a combination of cellular and humoral responses that are able to control intracellular infections. On the other hand, the absence of IL-

12 and the presence of cytokines such as IL-4, IL-5 and IL-13 result in Th cell differentiation skewing towards effector Th2 cells. These cells orchestrate the elimination of extracellular infections via activation of eosinophils and proliferation of antibody producing B cells (137,138). More recent studies into effector T cells have also uncovered both IL-6 and IL-21 involved in the differentiation of T cells into T follicular helper cells (Tfh). These specialised Th cells facilitate the selection and maturation of high-affinity antibody producing B cells and cell signalling from Tfh cells is required for maintenance of long-living memory B cells (139–142). Resultantly, protection against any infectious disease is significantly compromised in the absence of these cells (143). As different TLRs upregulate the expression of different cytokines, TLR agonists have been used to direct the adaptive immune response following vaccine administration. For example, mice administered with Ova antigen and the TLR2 ligand Pam$_3$Cys had pronounced secretion of IL-5 and IL-13, whereas mice given Ova with the TLR9 ligand immunostimulatory sequence oligodeoxynucleotides (ISS-ODN) did not upregulate these cytokines and instead had increased levels of IFNγ and IL-12. This resulted in mice primarily producing antibodies against Ova and mice with prominent cytotoxic T cell activity respectively (144).

Studies using mice with B cells devoid of TLR4 or the MyD88 protein downstream of TLRs indicated that interaction with antigen presenting T helper cells alone was not able to induce B cell production of specific antibodies. These studies suggested that activation of TLRs on B cells is also required for proliferation, activation and differentiation of B cells (145,146). The role of TLR signaling in B cells was further elucidated using the TLR4 agonist (lipopolysaccharides) LPS. When wild type mice and mice with MyD88 knock out B cells were vaccinated with a model antigen alone or in conjunction with LPS, only the wild type mice given both molecules had an amplified immune response. The knock-out mice were subsequently transfected with wild type B cells and given either just model antigen or the antigen with LPS. This resulted in only the transfected mice given both the antigen and TLR4 ligand displaying amplified antibody response (147). Collectively, this data indicates that B cell TLR activation is required for robust antibody production, further highlighting the ability of TLR to enhance adaptive immune response (Figure 1.5D).
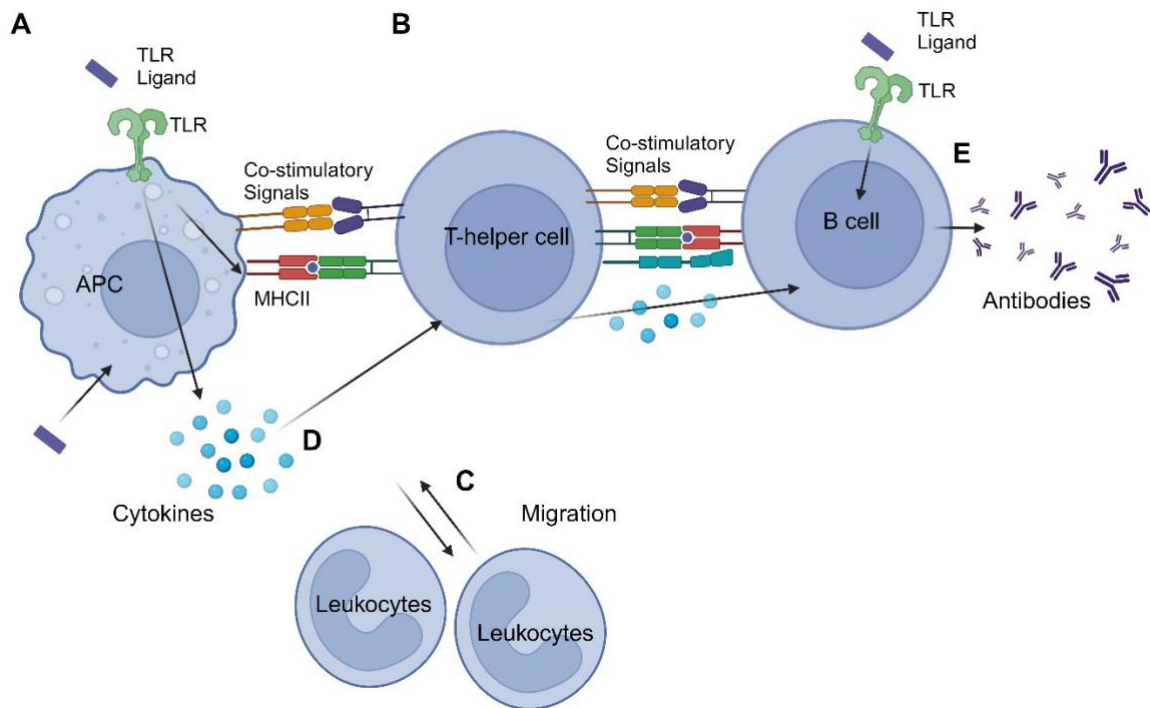
Figure 1.5. Schematic representation of examples of TLR activation bridging innate and adaptive immunity. (A) Activated TLR contributes to APCs displaying vaccine antigens on MHC to T helper cells. (B) Furthermore, TLR mediated expression of co-stimulatory signals aids in activation of these T helper cells. (C) TLR induced cytokine release aids in the migration of immune cells and (D) the polarisation of T helper cells. These T helper cells induce B cell activation alongside TLR expressed on the B cells themselves to (E) facilitate antibody production. Diagram created with biorender.com.

As TLR activation triggers a cascade of signaling pathways and processes, TLR agonists have applications in the clinical landscape. A major branch of this is the repurposing of these ligands as adjuvants, which are substances added to vaccine formulations to enhance immunogenicity of the vaccine and increase durability and magnitude of the adaptive immune response towards the antigens included (148). Adjuvants are generally employed to escalate vaccine mediated antibody response and protection in general populations, but have also found use in enhancing seroconversion rates in groups with low baseline immune responses such as children and the elderly, immunocompromised individuals and patients receiving immunosuppressing treatments (149,150). Furthermore, adjuvants can reduce the amount of antigens in the vaccine or the number of doses required for substantial antibody titers (151,152).

The mechanism behind adjuvants involves augmentation of the initial innate immune response to facilitate increased downstream humoral and/or cellular immune response (148,153). Thus

the use of TLR agonists as adjuvants has been a focal point due to the ability of these receptors to bridge the innate and adaptive immune response (154). Furthermore, adjuvants signaling through different TLRs are able to mediate polarization of the T helper cell response, and thus may also be used to elicit a functionally appropriate adaptive immune response towards a vaccine, such as ensuring high antibody production occurs or enhancing cytotoxic cell activity (137,138,148,155).

An example of a TLR agonist used extensively in both clinical and experimental settings is poly I:C, a synthetic double stranded RNA which induces inflammation through TLR3 (156). Poly I:C is a potent IFNγ inducer which can elevate Th1 activation and increase antibody production (157–159). As the T cell phenotype and cytokines induced by the molecule can promote cytotoxic effector cells, poly I:C is garnering particular interest in the space of cancer vaccines (160). However, there are some concerns around toxicity and studies around developing an efficacious derivative are ongoing (161). Another example is monophosphoryl lipid A (MPL), a TLR4 agonist derived from Gram negative bacterial LPS. This molecule skews T cell differentiation towards Th1, leading to its licensing for inclusion in vaccines against allergy (162). Another adjuvant triggering Th1 expansion is synthetic DNA containing CpG motifs, which activate TLR9 to effectively enhance cytotoxic T cell activity but have the disadvantage of being vulnerable to nuclease mediated degradation (163,164). A TLR5 based adjuvant that has reached clinical trials is flagellin (165). This compound triggers TNF production and a mixed Th response, unlike many other TLR adjuvants which polarise cells solely towards Th1 (166). Flagellin's overt stimulation of TLR5 resulted in the compound inducing systemic adverse effects when administered as part of an influenza vaccine however, signaling the need for further manipulation of the molecule to improve the safety profile (165). Although TLR agonists have shown promise in the space of vaccine adjuvants, there is currently a lack of commercial availability for many of these ligands (167). Further development is required to addresses issues surrounding current contenders and the exploration for efficacious TLR based adjuvants is still ongoing.

1.4.1 Innate Immune Response to GAS

Numerous studies conducted have indicated the role of innate immune cells in controlling GAS infection. For example, DCs have been found to be vital in this process, with transient depletion of DCs from mouse models resulting in increased systemic dissemination from a skin infection

(168). Similarly, depletion of macrophage from mouse models via clodronate liposome treatment resulted in enhanced spread of GAS from a soft tissue infection to the bloodstream. A decrease in GAS dissemination could then be observed when these mice received a macrophage graft (169). These findings are indicative of monocyte mediated control of GAS dissemination, a process involving the PRRs and associated signaling pathways detailed above. While the innate immune response is important for providing an early alert of infection and expediting GAS clearance, the resulting inflammatory reaction can at times be harmful (170).

The complement system is a soluble PRR key for elimination of GAS, with inhibition of this system in a mouse GAS infection model resulting in increased bacterial burden in both the blood and organs, as well as enhanced lethality (171). The plethora of mechanisms adopted by GAS to thwart the complement system and its associated soluble proteins such as pentraxins, is another testament to the importance of this system in the innate immune response to GAS (172). However, excessive complement activation in the kidneys can incite inflammatory cell recruitment and tissue damage responsible for the progression of post-streptococcal APSGN (173,174). Furthermore, certain complement factors were found to be elevated in ARF patients and in a mouse model contributed to heart valve inflammation, suggesting the complement system's role in the progression of post GAS infection sequelae (175,176).

Apart from the complement compounds, the large crux of innate immune responses against GAS is regulated by inflammatory mediators downstream of cellular PRRs (177). This was evident following knockout in mice of the gene encoding TNF, a major cytokine downstream of PRR stimulated NFκB. Deficiency of TNF significantly increased susceptibility to soft tissue GAS infections and greatly reduced immune cell recruitment to infection sites, as well as elevating rates of mortality (169). IFNγ, another cytokine induced by PRR recognition of GAS components, was also found to be key in defending the host against GAS infection. The cytokine appeared to regulate neutrophil infiltration, ensuring substantial amounts of phagocytic cells were translocated to infection sites and mice devoid of IFNγ receptor had heightened susceptibility to lethal GAS infection and tissue damage (178–180). Additionally, molecules secreted downstream of PRR activation, such as the antimicrobial peptide cathelicidin, was found to prevent invasive GAS from disseminating from skin infections (181).

Emerging information has been gathered that illustrates the importance of TLRs in innate immune response to GAS infections. Macrophages incubated with GAS were found to produce NFκB and pro-inflammatory cytokines such as the aforementioned TNF in a MyD88-dependent manner. As the MyD88 adaptor molecule is downstream of most TLRs, these results were indicative of TLR being one of the PRRs involved in GAS recognition (180). Furthermore, MyD88-/- mice infected with GAS had severely dampened release of pro-inflammatory cytokines such as IL-12 and IL-6 compared to wild type mice and attenuated chemoattractant release resulting in marred neutrophil and macrophage recruitment. These mice had accelerated morbidity following infection with GAS, compared to their wild type counterparts, further highlighting the role of TLR activation associated processes in eliminating GAS infection (125). TLRs also appeared to play a significant role in GAS induced dendritic cell maturation, with MyD88$^{-/-}$ mice infected with GAS failing to upregulate cell surface proteins required for cell activation and co-stimulation of adaptive immune cells (182,183). Loss of MyD88 additionally resulted in the abolishment of dendritic cell release of IL-12, a cytokine important for lymphocyte differentiation (182,184). GAS interaction with TLRs did not appear to be restricted to the receptors expressed on the immune cell surface, with the bacteria also found to interact with endosomal TLRs. GAS activated both TLR3 and TLR9 following their recognition of GAS derived DNA, such as CpG-rich DNA motifs (185). This prompted secretion of IFNγ and elicited the production of reactive oxygen species with the ability to mediate bacterial killing (186,187).

In spite of the evidence for the involvement of TLRs and downstream signalling in the immune response to GAS, there has been no general agreement on the interactions of specific TLRs and GAS components. Dendritic cells collected from mice models deficient in either TLR2, 4 or 9 did not lose the ability to secrete cytokines following exposure to GAS, and production of these signalling peptides was also preserved in TLR2/4/9 triple deficient mice macrophages (180,182). These results are most probably due to the multimodal interactions between PRRs and GAS. The host immune system will likely have a redundancy in PRR signalling, with various components of GAS being recognised by multiple PRRs. When a single receptor is not dominating pathogen recognition, it ensures the initiation of an immune response in circumstances where one of the individual PRR is defunct (188,189). For instance, NLRs also induces NFκB, albeit through a different signalling cascade to TLRs. As GAS is also recognised by NLRs, these complexes can offer defence against GAS infections through the

same mechanisms as TLRs (190). In fact, they are likely to have contributed to the NFκB associated clearance of GAS in studies introduced above which was not specifically initiated via MyD88 (169,180). NLRs have also been demonstrated to provide unique innate immune response pathways against GAS infections. An interesting aspect of this is NLRP4 regulating GTPase signalling following GAS infection. This has been shown to promote the formation of autophagosomes and result in GAS clearance via antibacterial autophagy (191). NLRX1 is another NLR described to trigger autophagic elimination of GAS, with GAS invasion markedly increasing when the receptor was knocked out in a mouse model (192). Cell anchored and secreted GAS components have also been implicated in NLR driven inflammasome formation. Deficiency in the IL-1 cytokine activated by this complex has been shown to reduce neutrophil recruitment to GAS infection sites and heighten susceptibility to systemic GAS infection in mouse models (193). Other cell bound PRRs such as CLR have also been depicted to contribute to GAS clearance through NFκB and independent pathways. Lipoteichoic acid on GAS is recognised by CLRs to upregulate signalling cascades through a tyrosine kinase to induce the secretion of pro-inflammatory cytokines, release of bactericidal reactive oxygen species and expression of cell surface receptors which co-stimulate adaptive immune cells (194).

As in the case of complement, the extensive range of innate immune responses elicited by the cell bound PRRs are crucial for GAS infection clearance but can also have a detrimental effect on the health outcomes of the infected individual. In particular for GAS, prolonged inflammation as a result of PRR stimulation can contribute to autoimmune disease, with cytokines and chemokines playing a key role in pathogenesis (195). In the context of ARF/RHD, an abundance of inflammatory cytokines such as TNF and IFNγ have been associated with disease progression, with TNF attracting cells to sites of inflammation and IFNγ inducing the presentation of autoantigens (196,197). Adhesion molecules which can be upregulated via PRR activation, such as vascular cell adhesion molecule, have also been depicted to contribute to valvular damage in RHD, due to the protein promoting T cell infiltration (198). Additionally, inflammasome associated cytokines have been implicated in linking innate and adaptive immune cells in autoimmune disorders and appear to be involved in the acute phase of rheumatic disease (199,200).

1.4.2 Innate immune Response to GAS pili

Being an abundant surface expressed structure, it is reasonable to assume that GAS pili can be recognised by innate immune PRRs. Numerous studies support the idea of pili from Gram-positive bacteria modulating host innate immune responses. For instance, piliated strains of *Streptococcus pneumoniae* were observed to evoke high levels of TNF release in mice following intraperitoneal challenge, whereas strains lacking pili induced low TNF response. Furthermore, mice administrated with a strain of *S. pneumoniae* with the pilus encoding gene islet deleted had decreased IL-6 and TNF secretion compared to mice given the wild type bacterium (201). Similar findings could be seen in Group B Streptococcus. A human endothelial cell line infected with a pilus expressing strain of the bacterium induced significantly greater release of neutrophil chemokines compared to cells treated with a pilus deletion mutant strain (202). Group B Streptococcus pili also appeared to possess the ability to modulate macrophage mediated phagocytosis, with the presence of the gene encoding pilus backbone protein correlating to increased macrophage uptake of the bacterium (203).

Supplementing these findings are results linking GAS pili and neutrophils of the innate immune system. When wild type GAS and a pilus deletion GAS mutant strain were exposed to human neutrophils, the wild type strain induced the release of neutrophil extracellular traps at 3-fold higher levels than the mutant strain (72). These neutrophil extracellular traps are a defence mechanism against bacteria produced downstream of PRR activation, which promotes further innate immune responses such as inflammasome activation (204,205). Pilus expressing WT GAS also appeared to induce elevated levels of IL-8, compared to mutant bacteria with abrogated pilus expression (72). These observations imply that GAS pili directly activate innate immune responses through PRRs and promote a state of inflammation, to tackle the clearance of the bacterium. Prior to this project, preliminary studies compared cytokine secretion from THP-1 cells exposed to GAS pili expressed on the *L. lactis* and cells exposed to W.T *L. lactis* devoid of pilus (135). This illustrated a strong increased secretion of IL-8 and TNF in response to pilus-expressing *L. lactis* compared to their unmodified wild type counterpart. This further solidifies the concept of GAS pili modulating the host innate immune response. At the same time, the preliminary evidence of a strong inflammatory response to GAS pili raises the notion of whether the structure contributes to the detrimental over stimulation of innate immunity associated with the inflammatory symptoms in GAS diseases. Although information is still

sparse, pili have been shown to induce TNF, and this is one of the cytokines associated with inflammation and progression of RHD (197,206). Additionally, pili are capable of triggering the release of neutrophil extracellular traps, and recent research has provided increasing evidence of these complexes playing a role in the perpetuation of autoimmune disorders (72,207). Currently, pili from M1 GAS have been the focal point of investigation into the relationship between innate immunity and pili but the immense inter-strain diversity of pili suggests possible divergence in the innate immune response between different types of pili. Therefore, investigation into pilus mediated inflammation may require a survey across pili from different GAS strains associated with differing clinical presentations.

Although the interaction between PRRs and GAS pili is yet to be extensively explored, studies on the closely related *S. pneumoniae* pili provide some insight into the possible relationship between receptors and this complex. Piliated *S. pneumoniae* was previously observed to induce the release of IL-8, a cytokine found downstream of multiple PRRs (208,209). Compared to a mutant strain devoid of pili, *S. pneumoniae* with pili was also found to induce significantly higher levels of IL-8 release from HEK cells expressing TLR2 but not in HEK cells expressing TLR4 (210). GAS pili and pneumococcal pili have similarity in structure, function, and even amino acid sequence of pilus subunits (56,73,211,212). Despite these similarities, there is little to no information on the innate receptor that recognise GAS pili. Investigation initiated prior to this project have begun to depict interaction between TLR2 and GAS pili but this relationship is yet to be fully elucidated (135).The emerging evidence for the roles of GAS pili in immune stimulation and TLR activation also opens up the avenue for its potential use as an adjuvant. To evaluate the suitability of GAS pili as a contender in the pursuit of effective TLR based adjuvants, the interactions between the complex and the innate immune response requires further mapping.

1.5   Aim

The global burden of GAS infection related diseases has prompted wide-spread investigation into the various virulence factors of the bacterium and its interactions with the host immune system, in an attempt to create prophylactic vaccines. GAS pili have garnered interest as a possible vaccine candidate, with promising evidence of the structure inducing protective host

adaptive immune responses. However, characterisation of the complex is incomplete, with a lack of knowledge around the innate immune response elicited by pili. This study aims to explore this undefined immunomodulation capacity of the pilus, to further consolidate its position as a GAS vaccine candidate but more extensively, to uncover the untapped adjuvanting potential of the structure. Preliminary studies into the pili elude to its immunostimulatory potential but more elaborate characterisation of the structure's interaction with the innate immune system and subsequent effect on the adaptive immune response is required.

The specific objectives to achieve this aim are:

1. To examine the link between pilus type and level of immune response/inflammation by exposing cell lines and *Galleria mellonella* (Great wax moth) larvae to a panel of GAS pili expressed on the avirulent *L. lactis* bacterium.

2. To generate recombinant proteins of pilus subunits and test on reporter cell lines expressing TLRs to further pinpoint receptor- pilus interactions and determine whether the pilus proteins are functional TLR ligands.

3. To generate fusion complexes consisting of pilus subunits conjugated to an antigen and confirm the integrity of the pilus proteins in this form.

4. To further use recombinant pilus subunits to perform cell based assays in order to elucidate the ability of pilus subunits to alter the immunomodulatory capacity of immune cells.

5. To test the aforementioned fusion complexes on a mouse model to investigate the ability of pilus proteins to enhance antibody response against the co-expressed antigen.

Chapter 2: Materials and Methods

2.1   Materials

2.1.1 Molecular Biology

All solutions were prepared using Type 1 Mili-Q water (Millipore) unless otherwise indicated.

2.1.1.1 Reagents

PCR buffer (10x)	500 mM KCI, 0.1% (v/v) Triton X-100, 100 mM Tris HCI (pH9.0)
6x DNA loading dye	30% (v/v) glycerol, 0.25% (w/v) bromophenol blue, 0.25% (w/v) xylene cyanol FF
TAE buffer	0.1% (v/v) glacial acetic acid, 2 mM EDTA, 40 mM Tris (pH8.0)
CutSmart buffer (10x)	50 mM potassium acetate, 20 mM Tris-acetate, 10 mM magnesium acetate, 100 µg/ml BSA (pH7.9)
Restriction Endonucleases	SalI, BamHI, PstI, XmaI, EcoRI, XhoI (NEB)
CCMB80 transformation buffer	10 mM KOAc, 80 mM CaCl2, 20 mM MnCl2, 10 mM MgCl2, 10% (v/v) glycerol (pH6.4)

2.1.1.2 Plasmids

pFW11	Vector for gene deletion containing the Spectinomycin-resistance gene *aad9*. Flanking regions of target genes are to be cloned into multiple cloning sites sandwiching *aad9*, which replaces the target gene via allelic replacement. Provided by Professor Andreas Podbielski from the University of Rostock, Germany.

pGEX-3C-M2e	*E. coli* expression vector modified from the pGEX-3C vector by Dr Catherine Tsai (UoA). It consists of a multiple cloning site with the *m2e* sequence inserted between the BamHI and EcoRI sites, an Ampicillin resistance gene, a GST-tag and a 3C protease recognition sequence.
pBC-Spy0125LPXTG	A standard cloning vector with Ampicillin resistance gene containing the sequence for *spy0125* including the LPXTG motif. Generated by Dr Jacelyn Loh (UoA).
pPROEX-Htb	*E. coli* expression vector from Life Technologies. It consists of an Ampicillin resistance gene, multiple cloning sites and 6× His-tag.
pBS-ccdB	A modified version of the pBluescript (pBS) cloning vector from Stratagene with Ampicillin resistance gene, β-galactosidase gene for blue/white selection and additional control of cell death B (ccdB) cassette for reducing background colonies introduced by Dr Jacelyn Loh (UoA).

2.1.1.3 Oligonucleotides

Table 2.1. Sequences of the oligonucleotide primers for the generation and confirmation of *SrtA* gene-knockout mutant. The restriction site in each primer is underlined.

Name	Sequence 5'-3'	Restriction Site
SrtA_FR1.fw	ctag<u>gtcgac</u>ctgacgaactgctaattc	SalI
SrtA_FR1.rv	ctag<u>ggatcc</u>gattctgtgaaaaatgcttttgag	BamHI
SrtA_FR2.fw	ctag<u>ctgcag</u>catctatatatgaccacc	PstI
SrtA_FR2.rv	ctag<u>cccggg</u>ggataaagccttaaaacttc	XmaI
SrtA-FR1.Ot	gcaagagaatcttcatctcc	-

SrtA-FR2.Ot	gatgtgacaaccastgggaac	-
SrtA.fw	gtcactttatcaaatgccttctc	-
SrtA.rv	cattgtcctattatttattgtggg	-
aad9.beg	ccttattggtacttacatgtttg	-
aad9.end	ccattcaatattctctccaag	-
aad9.fw	agagaatattgaatggac	-
aad9.rv	catgtaagtaccaataagg	-
Spy0128.fw	cgggatccgctacaacagttcacgg	-
Spy0128.rv	cggaattcttattcaaagactttttatttg	-

Table 2.2. Sequences of the oligonucleotide primers for the generation and confirmation of pilus protein-M2e fusion proteins. The restriction site in each primer is underlined.

Name	Sequence 5'-3'	Restriction Site
Spy0128Bam.fw	cgggatccgctacaacagttcacgg	BamHI
Spy0128Bam.rev	cgggatccttattcaaagactttttatttg	BamHI
Spy0128Eco.fw	cggaattcgctacaacagttcacgg	EcoRI
Spy0128Eco.rev	cggaattcttattcaaagactttttatttg	EcoRI
M2e.fw	cggatccctcgagtcacttttaactgaagttgaaaca cctattagaaatgaatgg	XhoI
M2e.rev	cggaattcctcgagatcagatgaatcattacatctacaaccc cattcatttctaatagg	XhoI
Spy0125Bam.fw	ggatccaagactgtttttggtttag	BamHI
Spy0125Sal.rev	gtcgacctctttattattttcaaaagc	SalI
Spy0125LPXTGXho.rev	ctcgagctaaccagtttctggcaaaggctctttattattttc	XhoI

2.1.1.4 Bacterial Strains

L. lactis MG1363   A plasmid-less strain of *L. lactis* used for cloning of a SrtA deletion strain and as a negative control when

studying cellular response to whole pilus expressed on *L. lactis* surface.

L. lactis plZ12-Km2:P23R_PilM1, PilM2, PilM4, PilM6, PilM28	*L. lactis* strains transformed with a plasmid containing the operon for expressing either FCT-2 GAS pilus from a serotype M1 strain (PilM1), FCT-6 GAS pilus from a serotype M2 strain (PilM2), FCT-5 GAS pilus from a serotype M4 strain (PilM4), FCT-1 GAS pilus from a serotype M6 strain (PilM6) or FCT-4 GAS pilus from a serotype M28 strain (PilM28) and a kanamycin-resistant gene. The expression of pili is driven by a strong, constitutive lactococcal promoter P23. These strains are used to study cellular response to assembled whole pilus expressed on the surface of *L. lactis* surrogate.
Streptococcus pyogenes	Wild type *S. pyogenes* SF370, an ATCC 700294 serotype M1 strain.
E coli. DH5α	A standard *E. coli* strain (ATCC 53868™) used for cloning.
E coli. BL21(DE3) pLysS	An *E. coli* strain used for the expression of recombinant proteins under the control of the T7 promoter. Contains the pLysS plasmid for chloramphenicol resistance. From Novagen.
E coli. BL21(DE3) pLysS pET32-3c: Spy0128	A BL21 *E. coli* strain transformed with a plasmid for expressing rSpy0128, the BP from the serotype M1 GAS pilus. The plasmid contains an Ampicillin

resistance gene and produces a recombinant protein fused to thioredoxin with a specific 3C protease cleavage site and 6×His tags at the N-terminal. Generated by Fiona Clow (UoA).

E coli. BL21(DE3) pLysS pPROEX-Htb_Spy0125 LPXTG	A BL21 *E. coli* strain transformed with a plasmid for expressing rSpy0125, the AP1 from the serotype M1 GAS pilus. The plasmid contains an Ampicillin resistance gene and produces a recombinant protein with 6×His tags at the N-terminal. Generated by Dr Jacelyn Loh (UoA).

2.1.1.5 Bacterial Media

Brain heart infusion broth (BHI)	3.7% (w/v) Brain Heart Infusion powder
Lysogeny broth	25 g/L Luria-Bertani Broth
GM17 broth	3.725% (w/v) M17 powder, 0.5% (w/v) glucose
Super optimal broth (SOB)	2% (w/v) bacto-tryptone, 0.5% yeast extract, 0.05% (w/v) NaCl, 0.018% (w/v) KCl, 1% (v/v) MgCl$_2$, (pH7.0)
Agar plate	Liquid media added with 1.5% (w/v) agar powder

2.1.1.6 Selective Antibiotics

Ampicillin	For the selection of *E coli.* DH5α and *E coli.* BL21 transformants containing ampicillin-resistance genes, used at 50 µg/ml

Chloramphenicol	For the selection of *E coli.* BL21 which contains the pLysS plasmid, used at 30 μg/ml
Kanamycin	For the selection of *L. lactis* containing plZ12-Km2:P23R plasmid, used at 200 μg/ml

2.1.2   Protein Purification and Analysis

2.1.2.1 Protein Purification

Protoplast buffer	40% sucrose, 10 mM MgCl2, 0.1 M KPO4 (pH6.2), 2 mg/ml lysozyme, 400 U mutanolysin, EDTA-free protease inhibitor (Roche)
Affinity purification wash buffer	150 mM NaCl, 1 mM EDTA, 1% Triton X-100, 10 mM Tris (pH7.4)
IPTG	Isopropyl-β-D-thiogalactoside induces expression of proteins under the control of the T7 promoter used at 0.1 mM.
PBS	2.7 mM KCl, 150 mM NaCl, 10 mM phosphate salts, (pH7.4)
MCAC-0	0.5 M NaCl, 10% (v/v) glycerol, 20 mM Tris HCl (pH8.0)
MCAC-1000	1 M imidazole, 10% (v/v) glycerol, 0.5 M NaCl, 20 mM Tris HCl, (pH8.0)

MCAC 10, 20, 40,100	MCAC1000+MCAC0 at imidazole concentrations of 10 mM, 20 mM, 40 mM, 100 mM
MCAC Lysis buffer	MCAC-0, 0.1 mM PMSF, 0.1% (v/v) Triton X-100
SEC buffer	10 mM Na_3PO_4, 0.14M NaCl, 3% glycerol (pH7.4)
GSH I buffer	1 mM EDTA, 50 mM NaCl, 25 mM Tris HCl (pH7.4)
GSH II buffer	1 mM EDTA, 500 mM NaCl, 25 mM Tris HCl (pH7.4)
GSH III buffer	1 mM EDTA, 5 mM reduced glutathione, 25 mM Tris HCl, (pH7.4)
GSH lysis buffer	1 mM EDTA, 50 mM NaCl, 1% (v/v) Triton X-100, 25 mM Tris HCl, (pH7.4)
Cleavage buffer	5 µg/ml 3C protease, 1.5 mM DTT

2.1.2.2 Protein Labelling

Fluorescent Red Mega 485 NHS-ester	Amine conjugated biolabel excitation 482 nm, emission 559 nm. Dissolved in amine-free DMF at 40 nmol/µl (Sigma-Aldrich)
Bicarbonate buffer	50 mM $NaHCO_3$ (pH9.0)

2.1.2.3 SDS-PAGE and Western Blot Solution

Acrylamide/Bis	30% (w/v) acrylamide, 0.8% (w/v) bisacrylamide

Resolving gel buffer	0.4% (w/v) SDS ,1.5 M Tris HCl (pH8.8)
Stacking gel buffer	0.4% (w/v) SDS ,0.5 M Tris HCl (pH8.8)
SDS running buffer	2.5 mM Tris HCl, 2.5 mM glycine, 0.01% SDS (pH8.6)
2× protein loading buffer	4.1% SDS, 20% glycerol, 300 mM 2-mercaptoethanol, 0.0001% (w/v) bromophenol blue, 125 mM Tris HCl (pH6.8)
Coomassie stain solution	50% ethanol (v/v), 7.5% (v/v) glacial acetic acid, 0.06% (w/v) coomassie brilliant blue R
Destaining Solution	25% (v/v) ethanol, 8% (v/v) glacial acetic acid
Tris-buffered saline (TBS)	20 mM Tris HCl, 150 mM NaCl, (pH7.6)
TBS-T	TBS + 0.1% (v/v) Tween-20
Western blot towbin transfer buffer	25 mM Tris HCl, 192 mM glycine, 20% (v/v) methanol (Merk), (pH8.3)
Western blot blocking solution	TBS-T plus 5% (w/v) skim milk powder (Anchor)
Western blot probing solution	TBS-T plus 2.5% (w/v) skim milk powder (Anchor)
Protoplast buffer	40% sucrose, 10 mM MgCl2, 0.1 M KPO4 (pH6.2), 2 mg/ml lysozyme, 400 U mutanolysin, EDTA-free protease inhibitor (Roche, Germany)

2.1.2.4 Antibodies for Western Blot

Table 2.3. Antibodies used for western blotting

Name	Host Species	Working Dilution	Supplier
rBP polyclonal antibodies	Rabbit	1:1000	In house
rAP1 polyclonal antibodies	Rabbit	1:1000	In house
Influenza A M2 Monoclonal Antibody (14C2)	Mouse	1:1000	ThermoFisher
Anti-rabbit IgG (HRP)-polyclonal	Goat	1:1000	Abcam
Anti-mouse IgG (HRP)-polyclonal	Goat	1:1000	Abcam

2.1.3   Cell Culture

2.1.3.1   Cell Lines

THP-1	Human monocyte-like cell line originally isolated from peripheral blood of a case of childhood acute monocytic leukaemia.
HEK-Blue hTLR	HEK293 cell lines engineered by InvivoGen to stably co-express human TLR gene along with a NF-κB inducible secreted embryonic alkaline phosphatase (SEAP) reporter gene, which can be detected using the HEK-Blue Detection SEAP detection media. HEK-Blue hTLR2, HEK-Blue hTLR4, HEK-Blue hTLR2/hTLR1 and HEK-Blue hTLR2/hTLR6 cell lines were utilised in this project.
J774A.2	BALB/C monocyte macrophage re-cloned from the J774A.1 cell line isolated from the ascites of an adult, female mouse with reticulum cell sarcoma.

2.1.3.2 Cell Propagation/ Media

THP-1

Roswell Park memorial institute medium 1640 (RPMI-1640) (Gibco™), 10% (v/v) fetal bovine serum (FBS), 1×PSG, 0.05 mM 2-β mercaptoethanol

HEK-Blue™ hTLR

Dulbecco's Modified Eagle Medium (DMEM), 4.5 g/l glucose, 10% (v/v) FBS, 100 U/ml penicillin, 100 µg/ml streptomycin, 100 µg/ml Normocin™, 2 mM L-glutamine,1×HEK-Blue™ Selection

J774A.2

DMEM, 2 mM L-glutamine, 4.5 g/l glucose, 10% (v/v) Fetal Bovine Serum,100 U/ml penicillin, 100 µg/ml streptomycin

2.1.3.3 Positive Controls for Cell Based Assays

Pam$_3$CSK$_4$

Synthetic triacylated lipopeptide (InvivoGen). Positive control for THP-1, HEK-Blue™ hTLR2/hTLR1, J774A.2 Utilised at a concentration of 1 µg/ml

Pam$_2$CSK$_4$

Synthetic diacylated lipopeptide (InvivoGen). Positive control for HEK-Blue™ hTLR2/hTLR6 cell lines. Utilised at a concentration of 1 µg/ml

ConA

Concanavalin A, a mannose/glucose-binding lectin isolated from Jack beans (InvivoGen). Positive control for J774A.2 , utilised at 1 µg/ml

LPS

E. coli lipopolysaccharide. Positive control for J774A.2, utilised at 1 µg/ml.

2.1.4 Functional Assays

2.1.4.1 Biosensor Binding Assay

Sensor Chip NTA | For capture of histidine-tagged molecules by metal chelation for use in Surface Plasmon Resonance (Cytiva)

Running buffer | 10 mM HEPES (pH7.4), 150 mM NaCl, 3 mM EDTA, 0.005% Tween-20

2.1.4.2 ELISA Based Assays

Carbonate-bicarbonate buffer | 0.01 M Na_2CO_3, 0.1 M $NaHCO_3$ (pH9)

PBS-T | 0.05% Tween-20 in PBS

Blocking solution | 3% BSA in PBS-T

Table 2.4. Antibodies and peptides used for ELISA based assays

Name	Host Species	Working Dilution	Supplier
rBP polyclonal antibodies	Rabbit	1 µg/ml	In house
rAP1 polyclonal antibodies	Rabbit	1 µg/ml	In house
Influenza A M2 Monoclonal Antibody (14C2 Clone)	Mouse	1 µg/ml	ThermoFisher
Anti-rabbit IgG (HRP)-polyclonal	Goat	1:1000	Abcam
Anti-mouse IgG (HRP)-polyclonal	Goat	1:1000-1:4000	Abcam
Anti-mouse IgA (HRP)-polyclonal	Goat	1:4000	Abcam

Name	Working Dilution	Supplier
Recombinant BP	1 µg/ml	In house
Recombinant AP1	1 µg/ml	In house
Recombinant human TLR2 extracellular domain (Met1-Arg587) with C-terminus 6×His tag	1 µg/ml	SinoBiological
Recombinant M2e with KLH conjugation	1 µg/ml	Scram Co., Ltd.

2.1.4.3 Flow Cytometry Based Assays

EDTA	Calcium chelator to detach adherent HEK-Blue™ hTLR cell lines, used at 10 mM
TrypLE	Recombinant enzyme to detach adherent J774A.2 cell lines, used at 10× dilution
FACS Buffer	PBS, 1% FBS, 5 mM EDTA
Blocking buffer	2% BSA in PBS

Table 2.5. Antibody panel used to detect expression of murine macrophage receptors. All antibodies supplied from BioLegend.

Target	Fluorophore	Working Dilution	Clone
CD80	PE/Cyanine7	1:200	16-10A1
CD86	PE	1:3200	GL-1
MHCII	Alexa Fluor® 647	1:40	M5/114.15.2
F4/80	FITC	1:500	BM8

2.1.4.4 Cytokine Detection Assays

Human TNFα ELISA   EK-0001 Human TNFα ELISA kit (Crux Biolab)

Luminex Discovery Assay   Premixed, 7-Plex, mouse Luminex assay kit containing
                                beads to detect IFNγ, IL-2, IL-4, IL-6, IL-10, IL-17 and
                                TNF (R&D systems)

2.1.4.5 TLR Activity Detection Assay

HEK-Blue Detection   HEK-Blue Detection powder, 50 ml endotoxin-free
                                water (InvivoGen)

Polymyxin B   Antibiotic to remove endotoxin (LPS) from proteins
                                expressed in *E. coli* before their use in assays, utilised
                                at a concentration of 100 µg/ml

Endotoxin-Free water   ToxOut™ Endotoxin Free Water (BioVision) used as
                                negative control for HEK-Blue™ hTLR cell lines

SSL3   Staphylococcal Superantigen-Like Protein 3. TLR2
                                antagonist derived from Staphylococcal aureus

2.1.4.6 Macrophage Activation Assay

MTT solution   5 mg/ml 3-(4,5-dimethylthiazol-2-yl)-2,5-
                                diphenyltetrazolium bromide in PBS

2.2 Methods

2.2.1 DNA Purification

2.2.1.1 Purification of Genomic DNA from *S. pyogenes/ L. lactis*

For isolation of DNA from GAS, bacteria was inoculated into 1.2 ml of BHI medium in an Eppendorf tube and incubated overnight at 37°C without agitation. For isolation from *L. lactis*, bacteria was inoculated into 1.2 ml of GM17 medium in an Eppendorf tube and incubated overnight at 28°C without agitation. The culture was subsequently spun at 5,000 g for 5 minutes and the supernatant was discarded. The pellet was washed twice with 1 ml of a 10 mM Tris (pH8.0) and 50 mM EDTA solution before the supernatant was discarded and the pellet was resuspended in 400 µl of a 10 mM Tris (pH8.0) and 50 mM EDTA solution. The solution was supplemented with 4 µl 10 U/ml mutanolysin, 4 µl 10 mg/ml RNase and 5 µl 100 mg/ml lysozyme and the tube was incubated at 37°C for 1 h with gentle agitation. This was followed by the addition of 80 µl proteinase K (1 mg/ml) and a further incubation for 30 min at 28°C. The genomic DNA was then isolated using a Monarch Genomic DNA Purification Kit (NEB) as per the manufacturer's instructions. DNA was eluted into 20 µl of pre-heated water and quantified by UV spectrophotometry using a Nanodrop ND-1000 Spectrophotometer (Thermo Scientific) before storage at -20 °C.

2.2.1.2 Purification of Plasmid DNA

E. coli DH5α was inoculated into 10 ml LB containing the appropriate antibiotics and incubated overnight at 37°C while being agitated at 200 rpm. The culture was spun at 4,000 g for 15 minutes and the supernatant was discarded. The plasmid DNA was subsequently isolated using a Nucleospin plasmid miniprep kit (Macherey-Nagel) according to the manufacturer's instructions provided with the kit. DNA was eluted into 30 µl of pre-heated water and quantified by UV spectrophotometry using a Nanodrop ND-1000 Spectrophotometer (Thermo Scientific) before storage at -20 °C.

2.2.1.3 Agarose Gel Electrophoresis

Agarose gels for DNA analysis were prepared by dissolving 1% (w/v) molecular grade agarose (Bioline) in TAE buffer and subsequently adding 1:10,000 SYBR™ Safe DNA gel stain (Invitrogen). The solution was poured into a gel caster with combs to create sample loading wells and submerged in TAE buffer after setting. DNA samples were mixed with 6 × DNA

loading dye at a ratio of 5:1 and loaded into wells. 1 Kb plus DNA ladder (Invitrogen) was loaded into the first well as a molecular-weight reference. The gel was run at 100 V and 400 mA for 30 minutes using a PowerPac™ basic power supply unit (Bio-Rad) and visualised using a ChemiDoc™ imaging system (Bio-Rad).

2.2.1.4 Gel Extraction of DNA

The agarose gel was placed over Dark Reader® DR46B transilluminator (Clare Chemical Research) and the desired DNA fragments were excised from the gel using a sterile scalpel. The gel fragment was placed in an Eppendorf tube and placed on dry ice to freeze, before being mashed using a sterile pipette. The pipette was left in the gel slurry and tube was frozen again with dry ice. The frozen gel piece was removed from the tube using the inserted pipette as a handle and transferred to the top of a filter pipette tip sitting in a clean Eppendorf tube. Once the gel was thawed, the tube was centrifuged at 13,000 g for 1 minute to elute DNA through the filter.

2.2.2 Molecular Cloning

2.2.2.1 PCR

Amplification of DNA fragments from single bacterial colonies or purified template DNA was undertaken using a Mastercycler Nexus thermocycler (Eppendorf). The reactions for single colony PCR were conducted using Taq polymerase (made in-house by Professor John Fraser group, UoA) using the reaction mixture and reaction conditions outlined in Table 2.6 and Table 2.7 respectively. Taq polymerase was also used for producing DNA fragments using overlapping PCR as outlined in

Table 2.8 and Table 2.9. Additionally, genes of interest were amplified using iProof High-fidelity DNA polymerase (Bio-Rad) as per the reaction mixture and conditions in

Table 2.10 and Table 2.11.

Table 2.6. Single colony PCR reaction mixture (for a 15 µl reaction)

Reagent	Final Concentration	Volume (µl)
10× PCR buffer	1×	1.5 µl
25 mM MgCl$_2$	2.5 mM	1.5 µl

10 mM dNTPs	0.2 mM	0.3 µl
10 µM Forward primer	0.2 µM	0.3 µl
10 µM Reverse primer	0.2 µM	0.3 µl
5 U/ µl Taq DNA polymerase	0.1 U/ µl	0.3 µl
UltraPure water	-	10.8 µl

Table 2.7. Thermal cycles for single colony PCR

Step	Temperature (˚C)	Time (s)	Cycles
Initial denaturation	95	300	1
Denaturation	95	30	
Annealing	X*	60	15
Extension	72	60/kb	
Final extension	72	600	1

*Annealing temperature based on the Tm of the primers

Table 2.8. Overlapping PCR reaction mixture (for a 100 µl reaction)

Reagent	Final Concentration	Volume (µl)
10× PCR buffer	1×	10 µl
25 mM MgCl$_2$	1.25 mM	5 µl
10 mM dNTPs	0.15 mM	1.5 µl
100 µM Forward primer	2 µM	2 µl
100 µM Reverse primer	2 µM	2 µl
5 U/ µl Taq DNA polymerase	0.075 U/ µl	1.5 µl
UltraPure water	-	78 µl

Table 2.9. Thermal cycles for overlapping PCR

Step	Temperature (˚C)	Time (s)
Denaturation	95	40
Annealing	50	45
Extension	72	600

Table 2.10. PCR amplification for genes of interest (for a 50 µl reaction)

Reagent	Final Concentration	Volume (µl)
5× iProof buffer	1×	10 µl
10 mM dNTPs	0.2 mM	1 µl
10 µM Forward primer	0.5 µM	2.5 µl
10 µM Reverse primer	0.5 µM	2.5 µl
2 U/ µl iProof polymerase	0.02 U/ µl	0.5 µl
Template DNA	50 µg	X ul
UltraPure water	-	Up to 50 µl

Table 2.11. Thermal cycles for genes of interest

Step	Temperature (˚C)	Time (s)	Cycles
Initial denaturation	98	30	1
Denaturation	98	10	
Annealing	X*	30	25-35
Extension	72	30/ kb	
Final extension	72	600	1

*Annealing temperature based on the Tm of the primers

2.2.2.2 Restriction Enzyme Digestion and Ligation

Vector and insert DNA was first digested with restriction enzyme(s) to gain compatible ends. Digestion was performed in a total volume of 10 µl consisting of 1 µg of DNA, 1 µl of 10× compatible reaction buffer and 1 µl of restriction enzyme(s) (NEB). The digestion mixture was incubated at 37˚C either overnight or for 2 hours if using high fidelity enzymes. The resulting linearised plasmids were treated with 1 µl of 5000 U/ml calf intestinal alkaline phosphatase for another 30 min at 37 ℃ to prevent self-ligation. Restriction enzymes were subsequently removed either by incubating the mixture at 65˚C for 20 minutes or by performing a gel extraction. Purified vector and insert were mixed at a molecular ratio of 1:3 in a total volume of 10 µl containing 1 µl of 10× ligation buffer and 1 µl of T4 DNA ligase. The reaction mixture was then incubated on ice overnight.

2.2.2.3 Preparation and Transformation of Chemically Competent *E. coli*

A single colony of DH5α or BL21 (DE3) *E. coli* was inoculated into 2 ml of SOB and grown overnight at 37˚C with agitation at 200 rpm. The next day, 1 ml of this culture was added to 100 ml of fresh SOB and incubated with agitation at 200 rpm at 37°C until an OD_{600} between 0.4-0.6 was reached. The cells were harvested by centrifugation at 4,000 rpm for 10 minutes at 4°C and resuspended in 32 ml of ice cold CCMB80 buffer. The cells were then incubated on ice for 20 minutes before being centrifuged for 10 minutes at 4,000 rpm at 4°C. The supernatant was completely removed and the bacterial pellet was resuspended in 4 ml of ice cold CCMB80 buffer. The cells were left to incubate on ice for another 20 minutes before being divided into 50 µl aliquots in pre-chilled Eppendorf tubes. The tubes were snap frozen in a dry ice ethanol bath and stored at -80°C until use.

A tube of chemically competent *E. coli* was thawed on ice and 5 µl of ligation mix or 1 µl of plasmid prep was added before the bacteria were incubated on ice for 10 minutes. The tube was heat shocked for 45 seconds on a heat block pre-heated to 42°C before being immediately transferred to ice. After a 2 minute incubation period 1 ml of LB was added for recovery and the cells were incubated at 37˚C for 30 min. After a 5 minute centrifugation at 5000 rpm, the media was removed and cells were resuspended in 100 µl of LB. The bacteria was then plated on a LB agar plate supplemented with the appropriate antibiotics and incubated overnight at 37°C.

2.2.2.4 Preparation and Transformation of Electrocompetent *L. lactis*

A single colony of *L. lactis* MG1363 was inoculated into 1.5 ml of GM17 broth and grown overnight at 28˚C without agitation. The next day, 1 ml of this culture was added to 50 ml of fresh GM17 and incubated without agitation at 28°C until the OD_{600} was between 0.4-0.6. The cells were harvested by centrifugation at 4,000 rpm for 15 minutes at 4°C and then underwent wash steps at 4,000 g at 4°C, 5 minutes per round of centrifugation. The bacteria were washed twice with 4 ml of ice cold sterile water, twice with 2 ml of ice cold 50 mM EDTA and twice with 2 ml of ice cold 0.5 M sucrose containing 10% glycerol. Finally, the cells were gently resuspended in 0.4 ml of ice cold 0.5 M sucrose containing 10% glycerol and used immediately for electroporation.

One microliter of plasmid DNA (0.2-1 µg) was mixed with 100 µl of cell suspension and incubated on ice for 5 minutes before being transferred to a pre-chilled 2 mm cuvette. The Gene Pulser Xcell Electroporation System (Bio-rad) was used to apply a single pulse of 2.5 kV, with capacitance at 25 µF and resistance at 200 Ω. The cells were recovered by immediately adding 1 ml of GM17 supplemented with 200 mM $MgCl_2$ and 20 mM $CaCl_2$ to the cuvette and incubating on ice for 10 minutes. The cells were transferred to an Eppendorf tube and incubated for 3 hours at 28°C without agitation. Additionally, at least 1 hour before the end of the bacterial incubation period, a GM17 agar plate containing the appropriate antibiotics was incubated at 28°C. Following the 3 hour incubation, cells were centrifuged for 5 minutes at 5,000 rpm before media was removed and the cell pellet was resuspended in 100 µl of GM17. The bacteria was then plated on the pre-warmed agar plate and incubated for 24 hours at 28°C.

2.2.3 Protein Expression and Purification

2.2.3.1 Cell Wall Extraction of *L. lactis*

A single colony of *L. lactis* was inoculated in 15 ml of GM17 media with appropriate antibiotics and incubated statically overnight at 28°C. This culture was centrifuged at 4,500 rpm for 10 minutes at 4°C and the resulting cell pellet was washed once with PBS. The pellet was resuspended in 1 ml of ice cold protoplast buffer and incubated for 3 hours at 37 °C with rotation. Cellular debris was removed via centrifugation at 15,600 g for 15 min at 4 °C and the extract was analysed using western blot or stored at -20 °C.

2.2.3.2 Affinity Purification of *L. lactis* Supernatant Pilus Proteins

A single colony of *L. lactis* was inoculated into 1 ml of GM17 with appropriate antibiotics and incubated overnight at 28°C under static conditions. The medium was diluted to a cell density of ~1×10^7 CFU/ml based on the conversion equation of OD_{600} 1.0=~1×10^8 CFU/ml and 1 ml of this bacterial suspension was centrifuged at 4,000 ×g for 15 minutes at 4°C and supernatant was collected. The Protein A agarose beads (ABT) (100 µl) were incubated with 1 µg of rBP polyclonal antibody for 4 hours at 4°C under rotary agitation. The mixture was then centrifuged for 2 minutes at 3,000 g at 4°C and supernatant was discarded. The beads were then washed by adding 1 ml wash buffer under agitation, before centrifugation was undertaken for 2 minutes at 3,000 ×g at 4°C. The wash step was repeated twice before beads were incubated with the prepared supernatant overnight at 4°C under rotary agitation. The mixture was centrifuged for

2 minutes at 3,000 ×g at 4°C, supernatant discarded and wash steps as above repeated. Beads were then incubated for 10 minutes with 100 µl of 0.2 M glycine (pH2.6) with frequent agitation and elution was undertaken by centrifugation at 300 ×g before equal volumes of Tris HCl (pH8) was added to neutralise the solution. This process was repeated two more times and elutant was pooled and analysed using western blot.

2.2.3.3 Recombinant Protein Expression in *E. coli*

A single colony of *E. coli* BL21(DE3) containing the plasmid for expressing the gene of interest was inoculated in 100 ml of LB media with appropriate antibiotics overnight at 37˚C with agitation at 200 rpm. The following morning the culture was added to 900 mL of fresh LB media (with appropriate antibiotics) and incubated at 37˚C with agitation at 200 rpm until the OD_{600} was between 0.6-0.8. The culture was transferred to an agitating incubator set at 28˚C and cooled for 30 minutes before the addition of 0.1 mM IPTG. The culture was incubated for a further 5 hours at 28˚C with 200 rpm agitation before centrifugation at 4,000 ×g for 30 mins at 4˚C. After removal of supernatant, the pellet was stored at -20˚C until purification was performed.

2.2.3.4 Nickle Affinity Chromatography Purification

The frozen *E. coli* pellet was resuspended in 6% w/v of MCAC lysis buffer and sonicated on ice using the Q700 sonicator (Qsonica). The cellular debris was pelleted by centrifugation for 30 minutes at 10,000 g at 4˚C and the supernatant was collected and filtered using a 0.22 µm filter unit (Merck). The clarified bacterial lysate was passed over a gravity flow column packed with 2 ml of nickel-charged nitrilotriacetic acid resin (Biorad) and pre-equilibrated with 10 column volume (CV) of MCAC-0. The column was then washed with 5 CV of MCAC-0 to remove unspecific binding and the protein was then eluted in a stepwise manner with 5 CV of MCAC-0 supplemented with increasing concentrations of imidazole from 10 mM to 100 mM (MCAC-10 to MCAC-100). The collected fractions were prepared and analysed using SDS-PAGE and the fractions containing the recombinant protein were pooled together.

Protein expressed in the pPROEX-Htb vector was dialysed overnight at 4°C against PBS and concentrated using the 50 kDa molecular weight cut-off Vivaspin protein concentrator (GE Healthcare) before further purification using size exclusion chromatography.

On the other hand, protein expressed in the pET32a3c vector was dialysed against MCAC-0 overnight at 4°C before incubation with 5 μg/ml 3C protease and 1.5 mM DTT at 37°C for one hour. The protein was then repassed through the column and the flow through was collected before MCAC-0 with 100 mM imidazole (MCAC-100) was used to elute and collect the cleaved tag. The final protein product was analysed by SDS-PAGE and dialysed against PBS overnight at 4°C. The following day, the proteins were concentrated using the 3 kDa molecular weight cut-off Vivaspin protein concentrator (GE Healthcare) and stored at -20°C.

2.2.3.5 Size Exclusion Chromatography

Protein expressed in the pPROEX-Htb vector and processed using affinity purification was passed over a Superdex 200 Column (GE Healthcare) connected to an ÄKTA protein purification system (GE Healthcare). Prior to protein loading the column was washed with 2 CV of H_2O and equilibrated with 5 CV of SEC buffer at a flow rate of 0.75 ml/min. The protein was loaded onto the column and eluted at a flow rate of 0.4 ml/min, with peak absorbance at 280 nm collected as fractions. The fractions were analysed by SDS-PAGE and clean fractions of the recombinant protein were pooled together and dialysed against PBS overnight at 4°C. Proteins were then concentrated using the 50 kDa molecular weight cut-off Vivaspin protein concentrator (GE Healthcare) and stored at -20°C.

2.2.3.6 Glutathione S transferase Purification

The frozen *E. coli* pellet was resuspended in 6% w/v of GSH lysis buffer and sonicated on ice using the Q700 sonicator (Qsonica). The cellular debris was pelleted by centrifugation for 30 minutes at 10,000 ×g at 4°C and the supernatant was collected and filtered using a 0.22 µm filter unit (Merck). The clarified bacterial lysate was passed over a gravity flow column packed with 1.5 ml of glutathione agarose resin (ABT) and pre-equilibrated with 10 CV of GSHI. The column was then washed with 10 CV of GSHII to remove unspecific binding and the protein was then eluted with 10 CV of GSHIII collected in ~2 ml fractions. The collected fractions were prepared and analysed using SDS-PAGE and the fractions containing the recombinant protein were pooled together.

Proteins were dialysed overnight against PBS at 4°C and concentrated using the 3 kDa molecular weight cut-off Vivaspin protein concentrator (GE Healthcare) before being stored at -20°C. Proteins requiring cleavage were treated with 5 μg/ml 3C protease and 1.5 mM DTT

whilst being dialysed against GSHI overnight at 4°C. The protein was then repassed through the column and the flow through containing protein was collected. Subsequently, the column was washed with GSHII and the GST tag was eluted with GSHIII and also collected. The final protein product was analysed by SDS-PAGE and dialysed overnight against PBS at 4°C. Finally, the proteins were concentrated using the 3 kDa molecular weight cut-off Vivaspin protein concentrator (GE Healthcare) and stored at -20°C.

2.2.4 Protein Characterisation and Analysis

2.2.4.1 Sodium Dodecyl Sulphate-Polyacrylamide Gel Electrophoresis (SDS-PAGE)

One-dimensional discontinuous SDS-PAGE under reducing conditions was performed to analyse purified proteins. This required the preparation of 12.5% polyacrylamide gels prepared in Hoefer Dual Gel Caster (GE Healthcare) and composed of resolving and stacking gels as per Table 2.12.

Table 2.12. Compositing of 12.5% SDS-PAGE gel

Reagents	Resolving Gel	Stacking Gel
Acrylamide/Bis	4.2 ml	0.5 ml
Resolving buffer	2.5 ml	-
Stacking buffer	-	0.83 ml
Water	3.3 ml	2 ml
TEMED	8 µl	3.3 µl
10% APS	60 µl	40 µl

Proteins were combined 1:1 with 2× protein loading buffer and heated for 5 minutes in a 90°C dry bath before loading onto the prepared gel. The first well was loaded with Benchmark protein ladder (Invitrogen) as a molecular-weight size marker comparison. Electrophoresis was undertaken at 200 V, 25 mA per gel in SDS running buffer for 1 hour. Gels were stained in coomaisse staining solution for 1 hour at room temperature before being detained in destaining solution for an adequate amount of time. The separated proteins were then visualised using the Chemidoc imaging system (Bio-Rad).

2.2.4.2 Western Blot Analysis

Protein samples were separated by SDS-PAGE, with the first well of the gel loaded with Benchmark Pre-stained Ladder (Invitrogen) which doubled as a molecular weight reference and a monitor for protein transfer efficiency from the gel to the blotting membrane. The SDS-PAGE gel was transferred onto a BioTrace™ NT nitrocellulose transfer membrane (Pall) in western blot towbin transfer buffer using a Hoefer TE77 semi-dry transfer unit (Amersham Biosciences) at 250 V, 50 mA for 1 hour. The membrane was then incubated in blocking solution for 1 hour on a shaker at room temperature before being washed with TBS-T. This was followed by the addition of probing solution containing primary antibody diluted to the appropriate concentration and incubation of the membrane at 4°C overnight with constant rotation. The membrane was then washed 3 times in TBS-T, with each wash cycle undertaken for 5 minutes on a shaker. Subsequently, probing buffer with HRP conjugated secondary antibody was added and the membrane was incubated at room temperature for 1 hour, on a shaker. Unbound antibodies were removed by 3× 5 minute wash steps in TBS, performed on a shaker. ECL detection reagent (Amersham Biosciences) was used to detect the desired proteins on the membrane, with the chemiluminescent signals captured using the Chemidoc imaging system (Bio-Rad).

2.2.4.3 Protein Labelling

Recombinant proteins were concentrated to at least 2 mg/ml and dialysed against 50 mM bicarbonate buffer (pH9) overnight at 4°C. Fluorescent Red Mega 485 NHS-ester label (Sigma-Aldrich) was added to proteins at an equimolar amount and incubated for 1 hour on a rotator at room temperature, in the dark. The conjugated protein was then separated from unreacted free dye using Hi-trap Sephadex G25 column (Cytiva) connected to an ÄKTA protein purification system (GE Healthcare). The column was washed with 2 CV of H_2O and equilibrated with 5 CV of PBS before sample was loaded onto the column. The protein was eluted with PBS at a flow rate of 0.2 ml/min with peak absorbance at 280 nm collected as fractions. The fractions were run on SDS-PAGE and the gel was imaged using a UV sample tray on the Chemidoc imaging system (Bio-Rad) to confirm the presence of fluorescently labelled recombinant proteins. The absorbance of the proteins at 280 nm and 485 nm (the maximum wavelength of the dye) was measured before degree of labelling (DOL) was calculated using the equation: $DOL = (A_{max} \times \varepsilon_{280}) / ((A_{280} - A_{max} \times CF) \times \varepsilon_{max})$.

2.2.4.4 Protein Integrity Sandwich ELISA

MaxiSorp Immuno-assay plates (Nunc) were coated overnight at 4°C with 100 µl/well of antigen (BP or AP1) diluted to 1 µg/mL in PBS. The plates were then washed 3 times using PBS-T and incubated with blocking solution for 1 hour at room temperature. Fusion protein samples were prepared in PBS as a three-fold serial dilution series and 100 µl added to each well before plates were incubated for 2 hours at room temperature. The plates were then washed 3 times with PBS-T and incubated for 2 hours at room temperature with 100 µl/well of Influenza A M2 Monoclonal Antibody (14C2) (Thermofisher) diluted in PBS-T to the appropriate concentration. The plate underwent 3 washes with PBS-T again and was subsequently incubated for 1 hour at room temperature with 100 µl/well of anti-mouse IgG (HRP)-polyclonal antibody (Abcam) diluted in PBS-T to the appropriate concentration. The plate was then washed 5 times with PBS-T and 100 µl/well of TMB was added to the plate. After the reaction was allowed to progress in the dark for 5 minutes at room temperature, 100 µl/well of 1 M HCI was used to stop the reaction. The absorbance was measured at 450 nm using the EnSightTM Multimode plate reader (Perkin Elmer, USA).

2.2.5 Protein Interaction with Immobilised Receptor

2.2.5.1 Biosensor analysis of Protein Affinity to TLR2

Kinetic binding analysis of recombinant pilus proteins was analysed using Biacore T200 (GE Healthcare, Sweden). Recombinant human TLR2 extracellular domain (Met1-Arg587) with C-terminus 6×His tag (SinoBiological) was immobilised onto a nitrilotriacetic acid sensor chip (GE Healthcare) using an amine coupling kit as per the manufacturer's instructions (GE Healthcare, Sweden). Following activation of the sensor chip using a mixture of 0.2 M N-ethyl-N'-(3-dimethylaminopropyl) carbodiimide and 0.05 M N-hydroxysuccimide at a 1:1 ratio, TLR2 was coated onto flow cell 2 (FC2) of the chip at 4 µg/ml in 10 mM sodium acetate (pH4.5) to 880 RU. The unoccupied surface on the chip was then blocked with 1 M ethanolamine (pH8.5). The reference flow cell (flow cell 1, FC1) was activated and deactivated following the same protocol but omitting coating ligand to prevent non-specific analyte interactions. Pilus proteins were diluted in running buffer at concentrations between 0-15 µM and passed over the chip at 30 µl/ min for 60 seconds. Between each cycle of protein injection, the chip surface was regenerated with 2 M guanidine HCl at 60 µl/ min for 10 sec between each cycle. Biacore T200 Evaluation software was used to display the binding response curve.

2.2.5.2 Solid Phase Binding Assay

MaxiSorp Immuno-assay plates (Nunc) were coated overnight at 4°C with 100 µl/well of TLR2 diluted to 1 µg/ml in carbonate bicarbonate buffer. The plates were washed 3 times using PBS-T and incubated with blocking solution for 15 minutes at room temperature. Recombinant protein samples were prepared in PBS as a 1.5-fold serial dilution series and 100 µl added to each well before plates were incubated for 3 hours at room temperature. The plates were then washed 3 times with PBS-T and incubated for 2 hours at room temperature with BP or AP1 polyclonal antibodies diluted in PBS-T to the appropriate concentration. The plates underwent 3 washes with PBS-T again and was subsequently incubated for 1 hour at room temperature with 100 µl anti-rabbit IgG (HRP)-polyclonal (Abcam) diluted in PBS-T to the appropriate concentration. The plates were then washed 5 times with PBS-T and 100 µl/well of TMB was added to the plates. After the reaction was allowed to progress in the dark for 5 minutes at room temperature, 100 µl/well of 1 M HCl was used to stop the reaction. The absorbance was measured at 450/570 nm using the EnSightTM Multimode plate reader (Perkin Elmer).

2.2.6 Cell Based Assays

2.2.6.1 Maintenance of Cell Lines

Adherent HEK-Blue hTLR and J774A.2 were grown in media as per Section 2.1.3.2 and passaged every 4 days or when confluency reached 70-80%. THP-1 cells were grown in suspension media as per Section 2.1.3.2 and passaged every 4 days to a cell density of 5×10^4 cells/ml. Handling and passaging of cells was performed as per the manufacturer's instructions for HEK-Blue™ hTLR (InvivoGen) or following the guidelines provided by ATCC.

2.2.6.2 Pili Induced Cytokine Secretion Assay

Lactococcus lactis strains, either WT or expressing pilus from different GAS serotypes (PilM1, PilM2, PilM4, PilM6 and PilM28), were inoculated from frozen stock into 1.5 ml of GM17 media with appropriate antibiotics and grown overnight at 28°C without agitation. After measuring the OD_{600}, bacterial cells were resuspended in RPMI-1640 medium to a cell density of $\sim 1 \times 10^7$ CFU/ml based on the conversion equation of OD_{600} 1.0=$\sim 1 \times 10^8$ CFU/ml. THP-1 cells were seeded into 96 well round bottom plates (Thermofisher) at a density of 1×10^6/ml, with 100 µl added to each well, and treated with 100 µl/well of *L. lactis* at 1×10^6 CFU/ml to achieve a multiplicity of infection (MOI) of 1. Pam3CSK4 (InvivoGen) diluted in RPMI-1640

medium to 1 µg/ml was used as a positive control. Plates were incubated at 37°C in the presence of 5% CO_2 for 20 hours and culture supernatant was collected by centrifuging the plate at 400 g for 15 minutes at 4°C. Cytokine levels were determined by testing supernatant on the Crux Biolab TNF human cytokine ELISA kit as per the manufacturer's instructions. The absorbance was measured at 450 nm using the EnSight™ Multimode plate reader (Perkin Elmer, USA) and based on the standard supplied in the kit, GraphPad prism was used to generate a four parameter logistic fit curve, from which absolute concentrations of TNF was quantified.

2.2.6.3 Flow Cytometry Based Binding Assay

HEK-Blue™ hTLR4 cell lines alongside either HEK-Blue hTLR2 or HEK-Blue hTLR2/6 cell lines were harvested by removal of growth media and treatment with PBS containing 10 mM of EDTA. Cells were centrifuged for 5 minutes at 280 ×g at room temperature before washing with PBS to remove cellular debris and proteins and resuspended in ice cold FACS buffer at a density of $1×10^7$ cells/ml. For assays using HEK-Blue hTLR2, 50 µl of cells was mixed with 2 nM of fluorescently labelled BP/AP1 in 50 µl FACS buffer and for assays using HEK-Blue hTLR2/6, 50 µl of cells was mixed with 8 nM of fluorescently labelled BP/AP1 in 50 µl FACS buffer. To assess non-specific binding 50 µl aliquots of HEK-Blue hTLR4 cells were given the same protein treatments and negative control cells were incubated with 50 µl of FACS buffer. The cells were incubated on ice for 30 minutes in the dark and supernatant was removed following centrifugation at 280 ×g for 5 minutes at 4°C. Centrifugation was then used to wash cells twice with 1 ml of ice cold FACS buffer before cells were resuspended in 0.5 ml of FACS buffer. Cells were strained through a cell strainer and fluorescent signal was analysed using a LSRII flow cytometer (Becton Dickinson), with 30,000 events collected for each experiment.

2.2.6.4 Competition Assay

THP-1 cells were seeded into 96 well round bottom plates (Thermofisher) at a density of $1×10^6$/ml, with 100 µl added to each well and co-incubated with 50 µl/well of BP or AP1 diluted in RPMI to 4 nM and 50 µl/well of SSL3 prepared in RPMI as a 3-fold serial dilution. Plates were incubated at 37°C in the presence of 5% CO_2 overnight and culture supernatant was collected by centrifuging the plate at 400 g for 15 minutes at 4°C. As per Section 2.2.6.2 supernatant cytokine levels were tested on the Crux Biolab TNF human cytokine ELISA kit as per the manufacturer's instructions. Cytokine levels detected from cells treated with

recombinant protein in the absence of SSL3 was defined as maximal cytokine production and used to calculate percentage cytokine secretion activity.

Alternatively, HEK-Blue hTLR2/6 cells were seeded into 96 well flat bottom plates (Thermofisher) at a density of 2.8×10^5/ml in HEK-Blue Detection solution, with 180 µl added to each well. Cells were co-incubated with 10 µl/well of BP or AP1 diluted in Endotoxin-Free water (Bio-Vision) to 80 nM and treated with 1 µg/ml of polymyxin B, as well as 10 µl/well of SSL3 prepared in Endotoxin-Free water as a 3-fold serial dilution. Plates were incubated at 37°C in the presence of 5% CO_2 for 9 hours and the absorbance was measured at 655 nm using the EnSight^{TM} Multimode plate reader (Perkin Elmer). Absorbance levels detected from cells treated with recombinant protein in the absence of SSL3 was defined as maximal TLR activation and used to calculate percentage TLR stimulation.

2.2.6.5 HEK-Blue hTLR Activation Assay

HEK-Blue hTLR2, HEK-Blue hTLR2/6 or HEK-Blue hTLR2/1 cells were seeded into 96 well flat bottom plates (Thermofisher) at a density of 2.8×10^5/ml in HEK-Blue Detection solution (InvivoGen), with 180 µl added to each well. Cells were incubated with 20 µl/well of proteins in Endotoxin-Free water pre-treated with 1 µg/ml of polymyxin B. Pam$_3$CSK$_4$ (InvivoGen) diluted in Endotoxin-Free water to 1 µg/ml was used as a positive control for HEK-Blue hTLR2 and HEK-Blue hTLR2/6 cells whilst 1 µg/ml Pam$_2$CSK$_4$ (InvivoGen) in Endotoxin-Free water was used as a positive control for HEK-Blue hTLR2/1. Endotoxin-Free water was added to negative control cell wells. Plates were incubated at 37°C in the presence of 5% CO_2 for 9 hours and the absorbance was measured at 655 nm using the EnSight^{TM} Multimode plate reader (Perkin Elmer).

2.2.6.6 MTT Cell Activity Assay

J774A.2 cell media was replaced with PBS and cells were detached using a cell scraper before being resuspended in complete media at a density of 1×10^6 cells/ml or 5×10^5 cells/ml and seeded into 96 well flat bottom plates (Thermofisher) with 50 µl added per well. Cells were then treated with 50 µl of 100 µg/ml BP or AP1 that had been pre-treated with 1 µg/ml of polymyxin B in RPMI-1640. As a positive control, 50 µl of 1 µg/ml ConA (Sigma-Aldrich) in RPMI-1640 was used and PBS was given to negative control cells. Plates were incubated at 37°C in the presence of 5% CO_2 for 24 hours before the plate was aspirated to remove media.

All sample wells were treated with 20 µl of MTT solution (Sigma-Aldrich) and 80 µl of fresh complete media. Plates were then incubated at 37°C in the presence of 5% CO_2 for 1 hour before addition of 100 µl/well of DMSO and incubation at room temperature on an orbital shaker for 15 minutes. The absorbance was measured at 540 nm using the EnSight™ Multimode plate reader (Perkin Elmer).

2.2.6.7 Luminex Based Cytokine Secretion Assay

J774A.2 cell media was replaced with PBS and cells were detached using a cell scraper before being resuspended in complete media at a density of 1×10^6 cells/ml and seeded 100 µl/well into 96 well flat bottom plates (Thermofisher). Cells were then treated with 100 µl of 2 nM rBP or rAP1 in media, with equal volumes of media and 1 µg/ml Pam₃CSK₄ added to negative and positive control cells respectively. Plates were incubated at 37°C in the presence of 5% CO_2 for 24 hours. Subsequently, plates were centrifuged at 280 g for 5 minutes at 4°C and supernatant was collected and stored at -80°C until analysis. The 7-plex Luminex Discovery assay (R&D systems) was used as per the manufacturer's instructions to detect cytokines in supernatant using the Luminex instrument system (Luminex Corporation).

2.2.6.8 Flow Cytometry Analysis of Receptor Expression

J774A.2 cell media was replaced with PBS and cells were detached using a cell scraper before being resuspended in complete media at a density of 2×10^6 cells/ml and seeded 0.5 ml/well into 24 well flat bottom plates (Thermofisher). Cells were then treated with 0.5 ml of 4 nM rBP or rAP1 in media, with equal volumes of media and 1 µg/ml LPS added to negative and positive control cells respectively. Plates were incubated at 37°C in the presence of 5% CO_2 for 24 hours and supernatant was removed. Cells were then incubated for 10 minutes at 37°C in the presence of 5% CO_2 with 160 µl/well of warm PBS and 1×trypLE to detach from the plate. 1 ml of complete media was added to each well and cells were transferred to Eppendorf tubes and centrifuged for 5 minutes at 300 g at 4°C before being suspended in 100 µl of ice cold blocking buffer. Cells were incubated on ice for 15 minutes before 1 ml of ice cold FCAS buffer was added and cells were centrifuged for 5 minutes at 300 g at 4°C. Supernatant was removed and cells were resuspended in 100 µl of antibody cocktail consisting of antibodies from Table 2.5 combined at the appropriate dilutions in FACS buffer. Negative control cells were resuspended in equal volumes of FACS buffer. Cells were incubated on ice in the dark for 30 minutes and supernatant was removed following centrifugation at 300 ×g for 5 minutes at 4°C.

Centrifugation was then used to wash cells twice with 1 ml of ice cold FACS buffer before cells were resuspended in 0.5 ml of FACS buffer. Cells were strained through a cell strainer and fluorescent signal was analysed using a Cytek Aurora CS cell sorter (Cytek Bioscience), with 30,000 events collected for each experiment.

2.2.7 *Galleria mellonella* Based Assays

Galleria mellonella larvae were purchased from Biosuppliers and kept in the dark at room temperature with antibiotic supplemented feed, until use. Larvae approximately 1.5 cm in size with no visible discolouration were used in all assays and shipments of larvae were used within 2 weeks of arrival.

2.2.7.1 Preparation of Bacterial Samples for Injection

WT *Lactococcus lactis* and strains expressing pilus from different GAS serotypes (PilM1, PilM2, PilM4, PilM6 and PilM28), were inoculated from frozen stock into 50 ml of GM17 media with appropriate antibiotics and grown overnight at 28˚C without agitation. After the OD_{600} was determined, the cells were then centrifuged at 4,000 ×g for 20 minutes at 4˚C and washed with sterile PBS. The bacterial cells were then resuspended in sterile PBS with 10% glycerol at a concentration where OD_{600} was equal to 10. Cells were divided into 1 ml aliquots and snap frozen in a dry ice ethanol bath and stored at -80°C until use. Aliquots from each strain were thawed, centrifuged at ×4,000 g for 10 minutes at 4˚C and were washed in sterile PBS before resuspension in 1 ml of PBS. A 10-fold serial dilution of the bacterial suspensions was prepared from 10^{-1} to 10^{-6} and the last 3 dilutions (10^{-4} to 10^{-6}) were plated in triplicate on GM17 agar plates with the appropriate antibiotics. The plates were incubated overnight at 28°C and enumerated to determine dilution factors required in order to inject wax moth larvae with equal concentrations of each bacterial strain.

2.2.7.2 Antibiotic Clearance in Larvae

Ten larvae were isolated from their antibiotic feed and individually placed in wells of 12 well flat bottomed plates (Thermofisher) without food 48 hours prior to inoculation. This process was repeated 24 hours prior to inoculation as well. Bacteria stock of WT *L. lactis* was thawed and washed once with PBS before being resuspended in PBS at 5×10^8/ml. Each group of larvae isolated from feed beforehand and another 10 larvae taken straight from the feed were inoculated with 20 µl of bacteria suspension using a 29G Micro-fine insulin syringe (BD

Biosciences) into the last proleg. Immediately after inoculation, 5 larvae from each group were homogenised in 0.5 ml of PBS by mechanical disruption and the homogenate was serially diluted and plated in triplicate on GM17 agar before being incubated at 28˚C overnight. The process was repeated for the remaining larvae 6 hours after inoculation. The agar plates were used for enumeration the following day.

2.2.7.3 Galleria mellonella Infection Model

To prepare for the experiment, 310 wax moth larvae were isolated from their antibiotic feed and individually placed in wells of 12 well flat bottomed plates (Thermofisher) for 48 hours. Following this period, frozen bacteria stock of WT *Lactococcus lactis* and strains expressing pilus from different GAS serotypes (PilM1, PilM2, PilM4, PilM6 and PilM28) was thawed and washed once with PBS, then resuspended in PBS at 5 concentrations: 5×10^{10} CFU/ml, 1×10^{10} CFU/ml, 2×10^9 CFU/ml, 4×10^8 CFU/ml or 2×10^7 CFU/ml . For each strain of bacteria, groups of 10 larvae were administered each concentration of inoculum in a 20 µl dosage to the lower left proleg using a 29G Micro-fine insulin syringe (BD Biosciences). Ten larvae were also injected with 20 µl of PBS. Larvae were incubated at 37°C and monitored daily for up to five days post-infection. Daily monitoring consisted of scoring each individual larvae on a health index scoring system scaling from 0-10 comprised of four phenotypes relating to overall larval health (activity, cocoon formation, melanisation, survival) (213,214).

Table 2.13. Galleria mellonella health index scoring system

Category	Description	Score
Activity	Active without stimulation	3
	Active with stimulation	2
	Minimal activity with stimulation	1
	None	0
Cocoon Formation	Full cocoon	1
	Partial cocoon	0.5
	None	0
Melanisation	None	4
	< 3 spots on beige wax larvae	3
	≥3 spots on beige wax larvae	2
	Brown or complete melanisation (black)	0
Survival	Alive	2
	Dead	0

2.2.7.4 Haemocyte Density Counts

In preparation for inoculation, 192 wax moth larvae were isolated from their antibiotic feed and individually placed in wells of 12 well flat bottomed plates (Thermofisher) without food for 48 hours. Following this period, frozen bacteria stock of WT *Lactococcus lactis* and strains expressing pilus from different GAS serotypes (PilM1, PilM2, PilM4, PilM6 and PilM28) was thawed and washed once with PBS, then resuspended in PBS at a concentration of 5×10^9/ml. Groups of 24 larvae were administered each strain of bacteria in a 20 μl dosage to the lower left proleg using a 29G Micro-fine insulin syringe (BD Biosciences). A group of larvae received 20 μl dosages of PBS and a larvae group was also sham injected with the needle to use as a baseline. Subsequent to injection, larvae were incubated at 37°C and at 6, 24, 48 and 72 hours post infection, haemocytes were collected from 6 larvae from each group. This was undertaken by placing larvae on a petri dish over ice to slow down movement and once immotile, pricking the lower left proleg with a 29G Micro-fine insulin syringe (BD Biosciences) while applying pressure to the top half of the body. A pipette was used to collect 10 μl of haemolymph from each puncture and 10 μl of PBS with 0.37% β-mercaptoethanol was added to each sample to prevent melanisation. Haemocyte density was then determined by loading samples mixed with 1:1 trypan blue on a haemocytometer, with counts from sham injected larvae subtracted as a baseline.

2.2.7.5 *L. lactis* Enumeration

For this experiment, 144 wax moth larvae were individually placed in wells of 12 well flat bottomed plates (Thermofisher) and isolated from feed for 48 hours prior to inoculation. In the same procedure as in Section 2.2.7.5, 5×10^9/ml inoculum of WT *Lactococcus lactis* and strains expressing pilus from different GAS serotypes (PilM1, PilM2, PilM4, PilM6 and PilM28) were prepared. Groups of 24 larvae were administered each strain of bacteria in a 20 μl injection to the lower left proleg using a 29G Micro-fine insulin syringe (BD Biosciences). Following inoculation, larvae were incubated at 37°C and at 0 (immediately after injection), 24, 48 and 72 hours post infection, 6 larvae from each group were homogenised in 0.5 ml of PBS by mechanical disruption. The homogenate was serially diluted and plated in triplicate on GM17 agar with appropriate antibiotics before incubation overnight at 28˚C. The agar plates were used for colony enumeration the following day.

2.2.8   Mouse Immunisations

All fusion proteins used to immunise mice were concentrated to 5 mg/ml and pre-treated with 50 µg/ml polymyxin B to neutralise endotoxins. Sterile PBS was used to adjust protein concentrations for dose response pilot immunisation.

2.2.8.1   Immunisation Schedule

For the pilot immunisation, six groups of female BALB/c mice aged 6-7 weeks, with 5 mice in each group, were immunised intranasally by administration of 10 µl of vaccine formulations as per Table 2.14 into the nostril. Mice were immunised three times at one-week intervals (i.e. vaccinated on days 0, 7, 14) and one week after the final immunisation (day 21), serum, bronchial alveolar lavage (BAL) and nasal wash (NW) samples were collected.

Table 2.14. Vaccine formulations administered to each immunisation group in pilot study

Immunisation Group	Vaccine formulation	Immunisation Group	Vaccine formulation
A	BP-M2e 1 µg	E	AP1-M2e 1 µg
B	BP-M2e 5 µg	F	AP1-M2e 5 µg
C	BP-M2e 50 µg	G	AP1-M2e 50 µg
D	BP 50 µg	H	AP1 50 µg

For the full panel immunisation, five groups of female BALB/c mice aged 6-7 weeks, with 6 mice in each group, were immunised intranasally by administration of 10 µl of vaccine formulations as per Table 2.15 into the nostril. Mice were immunised three times at one-week intervals (i.e. vaccinated on days 0, 7, 14) and one week after the final immunisation (day 21), serum and NW samples were collected.

Table 2.15. Vaccine formulations administered to each immunisation group in full panel

Immunisation Group	Vaccine formulation
A	M2e-BP 50 µg
B	BP-M2e 50 µg

C	AP1-M2e 50 µg
D	1 ul poly I:C + M2e 1 µg
E	M2e 1 µg

2.2.8.2 ELISA of Mouse Samples

MaxiSorp Immuno-assay plates (Nunc) were coated overnight at 4°C with 100 µl/well of antigen (BP, AP1 or M2e) diluted to 1 µg/mL in PBS. The plates were washed 3 times using PBS-T and incubated with blocking solution for 1 hour at room temperature. The plates were then incubated with serum or mucosal samples from the mice, with 100 µl added per well. For mouse samples from the pilot immunisation, serum samples were diluted 1:200 in PBS-T whilst NW and BAL samples were not diluted before addition to the ELISA. For samples from the full immunisation panel, PBS-T was used to produce a 2-fold serial dilution of serum samples from 1:200 and NW samples from neat, which were then added to the ELISA. The plates were then incubated for 2 hours at room temperature and washed 4 times with PBS-T. Subsequently, 100 µl/well of anti-mouse IgG (HRP)-polyclonal (Abcam) or anti-mouse IgA (HRP)-polyclonal (Abcam), was diluted to the appropriate concentrations in PBS-T and added. Plates were incubated for 1 hour at room temperature before being washed 4 times with PBS-T. Finally, 100 µl/well of TMB was added to the plate and after a 10 minute incubation at room temperature in the dark, 100 µl/well of 1 M HCl was used to stop the reaction. The absorbance was measured at 450 nm using the EnSight™ Multimode plate reader (Perkin Elmer, USA).

Chapter 3: Characterising Inflammatory Response to Different GAS Pili

As outlined previously, there is a large array of GAS strains, with particular strains associated with distinct disease manifestations. Some strains such as M6 are typically found within mild infections such as pharyngitis, whereas other strains such as M1 are commonplace in deeper systemic infections (29). Numerous GAS virulence factors contribute to the manifestation of these diseases of varying severity, although the degree of contribution of each component is not entirely clear (215). GAS pili have been shown to play key roles in adherence, invasion, biofilm formation and immune evasion (38,39,58,75), but this structure's role in GAS associated disease manifestation has not been studied. Of note, GAS strains linked to particular clinical presentations appear to harbour different pilus FCT variants (9,29). This insinuates the possibility that pilus types may have correlation with disease manifestation.

Many of the inflammatory symptoms seen in infectious diseases are triggered or exacerbated by cytokines produced during the innate immune response to the pathogen. In the case of GAS, a human challenge model has recently uncovered the chemokine and cytokine profile of pharyngitis, with the infection elevating serum levels of inflammatory signals such as IP-10 and IL-6 (216). Furthermore, cytokines released in response to bacterial infections can promote skewed differentiation of T cells into Th17, which can expedite the development of autoimmune diseases by causing prolonged inflammation and damage to tissues; in GAS infections, this has been implicated with rheumatic heart disease (217–219). During GAS sepsis, TNF has been pinpointed to propel disruption of the blood brain barrier and in patients with GAS associated necrotising fasciitis, an influx of IL-1β has been linked to increased mortality (190,220). Cytokine response is particularly crucial for the progression of such invasive infections, with the cytokine driven inflammation also propelling tissue haemorrhage and thrombosis (221). Although the relationship between cytokine mediated inflammation and GAS disease has been repeatedly illustrated, the bacterial components contributing to the release of these cell signals has not been entirely defined. I previously began to delve into this question and demonstrated the inflammatory properties of GAS pilus complex, illustrating its ability to induce highly inflammatory cytokines such as TNF and IL-8 (206). Thus it is possible that this virulence factor is one such component of GAS which enforces the sustained state of

inflammation required for the progression of GAS diseases. In order to explore this idea, the inflammatory response to a panel of pili across different GAS FCT types was studied.

The 9 different currently identified pilus types can be categorised into 6 antigenic variants. There is a possibility of different pilus types promoting inflammation to different degrees and in turn accelerating disease progression in a varied manner. It could tentatively be hypothesised that pilus types that are found on GAS strains associated with severe disease may induce greater inflammation, contributing to accelerated disease progression. Therefore, the panel used in this assay was selected in order to represent a wide range of pilus types across a range of disease manifestations. This included FCT-4 pilus from a M28 GAS strain associated with acute rheumatic fever (PilM28), FCT-2 type pilus from a M1 strain associated with invasive disease (PilM1) and a FCT-1 type pilus of a M6 strain linked to pharyngitis (PilM6). A FCT-6 pilus from a M2 strain (PilM2) and a FCT-5 pilus from M4 GAS (PilM4) was also incorporated for coverage of the main FCT types (26).In this chapter, pro-inflammatory responses to GAS pilus were assessed in cultured immune cells as well as the *Galleria mellonella* (greater wax moth) larvae infection model.

3.1 Isolation of GAS pilus from other virulence factors

The original plan for studying the immune response to GAS pilus sequestered from other GAS virulence factors was to generate fully assembled, cell-free pili expressed by the Gram positive host *L. lactis*, which does not produce endotoxin. Theoretically this could be achieved by expressing the pilus operon in a *L. lactis* strain with a deletion of the gene encoding the Sortase A enzyme. Sortase A (SrtA) is the housekeeping transpeptidase with the role of covalently anchoring proteins containing a cell wall-anchoring domain, including the base subunit of pilus complexes to peptides within the peptidoglycan on the bacterial cell surface (222). Thus, it was anticipated that in the absence of this mechanism for attachment of structures to the cell wall, the expressed GAS pili would be released into the culture media.

3.1.1 Creation of *L. lactis* Sortase A deletion mutants expressing GAS pilus

A SrtA knockout mutant was created via allelic replacement of the *srtA* gene in the WT *L. lactis* with the spectinomycin resistance gene *aad9*. Briefly, the flanking regions ~1000bp upstream and downstream of the *srtA* gene were amplified using primers listed in Table 2.1 before being cloned into pBS-ccdB and sequenced to confirm the absence of mutations. These

flanking regions were subsequently ligated into the pFW11 plasmid at the 2 multiple cloning sites sandwiching the *aad9* gene (Figure 3.1A). This plasmid was electroporated into WT *L. lactis* to facilitate homologous recombination resulting in the *srtA* gene becoming replaced with *aad9* (Figure 3.1B). Acquisition of spectinomycin resistance was used to screen successful mutants, and gene deletion was confirmed with PCR using a selection of primer pairs illustrated in Figure 3.1B and detailed in Table 2.1. The ~700bp *srtA* gene was absent from the *L. lactis* deletion strain (Figure 3.1C) and as indicated by primers for flanking regions and *aad9*, the spectinomycin resistance gene had been integrated into the genome (Figure 3.1C). Finally, the orientation of the inserted gene was confirmed with the use of *aad9* primers and diagnostic primers (SrtA-FR2.Ot and SrtA-FR1.Ot) annealing to regions outside of the two flanking regions (Figure 3.1C).
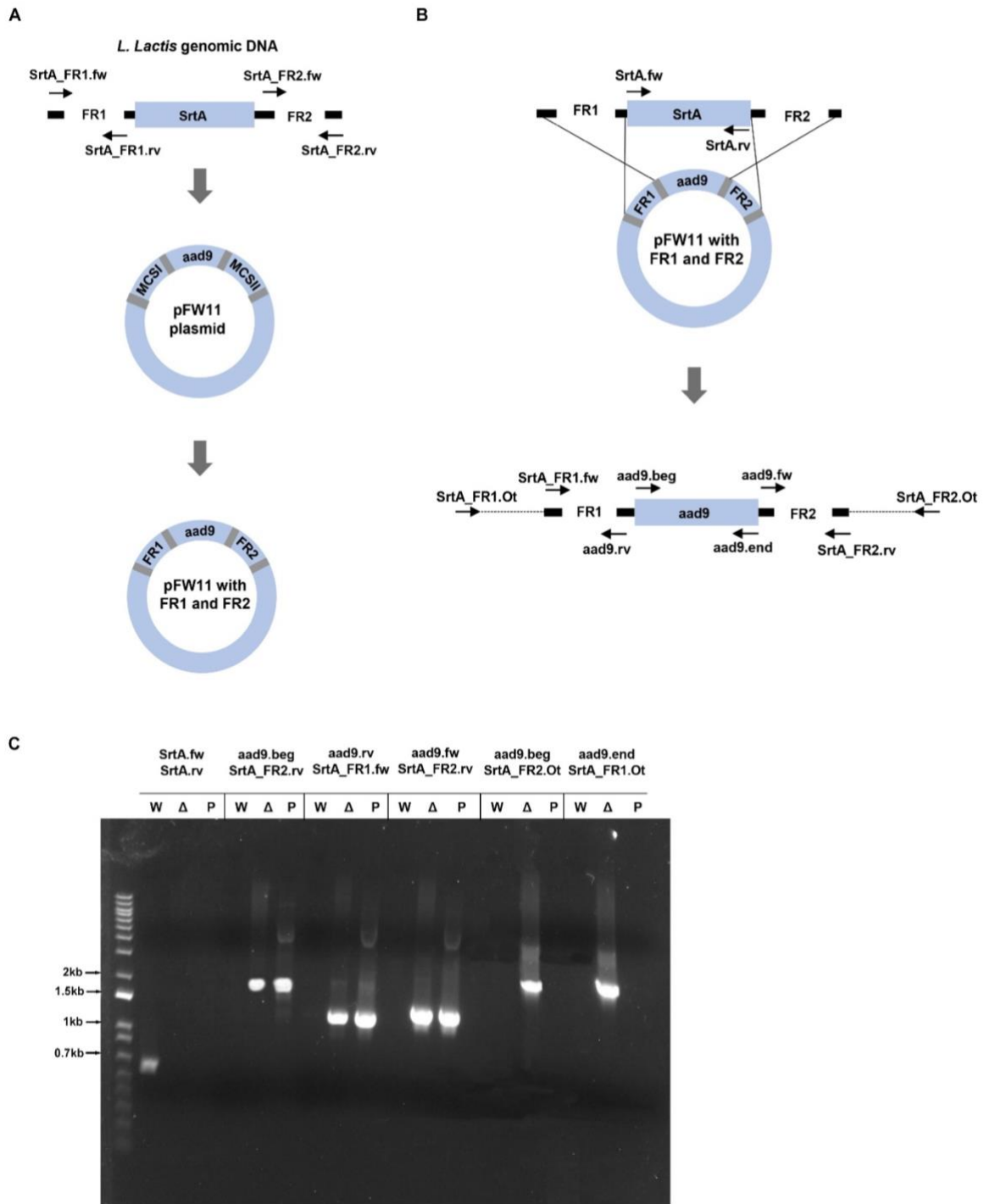
Figure 3.1. Allelic replacement strategy for generating *L. lactis* with SrtA deletion (A) Flanking regions upstream (FR1) and downstream (FR2) of the *srtA* gene were cloned into MCSI and MCSII of the pFW11 plasmid respectively, sandwiching the *aad9* gene. (B) Electroporation of the constructed pFW11 plasmid into WT *L. lactis* resulted in double crossover recombination, where *srtA* was replaced with *aad9* in the *L. lactis* genome. (C) Various primers illustrated in (B) were used in PCR to confirm integration of *aad9* in the correct orientation. L, 1 kb plus DNA ladder; WT, WT *L. lactis* chromosomal DNA; Δ, *L. lactis* SrtA deletion mutant; P, pFW11 plasmid with FR1 and FR2 of *srtA*

66

A plasmid encoding for M1 GAS pili expression (PilM1) was subsequently electroporated into this mutant *L. lactis* to generate GAS pili expressing, SrtA deleted *L. lactis*. Transformation of the plasmid was verified using a primer pair specific for the GAS pilus backbone gene *spy0128*, as indicated in Table 2.1 (Figure 3.2A). This strain was grown in liquid culture before cell wall extract and cell supernatant were run on a western blot using antibodies against the pilus (backbone) BP and (tip) AP1 subunits (Figure 3.2B). The corresponding samples from *L. lactis* expressing PilM1 were simultaneously run as a comparison. Both pilus subunits were detected in the cell culture supernatant of the deletion mutant, indicating the presence of pilus structures separate from the cell wall. In comparison, no pilus proteins were detected in the supernatant of PilM1 *L. lactis*, which possessed an intact SrtA enzyme (Figure 3.2B). Despite the initial success with cloning a SrtA deletion mutant, the secreted pilus structure proved difficult to purify from the culture supernatant. Protein A agarose beads were coupled to BP antibodies and incubated with the supernatant, before being eluted with glycine. The eluent was then imaged on a western blot using antibodies against BP (Figure 3.2C). This indicated that pili were not efficiently purified from the culture supernatant, with substantial loss of the pili occurring during this process. Despite a number of purification methods tested, the efficiency of pili recovery could not be enhanced.
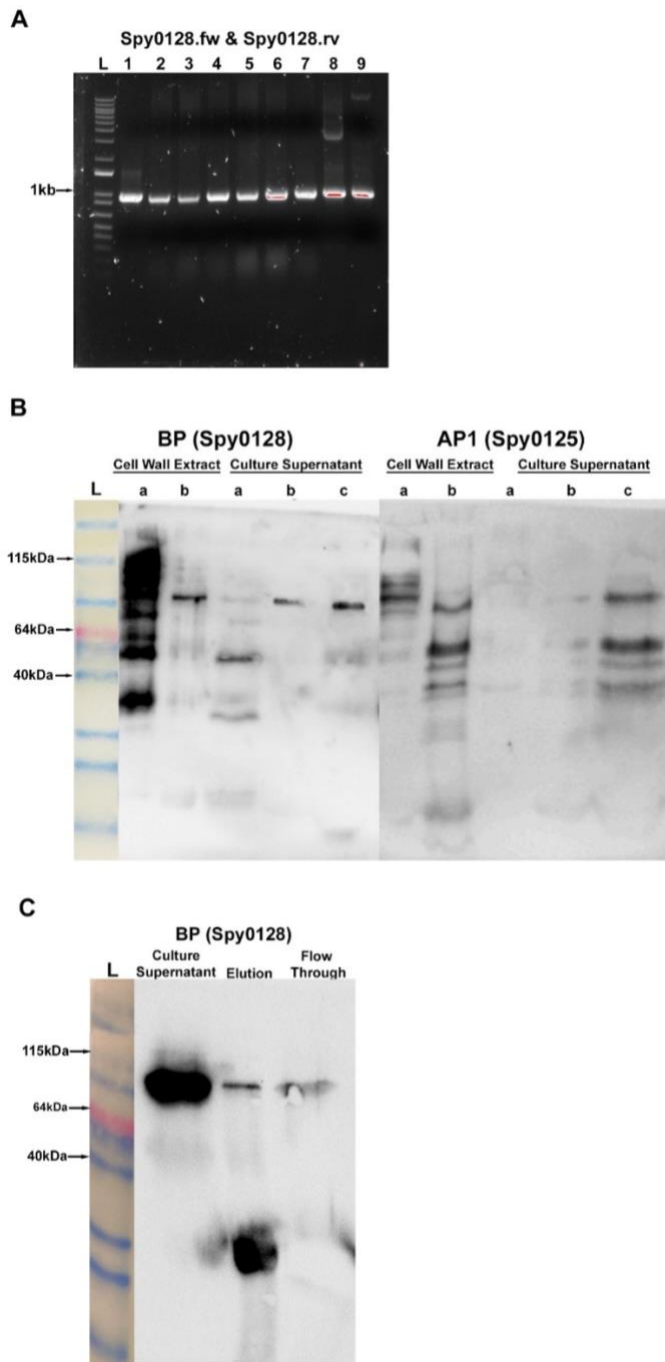
Figure 3.2 Transformation of plasmid for GAS pili expression into *L. lactis* with SrtA deletion results in secretion of pili into cell culture supernatant.(A) Transformation of *L. lactis* with a M1 GAS pili (PilM1) expression plasmid confirmed with PCR using primers annealing to start and end of pilin backbone gene (B) Western blot indicates detection of backbone (BP) and tip (AP1) pilus subunits in the cell culture supernatant of PilM1 *L. lactis* with SrtA deletion but not PilM1 *L. lactis*. (C) Western blot indicates that the process of purifying pili from the cell culture supernatant results in significant loss of the complex following collection of eluent. a- W.T PilM1 *L. lactis*, b- PilM1 *L. lactis* SrtA deletion strain, c- 10x Concentration PilM1 *L. lactis* SrtA deletion strain, L; 1kb plus DNA ladder used in (A) and benchmark protein pre-stained ladder used in (B) and (C)

This prompted a change of tactics and *L. lactis* was utilised as a vehicle to express cell wall-anchored GAS pili instead. These bacteria were constructed by electroporation of plasmids harbouring the pilus operons listed in our panel into WT *L. lactis*. This resulted in a collection of non-pathogenic bacteria serving as vehicles for delivery of surface expressed, fully assembled pili to inflammation models. Flow cytometry was used to confirm that the different strains had similar levels of pilus expression (223). WT *L. lactis* without pili were used throughout assays as a control to elucidate baseline changes in immune response generated by just the bacterial delivery platform.

3.2 Investigating GAS pili induction of cellular inflammation

3.2.1 The GAS pili panel induces inflammation in monocytic THP-1 cells

The inflammatory response against the panel of GAS pili was firstly assessed using monocytic THP-1 cells. These cells were seeded into a 96 well plate and incubated for 20 hours with the panel of *L. lactis* strains expressing PilM1, PilM2, PilM4, PilM6 or PilM28. The cell supernatant was collected following this incubation period and the secretion of the pro-inflammatory cytokine TNF was quantified using ELISA. TNF levels from the cells treated with pili expressing *L. lactis* were 3.2-fold (PilM1, P=0.04), 3.8-fold (PilM2, P=0.02), 3.5-fold (PilM4, P=0.04), 6.3 fold (PilM6, P<0.001) and 3.4-fold (PilM28, P=0.04) greater than that of cells treated with WT *L. lactis*, illustrating the highly inflammatory properties of pili (Figure 3.3). Although all pilus types appeared to elicit inflammation, there did not appear to be a distinct pattern between the level of inflammation and the disease severity associated with GAS yielding those particular pili. Of note, pilus derived from M6 GAS (PilM6) appeared to enhance cytokine release more than pilus from M1 GAS (PilM1), despite the former strain being more associated with superficial infections while strains in the latter serotype being frequently linked to invasive disease (29,224). Furthermore, despite M4 GAS (the strain that produces PilM4) being a common source of acute glomerulonephritis, which is characterised by inflammation driven renal damage (29), the cytokine response to this pilus was not particularly high. Similarly, despite the connection between GAS strains harbouring FCT-3/4 pili (such as PilM28) and acute rheumatic fever (9), these pilus types did not induce conspicuously high inflammation. This was contrary to the initial hypothesis which predicted that pilus derived from GAS strains linked to severe disease would elicit greater levels of inflammation. In order

to further explore these results, the assay was reiterated *in vivo*, with the *G. mellonella* infection model.
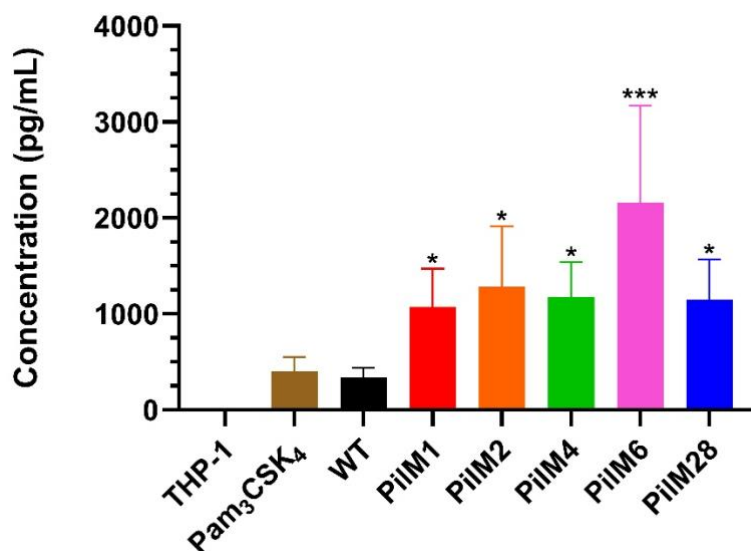
Figure 3.3. Different GAS pili induce varying degrees of inflammatory responses in THP-1 cells.THP-1 cells were incubated for 20 hours with either WT *L. lactis* or *L. lactis* strains expressing GAS PilM1, PilM2, PilM4, PilM6 or PilM28 at an MOI of 1. TNF release was subsequently measured using ELISA. Untreated cells served as a negative control and the Toll-like receptor 2 agonist Pam3CSK4 (1 µg/ml) was used as the positive control. The experiment was performed in duplicate and data from three independent biological repeats is shown as mean±S.D. Statistical significance was determined by one way ANOVA, and the P-values were calculated by Holm–Šídák's multiple comparisons test. ***$P \leq 0.001$, *$P \leq 0.05$ compared to cells incubated with WT *L. lactis*.

3.3 Exploring inflammatory characteristics of GAS pili panel in a wax worm infection model.

There has been expanding interest in recent years around the use of non-mammalian animal models for the assessment of host-pathogen interactions due to affordability, easy handling and lack of ethical concerns (225). *G. mellonella* is one such model which possesses an intact and complex innate immune system with the ability to mount both cellular and humoral immune responses (226). The larval humoral defence mechanisms involve soluble secreted peptides such as lysozyme, anti-microbial peptides and metalloproteinase inhibitors (227). The cellular response is dictated by the six types of phagocytic cells which have been identified in the wax moth immune system; oenocytodis, sphelurocytes, coagulocytes, plasmatocytes, prohaemocytes and granulocytes (228). Aside from phagocytosis, these haemocytes are also

implicated in nodulation and melanisation, a process which entraps and kills pathogens and coagulates as an initial response to wounding (227,229). Furthermore, in a process comparable to the human immune response, the amount of circulating haemocytes surge in number following infection (230). The parallels to the human immune system emphasise the suitability of the wax moth larvae for the investigation of human pathogens and the model has already been established as a way to study individual GAS virulence factors (214,231,232). The ability of *G. mellonella* to survive at 37 °C, which other non-mammalian models such as *C. elegans* cannot withstand, makes the moths especially beneficial when studying GAS as the transcriptome is vulnerable to alterations below this temperature (233,234).

3.3.1 Weaning *G. mellonella* off antibiotics

The sole supplier of G. *mellonella* in New Zealand (Biosupplies) grows and ships the larvae on antibiotic infused feed to maintain their health until the organisms are used in assays. To ensure *L. lactis* strains injected into *G. mellonella* were not killed off by circulating antibiotics prior to the moth immune system responding to the bacteria, the larvae required a wash-out phase for antibiotic clearance. This involved periods of isolating moths from feed to prevent further uptake of antibiotics, whilst allowing any drugs in the larvae to be eliminated. The required duration for the wash-out period was determined by firstly injecting 20 µl of WT *L. lactis* at 5×10^8 CFU/ml into moths isolated from feed for 0 hours, 24 hours or 48 hours. Larvae were then homogenised immediately or after a 6 hour incubation period and plated on agar to determine the CFU/ml of recovered bacteria. When larvae had not been removed from feed prior to inoculation with *L. lactis*, the CFU/ml of bacteria recovered was 10-fold lower than the injected amount, for both bacteria plated immediately after injection and 6 hours later (Figure 3.4). This was indicative of antibiotics circulating through the larvae exerting bactericidal properties on the injected *L. lactis*, resulting in the killing of bacteria. The CFU counts of *L. lactis* recovered immediately or 6 hours after injection into larvae starved for 24 hours was approximately 2-fold lower than the inoculated amount (Figure 3.4). Thus, at this time point, the antibiotics had been partially eliminated but there was still enough drug present to elicit some bactericidal effect. When *G. mellonella* were starved for 48 hours before inoculation, the CFU of *L. lactis* recovered immediately after injection matched the original inoculum, indicating the removal of antibiotics from the larval system. Furthermore, when bacteria were plated from these larvae 6 hours after injection, the CFU count was higher than

the injected amount, illustrating a lack of antibiotics allowing for further bacterial growth (Figure 3.4). This 48 hour starvation period was thus utilised across *G. mellonella* assays in order to assure the larvae were "antibiotic free" prior to the experiments.
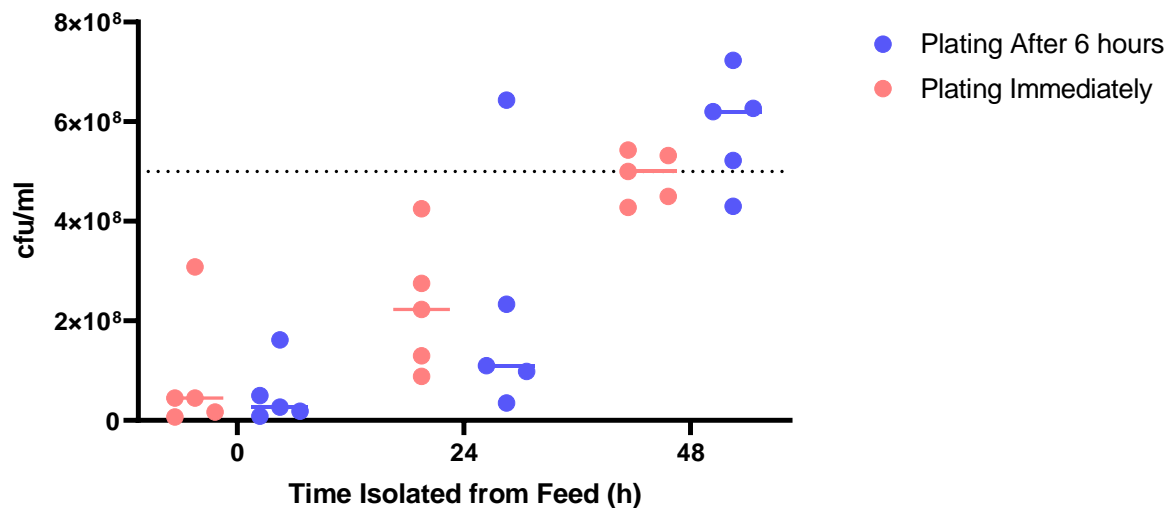
Figure 3.4. *G. mellonella* become antibiotic free following duration of wash out. *G. mellonella* were isolated from antibiotic feed for 0, 24 and 48 hours before inoculation with 20 µl of WT *L. lactis* at 5×10^8 CFU/ml. *G. mellonella* were homogenised and plated on agar immediately following injection or following a 6-hour incubation period and recovered CFU counts were enumerated. Data is shown for CFU recovered from each individual larvae as well as mean CFU. The dotted line indicates the initial concentration of *L. lactis* injected at 5×10^8 CFU/ml.

3.3.2 Different GAS pili exhibit varying degrees of virulence in the *G. mellonella* infection model

Following the results from the THP-1 cytokine assay, the same panel of gain-of-function *L. lactis* strains were tested on larvae to evaluate the inflammatory effects of pilus using an alternative method. To establish the *G. mellonella* infection model for evaluating the virulence associated with pili, the initial steps involved performing a dose titration of the *L. lactis* strains, including WT bacterium, to determine an optimal dosage for inoculation. *G. mellonella* were injected with 5 different concentrations of each strain of *L. lactis*: 1×10^9 CFU, 2×10^8 CFU, 4×10^7 CFU, 8×10^6 CFU or 4×10^5 CFU per larva. An additional group of *G. mellonella* were injected with PBS to serve as a control. Larvae were monitored across 5 days for survival, as well as health index based on visual characterisations such as melanisation and cocoon formation as seen in Table 2.13.

Whilst all *G. mellonella* in the control group survived the entirety of the time course, at high inoculum concentrations, all of the pilus expressing *L. lactis* were lethal to the larvae. The 1×10^9 CFU/larvae dosage resulted in a 100% death rate by the end of the time course and the 2×10^8 CFU/larvae injection resulted in 80-90% mortality by day 5 (

Table 3.1). The lethality of WT *L. lactis* in larvae was slightly dampened compared to pilus expressing strains, with death rates at the 1×10^9 CFU and 2×10^8 CFU dosages being 90% and 70%, respectively (

Table 3.1). Lowering the dosage to 4×10^7 CFU/larvae resulted in a significant drop in mortality, with 60-70% of the larvae injected with pili expressing *L. lactis* surviving the time course and 80% of the larvae inoculated with WT bacterium remaining alive at day 5 (

Table 3.1). These survival rates indicate that the presence of pili appeared to slightly enhance the lethality of *L. lactis*. Non-linear regression curves for larval death reiterated this observation, with the log LD_{50} values of pili-expressing *L. lactis* ranging between 7.71 and 7.87, while the log LD_{50} of WT *L. lactis* was marginally higher, at 8.05

(
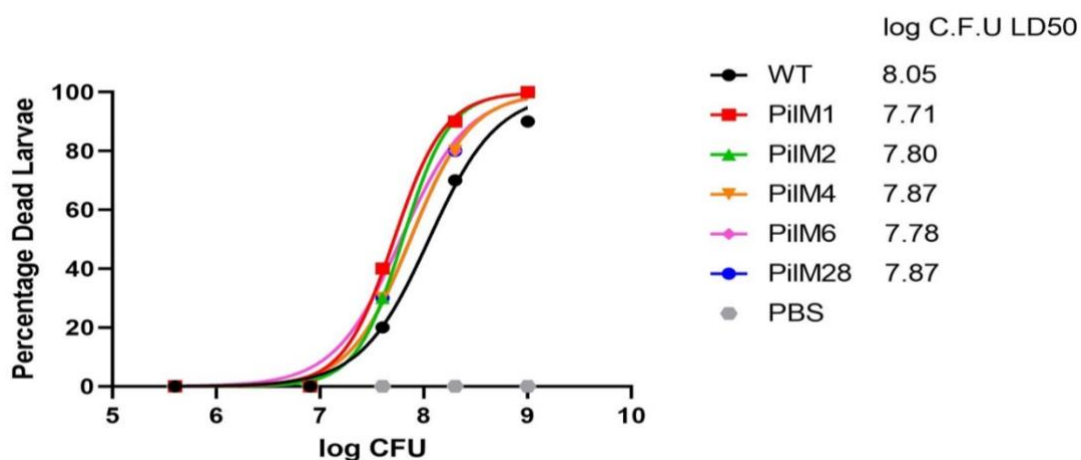
Figure 3.5).

Many larvae administered the lower dosages of bacteria remained viable throughout the monitoring period and therefore could not have their health defined by the metric of mortality. Accordingly, markers for decreased health preceding the event of death were required to detect more subtle differences between the health burden of different *L. lactis* strains. This was achieved with the use of the health index scoring system enveloping physical attributes associated with immune response and increased health burden such as melanisation and loss of

cocoon formation (Table 2.13). This scoring system allowed for detection of more refined differences in larvae health. Health index scoring generally followed the trends seen in survival rates, while providing extra information to distinguish more attenuated differences in larval health. At the aforementioned 4×10^7 CFU/larvae dosage where larvae administered with PilM2, PilM4 and PilM28 expressing bacterium had the same survival rate, *G. mellonella* inoculated with PilM28 had a lower health score than the larvae exposed to the other two *L. lactis* strains (

Table 3.1). This pointed towards PilM28 evoking a greater health burden on the larvae, an attribute not initially apparent when overviewing survival. At dosages where all larvae survived inoculation, the health scores of *G. mellonella* given WT *L. lactis* was up to 1.35-times higher than larvae administered pilus expressing bacterium, reiterating the slightly higher health burden posed by the expression of pilus (

Table 3.1).

Although the presence of pilus did have the effect of slightly increasing the health burden posed by the *L. lactis* injection, 1×10^7 CFU/larvae appeared to be an appropriate dosage to stimulate an immune response at a magnitude that would not overwhelm the larval immune system and result in extensive mortality.

Table 3.1. Day 5 mean death rates and health index scores of *G. mellonella* larvae receiving different dosages of *L. lactis* strains.

L. lactis strain Inoculum	WT	PilM1	PilM2	PilM4	PilM6	PilM28	PBS
Day 5 Mortality Rate							
1×10^9 CFU	90%	100%	100%	100%	100%	100%	0%
2×10^8 CFU	70%	90%	90%	80%	80%	80%	
4×10^7 CFU	20%	40%	30%	30%	40%	30%	
8×10^6 CFU	0%	0%	0%	0%	0%	0%	
4×10^5 CFU	0%	0%	0%	0%	0%	0%	
Day 5 Health Index Score							
1×10^9 CFU	0.5	0	0	0	0	0	9.7
2×10^8 CFU	1.8	0.5	0.6	0.8	0.8	0.6	
4×10^7 CFU	5.45	3.85	3.9	4.1	3.8	3.35	
8×10^6 CFU	8.9	7.55	8.05	7.9	8.1	8.2	
4×10^5 CFU	9.85	9.7	9.75	9.5	9.45	9.25	
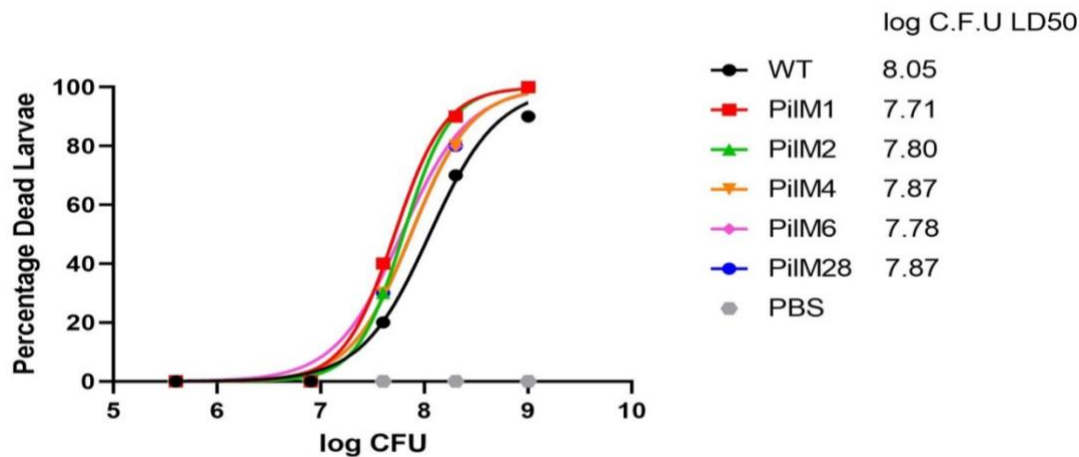
Figure 3.5. Dose titration of *L. lactis* in *G. mellonella* result in variable survival rates.*G. mellonella* were injected with 20 µl of WT *L. lactis* or *L. lactis* expressing GAS PilM1, PilM2, PilM4, PilM6 or PilM28 at dosages of 1×10^9 CFU, 2×10^8 CFU, 4×10^7 CFU, 8×10^6 CFU or 4×10^5 CFU, with 10 larvae used per experimental condition. Control larva were administered with PBS in equal volumes. Data is displayed as non-linear regression of wax moth larvae death rate at day 5 with dose titrations of each *L. lactis* strain.

3.3.3 Haemocyte density as a measure of GAS pili panel pro-inflammatory activity in *G. mellonella*

When investigating the immune response to pili expressing *L. lactis* at a non-lethal dose, it became important to utilise metrics such as the health index which capture more subtle differences than the binary events of death and survival. However, the health index scoring system relies on grading changes to external features of the larvae, which can be subjective and inconsistent. Furthermore, these physical alterations do not appear until about 24 hours after larval inoculation, so they do not illustrate the more immediate immune responses which occur in the hours following injection. In order to circumnavigate these issues, circulating haemocyte density was selected as a method to further assess GAS pili immune response in *G. mellonella*. Previous studies have reported circulating haemocyte numbers in *G. mellonella* surging as quickly as 4 hours post infection, indicating that an early indication of immune response can be provided by this metric (235). Additionally, compared to subjective visual cues, absolute haemocyte count is a more objective measurement of immune response.

G. mellonella were inoculated with 1×10^7 CFU/larvae of WT *L. lactis* or *L. lactis* expressing PilM1, PilM2, PilM4, PilM6 or PilM28. *G. mellonella* injected with PBS served as a control. It should be noted that the use of a needle during the process of inoculation can cause tissue damage to the larvae. Although inflammation is more heavily affiliated with microbial infection, sterile tissue damage can also result in the induction of inflammation. PRRs such as

75

TLRs can recognise non-infectious proponents of tissue damage or endogenous molecules released in the process of cellular injury, termed damage associated molecular patterns (DAMPs). These DAMPs are therefore able to induce similar inflammatory effects on the immune system to PAMPs, such the release of intracellular cytokines and the upregulation of activated immune cells (236). In *G. mellonella*, wound repairing melanin compounds are suspected of being DAMPs and wounding simulated by sham injections has been found to elicit immune responses such as increased haemocyte density and lysosome secretion (237–239). Therefore, sham injected larvae were included in this study to elucidate baseline haemocyte density following needle injury. This ensured that background DAMP associated inflammation induced by the act of injection was not mistaken to be an inflammatory response to *L. lactis* strains. At multiple time points across 3 days haemolymph was collected from larvae to assess haemocyte density. Across larvae administered with various *L. lactis* strains, circulating haemocyte density peaked at 24 hours, with the most prominent differences between groups being apparent at 6 hours post infection (Figure 3.6). At this time point, *G. mellonella* inoculated with pili expressing bacteria had significantly higher circulating haemocyte counts compared to larvae given WT *L. lactis*, with average cell counts between 1.5-fold (PilM1, $P=0.01$) and 2.5-fold (PilM6, $P<0.001$) greater (Figure 3.6). Consistent with the TNF release pattern seen in the THP-1 cell assay (Section 3.1), PilM6 had the highest haemocyte density 6 hours post infection, with mean cell counts between 1.4-fold (PilM2, $P<0.001$) and 1.6-fold higher (PilM1, $P<0.001$) than larvae inoculated with the other pili expressing *L. lactis* (Figure 3.6). *G. mellonella* exposed to pilus expressing *L. lactis* continued to exhibit elevated haemocyte density at 24 hours post infection, which was significantly greater ($P<0.001$) compared to that in larvae given WT bacterium. Although circulating haemocyte numbers dropped for all groups of larvae over the next 48 hours, *G. mellonella* inoculated with PilM6 *L. lactis* maintained haemocyte counts that were significantly greater ($P<0.001$) than larvae administered with WT *L. lactis* (Figure 3.6).
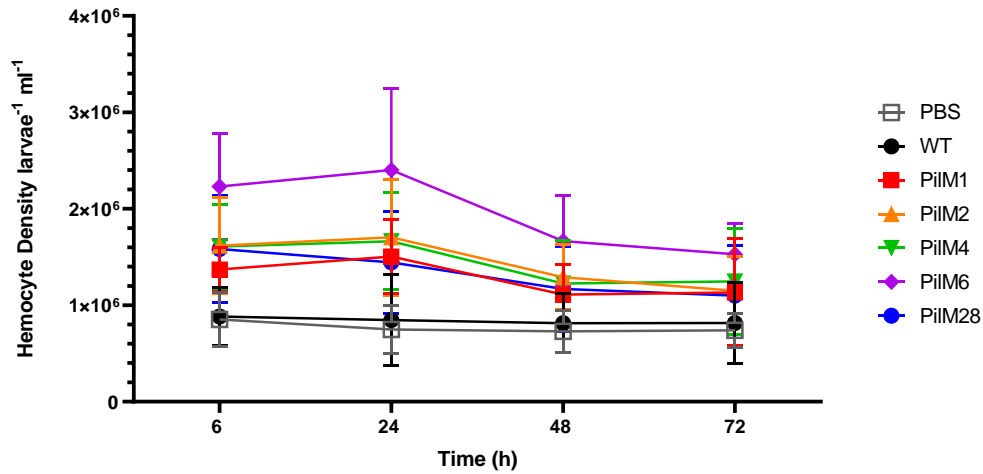
6 Hours Post Infection		24 Hours Post Infection		48 Hours Post Infection		72 Hours Post Infection	
WT vs PBS	>0.99	WT vs PBS	0.89	WT vs PilM6	<0.001	WT vs PilM6	<0.001
WT vs PilM1	0.01	WT vs PilM1	<0.001				
WT vs PilM2	<0.001	WT vs PilM2	<0.001				
WT vs PilM4	<0.001	WT vs PilM4	<0.001				
WT vs PilM6	<0.001	WT vs PilM6	<0.001				
WT vs PilM28	<0.001	WT vs PilM28	<0.001				
PilM6 vs PilM1	<0.001	PilM6 vs PilM1	<0.001				
PilM6 vs PilM2	<0.001	PilM6 vs PilM2	<0.001				
PilM6 vs PilM4	<0.001	PilM6 vs PilM4	<0.001				
PilM6 vs PilM28	<0.001	PilM6 vs PilM28	<0.001				

Figure 3.6. Haemocyte density increases with exposure to GAS pili. *G. mellonella* were injected with $1×10^7$ CFU of WT *L. lactis* or *L. lactis* expressing PilM1, PilM2, PilM4, PilM6 or PilM28, with 24 larvae used per group. A control group injected with PBS was also included. At 6, 24, 48 and 72 hours post infection, haemolymph was collected and haemocytes counted using a haemocytometer. Haemocyte counts of 24 sham injected *G. mellonella* was used as a baseline and subtracted from all cell counts. Data from three independent biological repeats is shown as mean±S.D. Statistical significance is determined by two-way ANOVA and P-values (shown in table) were calculated by Holm–Šídák's multiple comparisons test.

3.3.4 *L. lactis* expressing different GAS pili were cleared from *G. mellonella* at differential rates

Whether the expression of GAS pili affects the clearance of *L. lactis* in *G. mellonella* was also investigated by enumerating the recovered bacteria in *G. mellonella* homogenate collected at 6, 24, 48 and 72 hour time points post inoculation. The results show that bacterial CFU recovered from larvae administered with differing *L. lactis* strains diverged from 24 hours post infection. Pili expressing strains of *L. lactis* had significantly faster rates of clearance by the host compared to the WT bacteria, with recovered CFU counts between 1.6-fold (PilM2, P<0.001) and 5.2-fold lower (PilM6, P<0.001) (Figure 3.7). In particular, *L. lactis* expressing PilM6 had notably more rapid clearance from the larvae, with recovered colony counts

significantly lower than those from larvae inoculated with PilM1, PilM2 and PilM4 expressing *L. lactis* (Figure 3.7).
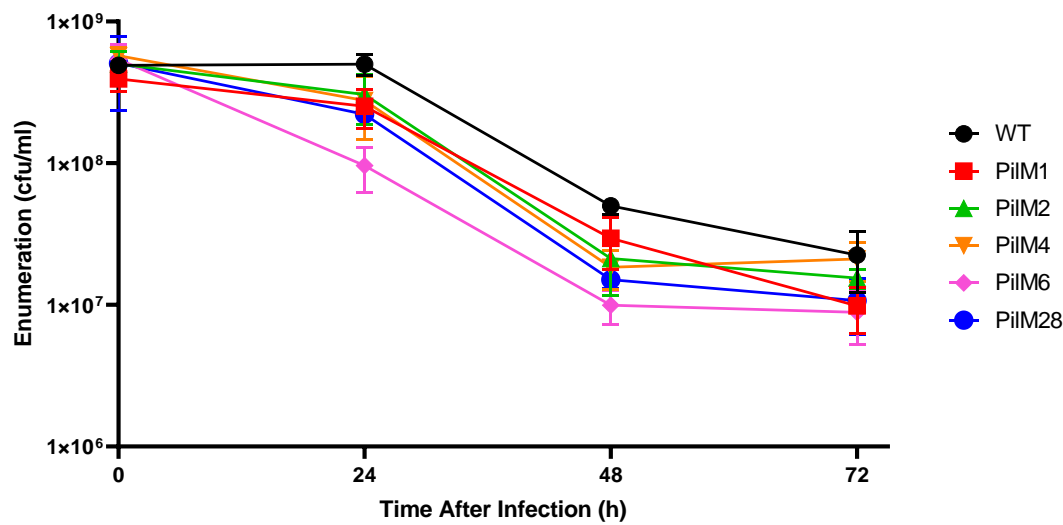
24 Hours Post Infection	
WT vs PilM1	<0.001
WT vs PilM2	<0.001
WT vs PilM4	<0.001
WT vs PilM6	<0.001
WT vs PilM28	<0.001
PilM6 vs PilM1	0.01
PilM6 vs PilM2	<0.001
PilM6 vs PilM4	0.002

Figure 3.7. GAS pili enhances clearance of *L. lactis* from *G. mellonella*. *G. mellonella* were injected with 1×10^7 CFU of WT *L. lactis* or *L. lactis* expressing PilM1, PilM2, PilM4, PilM6 or PilM28, with 24 larvae used per experimental group. At 0, 24, 48 and 72 hours post infection, individual larvae were homogenized in PBS and plated for colony enumeration. One representative data graph from three independent biological repeats is shown as mean±S.D. Statistical significance is determined by two-way ANOVA and P-values (shown in table) were calculated by Holm–Šídák's multiple comparisons test.

These results are complimentary to the haemocyte density assay. Pili expressing *L. lactis* induced higher circulating haemocyte density counts in *G. mellonella* and faster bacterial clearance in the first 24 hours following infection. In contrast, WT *L. lactis* induced lower circulating haemocyte counts in the larvae and slower rates of bacterial clearance. Of note, the PilM6-expressing strain induced the highest haemocyte density as well as the fastest clearance rate. This implies that the pili augment larval immune response, resulting in faster bacterial clearance.
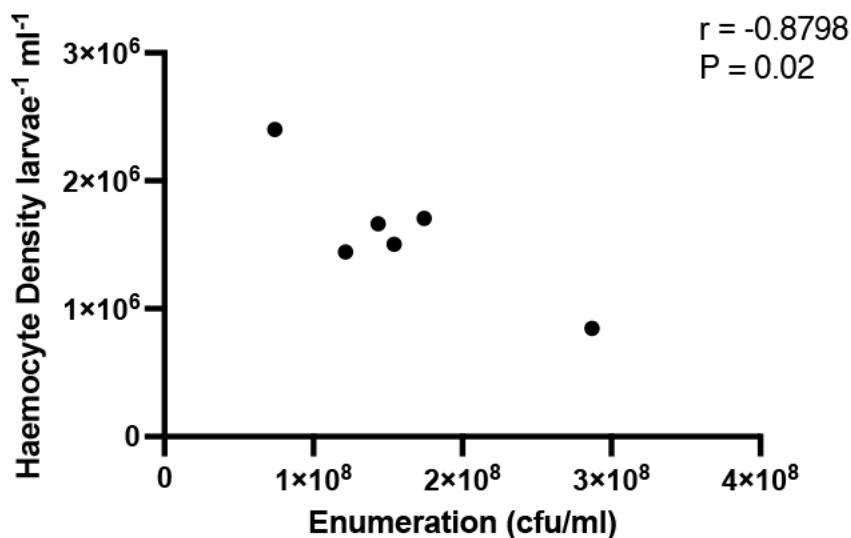
Figure 3.8. Haemocyte density correlates to enhanced clearance of *L. lactis* from *G. mellonella*. Correlation analysis of mean haemocyte density of larvae inoculated with WT *L. lactis* or *L. lactis* expressing PilM1, PilM2, PilM4, PilM6 or PilM28 and average CFU of bacteria recovered from each respective larval group 24 hours post infection. Linear correlation was determined using the Pearson correlation coefficient (r=-0.8798, P=0.02).

Correlation analysis between the average haemocyte counts of *G. mellonella* inoculated with the differing strains of *L. lactis* and the respective average bacterial CFU recovered from these larvae further visualised the relationship between immune response to pili and bacterial clearance. At 24 hours post infection, there was a strong negative correlation between larval circulating haemocyte density and bacterial CFU recovered (r = -0.8798), emphasising that the heightened immune response induced by pili is associated with enhanced bacterial clearance.

3.4   Discussion

Research on the GAS pili has been mainly focusing around defining their biological functions and their role as a virulence factor, as well as their potential as a GAS vaccine target (240). The innate immune response to GAS pili has been less investigated, despite the complex being a surface abundant structure. In order to explore this advent, there was a need to sequester the pili from other GAS virulence factors to avoid the immune stimulating effects exerted from other GAS components. This was achieved with the use of *L. lactis* as a surrogate to express GAS pili. *L. lactis* utilises the same mechanism of Gram-positive cell wall anchoring as GAS to display cell wall proteins, with the Lactococcal Sortase A enzyme being able to recognize the streptococcal cell wall anchoring domains, which contain a LPXTG motif conserved across

the two bacteria (241). This allows *L. lactis* to display the fully assembled GAS pili structure on the cell wall. Additionally, the bacterium is non-pathogenic, ensuring that the immune response to GAS pili can be studied isolated from other potentially virulent structures (242). In our group pilated *L. lactis* strains have already been utilised on numerous occasions, such as to investigate pili mediated adherence to host cells, and in vaccine studies (66,75).

In this project these pilated *L. lactis* strains were utilised to assess the immune response towards different GAS pilus types using monocytic THP-1 cells. The array of GAS pili all increased the THP-1 cell production of the pro-inflammatory cytokine TNF, demonstrated by cells co-incubated with pili expressing *L. lactis* strains having significantly higher TNF secretion than cells exposed to WT *L. lactis* devoid of pili (Figure 3.3). The variation in THP-1 stimulation between different pili recorded was somewhat surprising, with PilM6 inducing notably greater TNF production compared to the other pili, despite this complex being derived from a GAS strain more commonly associated with milder pathogenesis such as self-limiting pharyngitis (29).

In addition, the non-vertebrate *G. mellonella* larvae was used to model the virulence associated with different GAS pili. At the higher dosages, the larval immune system appeared to be overwhelmed by the sheer amount of bacteria introduced, with all *L. lactis* strains, including WT, instigating larval mortality. Larvae inoculated with pili-expressing *L. lactis* strains had slightly higher mortality rates to the group given WT bacterium, indicating that GAS pili appeared to exert a small increased health burden on the larvae (Figure 3.4). At the lower dosages, there was less pronounced larval death across all treatment groups. However, a difference in health index scoring could be discerned, with *G. mellonella* inoculated with pili expressing *L. lactis* scoring lower than larvae administered the WT strain.

Compared to *G. mellonella* studies using GAS, a much higher inoculum of bacteria was required to elicit notable changes in health (231). This is likely due to *L. lactis* being a non-pathogenic organism lacking virulence factors. Additionally, pili expression is controlled by an assemblage of transcriptional regulators (240). These mechanisms promote high pilus expression during the initial stages of infection, where the adhesive properties of the structure assist GAS attachment to cells and thus help establish an infection. Expression of these adhesive pilus complexes are subsequently inhibited, allowing the bacteria to gain increased ability to spread, aiding in the transition from local colonisation to dissemination (62,243).

Therefore, it was predicted that exposure of larvae to pili, which are not necessarily essential through the entire timeline of GAS infection, would have to be at higher dosages to induce similar outcomes in the larvae to constitutively expressed GAS virulence factors present throughout the entire cycle of infection. In line with this conjecture, when *L. lactis* was modified to display the GAS virulence factor deacetylase and inoculated into larvae, at the same dosage, the lethality of this gain of function mutant was much greater than the pili expressing *L. lactis* used in this chapter (232). This indicates that the pilus is not very virulent in the *G. mellonella* model and implies that the structure is relatively safe for biological use such as administration as part of a vaccine formulation. As the effects of pili on *G. mellonella* were more subtle than other virulence factors, dose exploration was found to be important for establishing an inoculum concentration high enough to accentuate the immune response to pili without the sheer amount of bacteria injected overwhelming the larvae and leading to mortality independent of the pilus complex.

The health index score, which is based on visual inspections of *G. mellonella* administered with pili expressing bacteria, was able to give an indication that the complex triggered larval immune response. In particular, these larvae became darkened in colour to a high degree, indicating the process of melanisation occurring (244). For example, the average melanisation score of larvae receiving bacteria at the non-lethal 8×10^6 CFU dosage was 3.6 for larvae administered WT bacteria and 2.6 for larvae inoculated with pilated bacteria, where a score of 4 indicated no melanisation. Melanisation occurs following larval oenocytoids releasing oxidative prophenoloxidase, which facilitates microbial encapsulation (238,245). The release of prophenoloxidase is subsequent to oenocytoids recognising PAMPs; this points to pili being a PAMP recognised by the larval immune system with the ability to induce the activation of defence mechanisms (245). The post-infection surge in circulating haemocyte density counts recorded in these melanised larvae ratifies the notion of GAS pili inciting the wax moth immune system. This surge was demonstrated across all larvae administered different pilus expressing bacteria. In fact, PilM1 expressing *L. lactis*, which had low stimulatory properties in the THP-1 cell based assay, still evoked a substantially greater surge in circulating haemocytes compared to WT *L. lactis* (Figure 3.6).

In the panel tested in this study, pro-inflammatory responses varied depending on the pilus type but the most prominent induction of both larval and monocytic cell line immunity was

facilitated by PilM6 expressing *L. lactis*. PilM6, encoded by FCT-1, has distinct properties compared to other FCT type pili (26,79). Previous studies on this pilus type identified its ability to propel the formation of biofilms irrespective of cell culture conditions (63). Furthermore, unlike other FCT type pili which primarily mediate biofilm formation subsequent to the establishment of a microcolony or via auto aggregation, FCT-1 pili were identified as being able to utilise its tip subunit as an adhesin for the initial cellular attachment required in the very early stages of biofilm formation (37,79). These characteristics may have increased the tendency of PilM6 expressing *L. lactis* to promptly form aggregates in contact with THP-1 cells or *G. mellonella* haemocytes, compared to *L. lactis* expressing other pilus types. The ensuing enhancement of interactions between pili and immune cells may have contributed to the high levels of immune response seen across both inflammation models. Further biofilm assays may shed light on whether this process is occurring.

The most important finding in this study is, disparities in the inflammatory response to GAS pili did not seem to correspond to the disease severity associated with GAS strains harbouring those particular pilus types. For instance, despite the highly inflammatory nature of PilM6 (FCT-1) observed here, the GAS strains displaying this FCT type are commonly associated with non-invasive superficial infections (29). Conversely, PilM1 (FCT-2) is found in GAS strains associated with more serious invasive infection but demonstrated lower immune response in these assays. Additionally, although a large portion of GAS strains associated with acute rheumatic fever express the FCT3/4 type pilus (9), PilM28 did not induce a strikingly high inflammatory response in the THP-1 cell line or an innate immune haemocyte surge in *G. mellonella*. GAS mediated pro-inflammation plays a multi-faceted role in disease progression that can appear antithetical; the induction of inflammation is pivotal for directing the immune system to resolve GAS infections but can also propel tissue damage associated with invasive GAS infection. The absence of positive correlation between pili and disease severity of GAS strains harbouring these specific pili can be better understood by casting eyes on the haemocyte and enumeration assays, which appear to indicate that pili mediated inflammation is more heavily weighted towards bacterial clearance rather than disease progression.

Surges in circulating haemocytes in *G. mellonella* are facilitated by the release of sessile haemocyte cells associated with the insect internal organs (246). Following infection, sessile cells are released into circulation, increasing the availability of haemocytes equipped with

fighting the invading bacteria (230). *G. mellonella* have been used to study the virulence of a plethora of pathogens both bacterial and fungal, and these studies have led to the consensus that circulating haemocyte counts is dynamic and dependent on the degree of pathogenicity of the organism the larvae is exposed to. When assessing haemocyte counts following inoculation of *G. mellonella* with *Actinobacillus pleuropneumoniae* for example, strains with lower virulence facilitated a rise in circulating haemocyte numbers in the initial hours following infection, while strains identified as being highly virulent induced a drop in circulating haemocytes (247). After 24 hours, circulating haemocyte counts decreased to baseline levels in larvae administered low virulence strains, whilst haemocyte density in *G. mellonella* receiving highly virulent strains dwindled remarkably below the initial pre-infection count (247). Similarly, investigations into different species of fungi revealed that larvae administered high pathogenicity yeast had a subsequent decline in circulating haemocyte numbers whilst lower pathogenicity yeasts facilitated increased circulating haemocytes (248). It is likely that this divergence in haemocyte counts occurs due to the cells ability to control and eliminate low virulence organisms, whilst more virulent organisms are able to evade the *G. mellonella* immune system and continue to proliferate, facilitating haemocyte death in the process. This is echoed in the study investigating fungal pathogens, where higher pathogenicity was correlated to both lower larval haemocyte densities and higher fungal load above the initial inoculation dosage (248).

Whilst the emphasis of wax moth larvae assays introduced above was on the virulence of whole microorganisms, the assays here honed into the immune response to one component of a pathogen. In fact, this study may be the first to utilise a combination of metrics to assess the immune response to a bacterial component. In this chapter, the presence of pili corresponded to surges in haemocyte density but this influx of haemocytes seemed to be able to mount an effective response to start eliminating bacteria. This was illustrated by bacteria recovered at the time points following the surge in haemocytes being at a CFU count markedly below the initial inoculation (Figure 3.7). The PilM6 expressing *L. lactis* in particular induced the highest surge in haemocyte counts and inversely the fastest rate of bacterial clearance during this period. Congruently, WT bacteria generated a less pronounced increase in haemocytes and had a corresponding slower rate of bacterial clearance (Figure 3.7). The association between haemocyte counts and bacterial clearance was reaffirmed following determination of the Pearson correlation coefficient, which illustrated surges in larval haemocyte density having a

very high negative correlation to bacterial CFU recovered from the larvae. (Figure 3.8). These results signal that pili induce the activation of the immune system, but pili mediated inflammation facilitates clearance of bacteria instead of promoting mechanisms such as tissue damage that intensify pathogenesis.

As briefly mentioned above, many features of the *G. mellonella* immune system resemble segments of the human innate immune system. For instance, the NFκB signalling pathway, which is responsible for activation of a plethora of pro-inflammatory genes, is conserved between mammals and Lepidopteran insects such as *G. mellonella* (249). The larvae produce peptides downstream to this transcription factor which have signalling properties equivalent to mammalian NFκB activated cytokines such as TNF, which was investigated in the THP-1 assay (249,250). Furthermore, both *G. mellonella* and human innate immune systems respond to the introduction of pathogens by mounting cells to perform phagocytosis and opsonisation and the release of pathogen damaging oxidative bursts is also generally conserved (249,251). Thus although these two systems do not perfectly mirror each other, the high degree of similarity allows the assumption that the *G. mellonella* immune response to GAS pili seen in this chapter roughly translates to the response the human innate immune system would uphold towards the complex.

The results of this chapter suggest that GAS pili are able to induce pro-inflammatory immune responses without high likelihood of consequential progression towards more severe disease and clinical outcomes. This work was also summarised in our paper (252). In the space of vaccine development, the implication of this observation is that incorporation of GAS pili into a vaccine formulation can aid in the invigoration of the immune system without posing serious safety concerns. As indicated previously, pili and pilus proteins have been proposed as a GAS vaccine candidate, with improved strain coverage compared to more conventional candidates such as the M protein (223,253). Compared to the M protein based vaccines, strategies using pili are not implicated in directly contributing to the pathogenesis of ARF and RHD as the pilus proteins do not have homology to human heart proteins (253–255). The results in this chapter further enforce the potential of GAS pili based vaccine, illustrating the highly inflammatory properties of the pili whilst simultaneously suggesting that this immune response does not exacerbate disease severity and that the structure by itself does not have high pathogenicity. Accordingly, pilus proteins may offer an approach to inducing strong antibody response with

low risk of causing damage to the recipient but a deeper investigation into these proteins is required to strengthen this proposition.

Chapter 4: Identifying the innate immune receptor for GAS pili

The pro-inflammatory characteristics of GAS pili across the multitude of pilus types was demonstrated in Chapter 3, which showed that the immune stimulating effect may facilitate the defence mechanism of the innate immune system and implied the potential of the complex as a vaccine component. However, more information on the GAS pili and its subunits is required before an assessment on the ability of pili to augment antibody response can be made. For instance, insight into the receptor through which the complex induces an inflammatory response can become important as this determines the downstream cytokine profile and which branch of the adaptive immune system is preferentially upregulated (256).

More comprehensive investigations into the immunostimulatory properties of GAS pili both in the fully assembled form and as individual protein subunits has begun to be undertaken using pilus from M1 GAS (PilM1). As we described in the pilot study, fully assembled PilM1 expressed on *L. lactis* induced the secretion of the pro-inflammatory cytokines IL-8 and TNF from THP-1 cells at a significantly higher level compared to wild type *L. lactis* lacking this complex (206). Furthermore, recombinant proteins of the tip (AP1) and backbone (BP) pilus subunits also had the ability to stimulate high TNF and IL-8 release. Moreover, whole pili on *L. lactis* and recombinant pilus subunits were tested against HEK-Blue hTLR cells. These reporter cell lines are co-transfected to express individual human TLR linked to a nuclear factor-kappa-B inducible downstream reporter protein, which is secreted into the cell supernatant upon TLR activation. The protein catalyses hydrolysis of substrates within the cell supernatant detection solution, driving a colourmetric change to the cell suspension. This can be utilised to quantify pili mediated activation of TLR. Both pili expressed on *L. lactis* and recombinant AP1/BP induced activation of HEK-TLR2 but not HEK-TLR4 or HEK-TLR5, the other cell surface TLRs associated with recognition of bacteria (206). On top of this, MCP-1 release was measured in the pili stimulated HEK-TLR2 cells whereas cytokine release was not detected from the HEK-TLR4 cells exposed to pili (206).

The results of these assays tentatively indicate that the GAS pili stimulate the innate immune response through TLR2. In this chapter, further investigation was conducted in order to characterise pili signaling through TLR2 and pinpoint the TLR2 heterodimeric form required for recognition of GAS pili.

4.1 Expression and Purification of Recombinant BP and AP1

4.1.1 Expression and Purification of BP

BL21 *E.coli* containing a pET32a3c vector for the expression of soluble BP, generated by Dr Jacelyn Loh at the Department of Molecular Medicine and Pathology (UoA), was used to produce recombinant BP. This expression system produced the pilin subunit as a ~50kDa fusion protein consisting of the soluble form of BP (devoid of the N-terminal signal peptide sequence and C terminal cell wall sorting domain), a N-terminal 6×hisitidine tag, a 3C protease cleavage site and a thioredoxin tag. The thioredoxin and 6×histidine tags' affinity to immobilised nickel ions allowed for protein purification using immobilised metal chelate affinity chromatography as outlined in 2.2.3.4. Sonicated bacterial lysate was loaded onto the nickel column, which underwent step-wise elution with 10-100 mM of imidazole to release the nickel-bound polyhistidine-tagged proteins. Visualisation of the eluents using SDS-PAGE revealed the presence of a protein band at about ~50kDa, indicating successful purification of the ~30kDa BP peptide and ~20kDa thioredoxin tag fusion protein (Figure 4.1).

Figure 4.1. Purification of BP using nickel affinity chromatography.The soluble fraction of bacterial lysate from *E. coli* BL21 pET32a3c BP was passed through the nickel column and the ~50kDa BP protein and thioredoxin tag fusion was collected after elution with increasing concentrations of imidazole. L; protein ladder.

Fractions from elution with 10 mM to 100 mM imidazole were pooled together and after overnight dialysis against MCAC-0, the thioredoxin tag was cleaved off using 3C protease.

Passage of this fraction through the nickel column resulted in the tag binding to the column and collection of standalone BP in the flow through, as indicated by the ~30kDa protein band on SDS-PAGE (Figure 4.2). Addition of 100 mM imidazole removed the tag from the column, as indicated by the ~20kDa protein band (Figure 4.2). BP was obtained with ~90% purity and underwent overnight dialysis in PBS in preparation for usage in assays.
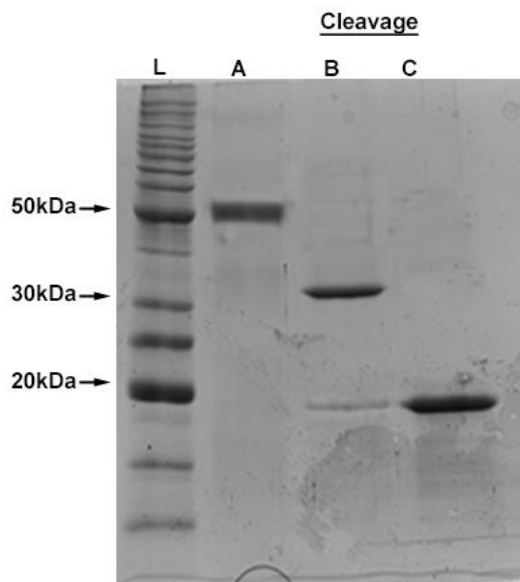
Figure 4.2. Cleavage of thioredoxin tag from recombinant BP protein. Fusion protein (A) was cleaved using 3c protease to separate the complex into ~20 kDa tag and ~30kDa BP subunit. The fraction was then passed through the nickel column to separate the BP subunit (B) from thioredoxin tag (C). L; protein ladder.

4.1.2 Expression and Purification of AP1

BL21 *E.coli* containing a plasmid constructed with the pPROEX-Htb vector and AP1 sequence, generated by Fiona Clow at the Department of Molecular Medicine and Pathology (UoA), was used to express the soluble portion of AP1. This protein consisted of AP1, with omission of the N-terminal signal peptide and C-terminal cell wall sorting domain, tagged with N-terminal 6×hisitidine. The recombinant protein was purified by a similar procedure as the one described for BP (as outlined in 2.2.3.4), and the protein was subsequently visualized on SDS-PAGE (Figure 4.3). A protein band at about ~100kDa eluted by 20-100 mM imidazole indicated the presence of AP1 in the eluent. However, native *E. coli* proteins also appeared to be present in these fractions, with several other bands evident on the SDS-PAGE. Thus, the eluted fractions were dialysed against PBS and concentrated for further protein purification.
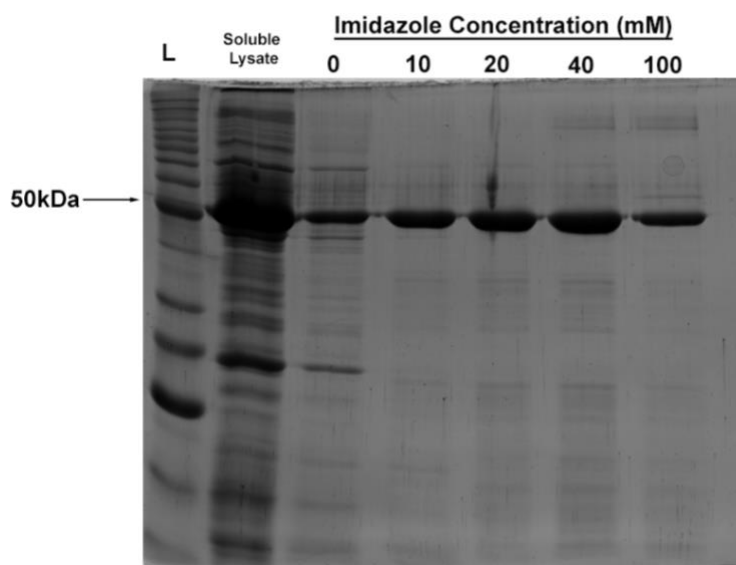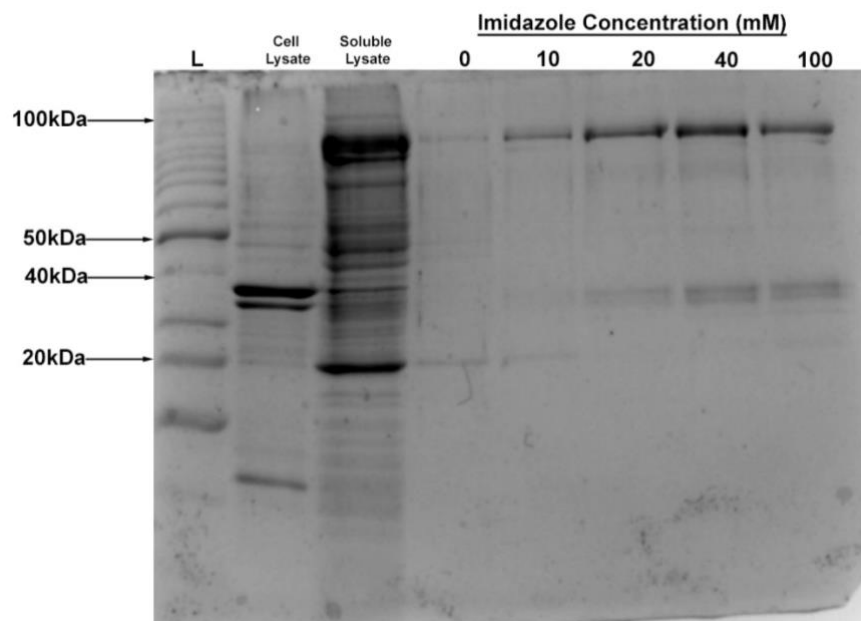
Figure 4.3. Purification of AP1 using nickel affinity chromatography.The soluble fraction of bacterial lysate from *E. coli* BL21 pROEX-Htb AP1 was passed through the nickel column and the ~100kDa AP1 protein was collected after elution with increasing concentrations of imidazole. L; protein ladder.

The second round of purification employed size exclusion chromatography (SEC) to separate the ~100kDa AP1 from the lower molecular weight *E. coli* protein contaminants. AP1 was eluted using phosphatase based SEC buffer with fractions collected based on the UV peaks recorded by the chromatogram. As before, fractions were visualised on SDS-PAGE to determine the outcome of purification (Figure 4.4). The first major absorbance peak on the chromatogram was collected as two fractions (Figure 4.4, fractions 1, 2) and was shown to be clean fractions solely containing the ~100kDa AP1 protein. The second, smaller absorbance peak collected over three fractions (Figure 4.4, fractions 3, 4, 5) appeared to contain both the AP1 protein and a lower molecular weight contaminant. Thus, the first two fractions, which were obtained with >95% purity, were pooled together and dialysed overnight against PBS for use in downstream assays.
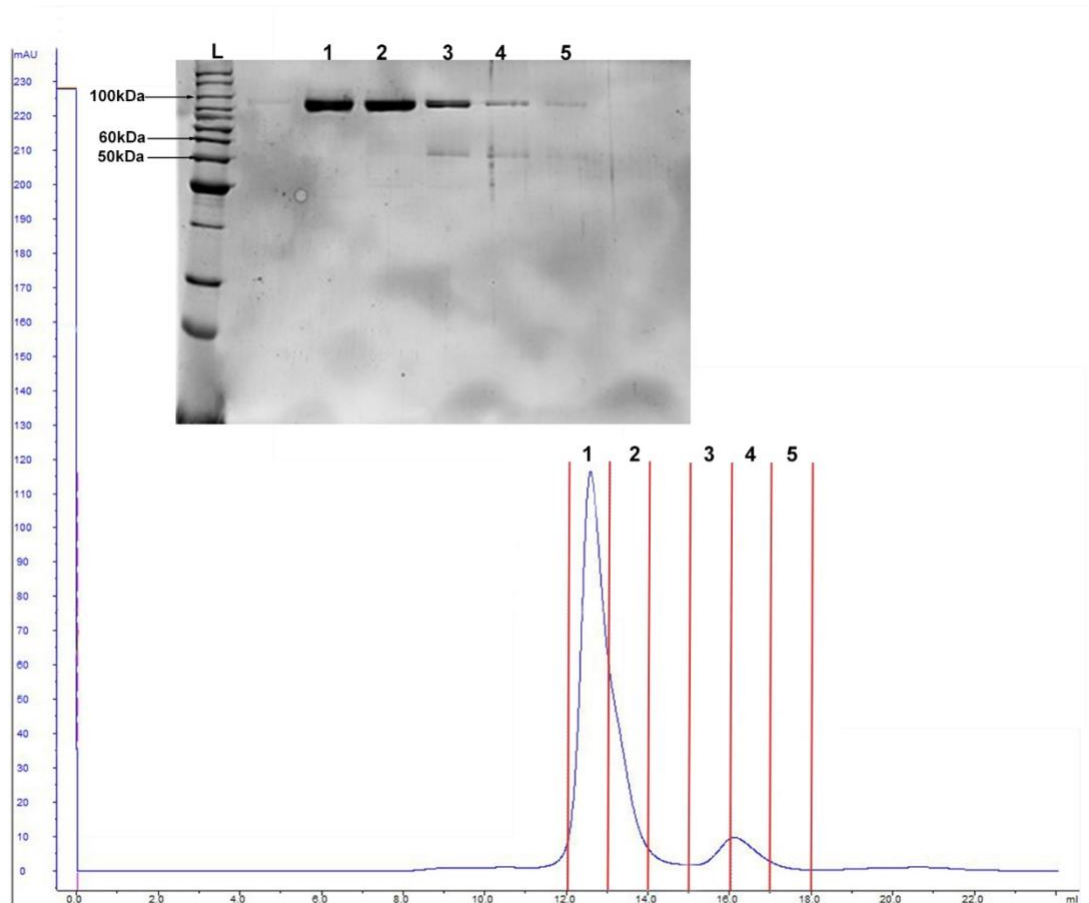
Figure 4.4. Purification of AP1 using size exclusion chromatography. Subsequent to nickel affinity chromatography, protein fractions containing AP1 were pooled and further purified using size exclusion chromatography. Fractions collected during elution (fractions 1-5) were analysed using 12.5% SDS-PAGE (lanes 1-5). Solid blue line indicates the UV absorbance during the elution period (mAU) and sections between red lines indicate the points at which fractions were collected. Fraction numbers correspond to numbered lanes on SDS-PAGE. L; protein ladder.

4.2   Interaction of pilus subunits and TLR2

Prior to this chapter, characterisation of physical interactions between pilus proteins and TLR2 had not been undertaken. Previous studies examining the interactions between *Neisseria meningitides* porin B (PorB) and TLR2 helped provide a possible framework for approaching this analysis. Analogous to the TLR2 stimulating capabilities of GAS pilus proteins, porin B from *Neisseria meningitides* has also been depicted to activate this specific TLR. For instance, incubation of PorB with HEK cells expressing TLR2 and NFκB inducible luciferase resulted in a dose dependent increase in luminescence not observed in the absence of TLR2 (257). However, the initial events leading to activation were not well understood. Massari et al (2006)

90

extrapolated from these findings to investigate whether binding of the porins to TLR2 could be captured (257). Firstly, TLR2 domains were incubated with immobilised PorB in an ELISA-like assay, illustrating dose dependent binding of the complexes to TLR2. Subsequent observed shifts in fluorescence following incubation of fluorescently tagged PorB with TLR2 expressing cells provided additional validation. Further assays portrayed PorB specificity to TLR2/1 and competition with other TLR2 ligands for binding sites (257).

As pilus proteins appear to activate TLR2 and downstream NFκB in a similar fashion to PorB, there was a high probability that a similar scheme of assays could help uncover physical interactions between pilus proteins and TLR2. Thus, a series of methods were deployed in this chapter to capture binding between pilus proteins and TLR2, competition with other TLR2 ligands for binding sites and protein recognition of TLR2 in its heterodimeric form.

4.2.1 Kinetic analysis of binding between TLR2 and Pilus Subunits

Surface plasmon resonance was deployed to measure the binding affinity of BP or AP1 to immobilized recombinant TLR2, with the biomolecular interaction analysis system (Biacore T200) utilised to record changes in refraction at the contact surface (258). Poly-histidine tagged recombinant TLR2 was immobilised onto a nitrilotriacetic acid sensor chip via amide linkages and an initial concentration series of BP and AP1 (0-15 µM) was passed over the chip in duplicate, with binding response detected using the Biacore T200 system. As seen in the run recording AP1 binding (Figure 4.5), despite maximum efforts being put on the optimal concentration and purity of the analyte proteins applied on the chip, readings between repeats were very inconsistent and a dissociation constant could not be calculated. This led to alternative methods of illustrating pilus protein binding being utilised.
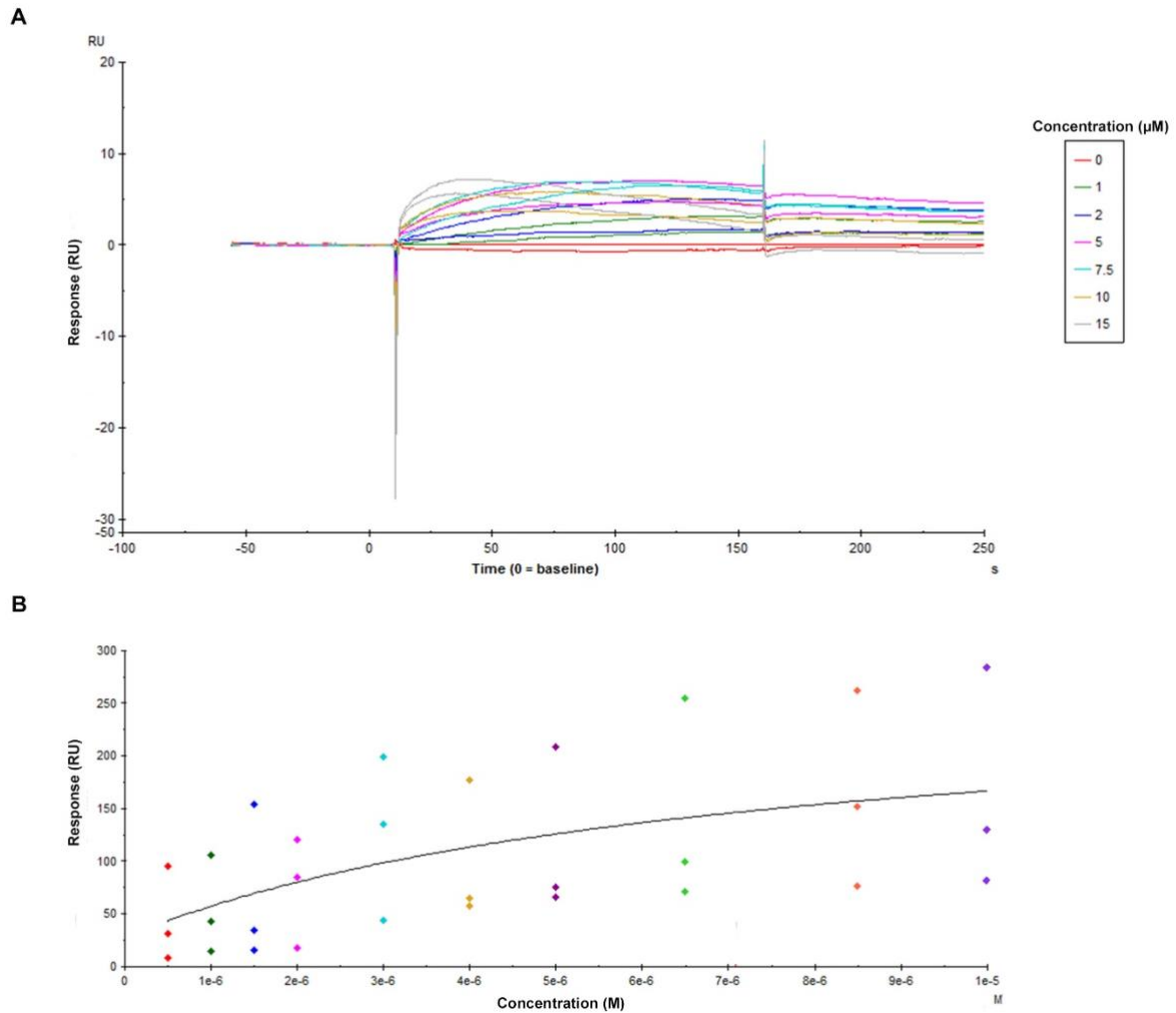
Figure 4.5. Kinetic analysis of AP1 binding to TLR2 using surface plasmon resonance resulted in inconsistent readings between runs.(A) The equilibrium binding response of a 0-15 µM concentration series of AP1 binding to TLR2 immobilised onto a nitrilotriacetic acid sensor chip was recorded on a sensogram using surface plasmon resonance. (B) The data was fitted into a single site binding model to calculate the dissociation constant. Experiment was performed in triplicate.

4.2.2 Solid phase binding assay demonstrates interaction between TLR2 and pilus subunits

In this alternative method, the physical interaction between pilus proteins and TLR2 was assessed using a solid-phase binding assay. Varying concentrations of recombinant BP or AP1 were added to a 96 well plate coated with recombinant TLR2 at 100 ng/well and binding was detected using purified antibodies against BP/AP1 in an indirect ELISA format. The AP1 subunit demonstrated dose dependent binding to TLR2, as shown by the 10-fold increase in absorbance when the concentration of the protein was incremented from 5 to 100 pM. In

contrast, the absorbance values for BP tested at the same concentration range showed negligible change, therefore binding could not be discerned (Figure 4.6)
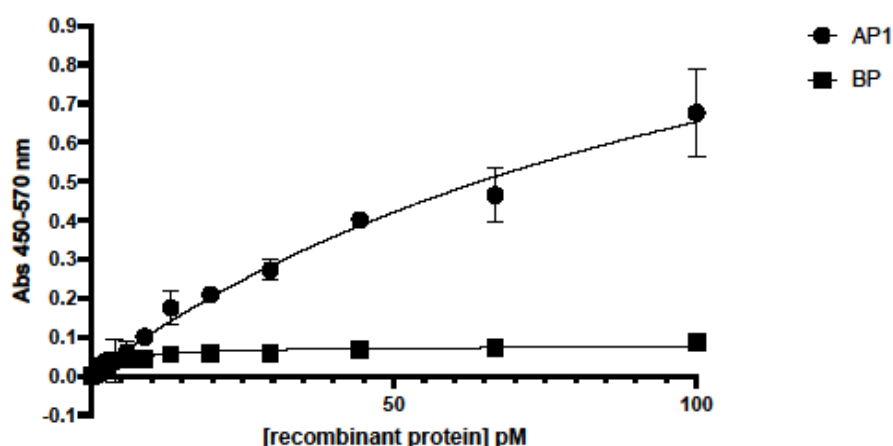
Figure 4.6 Subunits of M1 GAS pili interact with immobilised TLR2.Recombinant BP and AP1 of varying concentrations was incubated with 1 µg/ml of recombinant TLR2 immobilised on a 96 well plate. Protein binding was detected via ELISA using purified rabbit antibodies against AP1 and BP. Experiment was performed in duplicates and data shown as mean±S.D. A representative of three independently performed experiments is shown. Non-linear regression fitted using one site specific binding model on Graphpad Prism.

4.2.3 Usage of flow cytometry to demonstrate interaction between TLR2 and pilus subunits

Following the assessment of pilus protein binding to TLR2 using ELISA, the interaction between pilus subunits and the receptor was further evaluated by flow cytometry. This required the pilus proteins to firstly be labelled with a fluorescent dye for detection on the flow cytometer. Recombinant BP and AP1 were dialysed against bicarbonate buffer and incubated with Red Mega 485 NHS dye on a rotator for 1 hour at room temperature, before the samples were loaded onto a size exclusion chromatography (SEC) column. As the proteins labelled with the fluorescent dye were substantially greater in size than the dye molecules, the labelled proteins could be separated from free unbound dye based on their size, using SEC. For both BP and AP1, two absorbance peaks were observed on the chromatogram and these were collected as two separate fractions (Figure 4.7A). These peaks were analysed by loading the fractions onto a 12.5% SDS-PAGE gel, where the smaller peak fraction from BP and AP1 SEC were loaded into lanes 1 and 3, respectively (Figure 4.7B), and the BP and AP1 SEC fractions with the larger absorbance peak were loaded into lanes 2 and 4, respectively (Figure 4.7B). Visualisation of the proteins in each fraction using Coomassie staining indicated that for both

BP and AP1, the fraction with the larger absorbance peak could be seen on the gel as one clean band, with the molecular weight matching that of the pilus subunits, at ~30kDa and ~100kDa for BP and AP1 respectively (Figure 4.7B). The protein gel was also imaged using UV transillumination to confirm the addition of fluorescent tag to the pilus proteins (Figure 4.7C). For both BP and AP1, a single fluorescent band could be observed at a molecular weight corresponding to the protein band seen in the Coomassie stained image, marking the successful labelling of pilus proteins with the Red Mega dye. Finally, the degree of labelling (DOL), which illustrates the average number of dye molecules conjugated to each protein, was calculated to determine whether there was sufficient labelling of proteins. A DOL of around 1 for every 200 amino acids is indicative of adequate labelling and thus it was anticipated that the DOL of the ~340 amino acid BP and ~677 amino acid AP1 would be around 1.7 and 3.3 respectively. The absorbance of the two protein-fluorophore fractions at 280 nm and at the maximum wavelength of the Red Mega dye (485 nm) was measured before DOL was calculated using the equation: $DOL = (A_{max} \times \varepsilon_{280}) / ((A_{280} - A_{max} \times CF) \times \varepsilon_{max})$. This gave the BP and AP1 DOL values as 1.6 and 3.4 respectively, indicating that the majority of proteins had been successfully tagged with the fluorophore.
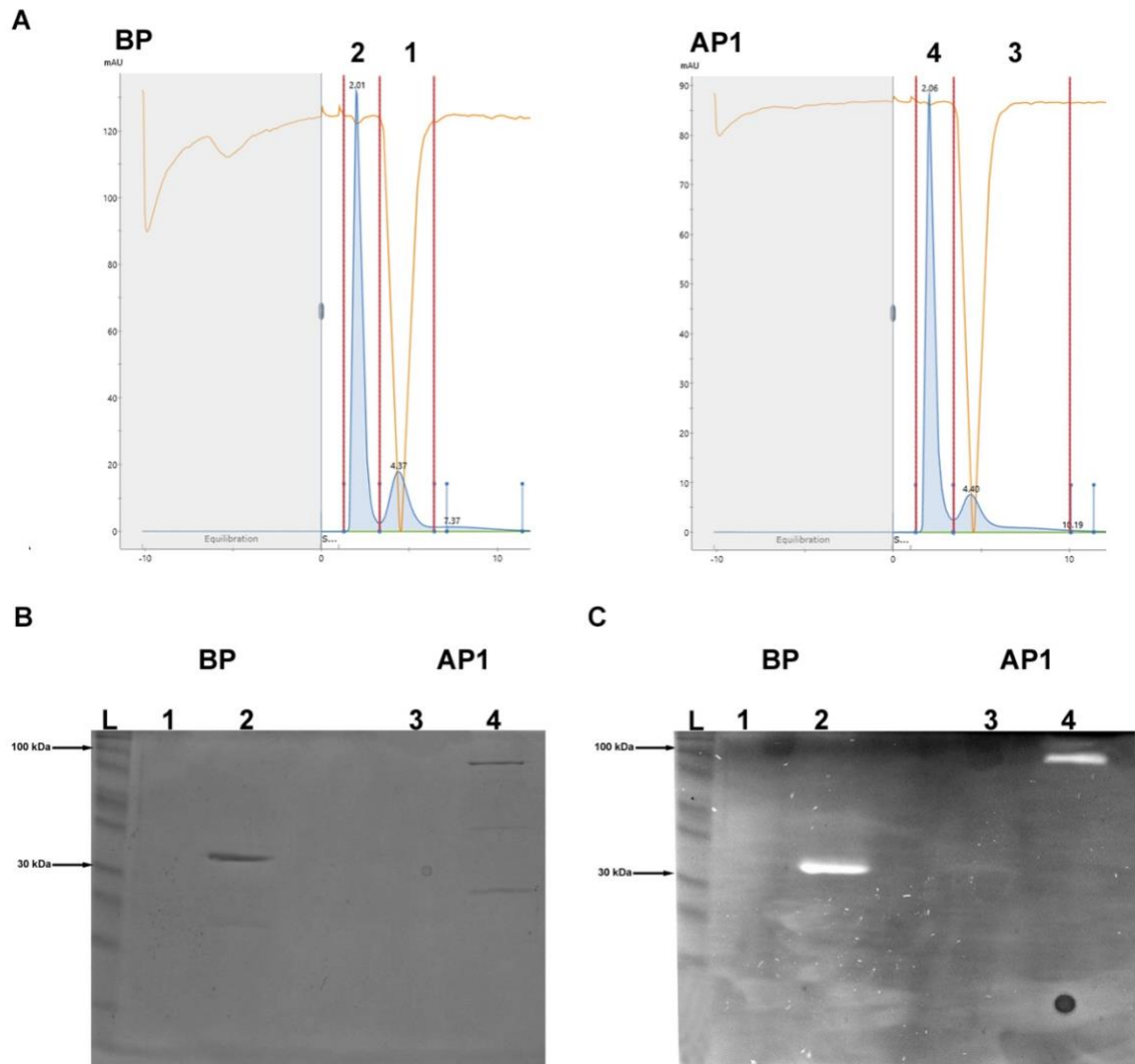
Figure 4.7. The AP1/BP subunits of M1 GAS pili were labelled with fluorescent Red Mega 485 NHS dye.(A) Following incubation with fluorescent dye, recombinant BP (left) and AP1 (right) were loaded onto size exclusion chromatography (SEC) columns, which resulted in both solutions eluting as two fractions. (B) The fractions from SEC were analysed by SDS-PAGE using Coomassie staining (C) and the proteins within these fractions labelled with the fluorescent tag were imaged using UV transillumination. Blue lines indicate the UV absorbance during the elution period (mAU) and sections between red lines indicate the points at which fractions were collected. Fraction numbers correspond to numbered lanes on SDS-PAGE.L; protein ladder.

Once BP and AP1 were fluorescently labelled, flow cytometry experiments were deployed to assess the interactions between pilus proteins and TLR2. One nanomole of each of the labelled proteins were mixed and incubated with 5×10^5 HEK-Blue hTLR2. The pilus proteins were also mixed with 5×10^5 HEK-Blue hTLR4, which has the same outer cell wall composition as the HEK-Blue hTLR2, to determine non-specific binding to components of the cell besides TLR2.

After performing washing steps to remove unbound proteins, the cells were analysed on a flow cytometer and the mean fluorescence intensity, which represents the relative amount of cell bound pilus protein, was calculated to deduce pilus protein-receptor interactions. HEK-Blue hTLR4 cells incubated with the fluorescent proteins did not have a markedly greater fluorescence compared to the untreated negative control cells, emphasising the lack of interaction between BP/AP1 and TLR4, as well as other HEK cell surface components (Figure 4.8A, B). In contrast, HEK-Blue hTLR2 cells incubated with fluorescently labelled AP1 had a fluorescence signal significantly shifted upwards compared to the untreated negative control cells, with a 2.5-fold greater mean fluorescence intensity (P<0.001; Figure 4.8A). This indicated binding between the fluorescent labelled tip pilus subunit and TLR2. On the other hand, HEK-Blue hTLR2 cells incubated with labelled BP did not display a statistically significant shift in mean fluorescence intensity compared to the negative control cells (Figure 4.8B). Thus, as consistent with the solid-phase binding assay, notable backbone subunit binding to TLR2 was not recorded.
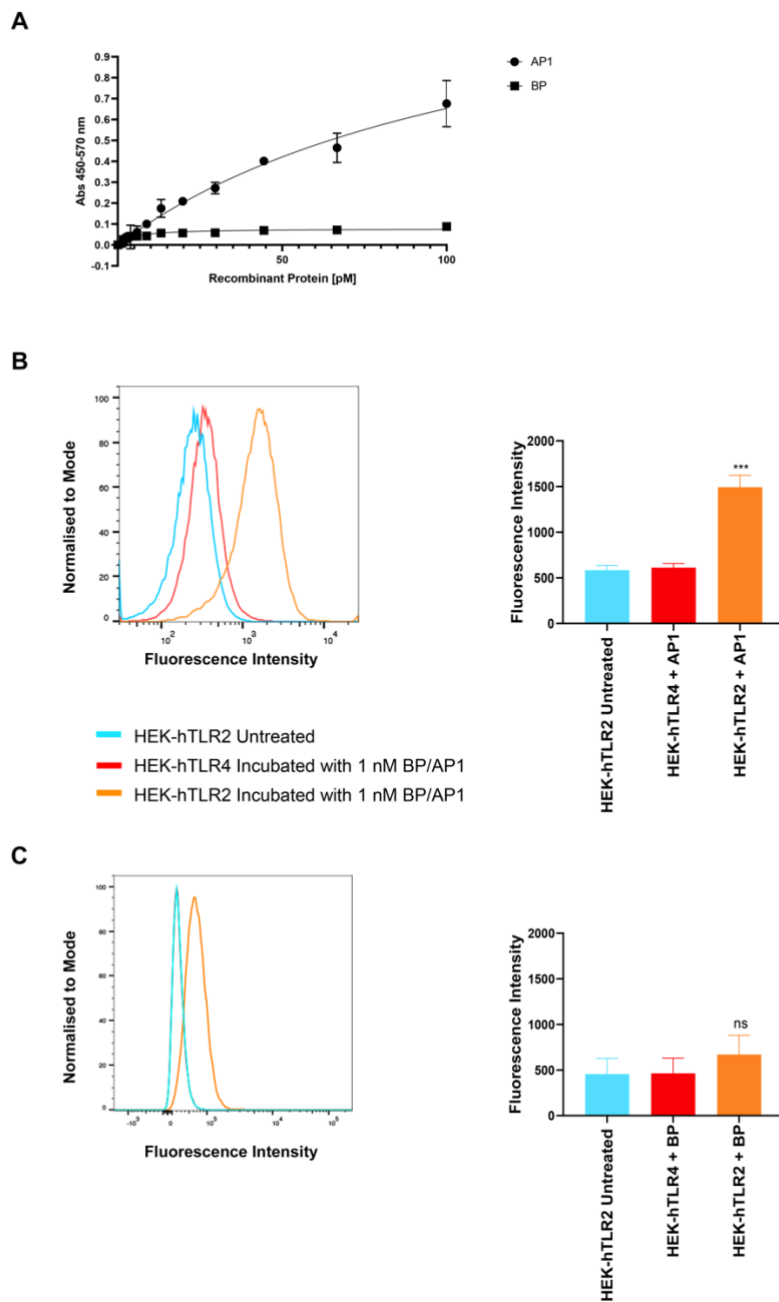
Figure 4.8. Fluorescently labelled M1 GAS pilus proteins physically interact with TLR2. Flow cytometry was used to analyse the interactions between TLRs expressed on HEK-293 cells and fluorescently labelled (A) AP1 or (B) BP. Untreated HEK-Blue hTLR2 was used as a negative control and proteins were also tested against HEK-Blue hTLR4. Fluorescence intensity was recorded for 30,000 events per group. Mean fluorescence intensity data was standardised against unstained control cells and is shown as bar graphs with mean±S.D from three independently performed experiments. Statistical significance was determined using one-way ANOVA followed by Holm-Šídák multiple comparisons test. ***P< 0.001 compared to untreated negative control.

4.2.4   Pilus proteins compete with TLR2 antagonist for receptor interactions

With both ELISA and flow cytometry based assays corroborating the binding of AP1 pilus protein to TLR2, a cell based competition assay was conducted to confirm the specificity of this interaction, and investigate whether this interaction was triggering stimulation of TLR2 and downstream immune signaling. In this assay THP-1 cells seeded into a 96 well plate were co-incubated with AP1 or BP alongside increasing concentrations of the TLR2 antagonist staphylococcal superantigen-like protein 3 (SSL3), derived from *Staphylococcal aureus* bacteria. SSL3 binds to the convex face of TLR2 and partially covers the lipopeptide binding pocket of the receptor, preventing further protein association and receptor stimulation (259). Therefore in the context of this assay, as the concentration of SSL3 is increased, decreased interaction between TLR2 and pilus proteins would be expected as the two ligands would compete for the same binding sites. If the pilus proteins activate TLR2, the competition with SSL3 for TLR2 binding sites will be reflected in changes to TNF secretion downstream of TLR2 stimulation. To test this conjecture, following an overnight incubation, the cell supernatant was collected from treated cells and the levels of TNF were quantified using an ELISA, with TNF production in the absence of SSL3 used as a baseline to calculate relative change in cytokine secretion. For both THP-1 cells incubated with BP (Figure 4.9A) and AP1 (Figure 4.9B), as the concentration of co-incubated SSL3 protein increased, the relative TNF production decreased. This indicates that as SSL3 displaced pilus subunits from TLR2, stimulation of the receptor decreased, affirming pili mediated TLR2 interaction and activation.

Figure 4.9. M1 GAS pilus proteins compete with SSL3 for TLR2 binding sites. Increasing concentrations of TLR2 antagonist SSL3 and BP (A) or AP1 (B) at 1 nM were co-incubated with THP-1 cells overnight. Cell supernatant was then harvested and secreted TNF concentration quantified using ELISA. Experiment was performed in duplicate and data shown as mean±S.D. One representative of three independently performed experiments is shown. Non-linear regression fitted using three-parameter dose response model on Graphpad Prism.

4.2.5 Pilus proteins activate the TLR2/6 heterodimer

Endogenous TLR2 requires heterodimersation with either TLR1 or TLR6 in order to become activated (260). The crystal structure of TLR2 in its heterodimeric form suggests that this activation requires the involvement of ligand, which stabilises the dimer and facilitates interactions between the intracellular moieties of each individual receptor to initiate downstream signaling (261,262). In order to determine whether TLR1 or TLR6 was interacting with TLR2 in pili mediated TLR2 activation, reporter cell lines co-expressing TLR2 with either TLR1 or TLR6 in the HEK-Blue cell collection were used. Recombinant BP and AP1 were incubated overnight with HEK-Blue hTLR2/hTLR6 or HEK-Blue hTLR1/hTLR2 in HEK-Blue detection substrate before absorbance was read at 655 nm to deduce TLR2 heterodimer activation. HEK-Blue hTLR2/hTLR6 incubated with either BP or AP1 had significantly greater absorbance readings compared to untreated cells, indicative of both pilus proteins activating TLR2 in its TLR2/TLR6 heterodimeric form (Figure 4.10A). On the contrary, a difference could not be discerned between the absorbance of HEK-Blue hTLR2/hTLR1 cells incubated with BP or AP1 and untreated cells, signaling a lack of pili mediated TLR2 activation in the TLR2/TLR1 heterodimeric form (Figure 4.10B).
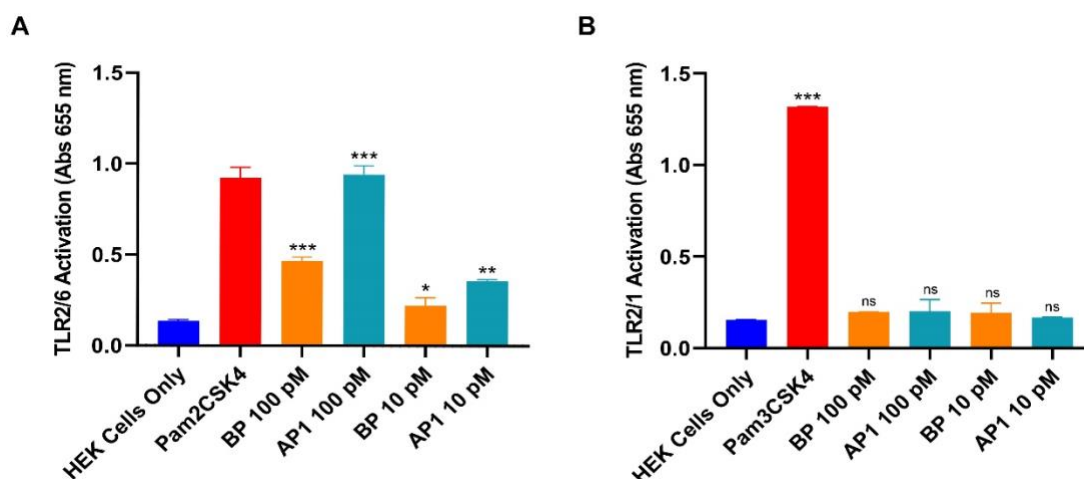
Figure 4.10. M1 GAS pilus proteins activate TLR2 when it is dimerised with TLR6 but not TLR1. (A) HEK-Blue hTLR2/hTLR1 cells or (B) HEK-Blue hTLR2/hTLR1 cells were incubated overnight with recombinant BP or recombinant AP1 or positive control (1 µg/ml Pam2CSK4 for TLR2/6 and 1 µg/ml Pam3CSK4 for TLR2/1) or left untreated. Level of TLR2 activation was determined by measuring absorbance of cell supernatant at 655 nm. Experiments were performed in duplicates and data are shown as mean ± S.D. One representative of three independently performed experiments is shown. Statistical significance was determined by one-way ANOVA, and P-values were calculated by Holm–Šídák's multiple comparisons test. *$P \leq 0.05$, **$P \leq 0.01$, ***$P < 0.001$ compared with the negative control.

Specificity of both BP and AP1 for TLR2/6 was further verified by co-incubating HEK-Blue hTLR2/6 cells in HEK-Blue detection substrate with BP/AP1 and increasing concentrations of the TLR2 antagonist SSL3 for 9 hours. After the incubation period, TLR2/6 activation was measured by recording absorbance at 655 nm, with pilus protein induced TLR2/6 activation in the absence of SSL3 serving as a baseline for the calculation of relative change in receptor stimulation. For both HEK-Blue hTLR2/6 cells incubated with BP (Figure 4.11A) and AP1 (Figure 4.11B), relative TLR2/6 activation decreased as the concentration of co-incubated SSL3 increased, affirming pili mediated TLR2/6 interaction and activation.
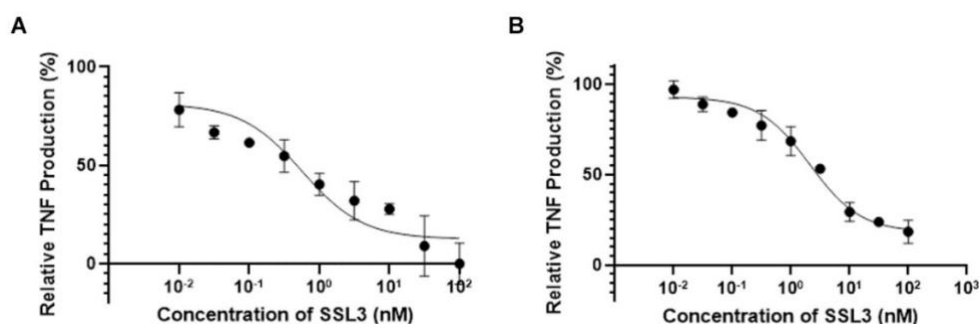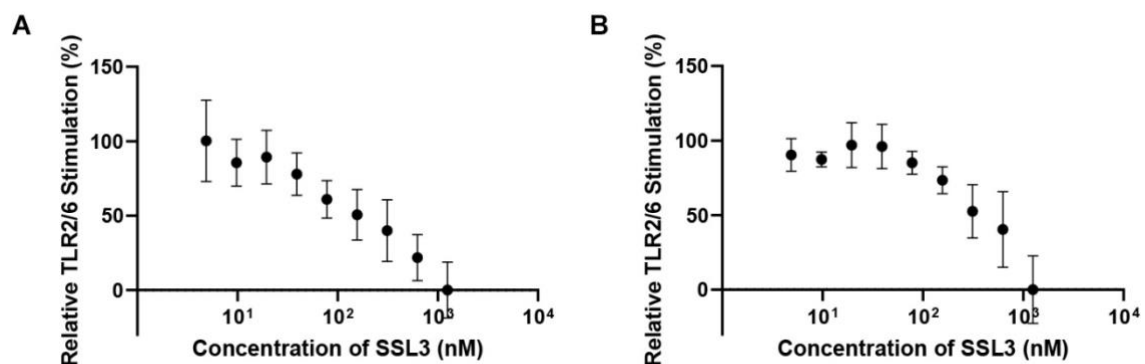

Figure 4.11. M1 GAS pilus proteins compete with SSL3 for TLR2/6 binding sites. Increasing concentrations of TLR2 antagonist SSL3 and BP (A) or AP1 (B) at 4 nM were co-incubated with HEK-Blue hTLR2/6 for 9 hours. Level of TLR2 activation was determined by measuring absorbance of cell supernatant at 655 nm. Experiments were performed in duplicates and data are shown as mean $\pm$ S.D of three independently performed experiments.

With the newfound knowledge of both BP and AP1 specifically interacting with TLR2 dimerised with TLR6, a flow cytometry based binding assay similar to the one reported in Figure 4.8 was performed using HEK-Blue hTLR2/6 cells. Four nanomole each of the BP and AP1 proteins labelled in Figure 4.7 were mixed and incubated with 5×10^5 HEK-Blue hTLR2/6. Proteins were also incubated with 5×10^5 HEK-Blue hTLR4 to account for any non-specific binding to the HEK cell aside from TLR2/6. Cells were analysed on a flow cytometer after undergoing wash steps to remove unbound proteins and mean fluorescence intensity was recorded as a representation of the relative amount of cell bound pilus protein. In line with the flow cytometry assay described in Figure 4.8, HEK-Blue hTLR4 cells incubated with the fluorescent proteins did not have a fluorescence signal distinctly higher than untreated negative control cells. This indicated a lack of interaction between the pilus subunits and TLR4, as well

as additional HEK cell surface molecules. In contrast, HEK-Blue hTLR2/6 cells incubated with fluorescently labelled BP had statistically significantly higher mean fluorescence intensity compared to untreated HEK-Blue hTLR2/6 cells, with 3.2-fold (P= 0.004) greater mean fluorescence recorded. This indicated binding between the labelled BP subunits and TLR2/6, an interaction which was not observed between labelled BP and TLR2. Aligned with observations from the HEK-Blue hTLR2 flow cytometry assay, fluorescently labelled AP1 was also depicted binding to TLR2/6, with HEK-Blue hTLR2/6 cells incubated with fluorescently labelled AP1 demonstrating 5.2-fold (P< 0.001) higher mean fluorescence intensity compared to untreated HEK-Blue hTLR2/6 cells.
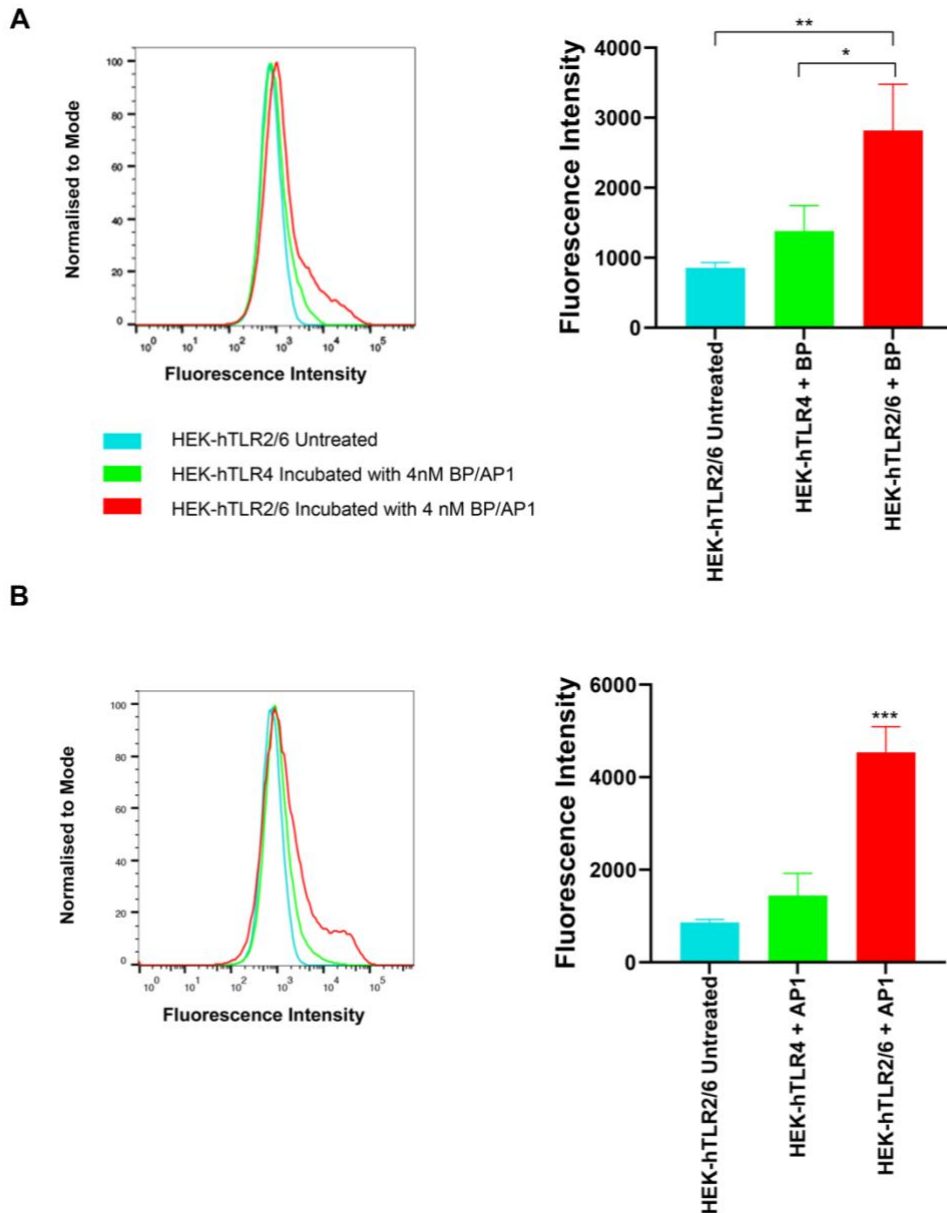
Figure 4.12. Fluorescently labelled M1 GAS pilus proteins physically interact with TLR2/6. Flow cytometry was used to analyse the interactions between TLRs expressed on HEK-293 cells and fluorescently labelled (A) AP1 or (B) BP. Untreated HEK-Blue hTLR2/6 was used as a negative control and proteins were also tested against HEK-Blue hTLR4. Fluorescence intensity was recorded for 30,000 events per group. Mean fluorescence intensity data was standardised against unstained control cells and is shown as bar graphs mean±S.D from three independently performed experiments. Statistical significance was determined using one-way ANOVA followed by Holm-Šídák multiple comparisons test. *P ≤ 0.05, **P ≤ 0.01, ***P < 0.001 compared to untreated negative control.

4.3   Discussion

Antecedent assays illustrated the ability of pilus proteins to cultivate an inflammatory response and to activate TLR2. This chapter expanded on the existing knowledge around the pilus protein subunits and their relationship with TLR2, firstly via different forms of binding assays to demonstrate physical interactions between the two structures.

The objective was initially attempted by utilising surface plasmon resonance (SPR). This optical technique depicts interactions between proteins passed over a chip and receptors immobilised on the chip surface by recording changes in refraction of light directed to the chip surface following binding events. This allows for measuring 'real-time' ligand-receptor association ('on-rate') and dissociation ('off-rate") and calculation of the equilibrium dissociation constant ('binding constant', kD) (263). However, in this research binding between the pilus proteins and TLR2 was highly variable between repeats, with fluctuations becoming more apparent as time progressed (Figure 4.5). Due to the sensitivity of this method, aggregate accumulation at the sensor surface can have a substantial effect on refraction and in turn, the binding constants (264). This is exemplified in SPR assays using soluble T-cell receptors, where there was an extremely limited window for data collection before the apparent dissociation constant fluctuated due to the tendency of the receptors to aggregate, resulting in the inability to amass adequate measurements (264,265). SPR experiments studying antibody binding also demonstrated an increase in signal variability when higher analyte concentrations were utilised, pertinent to the aggregating properties of the molecules (266). Assays comparing aggregation of wild type GAS and pilus deletion mutants have established the auto-aggregative properties of pilus, which appear to coalesce over the course of several hours (37,39). Thus it is probable that pilus proteins began to aggregate during the prolonged data collection period (up to 10 hours), resulting in the binding constant shifting as the read through progressed.

A plate based binding assay was employed to bypass the problems faced by SPR attributed to the aggregative properties of the pilus proteins. This assay utilised significantly lower concentrations of proteins and short incubation times, reducing the possibility and subsequent effect of homophilic protein interactions. Binding of the AP1 subunit to TLR2 was captured by this method of analysis, with increasing concentrations of AP1 incubated with the receptor resulting in increased absorbance (Figure 4.6). Results from the flow cytometry assays reiterated these outcomes, with AP1 binding to TLR2 expressed on HEK cells (Figure 4.8).

The lack of pilus protein adhesion to HEK-Blue hTLR4 further endorsed the specificity of pilus proteins interaction with TLR2, as this was indicative of the proteins associating with the cells solely through this receptor and not establishing nonspecific binding to other cell surface components. Although TLR2 recognises a wide scope of both Gram negative and Gram positive bacterial products, the majority of reported TLR2 ligands contain lipid moieties and few proteinaceous ligands have been chronicled (267). The binding assays in this chapter attempted to addressed this gap in the literature and cement the notion of GAS pilus proteins interacting with TLR2. Curiously, despite BP exhibiting activation of TLR2 cells expressed on HEK-Blue hTLR2 in our preliminary investigation (206), the binding assays in this chapter were unable to capture direct binding of this subunit to TLR2. Notably, protein-receptor association was not recorded despite the concentration of BP co-incubated with HEK-Blue hTLR2 in the flow cytometry assay being greater than the concentration of protein previously used to demonstrate BP mediated TLR2 activation in these cell lines. This seems contradictory as BP must interact with TLR2 to mediate its activation but this association to the receptor could not be demonstrated. One possible source for this discrepancy may be BP having low affinity for monomeric TLR2.

Although TLR dimerisation is often simply regarded as a result of ligand binding, there are some cases where the dimerisation event is simultaneously vital for formation of a stable receptor ligand complex. For example, although meningococcal PorB did bind to monomeric TLR2, binding increased over two-fold and receptor stimulation increased 5-fold when the porin was incubated with TLR2 in its heterodimeric TLR2/TLR1 form (268). In the case of TLR3, ligands failed to bind completely upon inhibition of TLR3 dimerisation (269). In this vein, BP binding to TLR2 may be severely reduced when the receptor is in its monomeric form and it is possible that robust binding to the receptor can only occur when TLR2 creates a binding site in conjunction with TLR6 or TLR1. Specific but low affinity interactions are often missed when undertaking adhesion assays with wash steps, such as the methods described in this chapter, due to dissociation of the ligand during these intermediate processes (270,271). This phenomenon may have occurred when BP was incubated with TLR2 in the solid-phase binding assay, which utilised recombinant TLR2 consisting solely of monomeric forms of the receptor. The multiple wash steps within the assay may have directed BP dissociation from TLR2, resulting in the weak interaction to the monomeric receptor eluding detection. The flow cytometry binding assay used HEK-Blue hTLR2, which express low levels of TLR1 and TLR6,

allowing for some extent of dimerisation events to occur. However, these receptors are heavily outnumbered by the abundance of overexpressed TLR2. While BP may have been able to tightly interact with the small number of TLR2 dimerised to the low expression endogenous TLRs on the HEK-Blue hTLR2 cells, the majority of BP-receptor interactions would have occurred between the pilus subunit and the overexpressed monomeric TLR2 molecules. Thus wash steps prior to the fluorescent measurements is likely to have removed the bulk of BP subunits interacting with TLR2, resulting in a cellular fluorescent signal not significantly different to untreated cells. On the other hand, as AP1 binding to TLR2 was recorded in these wash-type adhesion assays, it is likely that the subunit has less dependence on receptor dimerisation for stabilised binding. It should also be noted that unlike the binding assays performed using flow cytometry described herein, the TLR2 activation assay using the HEK-Blue hTLR2 cells in our previous work did not include any wash steps, with no manipulations performed to the protein/cell suspension during the 9 hour incubation period (206). On top of the small amounts of TLR2 heterodimers formed as a result of the low levels of endogenous TLR6 and TLR1 expression, this likely resulted in enough sustained BP-TLR2 interactions over the extended incubation period, despite potentially weaker binding to the monomeric receptor, to allow downstream TLR2 activity to be recorded. Despite the difficulty in directly observing BP binding to TLR2, the competition assay using SSL3 provided indirect evidence to substantiate this event occurring.

TLR2 heterodimersation with TLR1 or TLR6 is critical for initiation of the signaling cascade which induces an inflammatory response (260). The dimerisation event brings the associated intracellular domains of the two receptors in close enough proximity to consolidate a signaling scaffold, which facilitates recruitment of adaptor proteins, such as MyD88. These proteins in turn mediate downstream activation of transcription factors, which upregulate inflammatory mechanisms such as the production of pro-inflammatory cytokines (272,273). Thus in order for a ligand to induce TLR2 mediated immune responses, it must possess the ability to associate with both TLR2 and either TLR1 or TLR6. This results in ligands with specificity for TLR2 but not TLR1 or TLR6, such as SSL3, inhibiting inflammatory responses by occupying available binding sites and preventing TLR2 dimerisation (259,274). The cell based competition assay illustrated monocytic THP-1 cells, which express TLR2 and its dimer partners, co-incubated with SSL3 and either BP or AP1 exhibiting decreased cytokine secretion as the concentration of SSL3 was increased. This exemplified the pilus proteins competing

with SSL3 for TLR2 binding sites, as well as confirming that the subunits were inducing cytokine release downstream of TLR2, instead of simply binding to the receptor (Figure 4.9). This consolidated the pilus proteins as TLR2 agonists. On these THP-1 cells, where TLR2s were able to heterodimerise and there were no washing processes propelling dissociation of weaker affinity interactions, the amount of SSL3 required to displace either BP or AP1 from the receptor was at comparable concentrations.

Although several other bacterial pili/fimbriae have been touted as TLR2 agonists, the GAS pilus appears to be one of the few pili with protein monomers which can individually act as agonists for this receptor. While whole *Lactobacillus rhamnosus* pili stimulated TLR2, it was found that recombinant proteins of the pilus subunits failed to demonstrate measurable activity, leading to speculation that polymerisation of pilus subunits was required to form the topology and protein folds that could be recognised by the receptor (275). In the instance of *Streptococcus pneumoniae* pili, one ancillary protein was pinpointed as the subunit responsible for TLR2 stimulation but it was found that potent receptor activation required presentation in an oligomerised macromolecular form (210). Conversely, as seen illustrated in our previous publication and this chapter, both recombinant, monomeric BP and AP1 appear to be TLR2 agonists, indicating that the pilus proteins can induce inflammation on their own without assembly (206).

Incubation of BP and AP1 with HEK-Blue hTLR2/6 resulted in the upregulated release of the reporter protein downstream of TLR2/6 activation, whereas reporter protein downstream of TLR2/1 stimulation was not secreted when pilus proteins were incubated with HEK-Blue hTLR2/1 (Figure 4.10). This signified that both pilus proteins were associating with TLR2 in its TLR2/6 heterodimer form. Furthermore, a competition assay utilising the HEK-Blue hTLR2/6 cell line, where AP1 or BP was co-incubated with SSL3, indicated decreased TLR2/6 activation as the concentration of SSL3 was increased (Figure 4.11). This again demonstrated competition between the pilus proteins and a TLR2 antagonist for the TLR2 binding interface and further verified the pilus subunits binding to and activating TLR2 heterodimerised with TLR6. TLR2 recognises a wide variety of microbial cell surface constituents and is regarded as one of the most promiscuous TLRs. Whilst other TLRs are functionally active in a single homodimeric form, the ability of TLR2 to form two different heterodimers accounts for this broad spectrum of ligands (276). As indicated by crystallography, the binding pocket of TLR2

is lined with hydrophobic residues ideal for accommodating lipids and this lipid binding pocket is extended by TLR1, allowing for ligand binding mainly driven by hydrophobic chains (261). On the other hand, crystallography indicated that TLR6 has a binding pocket approximately half the size of TLR1, and thus ligand binding to the TLR2/TLR6 dimer is additionally heavily dependent on bridging hydrogen bonds between ligands TLRs (262). As documented through crystallization modelling, lipid moieties play a major role in agonist driven TLR2 heterodimersation and previously identified TLR2 agonists have exceedingly been lipids or proteins with post-translation lipid modifications (262,267). In fact, some bacterial proteins added to the list of TLR2 ligands have been redacted upon further investigation revealing that removal of lipid contaminants resulted in TLR2 no longer recognising the structure (277). Thus, there was considerable possibility of intrinsic lipidation attributing to the ability of GAS pilus subunits to interact with TLR2. However, online bioinformatics analysis using GPS-Lipid (28) suggests that the mature form of BP used in this chapter did not have a lipidation site and lipidation was not reported following resolution of the crystal structure of the subunit and mass spectrometry (67,278). Bioinformatics analysis indicated that AP1 had a small chance of palmitoylation at just one cysteine residue site. There is a chance that AP1 lipidation at this cysteine enhances binding to TLR2, whereas non-palmitoylated BP has less stringent association and may therefore be relying on hydrogen bonds with TLR6 to securely dock into the TLR2 heterodimer. However, this is merely speculative as the association of each protein to the receptor components is yet to be modelled. Moreover, this post-translation lipidation of AP1 appears to be reversible and in the case of the recombinant protein utilised throughout this chapter, it has not been confirmed if *E. coli* is able to actuate this modification in the same manner as GAS (278). Overall it appears highly probable that both pilus proteins directly bind to TLR2.

Upon confirmation of the pilus subunits signaling through TLR2 specifically when dimerised with TLR6, the flow cytometry binding assay using fluorescently labeled pilus subunits was repeated with HEK-Blue hTLR2/6 cells. Both pilus subunits were captured binding to the TLR2/6 heterodimers on the HEK cell surface, directly illustrating BP/AP1 binding to TLR2/6 (Figure 4.12). This provided more concrete evidence of TLR2 recognition of BP, which the solid-phase and previous flow cytometry based binding assays failed to capture. While BP association with TLR2 was not depicted by flow cytometry when HEK-Blue hTLR2 cells were utilised, applying the same methodology to HEK-Blue hTLR2/6 cells successfully captured

this interaction. This reconsolidated the theory explored extensively above that TLR2 heterodimersation was required for BP to robustly bind to the receptor. Identification of the exact binding mechanism of pilus proteins to TLR2/6 could be conducted in the future via co-crystallisation analysis to further clarify the physical association between BP and TLR2/6. There are only a small number of non-lipidated microbial compounds that have been identified to directly bind to TLR2 and these include SSL3, the meningococcal porin PorB and fungal chitin (259,279,280). All of the non-lipidated microbial peptides so far characterised have either been TLR2 antagonists with the ability to block receptor dimerisation, or have had specificity for TLR2/1. Therefore, the GAS pilus proteins are unique in that they are one of the first non-lipidated microbial proteins to directly associate with the TLR2/6 heterodimer.

The ramifications of the pilus proteins being TLR2 agonists extend beyond the immediate innate immune response generated, as the activated receptors can act as a bridging mechanism to promote humoral adaptive immune responses (256,281). TLR2 activation can upregulate a myriad of immune functions which collectively enhance antibody responses towards a target antigen. Firstly, TLR2 stimulation has been associated with early recruitment of dendritic cells with the capacity to present antigens to adaptive immune cells, ensuing higher antibody levels downstream (282). Moreover, activated TLR2 appears to recruit an enzyme that inhibits the formation of podosomes, which are adhesive structures utilised by dendritic cells for migration. The subsequent transient loss of migratory capacity allows for extended periods of contact between dendritic cells and antigens at inflammatory sites (283). Signaling downstream of TLR2 has been observed to facilitate T cell differentiation into effector T cells with the ability to upregulate antibody production. For instance, TLR2 agonists can upregulate the release of IL-13 and IL-5, and the expression of the co-stimulator ICOS, which facilitate Th2 and Tfh differentiation respectively (144,284–286). Moreover, activation of TLR2 expressed on B cells themselves have also been found to direct differentiation of these cells into antibody secreting plasma cells (287). As pilus proteins activate TLR2, they are likely to possess the ability to enhance antibody production through such processes and may be developed into effective vaccine adjuvants. The following chapters thus focus on investigating the adjuvant activity of GAS pilus proteins.

Chapter 5: Generation and validation of pilus protein fusion peptides

The preceding chapters establishing the GAS pilus proteins as immunostimulatory complexes with low risk of inducing detrimental inflammation suggested the possible suitability of the pilus proteins as vaccine adjuvants. Several bacterial TLR ligands have been explored for their adjuvant activity based on their ability to potentiate immune responses. The innate immune cell response augmented by these ligands include trafficking of cells, heightened antigen processing and presentation, up-regulation of adaptive immune cell co-stimulation receptors and the release of cytokines modulating adaptive immune cell maturation (288–290). These process in turn enhance adaptive immune cell activity and combined with the direct interaction of ligands and TLRs on B cells, amplifies B cell antibody production (288). For this reason, bacterial TLR ligands can be used as a tool to heighten the response to poorly immunogenic vaccines, which have become more commonplace with the rise of protein subunits replacing whole attenuated pathogens in vaccine formulations (289). As illuminated in the last chapter, GAS pilus proteins' specificity for TLR2 makes it a particularly promising potential adjuvant for vaccines which are designed to elicit production of protective antibodies. This is due to TLR2 activation having the ability to skew the immune response towards the generation of antibodies (267,288,291). This would be of particular use for vaccinations against infectious pathogens. It was thus determined that the adjuvanting capability of GAS pilus proteins would be explored, via examination of the proteins' effects on antibody response to a target antigen.

The influenza A matrix 2 protein (M2) was selected as the target antigen for testing the adjuvanting proficiency of the pilus proteins. M2 is a viroporin which is also incorporated into budding virions (292). Of particular interest is the 24-amino acid extracellular N-terminal domain with the sequence MSLLTEVETPIRNEWGCRCNDSSD, referred to as M2e (293). Cells infected with influenza A virus express copious amounts of M2, with M2e protruding from the cell surface (294,295). Studies in mice have shown that M2e elicits the production of protective antibodies, which work effectively against both homologous and heterologous strains of influenza A virus (296). The M2e antigen has garnered particular interest as a universal influenza A virus vaccine candidate due to the high levels of conservation observed across all influenza A strains and the lack of selection pressure, resulting in low antigenic shift (297). In contrast, hemagglutinin (HA), the current standard antigen for influenza vaccines, is

highly strain specific and prone to antigenic drift, resulting in the need for constant vaccine reformulation over time (298). However, M2e has not yet been successfully adopted into commercialised, circulating vaccine formulations due to its weak immunogenicity. This is likely due to its small size, low copy numbers in virions and the probable shielding of the antigen from immune cells by the larger influenza A surface proteins (299). Accordingly, M2e based vaccine formulations would greatly benefit from the addition of an adjuvant to encourage robust antibody production. This chapter covers the generation and validation of M2e-pilus protein formulations produced in preparation for the immunisation studies inspecting the adjuvanticity of pilus proteins.

5.1   Expression and purification of pilus protein-antigen fusion proteins

TLR ligands can be incorporated into vaccine formulations as adjuvants in two ways. The most straightforward method is to mix the proteins with antigen. Alternatively, they can be conjugated to the target antigen to create an adjuvant-antigen complex, where each individual immune stimulant is co-delivered with an antigen (300). The TLR ligand-antigen fusion proteins appear to induce better immune responses than their non-conjugated counterpart formulations, leveraging their use in vaccines. For instance, TLR ligand-adjuvant fusion proteins appear to enhance uptake and presentation of antigens by APCs, with studies indicating up to a 100-fold increase in uptake by DCs when the antigen was fused to the adjuvant as opposed to being delivered as an un-conjugated mixture (301,302). In addition, dendritic cell maturation and activation appears to be more pronounced when TLR4 agonist heat shock proteins are delivered to cells conjugated to the antigen, corroborated by higher levels of cytokine secretion and activation marker expression (303). Further downstream, protein antigens fused to the TLR5 agonist flagellin have been reported to demonstrate superior ability to induce T cell proliferation and T cell clustering compared to equimolar mixtures of separated flagellin and antigen (304). Resultantly, a wide range of adjuvant-antigen complexes have been observed to elicit higher levels of protective antibody production compared to their non-conjugated counterpart mixtures (302,305,306).

Although not yet entirely understood, the augmentation of immune response achieved by conjugation of protein adjuvants to antigens is thought to largely be a result of this system allowing simultaneous co-delivery of the vaccine components to immune cells at a fixed molar ratio (300). TLR ligand-antigen fusion proteins have been found to bind to TLRs specifically

recognising the adjuvant portion of the peptide, thereby efficiently targeting the antigen to relevant TLR expressing immune cells such as APCs. Examples of this include flagellin-antigen conjugates targeting TLR5 on DCs and monophosphoryl lipid A targeting myeloid DC TLR4. This co-delivery additionally cultivates a state of synergy where the adjuvant section of the fusion protein amplifies immune cell activation to encourage uptake of the antigen, which in turn primes the cell to upregulate TLRs, increasing interactions with the adjuvant portion of the fusion proteins (300,307). This is in contrast to a mixture of separate adjuvant and antigen molecules, where antigens do not receive adjuvant directed delivery to relevant immune cells and are thus more likely to elicit off-target effects. Furthermore, the two components are likely to be taken up independently by different cells resulting in varied ratios of molecules delivered and cell to cell fluctuations in the immune responses generated (302).

An assortment of different molecules have been identified to be potential TLR ligand adjuvants, including proteins, lipoproteins, lipopeptides, oligosaccharides and oligonucleotides (308,309). In the context of producing TLR ligand-antigen conjugated formulations, ligands of protein nature have the benefit of having a more straightforward conjugation process compared to the other types of molecules. Proteins can be conjugated to the antigen by molecular cloning at the DNA level to mass produce both components simultaneously as a single complex (310). On the other hand, the other type of molecules require individual preparation and chemical conjugation, a process which can be very expensive and time consuming (311,312).

In accordance to this information, it was concluded that the adjuvanting capacity of the TLR2 specific GAS pilus proteins could be maximized by conjugating the proteins to the M2e antigen. Thus pilus protein-M2e fusion proteins were synthesised to test the potential of GAS pili as an adjuvant. This required the construction of expression plasmids containing pilus protein-M2e fusion genes, which could then be transformed into *E. coli* BL21 (DE3) for high level recombinant protein expression. The initial design consisted of producing fusion genes for expression of conjugate proteins consisting of M2e fused to either the N or C terminus of BP (M2e-BP and BP-M2e) or AP1 (M2e-AP1 and AP1-M2e).

5.1.1 Expression and purification of GST-M2e-BP and GST-BP-M2e

The BP subunit is encoded by the *spy0128* gene. Thus primers (sequences provided in Table 2.2) specific to the 5' and 3' ends of the *spy0128* gene were designed to amplify the BP-

encoding sequence without the N-terminal signal peptide and the C-terminal cell wall anchor motif from the genomic DNA of GAS M1 SF370 strain. Two versions of this DNA fragment were produced, one with flanking EcoRI restriction sites and one flanked by BamHI restriction sites. The amplified gene sequences were subsequently inserted into the pGEX-3C vector containing the *m2e* sequence and an ampicillin resistance gene, as per Figure 5.1A. The pGEX-3C-M2e plasmid was generated previously by Dr Catherine Tsai (UoA) by inserting the *m2e* sequence between the BamHI and EcoRI sites within the MCS. Thus s*py0128-m2e* was created by BamHI restriction digestion of the plasmid, which allowed the s*py0128* sequence flanked with BamHI restriction sites to be inserted preceding the *m2e* sequence. Conversely, *m2e-spy0128* was generated by EcoRI digestion of the plasmid, which allowed s*py0128* flanked with EcoRI restriction sites to be inserted downstream of the *m2e* sequence (Figure 5.1A). Insertion of *spy0128* into the pGEX-3c vector in the correct orientation was confirmed by performing PCR using *m2e* and *spy0128* primers as detailed in Table 2.2, with successful cloning of both the ~850bp *spy0128-m2e* (Figure 5.1B) and ~850bp *m2e-spy0128* (Figure 5.1C) confirmed following visualisation on agarose gels. The resulting plasmids containing the fusion gene were transformed into *E. coli* BL21 (DE3) cells harbouring a chloramphenicol resistance gene and successful transformations were selected on LB plates containing both ampicillin and chloramphenicol.
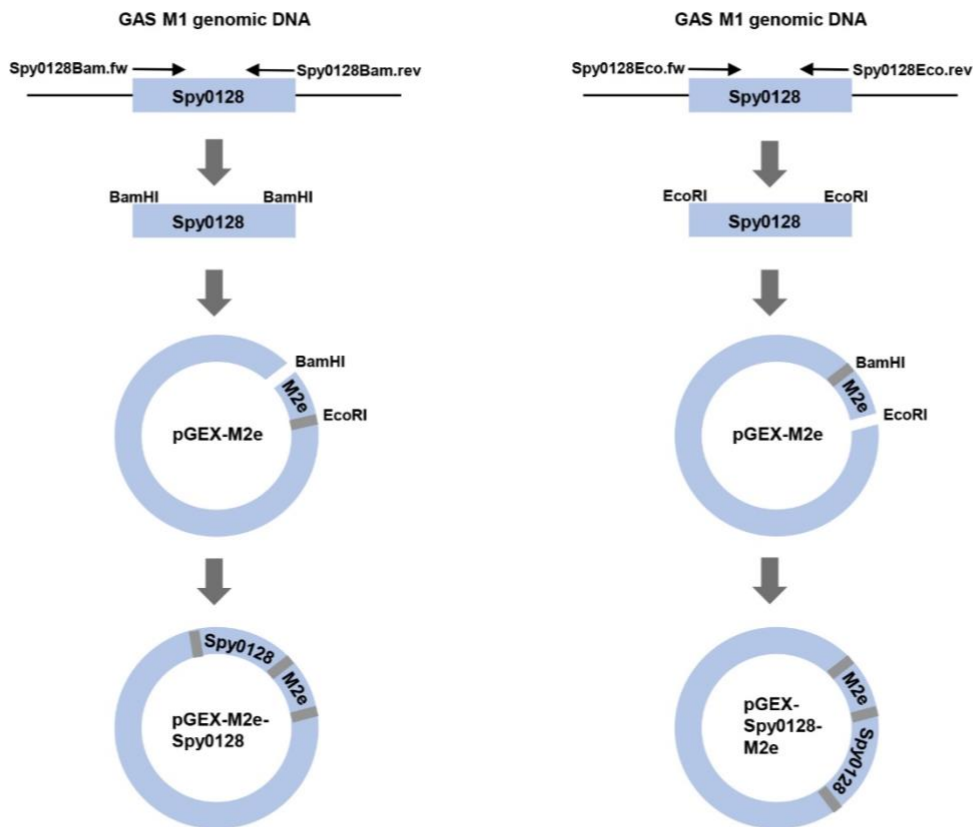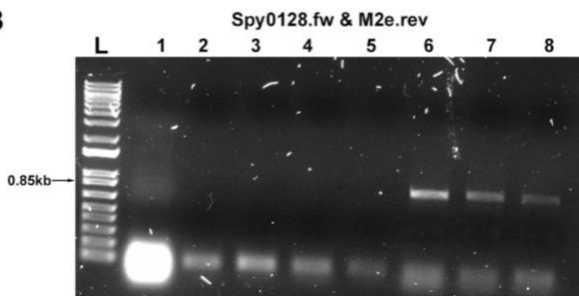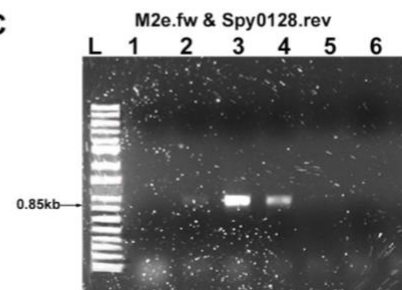
Figure 5.1. Cloning strategy for generating BP and M2e fusion protein gene constructs.(A) Schematic diagram of the *spy0128* gene being amplified from GAS genomic DNA and being inserted into pGEX-3C vector containing the DNA encoding the M2e peptide. (B) Successful cloning of *spy0128-m2e* confirmed by performing diagnostic PCR using appropriate primers and the results were visualised on 1% agarose gel. (C) Successful cloning of *m2e-spy0128* confirmed using appropriate primers and visualised on agarose gel. L, 1 kb plus DNA ladder

The BL21 (DE3) *E. coli* pGEX-3C *spy0128-m2e* and BL21 (DE3) *E.coli* pGEX-3C *m2e-spy0128* expression systems produced GST-BP-M2e and GST-M2e-BP fusion proteins respectively, with both proteins harbouring an N-terminal glutathione-S-transferase (GST) tag.

This GST tag at the N terminus helped maintain correct folding of the proteins and allowed for straightforward affinity purification of the fusion peptides by capitalising on the high affinity of GST to the reduced form of glutathione. As detailed in 2.2.3.6, sonicated bacterial lysate from BL21 (DE3) *E. coli* expressing GST-BP-M2e or GST-M2e-BP was loaded onto the glutathione column and subsequently subjected to elution with reduced glutathione in order to release proteins bound to the column via the GST moiety. Both the eluate containing GST-BP-M2e and GST-M2e-BP were collected as 2-ml fractions and visualised using SDS-PAGE (Figure 5.2A and B). Both gels illustrated the presence of protein bands in each fraction about ~50 kDa to ~60 kDa, indicating successful purification of the soluble fusion proteins consisting of ~26 kDa N-terminal GST tag followed by the ~30 kDa BP and M2e conjugated peptide (Figure 5.2A and B). Fractions containing the recombinant proteins, which were obtained with >95% purity, were pooled together and dialysed against PBS overnight before storage at -20 °C for use in future assays.
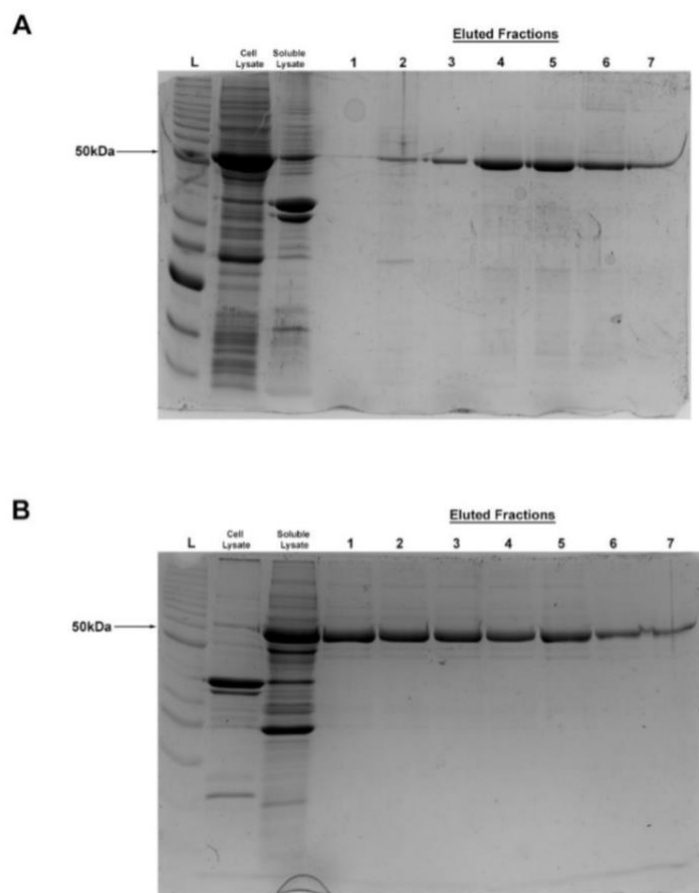
Figure 5.2. Purification of BP and M2e fusion proteins using glutathione affinity chromatography.(A) The soluble fraction of bacterial lysate from *E. coli* BL21 (DE3) pGEX-3C *spy0128-m2e* was passed through the glutathione column and the ~50 kDa GST-BP-M2e fusion peptide was collected in 2-ml fractions after elution with reduced glutathione. (B) The process was repeated using soluble fraction of bacterial lysate from *E. coli* BL21 (DE3) pGEX-3C *m2e-spy0128* to purify the ~50 kDa GST-M2e-BP fusion peptide. L; protein ladder.

5.1.2   Expression and purification of His-AP1(LPXTG)-M2e and His-AP1-M2e

The AP1 pilus subunit is encoded by the *spy0125* gene. Thus generation of the fusion protein of M2e and AP1 with the LPXTG motif was initiated with the amplification of the AP1(LPXTG) encoding sequence from pBC vector containing the full-length *spy0125* sequence. The primer pair listed in Table 2.2 was employed to generate *spy0125(lpxtg)* with BamHI and XhoI restriction enzyme sites at the 5' and 3' ends, respectively, and this DNA was inserted into the pPROEX-Htb vector (containing an ampicillin resistance gene) as illustrated in

Figure 5.3A. This was followed by insertion of the *m2e* sequence, which was synthesized using the primer pair indicated in Table 2.2 (

Figure 5.3A). In order to ensure all components of the resulting *spy0125(lpxtg)-m2e* fusion gene were inserted into the pPROEX-Htb vector in the correct orientation, a PCR was performed using an internal *spy0125* forward primer and the *M2e.rev* primer, which read from the end of the *m2e* sequence, as detailed in Table 2.2. Visualisation of the PCR fragments on agarose gel indicated the desired ~500 bp read through of the *spy0125(lpxtg)-m2e* sequence, verifying successful cloning (

Figure 5.3B).

This process was repeated to additionally generate the gene sequence for a fusion protein of M2e and mature AP1 without the LPXTG motif. Using the pBC *spy0125* vector as a template once more, primers listed in Table 2.2 were deployed to produce the *spy0125* gene, without the sequence encoding the LPXTG motif, sandwiched between BamHI and SalI restriction enzyme sites at the 5' and 3' ends respectively (

Figure 5.3C). This DNA fragment was subsequently inserted into the pPROEX-Htb vector, followed by synthesis and insertion of the *m2e* sequence to produce the *spy0125-m2e* fusion gene (

Figure 5.3C). Insertion of all gene sequences into pPROEX-Htb in the appropriate orientation was verified via PCR with the internal *spy0125* and *m2e.rev* primers used previously on *spy0125(lpxtg)m2e*. This resulted in the desired ~500 bp PCR product, as depicted on agarose gel, which confirmed successful cloning (

Figure 5.3D). The ensuing plasmids containing the fusion genes were subsequently transformed into *E. coli* BL21 (DE3) cells containing a chloramphenicol resistance gene and plated on LB plates with ampicillin and chloramphenicol to select successful transformations.

A

Spy0125Bam.fw → **Spy0125** ← Spy0125Sal.rev

PBC-
Spy0125
LPXTG

M2e.fw → ← M2e.rev

BamHI **Spy0125** SalI

XhoI **M2e** XhoI

BamHI **pPROEX** SalI

BamHI **Spy0125** SalI
pPROEX-
Spy0125

BamHI **Spy0125** SalI
pPROEX-
Spy0125

Spy0125 **M2e**
pPROEX-
Spy0125-M2e

B

CpaXho_fla.fw & M2e.rev

L 1 2 3 4 5 6 7 8 9

0.5kb →

C

Spy0125Bam.fw → **Spy0125** ← Spy0125LPXTGXho.rev

PBC-
Spy0125
LPXTG

M2e.fw → ← M2e.rev

BamHI **Spy0125LPXTG** XhoI

XhoI **M2e** XhoI

BamHI **pPROEX** XhoI

BamHI **Spy0125** XhoI
pPROEX-
Spy0125LPXTG

BamHI **Spy0125** XhoI
pPROEX-
Spy0125LPXTG

Spy0125 **M2e**
pROEX-
Spy0125LPXTG-
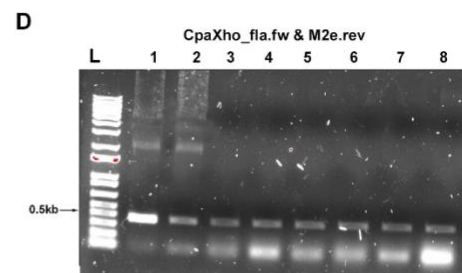M2e

D
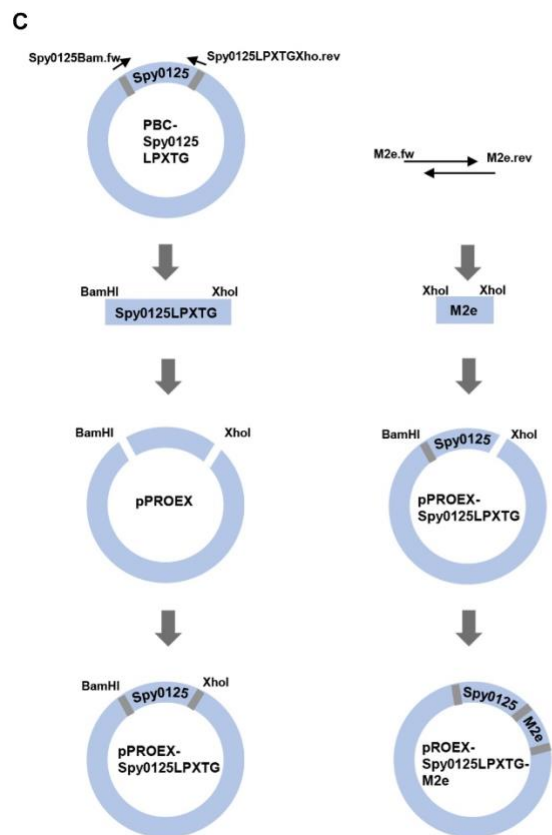
CpaXho_fla.fw & M2e.rev

L 1 2 3 4 5 6 7 8

0.5kb →

117

Figure 5.3. Schematic diagram of cloning strategy for generating AP1 and M2e fusion protein gene constructs.(A) The *spy0125(lpxtg)* gene was amplified from pBC *spy0125* and inserted into pPROEX-Htb vector, followed by synthesis and insertion of the *m2e* gene into this plasmid. (B) Successful cloning of *spy0125(lpxtg)-m2e* was confirmed by performing diagnostic PCR using appropriate primers and the results were visualised on 1% agarose gel. (C) Schematic diagram of cloning strategy for generating AP1 and M2e fusion protein gene constructs. The *spy0125* gene was amplified from pBC *spy0125* and inserted into pPROEX-Htb vector, followed by synthesis and insertion of the DNA encoding the *m2e* peptide into this plasmid. (D) Successful cloning of *spy0125-m2e* confirmed using appropriate primers and visualised on agarose gel. L, 1 kb plus DNA ladder.

The *E.coli* BL21(DE3) pPROEX-Htb *spy0125(lpxtg)-m2e* and *E.coli* BL21(DE3) pPROEX-Htb *spy0125-m2e* expression systems produced His-AP1(LPXTG)-M2e and His-AP1-M2e fusion proteins respectively, with both proteins possessing a N-terminal 6×hisitidine tags (denoted as His). This allowed for immobilised metal-chelate affinity chromatography (IMAC) purification of the complex via the tags' affinity to immobilised nickel ions. As described in 2.2.3.4, sonicated bacterial lysate from BL21 (DE3) *E.coli* expressing His-AP1(LPXTG)-M2e or His-AP1-M2e was loaded onto the nickel column. This was followed by applying an increasing concentrations of imidazole (10-100 mM) to release the polyhistidine tagged proteins from the nickel beads in fractions and visualisation of these eluted fraction on SDS-PAGE. The gel depicting elution fractions of His-AP1(LPXTG)-M2e (Figure 5.4A) illustrated a protein band at the predicted size of the fusion protein (~120 kDa) eluted by 100 mM imidazole. This elution fraction did not contain any other marked protein bands, with >95% purity His-AP1(LPXTG)-M2e. This fraction was thus concentrated and dialysed against PBS overnight and stored at -20 °C, ready for future assays.

The SDS-PAGE gel visualising purified fractions of AP1-M2e (Figure 5.4B) depicted proteins at the predicted size of the fusion protein (~120 kDa) being eluted by 20-100 mM imidazole. This confirmed the presence of His-AP1-M2e fusion protein across multiple elution fractions. However, these fractions appeared to be contaminated with either degraded fusion protein or native *E. coli* proteins, with a particularly distinct band at ~30 kDa evident on the SDS-PAGE (Figure 5.4B). Thus these fractions were concentrated, dialysed against PBS and run through size-exclusion chromatography (SEC) to separate the ~120 kDa AP1-M2e from the lower molecular weight protein contaminants. His-AP1-M2e was eluted with phosphate SEC buffer, with fractions collected at the UV peaks detected by the chromatogram. Visualisation of the protein contents in these fractions on SDS-PAGE marked the elution of the ~120 kDa His-

AP1-M2e occurring predominantly in the first major absorbance peak collected over two fractions (Figure 5.4C, fractions 1, 2). These fractions had relatively high concentrations of His-AP1-M2e and relatively low amounts of other contaminating proteins (~90% purity). The second, less striking absorbance peak collected over the next three fractions (Figure 5.4C, fractions 3, 4, 5) appeared to consist mainly of the lower weight contaminant. Thus the first two fractions were pooled together, concentrated and dialysed against PBS overnight and stored at -20 °C for usage in subsequent assays.
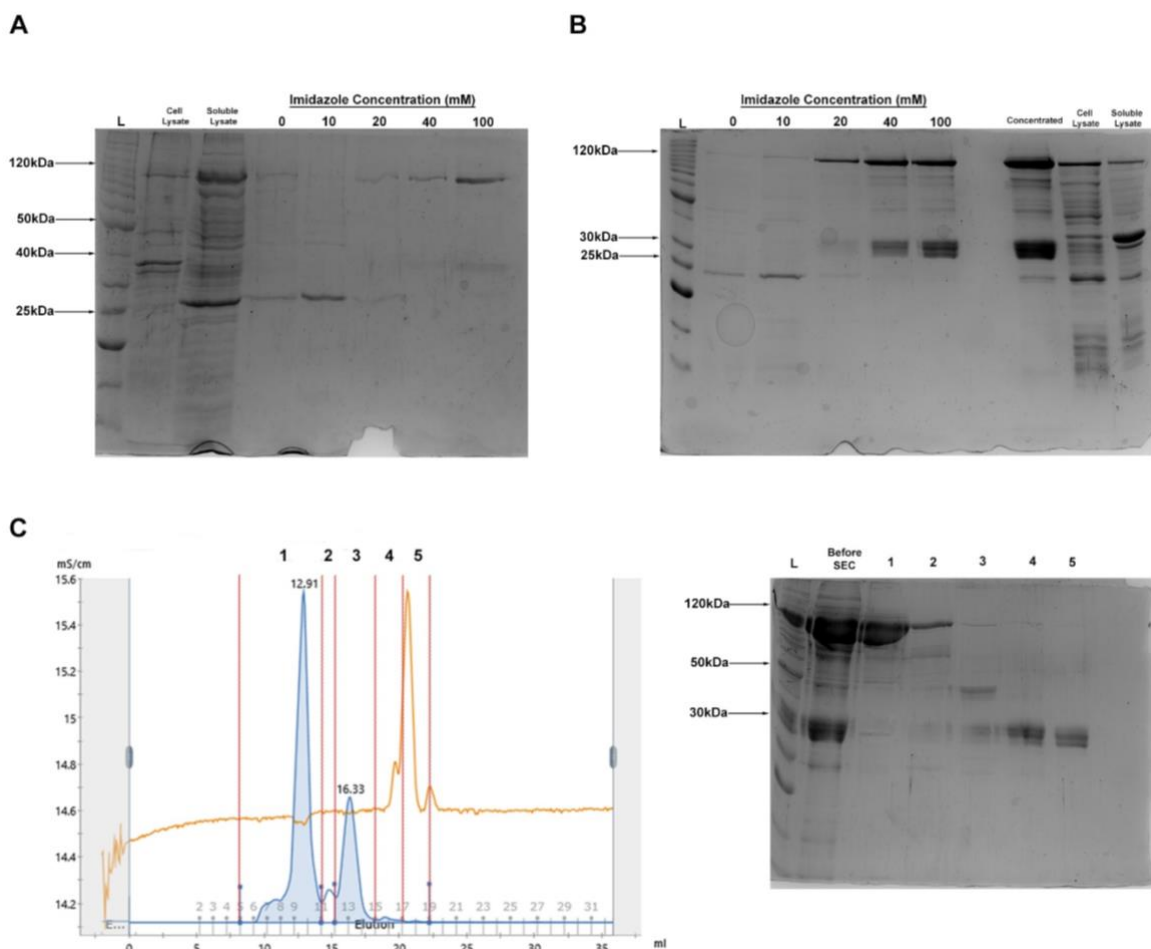
Figure 5.4.Purification of AP11 and M2e fusion proteins using nickel affinity chromatography. (A) The soluble fraction of bacterial lysate from *E. coli* BL21(DE3) pPROEX-Htb *spy0125(lpxtg)-m2e* was passed through the nickel column and the ~120 kDa His-AP1(LPXTG)-M2e protein was collected after elution with increasing concentrations of imidazole and visualised on 12.5% SDS-PAGE (B) Purification of His-AP1-M2e using nickel affinity chromatography. The process was repeated using soluble fraction of bacterial lysate from *E. coli* BL21 (DE3) pPROEX-Htb *spy0125-m2e* (C) Further purification of His-AP1-M2e using using size exclusion chromatography. Fractions from (B) containing His-AP1-M2e were pooled and purified further with size-exclusion chromatography. Fractions collected during the

elution process (fractions 1-5) were analysed with 12.5% SDS-PAGE. Blue line indicates the UV absorbance during the elution period (mAU), with peaks indicating eluted protein. Sections between red lines indicate the points at which fractions were collected. Fraction numbers correspond to numbered lanes on SDS-PAGE. L; protein ladder.

5.2 Validation of pilus protein-M2e fusion proteins

Before they could be used in their final application of studying the adjuvanticity of pilus proteins, the purified pilus protein-M2e complexes required validity testing. The accurate interpretation of pilus immunomodulation experiments using these fusion proteins hinges on the assumption that the recombinant proteins generated contain the protein of interest, are pure and homogenous, and are correctly folded into a functionally active state (313,314).

In the section above, SDS-PAGE gels indicated the presence of protein bands matching the predicted sizes of the fusion complexes and this was used to infer the successful production of the fusion proteins. However, it should be noted that due to its small size, the presence of the M2e peptide cannot be readily confirmed on the SDS-PAGE protein gel by Coomassie staining. Therefore, further testing was required to provide more definite confirmation that the purified proteins incorporated both the M2e peptide and pilus proteins. Thus additional assessments were conducted on the fusion proteins to confirm the integrity of the fusion protein samples generated.

5.2.1 Western blot of fusion proteins

The four fusion proteins purified in the section above were tested on a western blot using antibodies specific for M2e and the pilus proteins to verify their presence. Polyclonal antibodies against individual pilus protein were generated previously by Dr Jacelyn Loh (UoA) by immunising a rabbit with recombinant proteins. On the other hand, the protective murine monoclonal 14C2 antibody recognising the N-terminus of M2 was commercially sourced from Abcam to detect the presence of M2e (315). In order to concurrently examine stability of the proteins, an aliquot of each fusion protein was subjected to a 24-hour incubation period at room temperature and also included in these blots. Immunoblotting of GST-BP-M2e and GST-M2e-BP confirmed the presence of both BP and M2e in the fusion proteins, with detection of a single band at the predicted protein size of ~60 kDa following probing with BP and M2e antibodies (Figure 5.5A). Furthermore, the fusion proteins appeared to undergo very little degradation following a 24-hour period at room temperature, with no noticeable additional bands appearing

in the incubated sample. Additionally, immunoblotting of His-AP1-M2e and His-AP1(LPXTG)-M2e confirmed the presence of both AP1 and M2e in these fusion proteins, with the detection of bands at the predicted protein size of ~120 kDa subsequent to probing with M2e and AP1 antibodies (Figure 5.5B). However, for both fresh His-AP1(LPXTG)-M2e samples and aliquots incubated for 24 hours, immunoblotting revealed the existence of additional secondary bands, most noticeable at about ~40 kDa in the blot probed with AP1 antibodies. Interestingly, these bands were not detected with the M2e antibody. Thus His-AP1(LPXTG)-M2e appeared to experience significant levels of degradation during the incubation period.
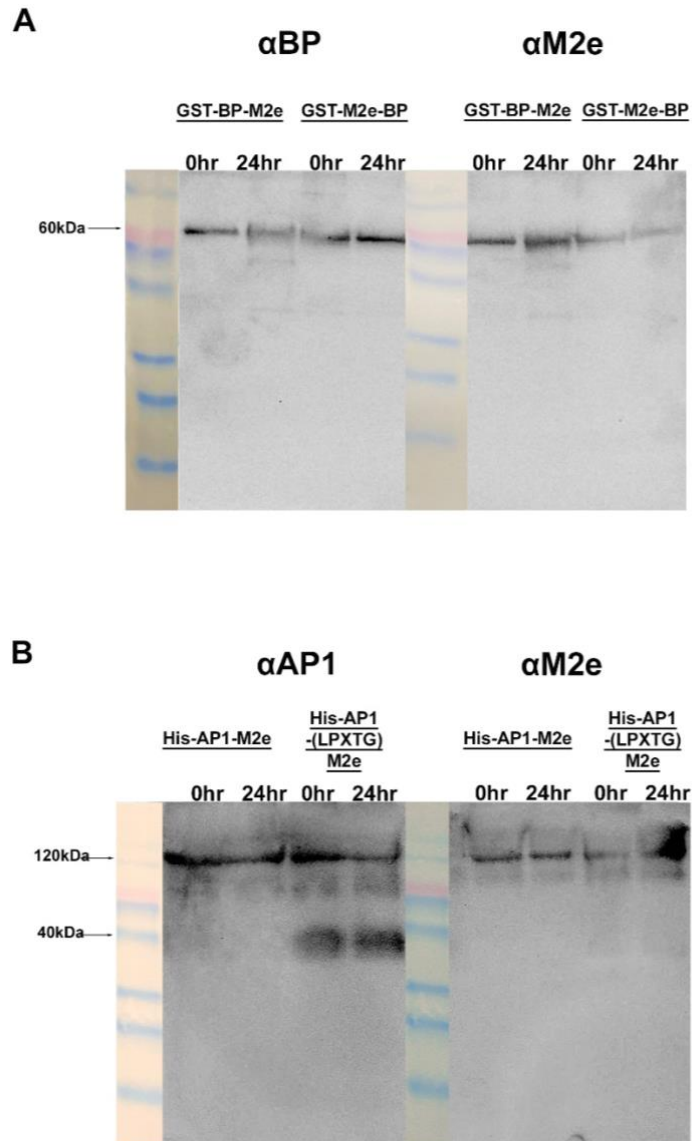
Figure 5.5 Western blot of pilus protein-M2e fusion proteins detect presence of both pilin subunits and M2e (A) BP and M2e fusion proteins taken immediately from stock (0 hr) or incubated at room temperature for 24 hours (24 hr) were analysed on a western blot by probing with αBP and αM2e. (B) AP1 and M2e fusion proteins taken immediately from stock (0 hr) or incubated at room temperature for 24 hours (24 hr) were analysed on a western blot by probing with αAP1 and αM2e. L; protein ladder

5.2.2 Sandwich ELISA of fusion proteins

Western blots of the fusion proteins confirmed the successful expression of pilus protein and M2e fusion peptides. A sandwich ELISA was subsequently performed to gain further confirmation of protein integrity, as well as affirm correct presentation of the M2e antigen and the co-existence of M2e and pilus proteins on one molecule. The ELISA was accomplished by adding varying concentrations of the fusion proteins to a 96 well plate coated with 1 μg/ml of capture antibodies against recombinant BP or AP1. Detection was then executed using the 14C2 antibody against M2e which in turn was bound to a horseradish peroxidase (HRP) linked secondary antibody. Both the ELISAs examining GST-BP-M2e (Figure 5.6 A) and GST-M2e-BP (Figure 5.6 B) illustrated a dose dependent relationship where increased concentration of fusion proteins added to the assay wells correlated to increased absorbance. This is indicative of both the BP antibodies recognising the fusion protein, allowing the complex to be captured on the assay plate, as well as the M2e mAb (monoclonal antibody) interacting with the fusion protein, resulting in its detection. Similarly, the ELISA for His-AP1-M2e (Figure 5.6 C) also exhibited this dose dependent relationship, indicating the ability of the fusion protein to interact to antibodies targeting both its structural components. In contrast, increasing the concentration of His-AP1(LPXTG)-M2e added to assay wells did not correspond to increased absorbance, suggesting that the AP1 and M2e antibodies failed to recognise this fusion protein (Figure 5.6 D). These ELISAs confirmed the structural integrity of GST-BP-M2e, GST-M2e-BP and His-AP1-M2e, with the ability to interact with pilus and M2e antibodies signifying simultaneous presentation of pilus proteins and M2e on the same molecule. On the other hand, the assay failed to detect His-AP1(LPXTG)-M2e, reiterating the instability of this protein illustrated in the western blot. Therefore, the following assays were only carried out with GST-BP-M2e, GST-M2e-BP, and His-AP1-M2e.
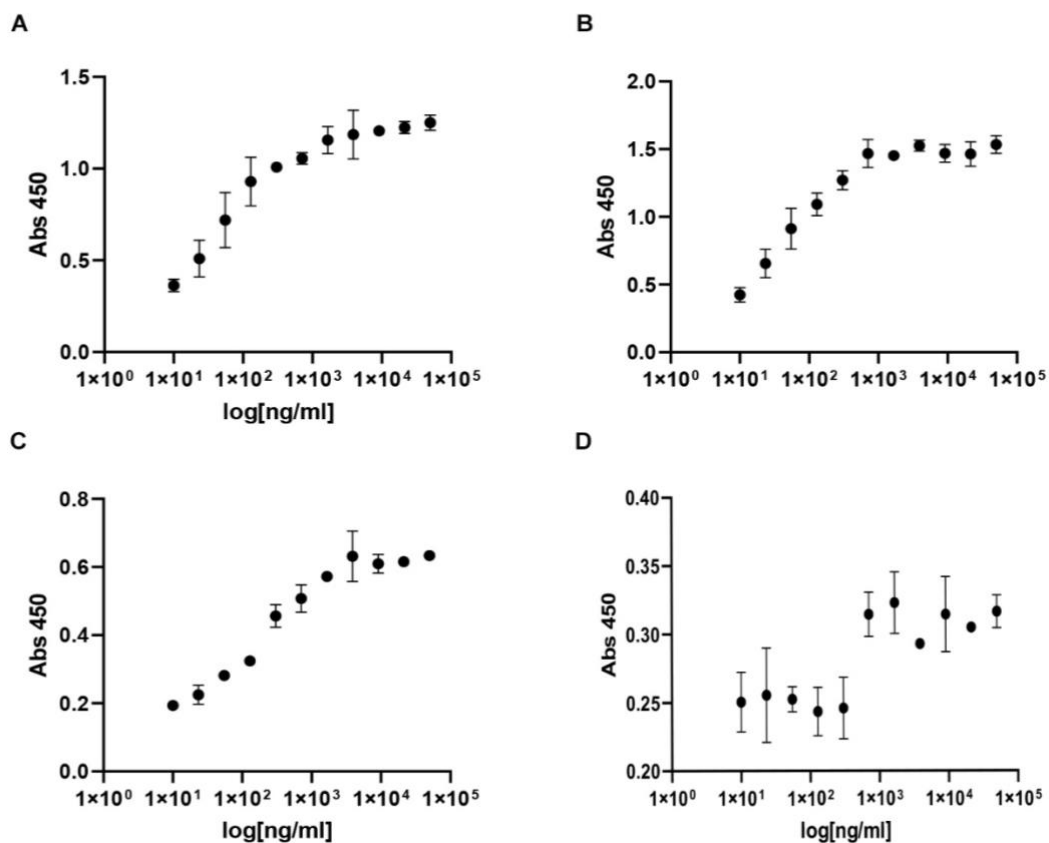
Figure 5.6. Pilus protein-M2e fusion proteins interact with antibodies against both pilin subunits and M2e in a sandwich ELISA. Varying concentrations of recombinant GST-BP-M2e (A) and GST-M2e-BP (B) were incubated with 1 µg/ml of purified BP rabbit antibodies immobilised on a 96 well plate, whilst varying concentrations of (C) His-AP1-M2e and (D) His-AP1(LPXTG)-M2e were incubated with 1 µg/ml of purified AP1 rabbit antibodies immobilised on a 96 well plate. Captured protein was detected using M2e mice primary antibody and HRP conjugated secondary antibody. Experiment was performed in duplicate and data of three repeats shown as mean±S.D.

5.2.3 Biological activity of fusion proteins

Next, the ability of the pilus protein to still activate TLR2 after being fused to the M2e peptide was assessed using the HEK- Blue hTLR2 receptor cell line, where TLR2 activation can be quantified by the downstream secretion of SEAP (secreted embryonic alkaline phosphatase) which drives a quantifiable colorimetric change to the cell suspension (206). The three fusion proteins established to have structural integrity in the assay above (GST-BP-M2e, GST-M2e-BP and His-AP1-M2e) were incubated for 9 hours with HEK-Blue hTLR2 in a media suspension containing HEK-Blue detection substrate before absorbance at 655 nm was read to evaluate TLR2 activation. All three fusion proteins caused significantly greater absorbance

readings compared to untreated cells, asserting that the pilus subunits was still able to mediate TLR2 activation when fused to M2e (Figure 5.7).

Figure 5.7. Pilus protein-M2e fusion proteins stimulate TLR2.HEK-Blue hTLR2 cells were incubated for 9 hours with recombinant GST-BP-M2e, GST-M2e-BP, His-AP1-M2e or positive control (1 µg/ml Pam2CSK4) or left untreated. Level of TLR2 activation was determined by measuring absorbance of cell supernatant at 655 nm. Experiments were performed in duplicates and data from three repeats is shown as mean±S.D. Statistical significance was determined by one-way ANOVA, and P-values were calculated by Holm–Šídák's multiple comparisons test. $*P \leq 0.05$, $***P < 0.001$ compared with the negative control.

5.2.4   GST protein tags do not contribute to the biological activity of fusion proteins

Although all three pilus protein-M2e fusion peptides activated HEK-hTLR2, the BP based fusion peptides GST-BP-M2e and GST-M2e-BP induced more pronounced TLR2 stimulation compared to His-AP1-M2e. This is somewhat opposite to the observation when the assays were carried out using the recombinant BP and AP1 proteins alone, where AP1 always exhibited a higher degree of TLR2 or TLR2/6 binding and activation (Figures 4.8, 4.10 and 4.12). One possible reason for this disparity could be the tag present in these fusion proteins. The original BP and AP1 recombinant proteins were both expressed as His-tagged proteins. However, the M2e fusion proteins discussed here were generated with different tags. Whilst His-AP1-M2e contains the small ~0.8 kDa His tag, the BP and M2e fusion proteins carry the ~26 kDa GST tag, which is almost as large as the BP subunit itself. This raised the question of whether the GST tag, which made up a considerable portion of the conjugated protein structure, played a

role in the capacity of the fusion proteins to activate immune cells via TLR2. In order to address this query, GST-BP-M2e and GST-M2e-BP protein solutions were incubated with 3c protease to separate the GST tag from the remaining part of the recombinant protein, as there is a 3c protease recognition site between the GST tag and the BP-M2e portion. These protein solutions were loaded onto a glutathione column and flow through, containing complexes without GST, was collected. Subsequently, elution with reduced glutathione was performed in order to release the GST moiety from the column. Visualisation on SDS-PAGE indicated that this enzymatic cleavage and subsequent protein purification resulted in the ~50 kDa proteins becoming segmented into a ~30 kDa portion consisting of BP-M2e (Figure 5.8A) or M2e-BP (Figure 5.8B) and a ~26 kDa portion containing the GST tag (Figure 5.8A, B).
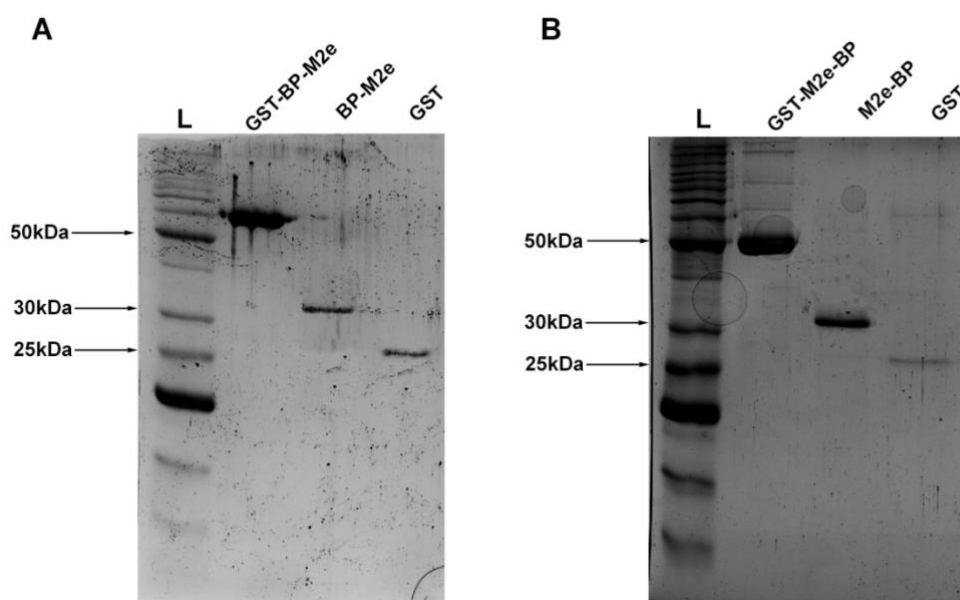
Figure 5.8 Separation of BP-M2e and M2e-BP from GST tag by 3c protease followed by glutathione affinity chromatography. As visualised on 12.5% SDS-PAGE, (A) ~50 kDa GST-BP-M2e protein solutions were incubated overnight with 3c protease before being passed through the glutathione column to collect ~30 kDa BP-M2e in the flow through. Reduced glutathione was then added to elute the ~26 kDa GST tag in 2ml fractions. (B) The process was repeated with ~50 kDa GST-M2e-BP to separate the ~30 kDa M2e-BP from the ~26 kDa GST tag. L; protein ladder.

The separated components of the fusion proteins were then tested on the established HEK-hTLR2 assay. The intact GST-BP-M2e and GST-M2e-BP proteins were incubated alongside BP-M2e, M2e-BP and the GST tag for 9 hours with the HEK-Blue hTLR2 cells in a media suspension containing HEK-Blue detection substrate. Absorbance was then read at 655 nm to

evaluate TLR2 activation. Both the cell suspensions exposed to intact pilus protein-M2e peptides and the cleaved versions lacking the GST tag (BP-M2e and M2e-BP) had significantly greater absorbance readings compared to unstimulated cells. On the other hand, the absorbance measurements from cell suspensions incubated with the GST tag alone were not significantly different to unstimulated cells. These observations signify that the GST tag itself does not possess the ability to activate TLR2-mediated cell signalling and lacks a biological function that could contribute to the simulative properties of the pilus protein-M2e peptides.

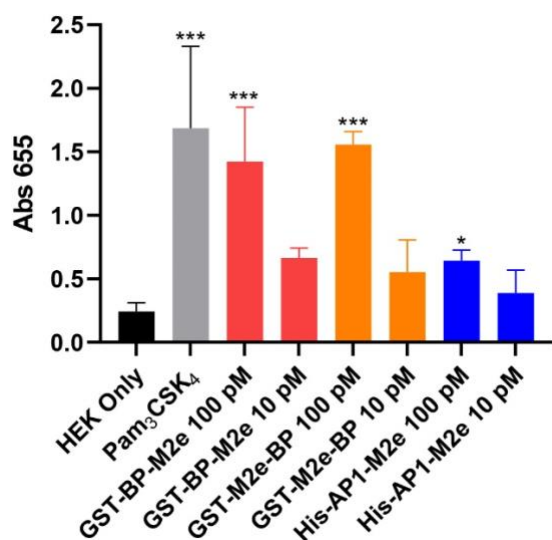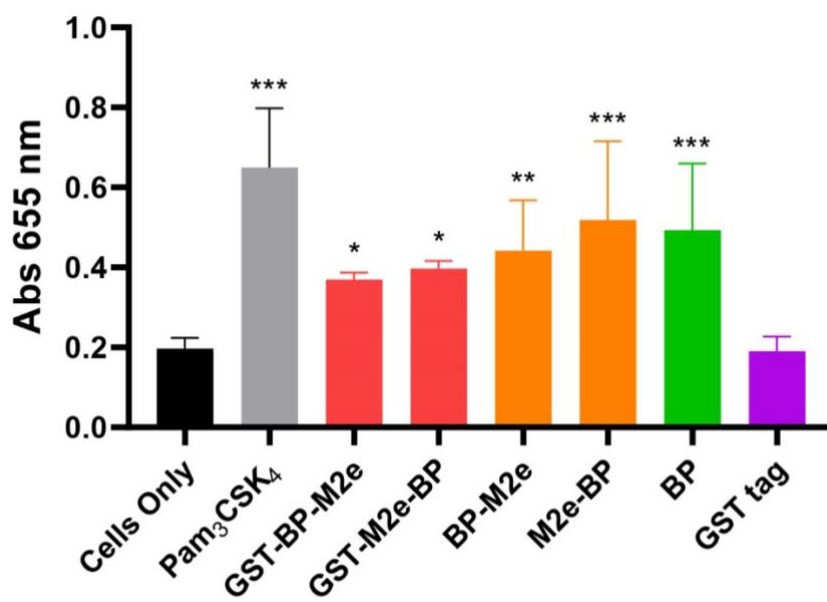Figure 5.9. GST tag does not contribute to the pilus protein-M2e fusion peptides' ability to stimulate TLR2.HEK-Blue hTLR2 cells were incubated for 9 hours with recombinant GST-BP-M2e, GST-M2e-BP, BP-M2e, M2e-BP, GST tag or positive control (1 µg/ml Pam₃CSK₄) or left untreated. Level of TLR2 activation was determined by measuring absorbance of cell supernatant at 655 nm. Experiments were performed in duplicate and data from three independent repeats is shown as mean±S.D. Statistical significance was determined by one-way ANOVA, and P-values were calculated by Holm–Šídák's multiple comparisons test. $*P \leq 0.05$, $**P \leq 0.01$, $***P < 0.001$ compared with the negative control.

5.3   Discussion

This chapter focused on the creation and subsequent validation of GAS pilus protein-M2e fusion proteins for ensuing exploration of the adjuvanting properties of the pilus.

Protein-protein conjugates can be manufactured via manipulation of different stages of the protein production pathway. Most commonly, the genes for the two proteins of interest can be expressed sequentially, resulting in the two proteins being translated as a single polypeptide chain (316). Alternatively, the two proteins can be expressed separately and post translationally linked using biochemical reactions (316). This route is often taken when expression of the two proteins from the former method fails to culminate in adequate yields of a correctly folded, functionally active complex (316,317). Creation of the GAS pilus protein-M2e conjugates was undertaken using the first approach by molecular cloning, as previous studies using this technique has resulted in the successful conjugation of flagellin (a TLR ligand) and M2e as a single recombinant protein (318). Studies have found that the order in which each protein is expressed can be consequential, with the placement of one protein observed in some cases to effect folding or functionality of the other (319,320). For this reason, four constructs were designed originally, which included all possible combinations of the pilus protein-M2e conjugation orders (GST-BP-M2e, GST-M2e-BP, His-AP1-M2e, and His-M2e-AP1). The most feasible way to generate these proteins within the limited timeframe of this project was to add the M2e peptide to existing plasmids that already contain the pilin gene.

As chronicled in the sections above, cloning of expression plasmids for the production of BP with N terminal M2e, BP with C terminal M2e and AP1 with C terminal M2e proved successful. Two versions of AP1 conjugated with M2e at the C terminus were constructed. The first version, AP1(LPXTG)-M2e, contained AP1 with the LPXTG sorting motif, which targets pilus proteins to the cell membrane and is cleaved to facilitate oligomerisation of subunits. The second variant contained mature AP1 without the sorting motif (AP1-M2e). Unfortunately, construction of the fusion gene for expression of AP1 with N terminal M2e proved unsuccessful despite several alterations to the cloning design and thus this fusion protein could not be generated within the timeframe of this project, making it an avenue for future work.

Once the conjugated proteins were produced in *E. coli* expression systems and purified, their authenticity was investigated using western blots. Immunoblotting of the purified GST-BP-M2e and GST-BP-M2e samples with both αBP and αM2e indicated that the BP and M2e portion can both be detected in the polypeptides (Figure 5.5A). The stability of the fusion proteins was emphasised upon examining the immunoblot of samples incubated at room temperature for 24 hours. The resulting blot did not show additional discernible bands that

would signify degradation. This was unsurprising considering BP has long been recognised for its thermal and proteolytic stability, which has been attributed to intramolecular isopeptide bonds (321,322). Both N and C terminal portions of BP contain isopeptide bonds, which join the first and last β strands of each domain together. This linkage of residues at distant points on the linear amino acids sequence results in a highly stable bond that is resistant to mechanical unfolding (321). Due to their intramolecular positions, terminal conjugation of M2e likely had no effect on these stabilising bonds.

Western blots of His-AP1-M2e and His-AP1(LPXTG)-M2e with αAP1 and αM2e also affirmed protein integrity, verifying expression of both the AP1 and M2e moieties within the conjugated proteins. However, the His-AP1(LPXTG)-M2e samples exhibited degradation, as evidenced by the additional protein bands visible on the αAP1 immunoblots (Figure 5.5B). Degradation products were present regardless of the prolonged incubation at room temperature, insinuating that the protein was prone to rapid degradation. Previous studies into the AP1 subunit have reported that the protein is susceptible to breakage at a proline rich sequence, resulting in the division of AP1 into an N terminal fragment spanning the first third of the intact protein and a larger C terminal fragment encompassing the remaining two thirds (70). Inspection of His-AP1(LPXTG)-M2e on the western blots appear to signal this phenomenon occurring. There is a palpable protein band detected by αAP1 at around ~40 kDa and as this is a third of the size of the ~120 kDa whole protein, it aligns in size to the N terminal fragment that tends to break off from the full-length AP1(70). Furthermore, this protein band was not visible in the αM2e-probed western blot, propounding the idea that the fragment originated from the N terminus, which does not carry the M2e antigen and would thus evade detection by αM2e. Fortunately, recombinant AP1 devoid of the N-terminal fragment does not have inhibited adhesion compared to full intact AP1 and this region is absent in some GAS serotypes (70,323,324). This suggests that the N-terminal fragment is less likely to be required for innate immune receptor recognition of AP1 and thus the degradation observed is anticipated to not heavily impact the interaction between fusion proteins and immune cells. As touched on above, BP contains stabilising intramolecular isopeptide bonds in both the N and C terminal domains (67). On the other hand, such isopeptide bonds have only been identified in the C-terminal domain of AP1 (325). The localisation of isopeptide bonds to solely the C-terminal region of AP1, coupled with the protein's vulnerable proline rich region, may be contributing to the AP1 fusion proteins possessing overall decreased stability compared to the BP fusion proteins.

Interestingly, the His-AP1-M2e fusion protein appeared to have greater stability than His-AP1(LPXTG)-M2e, with distinct degradation products not made apparent by the western. The presence of the LPXTG cell sorting sequence in His-AP1(LPXTG)-M2e may be the cause of this disparity. The LPXTG motif is found in the precursor pilus proteins synthesised in the cytosol, and upon translocation of the protein to the outer cellular membrane, the Sortase A enzyme cleaves LPXTG between threonine and lysine (326). This results in protein maturation and incorporation into the pilus structure via isopeptide bonding to the lysine residue in the next pilus subunit (70,240). Therefore, His-AP1(LPXTG)-M2e may be prone to breakage as the construct contains the pre-processed version of AP1 with the motif targeted for cleavage. Conversely, the AP1 subunit in His-AP1-M2e is in the mature form which does not contain the LPXTG motif and thus may be less susceptible to fragmentation as it does not possess an amino acid segment destined for cleavage.

Information on protein integrity provided by the western blots was supplemented by the sandwich ELISA, which aided in the selection of fusion proteins appropriate for further validation. GST-BP-M2e, GST-M2e-BP and His-AP1-M2e all exhibited a dose dependent relationship between concentration and absorbance on these ELISAs, where pilus subunit antibodies were used to capture the proteins and M2e antibodies were used to mediate protein detection (Figure 5.6A, B, C). This dose dependent relationship was indicative of the fusion proteins' being simultaneously recognised by both pilus protein and M2e antibodies. This verified the authenticity of the fusion proteins further by demonstrating that both the M2e and pilus proteins were extant on the same molecule. Furthermore, the assay provided assurance that the M2e antigen, which was presented in a linear peptide form by SDS-PAGE, was properly presented in the protein form. Additionally, recognition of the protein via the protective 14C2 antibody provided assurance that the complex contained the protective epitope of M2e. On the contrary, His-AP1(LPXTG)-M2e did not demonstrate this dose dependent relationship, with addition of increased amounts of the protein to the ELISA assay not equating to increased absorbance (Figure 5.6D). This insinuated that either the M2e antibody or the AP1 antibody, or both, failed to recognise the structure. As His-(LPXTG)-M2e did appear to express both M2e and AP1 peptides as per the western, it could be deduced that although both proteins were expressed as a single polypeptide, the complex was susceptible to breakage. Similar explorations into protein integrity using sandwich ELISAs have demonstrated that degradation of proteins results in a significant decrease in absorbance measured, with values at times falling

below the detection limit (327,328). The lack of signal detected from the ELISA may be indicative of breakage of the protein, resulting in the C-terminal fragment becoming washed off during the assay, leaving the M2 14C2 antibody unable to recognise the complex. This rearticulates the protein fragmentation illustrated in the western, where degraded product could only be recognised by the AP1 antibody.

This assay illustrated that the His-AP1(LPXTG)-M2e complex was not likely to be able to interact with immune cells as an whole, intact structure concurrently presenting both AP1 and M2e. Thus the construct was not subjected to further verification and the decision was made to omit the protein from the downstream studies investigating pilus protein facilitated M2e antibody response.

The three fusion proteins identified to have structural integrity (GST-BP-M2e, GST-M2e-BP, His-AP1-M2e) were finally verified for bioactivity using the HEK-Blue hTLR2 cell lines to confirm that conjugation to M2e had not impeded the ability of the pilus proteins to interact with TLR2. All three fusion proteins tested were able to stimulate TLR2 expressed on these reporter cell lines following an incubation period, as illustrated by significantly higher measured absorbance compared to untreated cells (Figure 5.7). It should be noticed that while GST-BP-M2e and GST-M2e-BP induced pronounced levels of TLR2 activation on par with the positive control, the ability of His-AP1-M2e to stimulate this receptor was not quite as high. Although additional information on the full structure of the fusion protein is required for an extensive explanation, some likely rationale can be raised. Firstly, although the pilus proteins were found to be recognised by TLR2 in the preceding chapter, the exact interface residues were not established. Thus there was possibility of the C terminal region of AP1 being crucial for the interaction with TLR2 and therefore tethering of M2e to this region may have obstructed access to the functional moiety, resulting in subdued interaction between AP1 and TLR2 (317). This was particularly of concern for His-AP1-M2e as the latter half of the AP1 complex, including the C terminal region, was solely responsible for the protein's adhesive properties and bacterial protein binding to host cells have previously been found to facilitate subsequent TLR activation (70,329–331). Furthermore, the fusion of proteins without a linker can impair the activity of proteins due to steric hindrance and a reduction in the degrees of freedom of the protein (317,332,333). Although the small size of M2e likely curtails complete disruption of

the interactions between AP1 and TLR2, there is possibility that the addition of this peptide without a linker imposed some level of inhibition on pilus protein signalling through TLR2.

As the pilus protein fusion complexes were expressed on different systems, they included different tags, adding variability in the composition of the structure. While the His tag is fairly small and not a major component of the fusion protein composition, the GST tag makes up a significant portion of the pilus protein-M2e fusion complex. This led to speculation of the GST tag having intrinsic immunostimulatory properties leading to the marked difference in TLR activation between His-AP1-M2e and GST-BP-M2e or GST-M2e-BP. If the GST tag did appear to have a biological function, additional manipulation of the GST-BP-M2e and GST-M2e-BP complexes to remove the tag would be required before use in antibody response studies in order to ensure any adjuvanting effects subsequently measured were due to BP alone and not a result of the combined impact of BP and GST. Thus a sample of GST-BP-M2e and GST-M2e-BP was cleaved at the GST tag and the split fusion protein components were tested on the HEK-hTLR2 cells (Figure 5.9). GST tag isolated from the fusion protein did not activate TLR2 signalling and both BP-M2e and M2e-BP triggered TLR2 stimulation in the absence of this tag at similar levels to their tagged counterparts. This confirmed that any apparent increase in immune response in the presence of the GST tag was not likely due to this component being inherently immunostimulatory. It is rather more likely that the GST tag increased antigen stability and elevated the interactions between TLR2 and intact fusion protein over the incubation period.

Despite some differences in the level of stimulation promoted by each of the fusion proteins, it could be concluded that the ability of the pilus proteins to activate TLR2 was preserved following conjugation to M2e. Thus GST-BP-M2e, GST-M2e-BP and His-AP1-M2e could be deployed to investigate whether BP or AP1 mediated TLR2 induction had an effect on the antibody response to the conjugated M2e peptide. This exploration into the adjuvanting properties of the pilus proteins was initiated in the following chapter.

Chapter 6: Exploring the adjuvanting capacity of the pilus proteins

The successful construction of pilin-antigen fusion proteins enabled the exploration of the adjuvanting capacity of the pilus proteins. This investigation was initiated by testing the ability of pilus proteins to activate immune cells. As touched on before, activation of TLRs expressed on APCs endows these cells with the ability to modulate adaptive immune responses. This is due to TLR signalling inducing the process of APC activation and maturation, resulting in secretion of immunomodulatory cytokines, upregulation of co-stimulatory transmembrane molecules, altered chemokine receptor expression and ability to display antigens on the cell surface (132,334). These upregulated APC features are able to activate T cells, which in turn gives these cells the capacity to stimulate antibody-generating B cells (335,336). Accordingly, one metric used to study the capacity of the pilus proteins to modulate adaptive immune response was the ability of BP and AP1 to induce maturation markers such as cytokine release and co-stimulatory molecule expression. Previous chapters have demonstrated the pilus proteins inducing the release of TNF, one of the cytokines associated with APC activation/maturation and adaptive immune cell regulation (337,338). This provided a glimpse into the potential of the pilus proteins to enhance the immunomodulatory abilities of APCs, but a more extensive assessment of the cytokine profile was required.

It should be noted that the ultimate goal of an adjuvant is to elevate antigen-specific immune response. Resultantly, the ability of the pilus proteins to enhance immunogenicity of an antigen provides clear indication of their adjuvant activity. Therefore, the pilus proteins were utilised in both *in vitro* cell-based assays and *in vivo* mouse immunisation studies to evaluate the adjuvanting properties of the structures. The results of their ability to activate immunomodulatory processes as well as their influence on downstream production of antigen specific antibodies are presented in this chapter.

6.1   Examining the ability of pilus protein to activate immune cells

Prior to mouse immunisation studies, a murine macrophage cell line (J774A.2) was utilised to investigate the ability of the pilus proteins to elicit enhanced cellular activity and maturation. A multitude of studies have previously evaluated potential adjuvanting systems using murine macrophage cell lines, including explorations of TLR based constructs (339–341). One of the

most common indicators used in such studies to highlight activation/maturation was the expression of the transmembrane co-stimulation molecules such as CD80 and CD86, which possess the ability to modulate T cells (340–342). Secretion of cytokines associated with an activated cell state was also commonly monitored either via direct measurements of released cytokines or through quantification at the mRNA level (340,341). GAS has been shown to induce macrophage activation, with exposure to the bacteria found to trigger the upregulation of co-stimulatory transmembrane proteins which can interact with adaptive immune cells including CD40, CD80, CD86 and the antigen presenting MHCII complex (168). Further evidence of the whole organism-driven cell activation by GAS has been confounded by the surge of secreted inflammatory cytokine and cell transmigration signals following incubation of macrophages with the bacteria (168,343). However, the contribution of pili in this process has not yet been explored. Resultantly, the effect of GAS pilus proteins on macrophage activation/maturation was examined in the section below by appropriating methods previously used to study the response evoked by other TLR adjuvants and whole GAS, such as in the aforementioned experiments.

6.1.1   Pilus proteins induce macrophage activation

Prior to delving into specific markers, a colourmetric assay using MTT (3-(4,5-dimethylthiazol-2-yl)-2,5-diphenyltetrazolium bromide) was performed to carry out an initial evaluation of whether the pilus proteins are able to activate mouse macrophages. MTT is a mono-tetrazolium salt with the ability to pass through the cell membrane into the mitochondrial inner membrane, where metabolically active cells can reduce the molecule to formazan crystals (344,345). Solubilisation of these crystals yields a colour change which can be correlated to the level of metabolic activity in the cells, signalling macrophage activation (346). Accordingly, J774A.2 cells were seeded into a 96 well plate at a density of 5×10^4 or 2.5×10^4 per well and incubated for 24 hours with negative control PBS, positive control ConA, BP or AP1 before the cell suspension was supplemented by MTT. At the end of the incubation, DMSO was added to solubilise crystals formed and absorbance was measured at 540 nm. At both cell densities, compared to untreated cells given PBS, cells incubated with positive control or the pilus proteins had significantly higher recorded absorbance levels (Figure 6.1). This demonstrated that exposure to the pilus proteins increased macrophage activation.
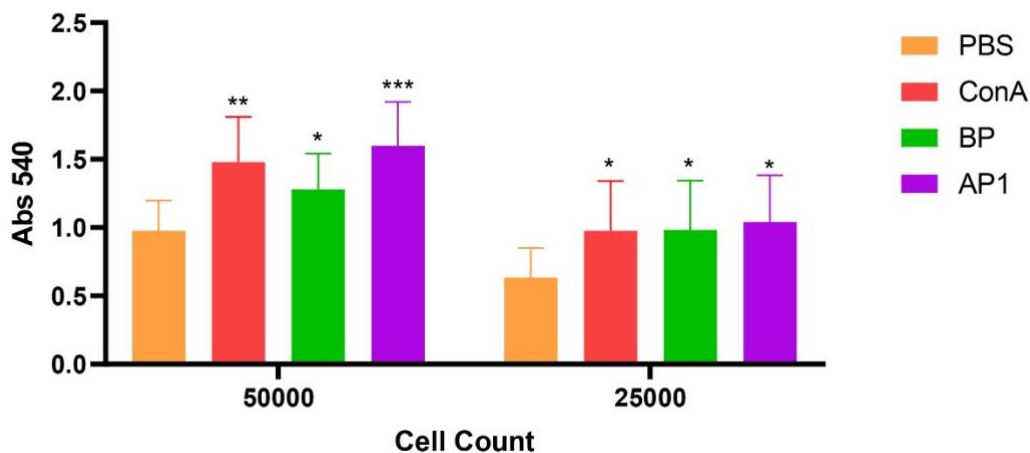
Figure 6.1. Pilus proteins induce macrophage activation. J774A.2 cells were incubated for 24 hours with recombinant BP, recombinant AP1, positive control (100 µg/ml ConA), or PBS. Subsequently, cells were incubated for 1 hour with 500 µg/ml MTT reagent followed by the addition of DMSO and a 15 minute incubation, before absorbance was measured at 540 nm. Experiments were performed in duplicate and data from three independently performed experiments is shown as mean ± S.D. Statistical significance was determined by one-way ANOVA, and P-values were calculated by Holm–Šídák's multiple comparisons test. *P ≤ 0.05, **P ≤ 0.01, ***P < 0.001 compared with the negative control (PBS).

6.1.2 Pilus proteins elicit macrophage secretion of cytokines associated with adaptive immune cell activation

Subsequent to confirmation of the pilus proteins inducing macrophage activity, the downstream effects of this interaction were explored. As demonstrated in previous chapters, pilus proteins have been implicated in the upregulation of TNF secretion. Following up on this observation, a Luminex assay was utilised to determine if the pilus proteins induced the expression of other cytokines associated with modulating adaptive immunity. Luminex assays make use of a repertoire of spherical beads coated with capture antibodies specific for different proteinaceous analytes. As each bead population bears a unique fluorescent signal, they can be detected via a flow-based detection system to determine the amount of bound analyte. As multiple bead types can be added to each sample of biological fluids, this assay allows for the simultaneous detection of a panel of selected cytokines (347,348). For the purposes of this experiment, a pre-existing panel containing mouse macrophage cytokines associated with adaptive immune cell modulation was utilised. This panel contained IL-2, IFNγ, TNF, IL-4, IL-10, IL-17 and IL-6, which are all cytokines associated with T cell differentiation into distinct Th lineages. J774A.2

cells were seeded into a 96 well plate at 1×10^5 / well and incubated for 24 hours with either recombinant BP, recombinant AP1, positive control Pam$_3$CSK$_4$ or left untreated before the cell supernatant was tested on the Luminex panel as per the manufacturer's protocol. As previously illustrated, both BP and AP1 induced the secretion of TNF, with cytokine levels detected 4-fold higher in the supernatant of cells incubated with the pilus proteins compared to cells left untreated (BP, P= 0.018, AP1, P=0.025) (Figure 6.2). Furthermore, pilus proteins appeared to enhance the secretion of IL-6, with cells exposed to AP1 displaying 9.5-fold higher supernatant concentrations of the cytokine compared to untreated cells (P=0.0275). Cells incubated with BP also had 2-fold higher supernatant IL-6 levels compared to untreated cells but this was not statistically significant, perhaps owing to the strong response induced by the positive control skewing the analysis of variance (Figure 6.2). The levels of IL-2, IL-4, IL-10, IL-17 and IFNγ secreted were below the limit of detection following incubation with pilus proteins.
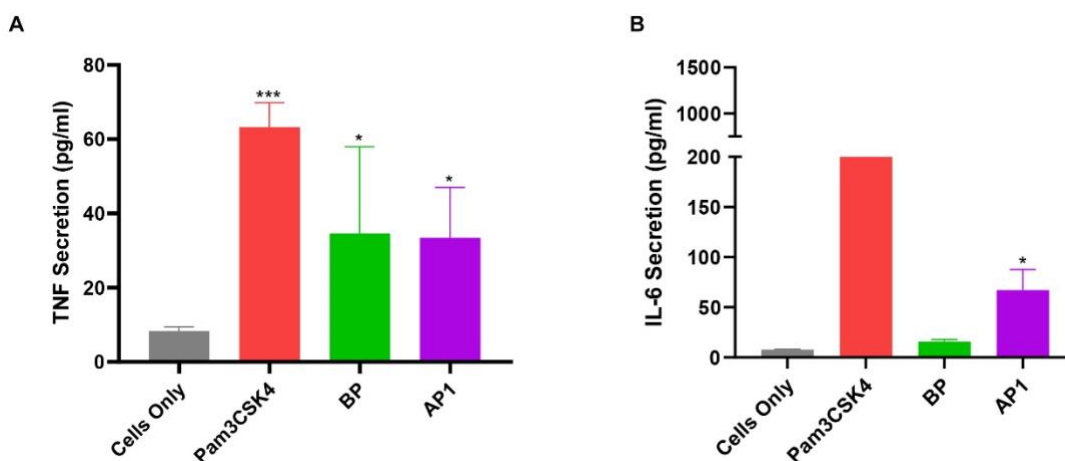
Figure 6.2. Pilus proteins induce cytokine secretion from macrophages. J774A.2 cells were incubated for 24 hours with recombinant BP or recombinant AP1 or positive control (1 µg/ml Pam$_3$CSK$_4$) or left untreated. Cell supernatant was then harvested and secreted TNF, IL-2, IL-4, IL-6, IL-10, IL-17 and IFNγ concentration quantified using Luminex. Samples from three independent runs were tested in duplicate and read using the same standard curve are shown as mean ± S.D. Statistical significance was determined by one-way ANOVA, and P-values were calculated by Holm–Šídák's multiple comparisons test. *P ≤ 0.05, ***P < 0.001 compared with the negative control.

6.1.3 Pilus proteins upregulate adaptive immune cell co-stimulation receptors on macrophages

The pilus proteins' effects on the macrophage expression of adaptive immune cell co-stimulation receptors was also examined. In particular, macrophage upregulation of the

adaptive immune cell modulating CD80, CD86, F4/80 (murine homologue of EMR-1, a well-established marker for macrophages) and MHC-II following exposure to the pilus proteins was studied using flow cytometry. In short, J774A.2 cells were incubated for 24 hours with pilus proteins, LPS, or left untreated, before they were harvested in PBS using TrypLE enzyme. LPS was included in the assay as a positive control to indicate the cells' capacity to upregulate co-stimulatory markers, due to its strong activation of the J774A cell lines (341). Harvested cells were then incubated with fluorescently labelled antibodies against CD80, CD86, F4/80 and MHC-II before undergoing washing steps to remove unbound antibodies. The cells were then analysed on a flow cytometer, with the mean fluorescence intensity of each antibody label determined to evaluate expression of the receptors. Incubation of cells with pilus proteins or positive control LPS appeared to increase expression of the co-stimulatory receptors, signified by the fluorescence signal recorded from these cells appearing to be markedly higher than the untreated cells (Figure 6.3A). A more detailed examination of the MFI recorded indicated that both BP and AP1 measurably induced the upregulation of CD86 and CD80. Measuring cells for fluorescent antibodies against CD86 illustrated BP treated cells and AP1 treated cells having 2.5-fold (P< 0.001) and 2.4-fold higher (P=0.002) MFI values compared to untreated cells respectively. Similarly, observations of the fluorescence from CD80 antibodies depicted the cells exposed to BP and AP1 having respectively 6.4-fold (P< 0.001) and 3.1-fold greater (P= 0.049) MFI compared to untreated cells. Additionally, BP appeared to considerably heighten expression of F4/80, with the MFI of cells incubated with BP being 5.9-fold greater than untreated cells (P= 0.008) (Figure 6.3B). AP1 also appeared to induce F4/80 upregulation, with the MFI recorded from AP1 incubated cells 3.9-fold higher than untreated cells, but this increase in fluorescence intensity was not statistically significant. Similarly, cells treated with pilus proteins appeared to express slightly greater amounts of MHCII compared to untreated cells, with a 1.6-fold difference in MFI values, but this discrepancy was not statistically significant (Figure 6.3B).
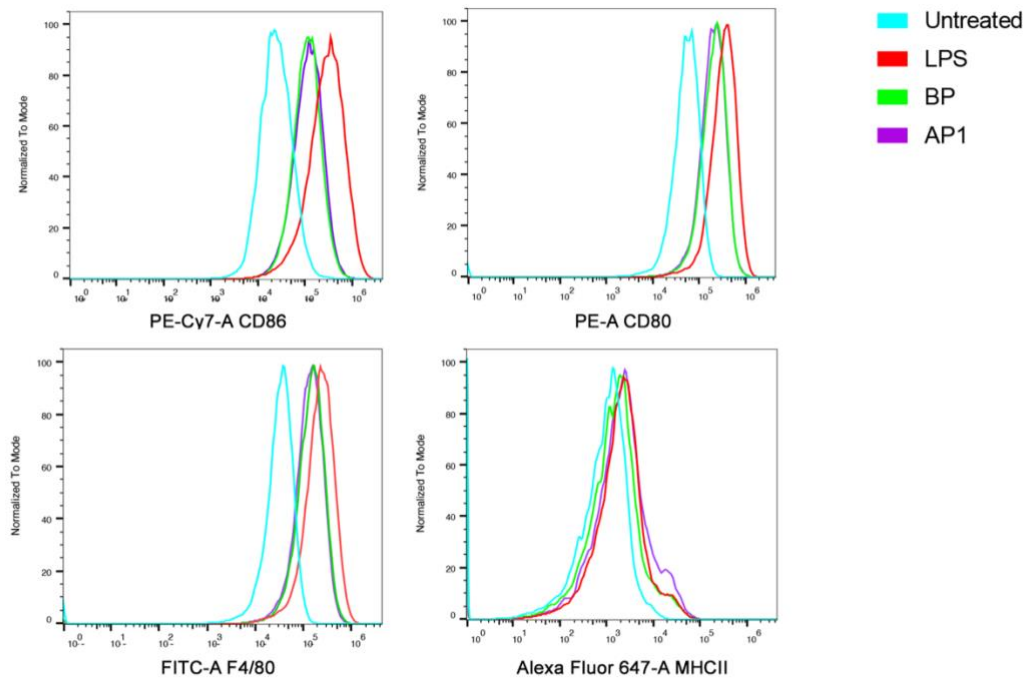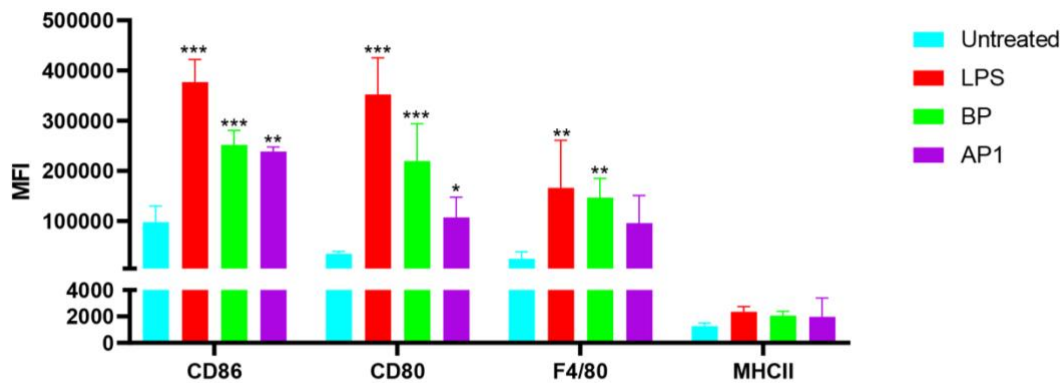
Figure 6.3 Pilus proteins upregulate expression of co-stimulation receptors on macrophages. J774A.2 cells were incubated for 24 hours with recombinant BP, recombinant AP1, positive control (1 µg/ml LPS) or left untreated. Cells were harvested using TrypLE and incubated with fluorescently labelled antibodies against CD86, CD80, F4/80 and MHCII. Flow cytometry was used to analyse the expression of these surface markers. Fluorescence intensity was recorded for 30,000 events per group. Mean fluorescence intensity data was standardised against unstained control cells and is shown as bar graphs mean±S.D from three independently performed experiments. Statistical significance was determined using one-way ANOVA followed by Holm-Šídák multiple comparisons test. *P ≤ 0.05, **P ≤ 0.01, ***P < 0.001 compared to untreated negative control.

6.2 Mouse Immunisation with pilin-M2e fusion proteins

The preceding sections portrayed the ability of the pilus proteins to augment processes on macrophages associated with adaptive immune modulation, such as the expression of co-stimulatory molecules and cytokine secretion. This substantiated the potential of the pilus proteins to enhance the production of antigen-specific antibodies when co-administered with an antigen. Accordingly, the adjuvanting ability of the pilus proteins was further explored by investigating antibody responses in mice vaccinated with the pilin-M2e fusion proteins generated in Chapter 5. In order to evaluate whether the pilus proteins elevated M2e antibody production, the levels of these specific antibodies generated in the fusion protein immunised mice was compared to that of mice exposed to synthetic M2e peptide alone. As a positive control, a group of mice were also immunised with a mixture of M2e peptide and poly I:C, an established TLR3 specific adjuvant with the ability to stimulate a robust inflammatory response (349).

The pilus protein-M2e fusion complexes and experimental controls were administered intranasally as a mucosal vaccine. Influenza infections originate from mucosal sites within the upper respiratory tract and thus a strong local immune response would be beneficial in preventing viral replication and penetration during the early stages of pathogenesis (350). Mucosal administration of influenza antigens has been touted as an effective method to achieve this, by inducing concentrated IgA antibody production in the upper respiratory tract, on top of systemically disseminated antibodies (351). In fact, previous immunisation studies where the M2e antigen was administered intranasally with a cholera toxin based adjuvant have demonstrated ameliorated protection against the influenza virus compared to parenteral M2e delivery (352). Furthermore, intranasal delivery of M2e with adjuvant was found to elicit IgA driven cross protection and reduction in viral transmission, whilst protective IgA was not generated at detectable levels following parenteral immunisation (352–354). As in the case of many proposed mucosal vaccines, M2e was not found to engender sufficient antibody response or elicit protection in the absence of an adjuvant and the probe for the most suitable molecule is ongoing (355–357). Few mucosal vaccines have been established for use in humans, in part due to a lack of effective adjuvant options for immunisations through this route. Cholera toxin and *E. coli* heat labile toxin are two of the most well studied potential mucosal adjuvants but despite their potency, these have not been approved for human use due to their enterotoxin

characteristics causing severe diarrhoea and potential to cause damage to the central nervous system via the olfactory nerves (358,359). Furthermore, efforts to reduce or eliminate the toxicity of such bacterial toxin based adjuvants without diminishing potency or stability have proven challenging and are ongoing (358). Explorations of other mucosal adjuvant candidates such as cytokines and synthetic lipids are in progress as well but have not yet led to the establishment of a licenced product and there is a need to ensure mechanisms of action can be precisely determined to circumvent excessive immunological activation which would prove harmful (358,360). As described in Chapter 3/4 and our publications (206,252), the pro-inflammatory properties and safety profile of pilus proteins make them a promising candidate in the development of a mucosal adjuvant. Accordingly, mucosal immunisation was incorporated into the experimental design to provide a contextually relevant example of how the potential adjuvanting properties of pilus proteins could be capitalised.

As detailed below, a dose-exploration immunisation study was firstly conducted using two of the pilus protein-M2e constructs to establish a vaccination regimen which was both safe and able to demonstrate antibody responses. This was followed by testing of the full panel of fusion proteins and control vaccine formulations. Both the pilot and full study were undertaken over a period of 28 days, with 3 rounds of weekly immunisation and sample collection one week after the final booster.

6.2.1 Immunisation with pilus protein-M2e fusion peptides shows dose-dependent response

In order to determine the effect of administered dosage and establish a vaccination protocol for the full immunisation panel, a pilot study using His-AP1-M2e and GST-BP-M2e was conducted. Six groups of female BALB/c mice, with 5 mice in each group, were administered varying dosages of the fusion proteins as a 100-µl intranasal vaccine. Two additional groups of mice were given recombinant AP1 or BP devoid of the M2e antigen, respectively. The 8 vaccination groups were thus as follows: His-AP1-M2e 50 µg, His-AP1-M2e 5 µg, His-AP1-M2e 1 µg, AP1 50 µg, GST-BP-M2e 50 µg, GST-BP-M2e 10 µg, GST-BP-M2e 1 µg, BP 50 µg (As per Table 2.14). Mice were immunised three times at one-week intervals and all animals did not develop any adverse health effects across the immunisation period, including the cohorts receiving the highest dosages. One week after completing the immunisation schedule, serum, bronchial alveolar lavage (BAL) and nasal wash (NW) samples were collected.

Antibody levels against M2e and pilus proteins were determined using ELISA with immobilised M2e peptide or pilus proteins, respectively.

Immunisation of mice with His-AP1-M2e resulted in a dose dependent antibody response against AP1. The highest IgG response against AP1 was seen in the mice given the 50 µg dosage, as illustrated in Figure 6.4A. The antibody response became less pronounced as the dosage was lowered, and this trend could also be seen in BAL and NW IgA. Although the trend was not as uniform, M2e antibody response also appeared to illustrate a dose dependent effect, with response apical in mice given the highest 50 µg dosage (Figure 6.4B). Mice immunised with GST-BP-M2e produced an analogous dose dependent antibody response to the His-AP1-M2e cohort. Highest response for IgG and IgA samples against BP were obtained from mice administered with the 50 µg dosage of fusion protein and antibody response curtailed as the dosages were stepped down (Figure 6.4B). Furthermore, M2e IgA response was greatest in the 50 µg dosage mice and appeared to decrease as the dosage was lowered. Of note, IgG response appeared to be relatively low for all three dosages (Figure 6.4B). For both His-AP1-M2e and GST-BP-M2e immunisation cohorts, each dosage group appeared to exhibit generally lower M2e antibody responses compared to pilus protein antibody responses. Interestingly, while mice administrated 50 µg of AP1 had similar AP1 specific IgG and IgA antibody responses compared to mice immunised with 50 µg of His-AP1-M2e (Figure 6.4A), the mice given 50 µg BP had a lower antibody response in comparison to their counterparts vaccinated with GST-BP-M2e (Figure 6.4B).

This pilot study indicated that the antibody response to both AP1 and BP based M2e fusion proteins was dose-dependent and vaccination with 50 µg of fusion proteins resulted in the highest serum and mucosal antibody titres. As this dosage elicited maximal antibody response and did not appear to trigger adverse effects in the mice, it was selected for the full immunisation panel.
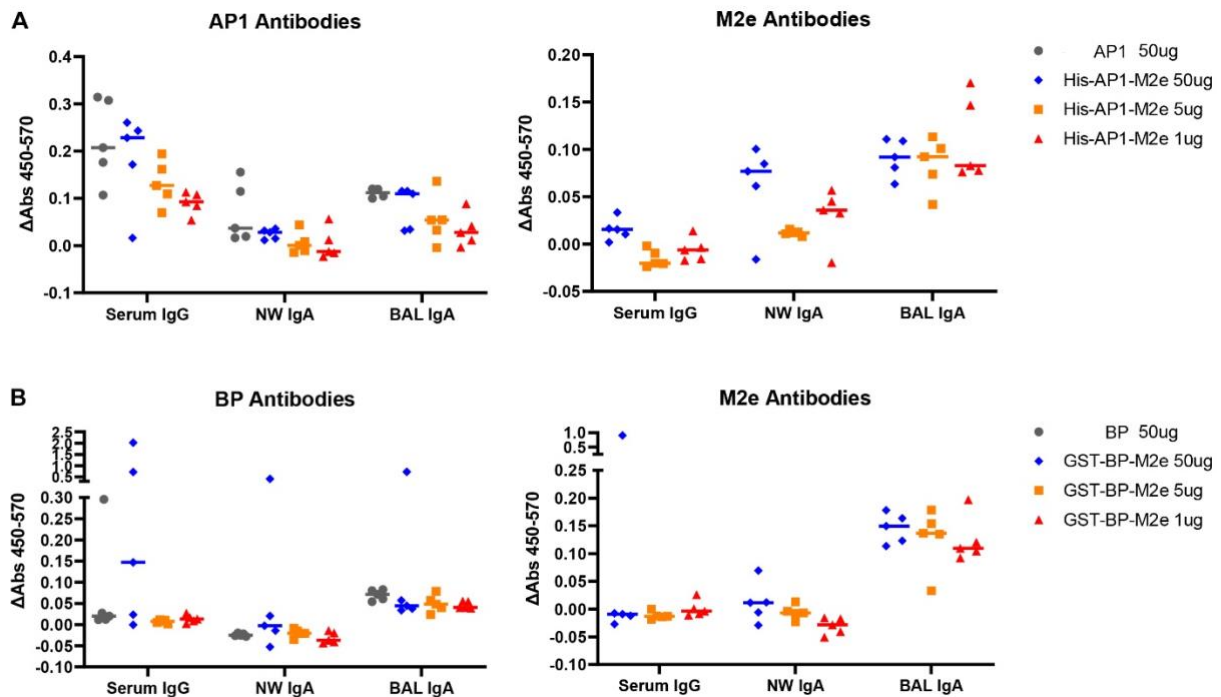
Figure 6.4. Immunisation with His-AP1-M2e and GST-BP-M2e induces M2e/pilus protein IgG antibody response. BALB/c mice (n=5) were intranasally immunised with either His-AP1-M2e or GST-BP-M2e at 50 µg, 5 µg or 1 µg. Additional groups of mice were administered 50 µg BP or AP1.Serum, nasal wash and bronchial alveolar lavage samples were collected and serum samples were diluted 1:200. (A) AP1 and M2e antibody response of mice immunised with His-AP1-M2e, as well as (B) BP and M2e antibody response of mice immunised with GST-BP-M2e was determined by ELISA performed in duplicates. Each data point represents the antibody response in an individual mouse determined by measuring change in absorbance from baseline at 450 nm (with absorbance at 570 nm subtracted to correct for background absorbance). The median of each group is shown as a horizontal line.

6.2.2 Immunisation with pilus protein-M2e fusion peptides results in M2e specific mucosal antibody production

Following establishment of the optimal dosage for pilin-M2e fusion protein immunisations, the full vaccination panel was tested on mice. Five groups of female BALB/c mice (n=6) were immunised intranasally with three weekly doses. The 5 vaccination groups were as follows: GST-BP-M2e, GST-M2e-BP, His-AP1-M2e, poly I:C+M2e and M2e only. A week after completing the immunisation schedule, serum and NW samples were collected. ELISAs were performed using serum samples starting at 1:200 dilution and NW samples starting from NEAT, to determine M2e specific IgG and IgA responses. Endpoint titre was determined as the minimum serial dilution where absorbance was above mean absorbance + 3 standard deviations of control wells.

M2e specific mucosal IgA response was found to be varied between groups. While overall antibody response was not strikingly robust, mice vaccinated with the pilus protein-M2e fusion peptides possessed statistically significantly higher M2e-specific IgA titres compared to mice administered M2e alone (Figure 6.5A). Mice immunised with GST-M2e-BP had the highest amounts of M2e specific antibodies, compared to mice vaccinated with just M2e (P= 0.0005). These mice additionally had greater levels of M2e IgA compared to mice administered poly I:C+M2e (P=0.01) (Figure 6.5A). Compared to mice immunised with M2e alone, M2e IgA production was also significantly higher in mice vaccinated with GST-BP-M2e (P= 0.032) and His-AP1-M2e (P= 0.025) (Figure 6.5A).

Whilst immunisation with pilus protein-M2e fusion peptides induced somewhat higher mucosal antibody responses in mice than administration of M2e alone, the fusion proteins did not appear to enhance serum IgG responses (Figure 6.5B). In fact, mice administered GST-BP-M2e, GST-M2e-BP and His-AP1-M2e all did not produce levels of M2e specific serum IgG above the titre cut-off. The mice vaccinated with poly I:C+M2e did however generate substantial M2e IgG, with antibody titre significantly greater than mice in the M2e alone group (P= 0.026) (Figure 6.5B).

Figure 6.5. Immunisation with pilus protein-M2e fusion peptides induce significant M2e IgA antibodies but not IgG antibodies. BALB/c mice (n=6) were intranasally immunised with either GST-BP-M2e, GST-BP-M2e, His-AP1-M2e poly I:C+M2e or M2e alone. Serum and nasal wash samples were collected and serum samples were diluted 1:200 before all samples were titrated and analysed using ELISA with immobilised M2e in duplicate to determine (A) IgA M2e endpoint antibody titre and (B) IgG M2e endpoint antibody titre. Each data point

represents the endpoint antibody titre in an individual mouse, defined as the minimum serial dilution where absorbance was above mean absorbance + 3 standard deviations of control wells. The median of each group is shown as a horizontal line and statistical significance was determined using Kruskal-Wallis analysis with a Dunn's test for multiple analysis. *P ≤ 0.05, **P ≤ 0.01, ***P < 0.001

6.2.3 Serum antibody response to pilus protein-M2e is skewed towards pilus proteins

The lack of serum IgG antibodies against M2e detected in mice immunised with pilus-protein M2e peptides prompted a probe into the vaccination efficiency and verification of whether there was antibody induced towards the pilus subunits portion of the vaccine. To this end, ELISAs using 1:200 diluted serum samples collected from the immunisation panel were performed to determine pilus protein specific IgG response. End point titre was determined as the minimum serial dilution where absorbance was above mean absorbance + 3 standard deviations of control wells.

The ELISAs showed significant levels of pilin-specific IgG in the serum samples. Mice given His-AP1-M2e had median endpoint AP1 IgG antibody titre of 5300, whilst the cohorts immunised with GST-BP-M2e and GST-M2e-BP had median endpoint BP IgG titres of 5500 and 2700 respectively (Figure 6.6). The presence of these pilus specific antibodies gave assurance that the immunisation was effective and the lack of serum M2e IgG measured previously was not due to the vaccine lacking efficiency. However, coupled with the observation of the fusion protein vaccinated mice not exhibiting substantial levels of serum M2e IgG, these results suggest that serum antibody response to pilus protein-M2e peptides was dominated by the production of antibodies against the pilus component of the structure.
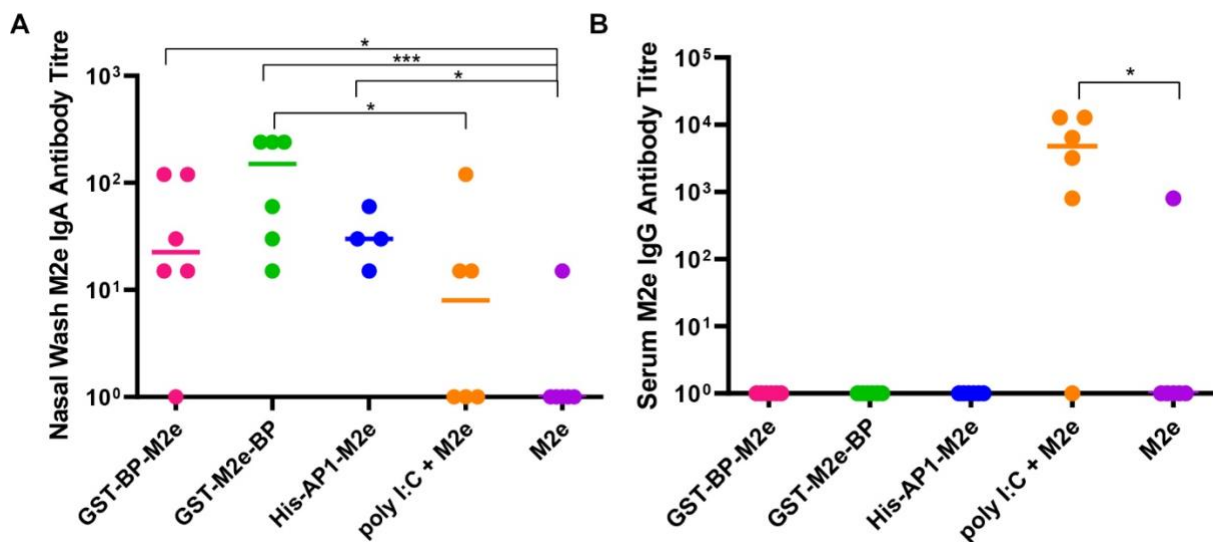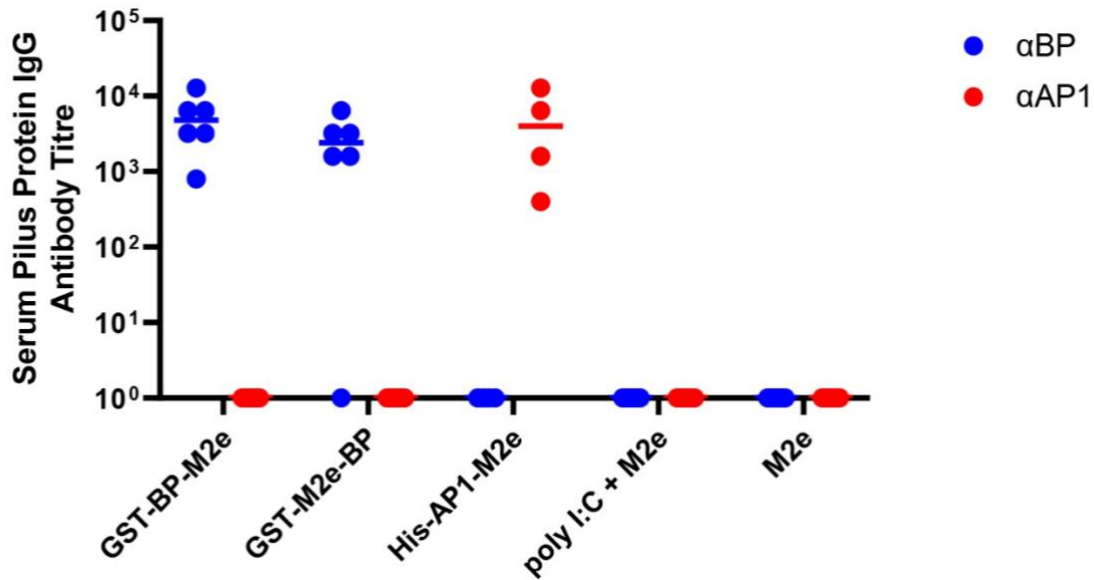
Figure 6.6. Immunisation with pilus protein-M2e fusion peptides induce significant pilus protein IgG antibodies. BALB/c mice (n=6) were intranasally immunised with either GST-BP-M2e, GST-BP-M2e, His-AP1-M2e poly I:C+M2e or M2e alone. Serum samples were collected and diluted 1:200 before being titrated and added to ELISA with immobilised BP or AP1 in duplicate to determine BP and AP1 specific IgG antibody endpoint titre. Each data point represents the endpoint antibody titre in an individual mouse, defined as the minimum serial dilution where absorbance was above mean absorbance ± 3 standard deviations of control wells. The median of each group is shown as a horizontal line.

6.3 Discussion

This chapter surveyed the capacity of pilus proteins to modulate adaptive immunity using both *in vitro* and *in vivo* systems. The first block of *in vitro* assays addressed whether the pilus proteins enhanced the capacity of APCs to interact with and modulate portions of the immune system. Before specific modulatory factors upregulated by the pilus proteins were pin-pointed, an initial survey into whether these structures activated macrophages, an initiative step of the immune cell maturation, was performed using the MTT assay. As touched on above, MTT can be reduced by mitochondrial dehydrogenases in metabolically active cells to form crystals, which can be measured in a colourmetric assay (361). Resultantly, colourmetric measurements of cell suspensions with MTT are proportional to the level of activity of the cells. For example, activated lymphocytes demonstrate ten-fold higher colourmetric measurements compared to resting cells (362). These properties of the MTT assay have confounded in its usage in a variety of adjuvant studies to scope whether the molecules induced macrophage activation and

proliferation prior to investigations delving into specific pathways activated (361,363,364). For instance, the MTT assay has assisted in illustrating the ability of aluminium based adjuvants to enhance THP-1 activity and were also used to highlight the increased macrophage stimulation driven by TLR4 activating polysaccharides, prior to measuring upregulation of downstream immunomodulatory processes such as cytokine secretion (364). In a similar fashion, the MTT assay here confirmed the pilus proteins triggering murine macrophage activation, with cellular exposure to pilus subunits resulting in increased absorbance and therefore greater metabolic activity, compared to untreated cells (Figure 6.1). This heightened absorbance was on par with measurements from cells receiving the lymphocytic ConA mitogen, emphasising the high capacity of the pilus proteins to induce macrophage activation (365). It can be noted the macrophages not exposed to the pilus protein stimulants or positive control ConA still exhibited fairly high baseline activity. This was expected as all cells will have some level of metabolic activity to fulfil biological functions and this property has in fact made MTT assays a convenient way to gauge viable cell numbers (366).

The MTT assay provided evidence of pilus proteins inducing immune cell activation and it could be implied that the enhanced metabolic activity of the cells was indicative of increased activity of immunomodulatory pathways, stipulating the adjuvanting properties of pilus. This ramification was directly addressed via cytokine and co-stimulatory molecule measurements.

Simultaneous testing of multiple cytokines was required to understand the type of T cell response to the pilus proteins. T cells differentiate into variable effector Th types based on the surrounding cytokine milieu and are then able to exert distinct influences on the adaptive immune response (367,368). For example, IFNγ is key for the polarisation of T cells towards effector Th1 cells, which propel cell-mediated immunity towards intracellular pathogens (369,370). IL-4 and IL-10 on the other hand, drive differentiation into effector Th2 cells, which provide antibody facilitated defence against extracellular pathogens (361,362). IL-6 drives the maturation of T cells into the more recently defined Tfh cells, which are crucial for the generation of effective long-term protective antibody responses against pathogens. This is achieved through the ability of Tfh cells to mediate activation of high-affinity antibody producing B cells and memory B cells (139–141). Conversely, some cytokines such as TNF are associated with several Th phenotypes, depending on the combination of cytokines that are simultaneously present (371,372). There are additional subsets of Th cells which also

experience cytokine driven differentiation such as the IL-17 secreting Th17 cells (369). An effective vaccine adjuvant should therefore induce a cytokine environment which favours differentiation of T cells into a Th cell subset which can mediate protection against the target pathogen. Consequently, a Luminex assay covering the detection of cytokines associated with variable effector Th profiles was employed in this chapter, to gain some insight into the T cell driven adaptive immune response induced by the pilus proteins.

The conspicuous BP and AP1 driven release of TNF from the murine macrophages detected by the Luminex assay (Figure 6.2A) was in line with the ELISA results seen previously (206). The ability of pilus protein to induce TNF secretion highlights the potential adjuvanting properties of the pilus as this cytokine directly and indirectly modulates adaptive immune cells in a variety of ways (373). TNF release from innate immune cells results in maturation of that particular cell population via a feedback system, while also triggering maturation of other APCs in proximity. This results in enhanced T cell activation as it increases APC expression of T cell co-stimulation molecules such as CD86 (374). Additionally, this cytokine can interact with T cells directly via tumour necrosis factor receptor 2 (TNFR2) to augment T cell proliferation and sustain cell survival (375,376). The influence of TNF on T cell activity has been confirmed with TNF knock-out mice displaying reduced DC maturation and T cell response, as well as heightened T cell activation achieved in cell lines supplemented with the cytokine (338,377). Additionally, TNF has been demonstrated to elevate antibody production by increasing the level of activated T cells required for proliferation and differentiation of antigen specific B cells (378). TNF has also been reported to induce DC secretion of B cell activating factor (BAFF), which is a potent enhancer of B cell maturation, proliferation and immunoglobulin production (379,380). Furthermore, TNF is able to induce expression of endothelial adhesion molecules and stimulates chemotaxis to direct the migration of antigen-specific lymphocytes and APCs to the sites were antigens are present (381,382). Conversely the TNF mediated enhancement of migration can result in the translocation of APCs to the draining lymph nodes, where they are able to stimulate naïve adaptive immune cells (383,384). The pilus protein triggered release of TNF from innate immune cells is predicted to modulate the adaptive immune cells through such pathways to drive antibody production.

The adjuvanting potential of the pilus proteins was also suggested by their ability to upregulate IL-6 secretion in the murine macrophages (Figure 6.2B). IL-6 is a prominent pro-inflammatory

147

cytokine alongside TNF with a role in many different signalling pathways. Akin to TNF, IL-6 upregulates the expression of adhesion molecules to facilitate migration of immune cells (385). Moreover, analysis of IL-6 knockout mice has identified the necessity of IL-6 for T cell recruitment, with the cytokine triggering the expression of T cell attracting chemokines such as CCL4 (386). As mentioned above, another important caveat of this cytokine is its association with Tfh cell expansion (141). IL-6 has been observed to be essential for initiation of T cell differentiation into the Tfh lineage, with naïve CD4 T cells exposed to the cytokine found to upregulate the transcription factor responsible for Tfh cell specific gene expression (142,286). Contrarily, T cell maturation into Th1 cells was inhibited in the presence of IL-6, with the cytokine supressing IL-12 driven Th1 differentiation (387,388). The ability of pilus proteins to upregulate IL-6 is hence beneficial as the release of this cytokine can have the potential to shift the adaptive immune response towards Tfh cell expansion, in turn elevating the selection and maturation of B cells producing high affinity antibodies. This may be compounded by the ability of IL-6 to directly promote differentiation of B cells into antibody producing plasma cells, as illuminated in mice models (389) .

Pilus protein induced secretion of IL-2, IL-4, IL-10, IL-17 and IFNγ were not captured in this assay. As IL-2 is indicated to be a potent inhibitor of Tfh cell differentiation, its absence suggests that the pilus proteins do not trigger substantial cytokine driven negative regulation of Tfh cell activity (390). However, as innate immune cell synthesis of IL-2 occurs in small amounts, pilus protein induced cytokine release from adaptive immune cells should be studied before this conclusion is drawn (391). IL-4, which is synonymous with T cell differentiation into effector Th2 cells and antagonises TNF mediated dendritic cell stimulation, was also not detected (367,392). Similarly, IL-10 is an effector Th2 cell associated cytokine that has been observed to become upregulated following activation of TLRs including TLR2, which the pilus proteins have specificity for (206,393). However, this cytokine was also not detected following exposure of cells to pilus proteins. This is likely attributed to the cytokine being immune-inhibitory in nature, opposing the potently inflammatory properties of the pilus subunits (394). The apparent lack of IL-10 and IL-4 secretion measured following cellular exposure to pilus proteins could be regarded in a positive light as it is an indication that the adjuvanting properties of the pilus complexes are not self-limiting. IFNγ, which facilitates effector Th1 cell differentiation, was additionally not seen at levels above the limit of detection. IL-17 expression also did not appear to be promoted by the pilus proteins. This was not a cause of

major concern as the immunomodulatory properties of this cytokine, such as promotion of lymphocyte chemotaxis expression and B proliferation, were redundant and attainable through IL-6/TNF (379,381,395,396). Furthermore, as an overabundance of IL-17 has been implicated in autoimmune diseases such as rheumatoid arthritis, the lack of IL-17 induction by this potential adjuvant decreases associated safety concerns (397). It should also be noted that the cellular production of some cytokines in the panel, namely IL-4, IL-17 and IFNγ, has been illustrated to be more commonly associated with lymphocytes (398–400). This may have compounded to the lack of detectable levels of these cytokines in this assay, which utilised a cell line of the macrophage lineage.

The Luminex assay illuminated pili induced release of TNF, which enhances overall adaptive immune cell activity and IL-6, a cytokine heavily involved in differentiation of T cells into the Tfh subset. Th2 differentiation inducing IL-4 and IL-10, Th1 associated IFNγ and the Tfh inhibitory IL-2 was not detected in this assay. This suggests that pilus induced cytokine release may skew T cell differentiation towards Tfh cells over other effector Th cell phenotypes. Consequently, pili may possess the ability to enhance long lived humoral responses by regulating the activity of T cells which support robust B cell antibody production. Increased T cell differentiation towards the Tfh cell lineage has previously been depicted to occur downstream of TLR2 activation (285,401). Therefore, the outcome of this cytokine assay aligns with the preceding chapter depicting the capacity of the pilus proteins to stimulate TLR2.

As the panel of cytokines tested here was not exhaustive, a larger array would be required to cement the proposed cytokine profile induced by the pilus proteins and its effects on T cell differentiation. Pilus proteins have already been established to trigger secretion of one cytokine not included in this test, the inflammatory IL-8, highlighting the benefits of an expanded panel. Capturing the presence of additional cytokines, such as IL-21, which is another signal instrumental in Tfh cell maturation, would also help solidify the current proposed capacity of pilus proteins to polarise T cells towards differentiating into the Tfh subtype (402).

An alternative method for exploring pilus protein transduced adaptive immune cell modulation came from flow cytometry assays, where the upregulation of the co-stimulatory molecules CD80, CD86, F4/80 and antigen presenting MHCII on murine macrophages was measured following exposure to pilus subunits. F4/80 has widely been used as a marker of murine macrophages and expression level is related to the physiological state of the cell, where

increased display of the molecule can be interpreted as elevated cell activation and progression towards a matured state (403). As depicted in Figure 6.3B, incubation of murine macrophages with BP resulted in a significant, nearly 6-fold increase in F4/80 expression compared to unstimulated cells. This highlighted the ability of BP to drive macrophage activation and mirrored the outcome of the MTT assay. Exposure of macrophages to AP1 did not result in a change to F4/80 upregulation deemed statistically significant. However, as MFI values indicated close to 4-fold higher F4/80 expression in these cells compared to untreated cells and as the MTT assay depicted significant changes to metabolic activity following macrophage exposure to AP1, it is plausible to assume this pilus subunit also yields the ability to initiate macrophage maturation.

Two distinct signals from APCs are required for T cell activation and proliferation. The first is the presentation of antigens to the T cell receptor (TCR) via MHCII, which immobilises peptides for effective display. MHCII and TCR interactions occur in parallel to CD80 and CD86 interacting with CD28 on T cells to transduce a second signal and the combined effect is the activation, expansion and differentiation of T cells, which are then able to activate antibody production in B cells (404,405). MHCII presentation of antigens is a key component of T cell activation, with impairment to MHCII expression markedly reducing the population of developed T cells (406,407). Furthermore, the importance of the tandem effect of APC CD80 and CD86 expression can be seen in cellular CD80/CD86 blockade models, where T cell activation and associated cytokine upregulation was diminished (405,408). Deletion of these co-stimulation molecules was also found to significantly impair antibody response (409). Preceding results illustrated pilus protein driven cell activation and the pilus dependent secretion of cytokines associated with upregulation of CD86 and CD80. Aligned with these findings, the flow cytometry assay revealed both BP and AP1 stimulating over 2-fold higher CD86 expression and 3.1- and 6.4-fold higher CD80 expression, respectively. CD86 and CD80 expression is downstream of TLR activation, so this result is also in line with the narrative established in previous chapters of pilus proteins being TLR2 agonists (410,411).

MHCII is also under the regulation of TLR signalling pathways, with activation of the receptors promoting loading of endocytosed or phagocytosed antigens onto MHCII and redistribution of the molecules to the cell surface (412,413). Furthermore, MHCII biosynthesis has been shown to become transiently upregulated in response to cell activation, a process which was

demonstrated in prior assays (414,415). Thus it was anticipated that the TLR2 agonist pilus proteins would upregulate the expression of MHCII on murine macrophages. However, as portrayed in Figure 6.3B, flow cytometry following incubation of mouse macrophages with the pilus proteins was not able to capture a significant increase in the upregulation of MHCII. Despite the MFI of pilus treated cells being similar to the positive control cells, the 1.6-fold shift in MFI between unstimulated cells and cells exposed to pilus proteins was not deemed to be statistically significant. The abundant evidence of macrophage activation/maturation seen across the J774A.2 cell line assays and the fact that MHCII shares induction pathways with CD86 and CD80, suggests that it is conceivable that pilus mediated MHCII upregulation occurred but was not successfully captured by the flow cytometry assay. It should be noted that prior to testing pilus stimulated macrophages on the flow cytometer, each of the antibodies used was titrated to determine optimal working concentrations. At this point, the antibodies against MHCII was noted to generate a markedly lower signal than the other antibodies, with up to 80-times more antibody required to get similar fluorescence intensity as the other labels. The differences in MHCII expression between treatment groups as reported by MFI may thus have lacked statistical power due to the seemingly subordinate labelling efficiency of the antibody used. In fact, the difference in MFI between unstimulated cells and positive control treated cells following labelling with MHCII antibody was also not statistically significant, an outcome which diverges from the results of the positive control group for the other three co-stimulatory molecules (Figure 6.3). A repeat of the flow cytometry assay using different antibodies against MHCII, possibly including ones binding to different MHCII variants, may assist in defining statistically powerful changes in MHCII expression following treatment with the pilus proteins. The inability of this assay to successfully illustrate strong MHCII expression may have been compounded by suboptimal cell environmental conditions. For instance, IFNγ is a primary signaling cytokine for induction of MHCII expression on macrophages. The presence of this cytokine has been found to establish a positive feedback loop *in vivo,* where IFNγ directed MHCII expression on macrophages allows the cells to interact with T cells, which in turn are stimulated to produce more IFNγ to further upregulate MHCII expression (416,417). As evident by the Luminex assay, IFNγ was not secreted by the J774A.2 cells following incubation with pilus proteins and as macrophage cells were investigated isolated from adaptive immune cells, there was little leeway for the establishment of a feedback loop to increase MHCII expression. Nonetheless, the ability of the pilus proteins to establish

increased expression of co-stimulatory factors on APCs necessary for proliferative adaptive immune cell response alluded to the adjuvanting potential of the pili.

The preceding assays demonstrated the ability of the pilus proteins to enhance APC derived adaptive immune cell immunomodulation factors and hinted at the pili having the potential to create an environment where the adaptive immune response is skewed towards the high antibody producing Tfh phenotype. The projected downstream culmination of these observations is enhanced antigen specific antibody production, and thus immunisation studies were carried out using the pilus protein-M2e fusion peptides generated in Chapter 5.

A pilot immunisation round using His-AP1-M2e and GST-BP-M2e assisted in establishing a vaccination protocol prior to the expansion of the mouse immunisation model to include all fusion proteins and controls. Although the wax moth larvae experiments in Chapter 3 indicated that pilus protein mediated inflammation was not likely to cause adverse effects, there was still some concerns surrounding the effects of this potent ligand in a mammalian model. These concerns were fuelled by reports of inclusion of TLR agonists in murine intranasal flu vaccines causing atypical immune responses associated with toxicity (418). Across all vaccination groups, mice were not recorded experiencing behavioural or weight changes following immunisation. The sustained health of all mice involved in the pilot study throughout the course of immunisations provided assurance that the pilus proteins were inflammatory but did not elicit adverse health effects.

Casting attention to the pilus antibody responses to His-AP1-M2e (Figure 6.4A), mice immunised with recombinant AP1 had similar IgG and IgA responses compared to mice administered His-AP1-M2e at equal dosages. This provided some affirmation that the pilus protein interaction with immune cells was maintained in the fusion protein. Antithetical to His-AP1-M2e, mice immunised with GST-BP-M2e had more pronounced antibody response compared to mice immunised with recombinant BP (Figure 6.4B). This appears to highlight BP having a higher adjuvant activity than AP1 when incorporated into a fusion protein conjugated to antigen. One reason for this discrepancy in antibody response could be due to variability in the efficiency of uptake by APCs. For example, the BP based fusion protein may have a higher tendency to form aggregates, which appear to enhance APC uptake (419). The GST tag on the BP based fusion protein may have increased the likelihood of this occurrence, due to its ability to form dimers (420).

M2e antibody response was ascertained in both GST-BP-M2e and His-AP1-M2e immunised mice (Figure 6.4A, B). M2e antibody response was lower overall compared to response towards pilus proteins, reflecting their intrinsic difference in immunogenicity. While there was some variance in antibody responses, the highest 50 µg dosage appeared to elicit a detectable response across samples. As this dosage also did not induce any eminent health effects, it was selected as the vaccination concentration for the full immunisation panel (Figure 6.4).

The full vaccine panel allowed immunisation with the three different pilus protein-M2e fusion complexes to be compared with M2e alone and M2e supplemented with the established poly I:C adjuvant. Focusing first on the mucosal IgA response (Figure 6.5A), only one mouse in the M2e only immunisation group had antibody titres above the cut-off, re-emphasising the poorly immunogenic nature of this antigen. In contrast, though not dramatic, all three fusion proteins (GST-M2e-BP, GST-BP-M2e and His-AP1-M2e) induced enhancement of M2e specific IgA antibodies. This was backed by statistical analysis, which indicated that median titres were higher compared to that of the group administered M2e alone.

GST-M2e-BP invoked the most noticeable levels of M2e IgA titres in the mice, with the end point titre statistically significantly higher than mice immunised with M2e in combination with the widely used poly I:C adjuvant. Thus GST-M2e-BP appeared to possess higher immunogenicity compared to His-AP1-M2e and GST-BP-M2e, despite the latter protein consisting of the same peptide components. The cause for this discrepancy may lie in the differing configurations between the two fusion proteins. As discussed previously, the conjugation of proteins without a linker can reduce the degrees of freedom of a protein and incite steric hindrance. Such disruption may have been more substantial when M2e was conjugated at the C terminus and resulted in impaired adjuvanting ability of pilus proteins (317,332,333). Furthermore, the GST-M2e-BP structure sandwiches the M2e peptide between BP and the GST tag, which may have resulted in M2e remaining intact and attached to the immunostimulatory BP subunit for longer periods. In contrast, M2e in GST-BP-M2e and His-AP1-M2e is exposed at the end of the protein complex. Thus it may have been more susceptible to degradation and separation from the immunostimulatory pilus subunit. The peptide may have also been more liable to exoprotease driven cleavage, as these enzymes attack terminal amino acids (421).

While pilus proteins elevated antibody response towards M2e, the ensuing titres were conservative and there appears to be room for improvement of the adjuvant activity. One characteristic of the pilus subunits which may need to be considered is the fact that there will be an adjuvant specific antibody response to the proteins, which may interfere with the antigen-specific antibody responses. This has been observed in other adjuvants such as flagellin, where the adjuvant moderately induced antigen specific antibody levels to a low immunogenicity antigen but not to the anticipated magnitude. This was linked to the adjuvant antibody response outcompeting the immune response to the antigen (422). The balance between immunogenicity and adjuvanticity of flagellin has played a large role in the development of the protein as an adjuvant, with focused efforts to truncate the protein to reduce flagellin-specific antibody responses and skew activity towards adjuvanticity (423–425). In the context of mucosal adjuvants, when utilised as an adjuvant for HIV protein, recombinant flagellin with deleted domains was shown to elicit higher HIV protein specific mucosal antibody levels compared to wild type protein (426). Thus similar modifications to the pilus proteins may be the next step in developing the structures as vaccine adjuvants.

The primary target for intranasally administered vaccines is the nasal-associated lymphoid tissues (NALT) (427). In the NALT, APCs can present antigens to T cells which induce B cell differentiation into IgA secreting plasma cells in the presence of cytokines/ co-stimulatory factors (427,428). These plasma cells can secrete IgA which can be transported back to the vaccination site and in parallel, the cells can also migrate throughout the mucosa of the respiratory tract to induce further IgA response (427,428). In parallel to this localised response, antigen carrying APCs can migrate to regional lymph nodes and activate adaptive immune cells to translocate into the bloodstream and induce serum IgG response (428–430). Antigens can also diffuse through the nasal mucosa directly into the bloodstream to interact with circulating adaptive immune cells and trigger IgG production (431). In this vaccination schedule, serum IgG response elicited through such processes was not reported in the fusion protein immunised mice (Figure 6.5B), indicating that the conjugated protein complexes appeared to be effective in eliciting an immediate local mucosal immune response but did not seem to stimulate a systemic response upon direct or APC mediated transportation from the mucosa.

Despite there being other reported cases of mucosal immunisation resulting in a IgA response in the mucosa without evidence of substantial IgG generation or considerably lower IgG

production, the cause of this response profile was not concretely defined (432,433). One possible theory arising from such studies was the rate of mucociliary clearance effecting antibody production (433,434). It was observed that substantial mucosal IgA was induced even in rapidly cleared immunisations but prolonged residence of vaccines in the mucosa was required for IgG production on par with intra-muscularly administered vaccines (433,434). Thus fusion proteins may have had relatively faster clearance from the immunisation sites compared to poly I:C+M2e, a theory especially likely considering studies signifying the potential of poly I:C to disrupt respiratory clearance mechanisms (435). Reducing the size of the fusion proteins could circumnavigate extensive mucociliary clearance by improving the rate of absorption so that the vaccine passes through the nasal mucosa before it can be cleared (436).

Additionally, the pilus proteins are likely to not be as stable of an adjuvant as poly I:C. Whilst fusion proteins may have remained relativity intact during induction of localised mucosal responses, large amounts of the complexes may have become degraded by the time they became disseminated throughout the immune system. Breakage could have occurred at the TLR2 interacting domain during translocation from the nasal cavity, reducing the level of immunostimulation conferred. Furthermore, degradation resulting in separation of the M2e antigen from the pilus protein would abolish the state of synergy achieved by co-delivery of antigen and adjuvant to the same cell, where the adjuvant amplifies cell activation and antigen uptake, which in turn increases the availability of adjuvant recognising receptors (300,307). As alluded to above, terminally conjugated M2e would be especially prone to degradation. As the entire M2e amino acid sequence constitutes a single T cell epitope, even partial degradation of M2e can result in a low serum antibody response to the peptide (357). The lack of serum IgG elicited by the fusion proteins including GST-M2e-BP suggests sandwiching of the peptide may not have been sufficient to entirely protect M2e from degradation throughout the protein dissemination process.

The low IgG antibody response against M2e recorded in the fusion protein immunised mice prompted an investigation into the pilus specific serum IgG response in these cohorts. As illustrated in Figure 6.6, mice administered His-AP1-M2e had high antibody titres against AP1 and the immunisation cohorts receiving GST-BP-M2e and GST-M2e-BP generated high titres

of antibodies against BP. These observations appear to illustrate a strong antibody response against the pilus proteins overwhelming M2e specific antibody responses in the sera.

As described above, protein based adjuvants can suffer from the drawback of inducing adjuvant-specific antibody responses. The serum samples indicate an especially strong dominance of adjuvant specific response, with antibody production being entirely skewed towards the pilus proteins. The degradation of fusion proteins during trafficking from the nasal cavity could have compounded to this immunodominance in the serum. Pilus proteins contain multiple epitopes and thus compared to M2e, are more likely to continue to display intact epitopes subsequent to breakage. Additionally, antibody production may also have been directed to the respective tags on each fusion protein, which are more stable structures. The tags may have provided another additional epitope that antibody production could be directed towards instead of the M2e peptide, resulting in further divergence of the immune response from M2e specific antibody production. Of note, many immunisation studies using protein-derived adjuvants have reported the occurrence of "immune imprinting", where the presence of dominant epitopes results in the immune response towards booster vaccinations becoming heavily directed towards these epitopes (437). This phenomenon also seems to have occurred on a global scale during the circulation and use of successive variants of COVID-19 vaccines (437). As the vaccination schedule for the pilus protein-M2e fusion peptides consisted of consecutive booster immunisations, "immune imprinting" may have amplified the dominance of non M2e antibodies in the sera.

As touched on previously, mucosal IgA production is crucial for providing protection against influenza (352–354). Protection conferred from local IgA in fact, appears to be as important or more than the effects of serum IgG. For instance, nasal murine influenza infections models indicated that IgA but not IgG successfully prevented viral pathology in the upper respiratory tract, and transfer of nasal IgA to naïve mice has been demonstrated to be sufficient for protection against infection (438,439). Furthermore, local IgA was found to correlate to protection in a human challenge study using participants pre-screened for low antibody titres (440). Therefore, the M2e IgA response elicited by the pilus protein-M2e fusion complexes alone may provide some level of protection against influenza infection, although re-modelling of the fusion construct to ensure serum IgG response and a more robust IgA response is still desirable.

Parenteral vaccination often does not elicit sufficient localised IgA response due to a lack of mucosal homing receptors induced on immune cells activated in peripheral lymph nodes (429,441). Thus, for this immunisation schedule testing pilus protein-M2e fusion complexes, routes of administration such as subcutaneous injection were not tested. However, it would be of interest to see the adjuvanting properties of the pilus proteins when delivered parenterally, where there is often faster drainage to lymph nodes and systemic circulation (442) .

The first portion of this chapter alluded to the pilus proteins enhancing humoral immunity by demonstrating the upstream immune modulatory pathways elevated by these proteins. The subsequent mouse immunisation assay gave further weight to the idea that both BP and AP1 pilus subunits operated as adjuvants with the ability to leverage antigen specific IgA production downstream of these pathways. However, the pilus subunits were not able to enhance the generation of antigen specific serum IgG antibodies and the enrichment of IgA response was not as robust as it could be. Further work is required to fully realise and elucidate the adjuvanting potential of the GAS pilus.

Chapter 7: Summary and Future Directions

As Group A Streptococcus is a successful human pathogen which exerts a significant health burden on the global population, the virulence factors supporting the initiation of infection are of great interest. GAS pili are a key player in this process and thus their functional characteristics and potential as a vaccine target has been examined. However, the interaction between GAS pili and innate immune system has been left largely undefined. Prior to this project, our preliminary probe into the innate immune response towards GAS pili pointed towards the complex being inflammatory in nature. This raised the question of whether this property of GAS pili was associated with the presentation of GAS disease, as inflammation contributes to some of the more severe clinical presentations of GAS infection. Additionally, the complex appeared to have the ability to induce TLR, a molecule which facilitates immune potentiating signals and is recognised to act as a bridging mechanism between innate and adaptive immunity. These observations suggested that the complex may have immunomodulatory properties that could be exploited in the development of an immunogenicity increasing adjuvant. Thus the overarching aim of this project was to characterise the innate immune response to GAS pili to assess the potential of the complex as a vaccine adjuvant.

7.1   Summary

The inflammatory response to a range of different GAS pilus types was investigated in non-pathogenic *L. lactis* surrogate strains each expressing a different FCT-type pilus. *In vitro* assays using monocytic cell lines indicated all pilus types inducing a cytokine response and highlighted the particular strong cytokine secretion elicited by the FCT-1 type pilus derived from M6 GAS (PilM6). This divergence in inflammatory response was not surprising considering the variation in both gene sequence and regulation of expression between different pilus types (26,61,62). The same trend of pilus-mediated immune response could be modeled in *Galleria mellonella* larvae, which possess an innate immune system functionally and anatomically similar to vertebrates (443). PilM6 has distinct properties such as being a strong proponent of biofilm formation irrespective of cell culture conditions and facilitating this process through use of the tip subunit as an adhesin, as opposed to pilus-driven auto aggregation (37,63,79). The high inflammatory response elicited by this structure could possibly be a result of these properties, which may have increased the tendency for bacterial

aggregation and enhanced interactions between pili and host immune cells. Further testing of the *L. lactis* strain expressing this pilus, such as recording the incidence of biofilm formation, required to confirm this conjecture.

Both *in vitro* and *in vivo* models indicated that the disparities in pilus-induced inflammatory response did not correlate to the severity of disease associated with the GAS strain from which the pili were derived from. The most inflammatory PilM6 is produced in a M6T6 serotype strain which is associated with non-invasive superficial infections (29). Conversely, pili inducing more subdued immune responses were grouped into FCT-types seen in GAS strains associated with more invasions infection or post immune sequalae (9). Assays documenting haemocyte counts and bacterial clearance following administration of the pilus-expressing *L. lactis* strains into *G. mellonella* provided some explanation to this seemingly counterintuitive result. These experiments illustrated a post-infectious surge in circulating haemocyte density and decreased bacterial counts recovered from larvae at time points following this surge. It could be deduced that the presence of pili was stimulating an innate immune response/inflammation but the resulting influx of haemocytes was able to mount an effective response to eliminate the bacteria expressing the pili. Therefore, pilus-mediated inflammation was more likely to promote the clearance of bacterial infections as opposed to driving disruptive damage contributing to the progression of pathogenesis.

Preliminary results prior to the commencement of this project pointed towards GAS pili having the ability to stimulate TLR2 (206). A competition assay using the TLR2 antagonist SSL3 provided indirect evidence to substantiate this interaction. The assay indicated that BP and AP1 driven monocyte cytokine secretion decreased with the presence of increasing concentrations of co-incubated SSL3. SSL3 exerts its inhibitory activity by occupying TLR2 binding sites and prevents the TLR2 dimerisation required for initiation of the downstream signaling cascades (259,260,274). Thus the results of the experiment implied that BP and AP1 subunits have physical interaction with TLR2, which is required for the activation of the receptor. While bacterial pili/fimbriae from other microorganism have been described as stimulants of TLR2, the individual pilus proteins did not induce receptor activation unless they were assembled in an oligomerised macromolecular structure (210,275). Thus the aforementioned assays provided evidence of GAS pilus being one of the few pili with monomeric subunits that could individually act as TLR2 agonists.

An assay utilising HEK-cells individually expressing either TLR2/1 or TLR2/6 provided further information on the pilus protein interaction with TLR2, exhibiting both BP and AP1 having specificity for TLR2 heterodimerised with TLR6. This was reiterated with a competition assay using the SSL3 TLR2 antagonist, which demonstrated the subunits competing with SSL3 for recognition and stimulation of this heterodimeric receptor. The specificity of pilus proteins for TLR2/6 and their ability to induce the heterodimer is unique as all of the microbial compounds identified thus far to associate with TLR2 have either been antagonists, or shown specificity for TLR2/1 (259,279,280).

Pilus protein binding to TLR2 was also directly demonstrated using solid phase or cell based assays. AP1 was illustrated binding to immobilised monomeric TLR2 in a dose dependent manner and associated to both TLR2 and TLR2/6 expressed on HEK-cells. On the other hand, clear binding to immobilised TLR2 monomers or cell surface TLR2 could not be established for BP, and the association between this pilus protein and TLR2 was only clearly depicted in the TLR2/TLR6 dimer. This shows that whilst AP1 appears to robustly associate with monomeric TLR2, BP appears to require dimerisation of TLR2 with TLR6 in order to maintain stable receptor protein interactions. The lack of association seen in the solid phase and cell based binding assays is likely due to the washing steps dislodging the weaker interaction between BP and TLR2 (270,271). An optimised surface plasmon resonance assay may be required to illustrate the lower affinity interaction between BP and TLR2.

Cloning using pGEX-3C and pPROEX-Htb expression vectors and protein purification using affinity chromatography and size exclusion chromatography resulted in the successful expression and purification of four different GAS pilus and influenza A M2e peptide fusion proteins. These fusion proteins underwent protein integrity testing and functional validation, with the GST-BP-M2e, GST-M2e-BP and His-AP1-M2e successfully validated and utilised in downstream assays.

A cell based assay established that exposure of macrophages to pilus proteins increased cellular metabolic activity. This provided an initial indication of the ability of the proteins to activate macrophages and propel the process of immune cell maturation, which accounts for upregulated expression of immunomodulatory molecules. A more detailed analysis of downstream upregulated factors was undertaken using a multiplex cytokine assay. This revealed pilus protein inducing the release of TNF, which is involved in enhancing processes

such as T cell activation and proliferation, APC translocation and secretion of B cell activating factors (374–376,379–382). The proteins also upregulated IL-6, which provides signals for lymphocyte migration and drives polarisation of T cells towards the Tfh phenotype associated with high antibody production (139,385,386,401). These results were indicative of the pilus proteins stimulating processes related to an intensified humoral response. Staining of macrophages using fluorescent antibodies also revealed pilus protein mediated upregulation of CD80 and CD86 ligands. These co-stimulatory receptors operate in concert with MHC class II antigen presentation and are essential for T cell activation as well as robust antibody production (405,408,409).

The immune potentiating properties of pilus were further investigated by immunising mice intranasally with the pilus-M2e fusion proteins constructed earlier. Whilst mice administered with only M2e had negligible antibody titres, the mice immunised with GST-BP-M2e, GST-M2e-BP or His-AP1-M2e had detectable titres of M2e specific IgA antibodies, confirming both BP and AP1 have the ability to elevate antigen specific antibody production. In general, conjugation with BP showed a more prominent effect in the elevation of immunogenicity, and the N-terminal conjugated configuration (GST-M2e-BP) appeared to induce stronger M2e antibody production compared to C terminal M2e conjugation (GST-BP-M2e). It is possible that steric hindrance of the pilus protein may have been greater with C terminal conjugation, resulting in impaired adjuvanting ability of the pilin or reduced M2e recognition (317,332,333). The sandwiching of M2e peptide between the GST tag and BP may also have reduced degradation of the antigen, as well as provided protection against exoprotease cleavage and this was also raised as a possible cause for discrepancy in antibody responses (421). While IgA responses showed potential of pilus proteins to act as adjuvants, further work around honing the protein domains included would be needed to improve the immune potentiating ability of the pilus proteins.

The pilus proteins were unable to enhance the IgG response, with M2e specific IgG antibody levels in mice administrated the fusion proteins below the titre cut-off. This was proposed to be due to a lack of stability of the small M2e peptide, especially in the fusion proteins with terminal M2e conjugation. ELISA demonstrated a dominance of pilus protein antibodies in the serum. This suggested that progression of M2e degradation as the fusion proteins disseminated from the mucosa could have resulted in antibody response against this antigen becoming

overpowered by generation of antibodies against the fusion peptide tags and the multi-epitope pilus proteins. Additionally, rapid mucociliary clearance of the fusion proteins was hypothesised to be another contributor to the low IgG response, with the peptides possibly removed from the mucosa before they could be translocated for accelerated IgG production (433,434). This further accentuated the need for changes to the fusion protein construct to fully exploit the adjuvanting properties of pilus proteins. In the context of protection against influenza, nasal IgA has been sufficient in mouse models for prevention of infection and correlated to protection in a human challenge (438–440). Thus the pilus protein induced IgA response may still provide some protection in the absence of IgG antibodies. A challenge model using the fusion proteins could corroborate this idea.

7.2 Significance

The work in this project has started to characterise the interaction between GAS pili and the host immune system, an avenue of GAS research which has previously not been explored. The variations in inflammatory and immune responses to different pilus types was showcased and this project provided the first evidence of GAS pilus proteins being a TLR2 agonists and was also able to pinpoint the specific heterodimer recognising the structure.

The findings from this project also illustrated the GAS pili increasing the immunomodulatory potential of innate immune cells and suggested that with further development, the GAS pili have the potential to be developed into an adjuvant. The inclusion of an adjuvant in vaccine formulations has become increasingly important in recent years due to greater emphasis on the development of subunit vaccines (444). As these vaccines rely on the capacity of one or a select panel of defined antigens, there is often a much more subdued immune response compared to traditional vaccines consisting of entire pathogens which display the full library of intrinsic innate immune stimulating cell surface components (445).

There is currently high interest in producing adjuvants derived from immune potentiating molecules with the ability to target TLRs, such as the GAS pili. As the pathways through which TLR activation can result in enhanced adaptive immune response have been mapped, the mechanism in which these adjuvants work is more defined then traditional adjuvants. Although studies have been conducted on defining and utilising the adjuvanting ability of TLR2 agonists, these experiments have all been pre-clinical (446). Thus there is still a vacuum in the space of

TLR2 based adjuvants, which could be filled by the GAS pilus proteins. This project depicted the ability of individual GAS pilus subunits to act as fully proteinaceous TLR2 agonists. In contrast, other TLR2 agonists interact with the receptor via surface lipid moieties, instead of the protein structure itself. Thus when utilising the pilus proteins as adjuvants, there is no requirement for lipid moiety synthesis and coupling, which can further complicate the production process and inflate costs related to manufacturing.

Disparate to many of the TLR adjuvants currently being refined, this project appeared to indicate that GAS pili may encourage the expansion of Tfh cells. This makes the proteins an especially promising vaccine adjuvant as Tfh cells have potent B cell supporting ability, facilitating the formation of memory B cells and B cell production of protective antibodies (142). In fact, studies on vaccine derived humoral immunity, such as investigations into the Astra-Zeneca COVID vaccine, have demonstrated that neutralizing antibodies and vaccine-reactive memory B cells are nominal in the absence of Tfh cells (447). Due to the complexity of T cell differentiation *in vivo*, further cytokine panels and cellular characterisation assays would assist in confirming the suggestion drawn from this project that the pilus proteins induce a cytokine environment which skews T cells towards the Tfh cell type.

Of note, the downstream effects of TLR2 have been observed to become altered depending on whether it heterodimerises with TLR1 or TLR6 (448). The GAS pilus proteins AP1 and BP are TLR2 agonists signaling through the TLR2/6 heterodimer in particular. Compared to TLR2/1, activation of this heterodimer appears to induce the upregulation of more cytokine types associated with skewing of the immune response towards expanding Tfh cell activity, such as IL-6 and IL-21 (367,449,450). Thus GAS pili may be a TLR2 based agonist notably suited to instill a strong antibody based immune response. TLR agonists which mediate Th2 cell expansion, such as the TLR5 ligand flagellin, have had high interest in the space of adjuvant design as these effector T cells have also been implicated in enhanced antibody production (304). However, skewing of the immune system towards cytokine patterns favouring Th2 differentiation and the effector Th2 cell driven formation of IgE antibodies against vaccine antigens has been found to promote allergy in pre-disposed populations (451,452). As Tfh cells are not associated with allergic pathology, a TLR agonist which promotes expansion of this effector T cell phenotype, such as GAS pili, may be a safer potential adjuvant.

Furthermore, in the case of flagellin, issues may also arise when administering this complex as part of a vaccine due to its highly inflammatory nature (165). On the contrary, despite pili being potent innate immune inducers, this project has demonstrated that pilus-mediated inflammation did not appear to contribute to disruptive damage and thus the complex could be used to galvanise the immune system with low risk of causing damage to the recipient (252).

The need for investigating new adjuvants is also highly relevant in the design of mucosal vaccines. There has been heightened interest in mucosal vaccination as it offers the option of triggering protective immune responses directly at the site of initial pathogen colonisation, thus curtailing establishment of infection (453). However, the mucosa is constantly exposed to antigens through inhalation and ingestion and is thus inherently less immunogenic to prevent hyperactivity, resulting in the necessity of adjuvants when delivering a vaccine to the mucosal immune system (454). However, adjuvants generated for parenteral administration may not always translate to effective mucosal adjuvants and compounds may have to be designed separately for use in the mucosa. For example, despite its commercialization and widespread use as a delivery adjuvant, alum is not suited for oral or intranasal immunisation due to its properties of forming antigenic deposits at the site of administration and poor mucosal immunogenicity (455). The most chronicled mucosal adjuvants are the B subunit of bacterial ADP-ribosylating enterotoxins, which includes compounds such as cholera toxins. These molecules induce TLR independent signaling pathways in APCs to amplify downstream adaptive immune cell modulators and have also been demonstrated to enhance permeability of epithelium for antigen translocation (358,456–458). However, the high risk of these toxins to induce dire side effects has posed a roadblock in the standardisation of the compounds into adjuvants (358,359). Chitosan is another notable mucosal adjuvant, consisting of a biopolymer derived from crustacean shell, which can be used as an antigen transport system. This adjuvant improves transport of antigens through the epithelium and reduces mucociliary facilitated vaccine clearance by inducing translocation of cellular tight junctions (459). However, research on this adjuvant is still in the preclinical phases and the variability in deacetylation and molecular weight of chitosan molecules, due to its derivation from organic shell material, creates difficulties in standardisation of experimental processes (460,461).

In this project, intranasally administered antigen conjugated to GAS pilus proteins showed some enhancement of mucosal IgA response, indicating that pili could be used as an adjuvant

administrated through mucosal routes. However, the results from this project seem to indicate that the pilus subunit requires further modification to avoid the overwhelming antibody response towards the immunodominant pilus protein, which appears to be detracting from the enhancement of antigen targeted humoral responses. TLRs are implicated in protective immunity across different mucosal sites such as the upper respiratory tract, cervix and the gastric tract. Furthermore, the receptor is present on both professional immune cells and epithelial cells lining these mucosal surfaces (462–464). Thus with further development, a TLR agonist such as GAS pili is likely to be a particularly effective amplifier of immunogenicity in the mucosa, where there is substantial TLR expression. On top of this, this project demonstrated that GAS pili are not likely to conflict significant damage to host cells or proteins and thus may have an improved safety profile compared to bacterial enterotoxin based adjuvants (358,359). Also, the pilus based adjuvanting system in this project was protein based and did not require any chemical conjugation. Thus the complex was able to be successfully produced using bacterial expression systems. This process could be scaled up for mass production whilst ensuring the compound is not subjected to issues in product variability such as seen in the mucosal adjuvant chitosan (461).

It should be noted that whole assembled pili and the backbone subunits are currently being explored as vaccines against GAS (223,253). GAS pili have also been repurposed as an experimental vaccine delivery platform, where antigens are engineered to be incorporated into the backbone subunits (96,97). The immune modulating activity of GAS pili explored in this project further strengthens its position as a vaccine candidate against GAS, as it suggests that the pili have high immunogenicity without the addition of extrinsic adjuvants and may function as a self-contained vaccine formulation. Furthermore, the findings propound the effectiveness of pili as a vaccine delivery platform, as they are indicative of the delivery mechanism having the dual effect of stabilising peptides via incorporation into the pilus structure and acting as immune potentiator. This may be compounded by the adhesive properties of the pilus proteins, which may assist in antigen retention, a feature especially useful for mucosal vaccines.

7.3 Conclusion and Future Perspectives

This project unravelled many aspects of the interaction between GAS pili and innate immune cells and detailed the immunomodulation capacity of these structures. These results suggest

refinement and continuous exploration into the adjuvanting capability of this structure and the further investigation into its interaction with components of the immune system.

This research demonstrated the usefulness of using *G. mellonella* to assist in depicting the inflammatory properties of GAS pili. With the expanding utility and increasing genomic information of this alternative infection model, it can be expected that additional knowledge can be drawn from using the *G. mellonella* model. In this project, measuring the haemocyte density helped evaluate the innate immune response towards pili based on the amount of cells deployed against the PAMP. This information could be further supplemented by identifying differences in the level of downstream process induced in these recruited innate immune cells. For example, release of antimicrobial peptides have been shown to be a consequence of innate immune cell activation in *G. mellonella* (465). The amount of anti-microbial peptides secreted in response to different pili could be investigated via proteomic profiling to gain further understanding of differential innate immune response to pilus types.

This project established the interaction between GAS pili and the important PRR TLR2. Further investigation is warranted to identify the exact domains in pilus proteins at the interface of this interaction. This could be done by cloning and expression of the separate domains from which BP and AP1 are formed and a repeat of the binding/competition assays in this project to determine the domains contributing to the role of pili as a TLR2 agonist. Surface plasmon resonance could be re-visited when testing domains as the smaller size test proteins would allow for the use of a less densely immobilised chip. This would reduce steric hindrance and non-specific electrostatic binding and could decrease the variability in binding between test runs which was an issue when using SPR in this project. Determination of the exact TLR2 interaction domain may also be useful when considering the use of GAS pili as an adjuvant. Conjugation of antigen to the domain responsible for TLR2 stimulation could be avoided to prevent the antigen introducing steric hindrance that blocks interactions with TLR2. Furthermore, an adjuvant could be designed to incorporate just the TLR2 recognition domain instead of using the whole pilus protein. Inclusion of just the interaction domain would likely decrease the pilus epitopes present and thus reduce the divergence of antibody production away from the M2e antigen seen in this project.

The cytokine response elicited by pilus proteins was investigated in this project, by measuring cell supernatant after overnight expression to the complexes. However, cytokine secretion can

be a transient process and this assay did not account for the produced, degraded and absorbed cytokines resulting in the net outcome measured (466). Furthermore, the assay was not able to differentiate between biologically active and inactive molecules and could only detect specific cytokines selected for in the panel (467). An experimental procedure analysing gene expression may provide such information not captured by an assessment of secreted biological protein present at the time of sample collection. Thus cytokine profiling could be done using RNA sequencing coupled with predictive modelling of the associated signalling cascades (468). As pili appear to enhance cell signalling for Tfh expansion, it would be of interest to determine if additional cytokines associated with this phenotype have upregulated expression. Furthermore, cytokines observed to have specifically notable secretion downstream of TLR2/6 stimulation may also be elucidated (469). Cytokine profiles of PBMCs isolated from mice immunised with the pilus proteins could also provide further insight into the inflammatory response elicited by the pili and the degree of skewing towards a Tfh cell phenotype. Similarly, pilus-induced co-stimulatory ligand expression on APCs could be further detailed by recording gene expression. Alternatively, as MHCII expression was not effectively captured using flow cytometry in this project, MHCII antibody with stronger fluorescence could be utilised or the current antibody could be used in tandem with another antibody recognising a different set of MHCII types, to increase the probability of successfully illustrating the specific MHCII upregulation induced by pili. Further investigation would be useful for confirming the upregulation of this molecule as well as surveying other cell surface ligands induced following pilus-interaction with TLR2

This project demonstrated GAS pilus proteins elevating M2e specific IgA antibody production but not serum IgG production, following intranasal immunisation. However, the effectiveness of GAS pilus protein as a parenteral vaccine adjuvant has not been verified. Apart from evaluating the adjuvanting potential of pilus protein in this more conventional administration route, this experiment could provide some indication of whether degradation as the fusion peptides translocate from mucosa to bloodstream is contributing to the low IgG response seen in the intranasal immunisation assay conducted here.

As suggested prior, a redesign of the pilus protein-M2e fusion peptides will be key for fully potentiating the immunomodulatory characteristics of GAS pili. Truncation of the pilus structure will be a major focus, as this will reduce the immunodominance of pilus proteins and may improve rates of absorption. Pilus proteins consist of 2-3 domains which can be expressed

individually in recombinant forms; this may be a starting point in producing an improved pilus based adjuvant. Insertion of the M2e peptide within the pilus subunit structures is another way the fusion proteins could be modulated. This design may protect the antigen against degradation and prevent steric hindrance. Proteins with adhesive properties can retain antigen in mucosa for longer and are thus suitable mucosal vaccine delivery agents. As pili and in particular the AP1 subunits have adhesive properties, a pilus-antigen fusion protein which incorporates the adhesive determinant of AP1 and ensures antigen is conjugated at a position not blocking adhesion, may create an adjuvant which is both immunopotentiating and an effective delivery system. Thus further re-design of fusion proteins and investigation in mucosal immunisation models could be directed towards augmenting the potential of GAS pili specifically for use as a mucosal adjuvant.

Overall, this project portrayed GAS pili as complexes which could induce high levels of inflammation without propagating damage in the process. Both BP and AP1 subunits of the investigated GAS pili were ascertained to be TLR2 agonists, with specificity for TLR2 heterodimerised with TLR6. The pilus proteins enhanced the innate immune cells' ability to interact with and influence adaptive immune cells and in mucosally immunised mice was found to enhance the production of antigen-specific antibodies. These findings illuminate the possibility of exploiting the immune stimulating property of GAS pili in adjuvant development. At the same time, it highlights the supplementary characterisation of pili, such as determining the exact PRR recognition domains and modulation of pilus-based adjuvanting systems, such as making changes to reduce pilus epitope domination, required to fully realise the capacity of GAS pili as an immune potentiating tool.

References

1. Ferretti J, Köhler W. History of Streptococcal Research [Internet]. Streptococcus pyogenes [Internet]. University of Oklahoma Health Sciences Center; 2016. Available from: http://www.ncbi.nlm.nih.gov/pubmed/26866232

2. Hand RM, Snelling TL, Carapetis JR. Group A Streptococcus. In: Hunter's Tropical Medicine and Emerging Infectious Diseases [Internet]. Elsevier; 2020 [cited 2023 Nov 1]. p. 429–38. Available from: https://linkinghub.elsevier.com/retrieve/pii/B9780323555128000405

3. Excler JL, Kim JH. Accelerating the development of a group A Streptococcus vaccine: an urgent public health need. Clin Exp Vaccine Res. 2016 Jul;5(2):101–7.

4. Carapetis JR, Steer AC, Mulholland EK, Weber M. The global burden of group A streptococcal diseases. Lancet Infect Dis. 2005 Nov 1;5(11):685–94.

5. Lior Z, Lior C, Gideon C. Current Microbiological, Clinical and Therapeutic Aspects of Impetigo. Clin Med Rev Case Rep. 2018;

6. Henningham A, Barnett TC, Maamary PG, Walker MJ. Pathogenesis of group A streptococcal infections. Discov Med. 2012;

7. Lin JN, Chang LL, Lai CH, Lin HH, Chen YH. Group a streptococcal necrotizing fasciitis in the emergency department. J Emerg Med. 2013;

8. Spaulding AR, Salgado-Pabón W, Kohler PL, Horswill AR, Leung DYM, Schlievert PM. Staphylococcal and streptococcal superantigen exotoxins. Clin Microbiol Rev. 2013;

9. Walker MJ, Barnett TC, McArthur JD, Cole JN, Gillen CM, Henningham A, et al. Disease manifestations and pathogenic mechanisms of group A Streptococcus. Clin Microbiol Rev. 2014;27(2):264–301.

10. Efstratiou A, Lamagni T. Epidemiology of Streptococcus pyogenes. Streptococcus pyogenes. 2016.

11. Ralph AP, Carapetis JR. Group A Streptococcal Diseases and Their Global Burden. In Springer, Berlin, Heidelberg; 2012 [cited 2019 Mar 13]. p. 1–27. Available from: http://link.springer.com/10.1007/82_2012_280

12. Craik N, Hla T, Cannon J, Moore H, Carapetis JR, Sanyahumbi A. Global Disease Burden of Streptococcus pyogenes. In: Ferretti JJ, Stevens DL, Fischetti VA, editors. Streptococcus pyogenes: Basic Biology to Clinical Manifestations [Internet]. 2nd ed. Oklahoma City (OK): University of Oklahoma Health Sciences Center; 2022 [cited 2023 Nov 12]. Available from: http://www.ncbi.nlm.nih.gov/books/NBK587099/

13. Steer AC, Carapetis JR, Nolan TM, Shann F. Systematic review of rheumatic heart disease prevalence in children in developing countries: The role of environmental factors. J Paediatr Child Health. 2002;38(3):229–34.

14. Barnett TC, Bowen AC, Carapetis JR. The fall and rise of Group A Streptococcus diseases. Epidemiol Infect. 2019;147:1–6.

15. World Health Organization. The Current Evidence for the Burden of Group A Streptococcal Diseases. Discussion papers on Child Health [Internet]. 2005. Available from: http://whqlibdoc.who.int/hq/2005/WHO_FCH_CAH_05.07.pdf

16. Hambling T, Galloway Y, Jack S, Morgan J. Invasive group A streptococcal infection in New Zealand, 2016 [Internet]. New Zealand: Institute of Environmental Science and Research Ltd; 2017 [cited 2019 Mar 13] p. 1–25. Report No.: FW17051. Available from: www.surv.esr.cri.nz

17. Lee JL, Naguwa SM, Cheema GS, Gershwin ME. Acute rheumatic fever and its consequences: A persistent threat to developing nations in the 21st century. Autoimmun Rev. 2009;9(2):117–23.

18. Galloway Y, Jack S, Hambling T. Rheumatic Fever in New Zealand Annual Report July 2014 to June 2015 [Internet]. 2017. Available from: www.surv.esr.cri.nz

19. Milne RJ, Lennon DR, Stewart JM, Vander Hoorn S, Scuffham PA. Incidence of acute rheumatic fever in New Zealand children and youth. J Paediatr Child Health. 2012 Aug;48(8):685–91.

20. Milne RJ, Lennon D, Stewart JM, Vander Hoorn S, Scuffham PA. Mortality and hospitalisation costs of rheumatic fever and rheumatic heart disease in New Zealand. J Paediatr Child Health. 2012 Aug;48(8):692–7.

21. McMillan DJ, Drèze PA, Vu T, Bessen DE, Guglielmini J, Steer AC, et al. Updated model of group A Streptococcus M proteins based on a comprehensive worldwide study. Clin Microbiol Infect. 2013 May 1;19(5):E222–9.

22. Bessen DE, Smeesters PR, Beall BW. Molecular Epidemiology, Ecology, and Evolution of Group A Streptococci. Microbiol Spectr [Internet]. 2018 Oct 5 [cited 2020 Aug 14];6(5). Available from: http://www.asmscience.org/content/journal/microbiolspec/10.1128/microbiolspec.CPP3 -0009-2018

23. Spellerberg B, Brandt C. Laboratory Diagnosis of Streptococcus pyogenes (group A streptococci). In: Ferretti JJ, Stevens DL, Fischetti VA, editors. Streptococcus pyogenes : Basic Biology to Clinical Manifestations [Internet]. Oklahoma City (OK): University of Oklahoma Health Sciences Center; 2016 [cited 2020 Jul 21]. Available from: http://www.ncbi.nlm.nih.gov/books/NBK343617/

24. McArthur JD, Walker MJ. Domains of group A streptococcal M protein that confer resistance to phagocytosis, opsonization and protection: Implications for vaccine development. Mol Microbiol. 2006;

25. Bessen DE, Kalia A. Genomic localization of a T serotype locus to a recombinatorial zone encoding extracellular matrix-binding proteins in Streptococcus pyogenes. Infect Immun. 2002;

26. Falugi F, Zingaretti C, Pinto V, Mariani M, Amodeo L, Manetti AGO, et al. Sequence Variation in Group A *Streptococcus* Pili and Association of Pilus Backbone Types with Lancefield T Serotypes. J Infect Dis. 2008 Dec 15;198(12):1834–41.

27. Bessen DE, McShan WM, Nguyen SV, Shetty A, Agrawal S, Tettelin H. Molecular epidemiology and genomics of group A Streptococcus. Infect Genet Evol. 2015;

28. Streptococcus Laboratory: M Protein Gene (emm) Typing | CDC [Internet]. 2019 [cited 2020 Jul 24]. Available from: https://www.cdc.gov/streplab/groupa-strep/emm-background.html

29. Metzgar D, Zampolli A. The M protein of group A Streptococcus is a key virulence factor and a clinically relevant strain identification marker. Virulence. 2011 Sep;2(5):402–12.

30. Williamson DA, Smeesters PR, Steer AC, Morgan J, Davies M, Carter P, et al. Comparative M-protein analysis of Streptococcus pyogenes from pharyngitis and skin infections in New Zealand: Implications for vaccine development. BMC Infect Dis. 2016;

31. Kaplan EL, Wotton JT, Johnson DR. Dynamic epidemiology of group A streptococcal serotypes associated with pharyngitis. The Lancet. 2001 Oct 20;358(9290):1334–7.

32. Martin JM, Green M, Barbadora KA, Wald ER. Erythromycin-Resistant Group A Streptococci in Schoolchildren in Pittsburgh. N Engl J Med. 2002 Apr 18;346(16):1200–6.

33. Courtney HS, Hasty DL, Dale JB. Molecular mechanisms of adhesion, colonization, and invasion of group A streptococci. Ann Med. 2002 Jan;34(2):77–87.

34. Nobbs AH, Lamont RJ, Jenkinson HF. Streptococcus Adherence and Colonization. Microbiol Mol Biol Rev MMBR. 2009 Sep;73(3):407–50.

35. Beachey EH, Ofek I. Epithelial cell binding of group A streptococci by lipoteichoic acid on fimbriae denuded of M protein. J Exp Med. 1976 Apr 1;143(4):759–71.

36. Hasty DL, Ofek I, Courtney HS, Doyle RJ. Multiple adhesins of streptococci. Infect Immun. 1992 Jun;60(6):2147–52.

37. Becherelli M, Manetti AGO, Buccato S, Viciani E, Ciucchi L, Mollica G, et al. The ancillary protein 1 of Streptococcus pyogenes FCT-1 pili mediates cell adhesion and biofilm formation through heterophilic as well as homophilic interactions. Mol Microbiol. 2012 Mar 1;83(5):1035–47.

38. Abbot EL, Smith WD, Siou GPS, Chiriboga C, Smith RJ, Wilson JA, et al. Pili mediate specific adhesion of Streptococcus pyogenes to human tonsil and skin. Cell Microbiol. 2007;9(7):1822–33.

39. Manetti AGO, Zingaretti C, Falugi F, Capo S, Bombaci M, Bagnoli F, et al. Streptococcus pyogenes pili promote pharyngeal cell adhesion and biofilm formation. Mol Microbiol. 2007;64(4):968–83.

40. Amelung S, Nerlich A, Rohde M, Spellerberg B, Cole JN, Nizet V, et al. The FbaB-type fibronectin-binding protein of Streptococcus pyogenes promotes specific invasion into endothelial cells. Cell Microbiol. 2011 Aug;13(8):1200–11.

41. Fontaine MC, Lee JJ, Kehoe MA. Combined Contributions of Streptolysin O and Streptolysin S to Virulence of Serotype M5 Streptococcus pyogenes Strain Manfredo. Infect Immun. 2003 Jul;71(7):3857–65.

42. Nizet V, Beall B, Bast DJ, Datta V, Kilburn L, Low DE, et al. Genetic locus for streptolysin S production by group A streptococcus. Infect Immun. 2000 Jul;68(7):4245–54.

43. Kansal RG, McGeer A, Low DE, Norrby-Teglund A, Kotb M. Inverse Relation between Disease Severity and Expression of the Streptococcal Cysteine Protease, SpeB, among Clonal M1T1 Isolates Recovered from Invasive Group A Streptococcal Infection Cases. Infect Immun. 2000 Nov 1;68(11):6362–9.

44. Timmer AM, Timmer JC, Pence MA, Hsu LC, Ghochani M, Frey TG, et al. Streptolysin O promotes group A streptococcus immune evasion by accelerated macrophage apoptosis. J Biol Chem. 2009;

45. Nelson DC, Garbe J, Collin M. Cysteine proteinase SpeB from Streptococcus pyogenes - a potent modifier of immunologically important host and bacterial proteins. Biol Chem. 2011 Dec;392(12):1077–88.

46. Collin M, Svensson MD, Sjöholm AG, Jensenius JC, Sjöbring U, Olsén A. EndoS and SpeB from Streptococcus pyogenes inhibit immunoglobulin-mediated opsonophagocytosis. Infect Immun. 2002 Dec;70(12):6646–51.

47. Laabei M, Ermert D. Catch Me if You Can: Streptococcus pyogenes Complement Evasion Strategies. J Innate Immun. 2019;11(1):3–12.

48. Yamaguchi M, Terao Y, Kawabata S. Pleiotropic virulence factor - *Streptococcus pyogenes* fibronectin-binding proteins: Multiple role of *S. pyogenes* Fn-binding proteins. Cell Microbiol. 2013 Apr;15(4):503–11.

49. Whitnack E, Beachey EH. Inhibition of complement-mediated opsonization and phagocytosis of Streptococcus pyogenes by D fragments of fibrinogen and fibrin bound to cell surface M protein. J Exp Med. 1985 Dec 1;162(6):1983–97.

50. Brouwer S, Rivera-Hernandez T, Curren BF, Harbison-Price N, De Oliveira DMP, Jespersen MG, et al. Pathogenesis, epidemiology and control of Group A Streptococcus infection. Nat Rev Microbiol. 2023 Jul;21(7):431–47.

51. Barnett TC, Cole JN, Rivera-Hernandez T, Henningham A, Paton JC, Nizet V, et al. Streptococcal toxins: Role in pathogenesis and disease. Cell Microbiol. 2015;17(12):1721–41.

52. Shannon BA, McCormick JK, Schlievert PM. Toxins and Superantigens of Group A Streptococci. Microbiol Spectr [Internet]. 2019 Feb 8 [cited 2020 Sep 1];7(1). Available from: https://www-asmscience-org.ezproxy.auckland.ac.nz/content/journal/microbiolspec/10.1128/microbiolspec.GPP3-0054-2018

53. Telford JL, Barocchi MA, Margarit I, Rappuoli R, Grandi G. Pili in Gram-positive pathogens. Nat Rev Microbiol. 2006;

54. Fronzes R, Remaut H, Waksman G. Architectures and biogenesis of non-flagellar protein appendages in Gram-negative bacteria. EMBO J. 2008 Sep 3;27(17):2271–80.

55. Linke-Winnebeck C, Paterson NG, Young PG, Middleditch MJ, Greenwood DR, Witte G, et al. Structural model for covalent adhesion of the Streptococcus pyogenes pilus through a thioester bond. J Biol Chem. 2014;

56. Mora M, Bensi G, Capo S, Falugi F, Zingaretti C, Manetti AGO, et al. Group A Streptococcus produce pilus-like structures containing protective antigens and Lancefield T antigens. Proc Natl Acad Sci. 2005;102(43):15641–6.

57. Kratovac Z, Manoharan A, Luo F, Lizano S, Bessen DE. Population genetics and linkage analysis of loci within the FCT region of Streptococcus pyogenes. J Bacteriol. 2007 Feb 15;189(4):1299–310.

58. Nakata M, Köller T, Moritz K, Ribardo D, Jonas L, McIver KS, et al. Mode of expression and functional characterization of FCT-3 pilus region-encoded proteins in Streptococcus pyogenes serotype M49. Infect Immun. 2009;77(1):32–44.

59. Luo F, Lizano S, Bessen DE. Heterogeneity in the polarity of Nra regulatory effects on streptococcal pilus gene transcription and virulence. Infect Immun. 2008;

60. Beckert S, Kreikemeyer B, Podbielski A. Group A streptococcal rofA gene is involved in the control of several virulence genes and eukaryotic cell attachment and internalization. Infect Immun. 2001;

61. Liu Z, Treviño J, Ramirez-Peña E, Sumby P. The small regulatory RNA FasX controls pilus expression and adherence in the human bacterial pathogen group A Streptococcus. Mol Microbiol. 2012;

62. Danger JL, Cao TN, Cao TH, Sarkar P, Treviño J, Pflughoeft KJ, et al. The small regulatory RNA FasX enhances group A Streptococcus virulence and inhibits pilus expression via serotype-specific targets. Mol Microbiol. 2015 Apr;96(2):249–62.

63. Manetti AGO, Köller T, Becherelli M, Buccato S, Kreikemeyer B, Podbielski A, et al. Environmental acidification drives S. pyogenes pilus expression and microcolony formation on epithelial cells in a FCT-dependent manner. PLoS ONE. 2010;

64. Zähner D, Scott JR. SipA is required for pilus formation in Streptococcus pyogenes serotype M3. J Bacteriol. 2008;

65. Kang HJ, Coulibaly F, Proft T, Baker EN. Crystal Structure of Spy0129, a Streptococcus pyogenes Class B Sortase Involved in Pilus Assembly. PLOS ONE. 2011 Jan 11;6(1):e15969.

66. Loh JMS, Lorenz N, Tsai CJY, Khemlani AHJ, Proft T. Mucosal vaccination with pili from Group A Streptococcus expressed on Lactococcus lactis generates protective immune responses. Sci Rep. 2017;7(1):7174.

67. Kang HJ, Coulibaly F, Clow F, Proft T, Baker EN. Stabilizing isopeptide bonds revealed in gram-positive bacterial pilus structure. Science. 2007 Dec 7;318(5856):1625–8.

68. Linke C, Young PG, Kang HJ, Bunker RD, Middleditch MJ, Caradoc-Davies TT, et al. Crystal structure of the minor pilin FctB reveals determinants of Group A streptococcal pilus anchoring. J Biol Chem. 2010 Jun 25;285(26):20381–9.

69. Quigley BR, Zähner D, Hatkoff M, Thanassi DG, Scott JR. Linkage of T3 and Cpa pilins in the Streptococcus pyogenes M3 pilus. Mol Microbiol. 2009;

70. Smith WD, Pointon JA, Abbot E, Kang HJ, Baker EN, Hirst BH, et al. Roles of minor pilin subunits Spy0125 and Spy0130 in the serotype M1 Streptococcus pyogenes strain SF370. J Bacteriol. 2010;

71. Nakata M, Kimura KR, Sumitomo T, Wada S, Sugauchi A, Oiki E, et al. Assembly Mechanism of FCT Region Type 1 Pili in Serotype M6 Streptococcus pyogenes. J Biol Chem. 2011 Oct 28;286(43):37566–77.

72. Crotty Alexander LE, Maisey HC, Timmer AM, Rooijakkers SHM, Gallo RL, von Köckritz-Blickwede M, et al. M1T1 group A streptococcal pili promote epithelial colonization but diminish systemic virulence through neutrophil extracellular entrapment. J Mol Med Berl Ger. 2010 Apr;88(4):371–81.

73. Kreikemeyer B, Nakata M, Oehmcke S, Gschwendtner C, Normann J, Podbielski A. Streptococcus pyogenes collagen type I-binding Cpa surface protein: Expression profile, binding characteristics, biological functions, and potential clinical impact. J Biol Chem. 2005;280(39):33228–39.

74. Edwards AM, Manetti AGO, Falugi F, Zingaretti C, Capo S, Buccato S, et al. Scavenger receptor gp340 aggregates group A streptococci by binding pili. Mol Microbiol. 2008;

75. Tsai JYC, Loh JMS, Clow F, Lorenz N, Proft T. The Group A Streptococcus serotype M2 pilus plays a role in host cell adhesion and immune evasion. Mol Microbiol. 2017;103(2):282–98.

76. Chen YH, Li SH, Yang YC, Hsu SH, Nizet V, Chang YC. T4 Pili Promote Colonization and Immune Evasion Phenotypes of Nonencapsulated M4 Streptococcus pyogenes. mBio. 11(4):e01580-20.

77. Lizano S, Luo F, Bessen DE. Role of streptococcal T antigens in superficial skin infection. In: Journal of Bacteriology. 2007.

78. Maisey HC, Hensler M, Nizet V, Doran KS. Group B Streptococcal Pilus Proteins Contribute to Adherence to and Invasion of Brain Microvascular Endothelial Cells. J Bacteriol. 2007 Feb 15;189(4):1464–7.

79. Kimura KR, Nakata M, Sumitomo T, Kreikemeyer B, Podbielski A, Terao Y, et al. Involvement of T6 Pili in Biofilm Formation by Serotype M6 Streptococcus pyogenes. J Bacteriol. 2012 Feb 15;194(4):804–12.

80. Manetti AGO, Zingaretti C, Falugi F, Capo S, Bombaci M, Bagnoli F, et al. Streptococcus pyogenes pili promote pharyngeal cell adhesion and biofilm formation. Mol Microbiol. 2007;64(4):968–83.

81. Köller T, Manetti AGO, Kreikemeyer B, Lembke C, Margarit I, Grandi G, et al. Typing of the pilus-protein-encoding FCT region and biofilm formationas novel parameters in epidemiological investigations of Streptococcuspyogenes isolates from various infection sites. J Med Microbiol. 2010;59(4):442–52.

82. Rouchon CN, Ly AT, Noto JP, Luo F, Lizano S, Bessen DE. Incremental Contributions of FbaA and Other Impetigo-Associated Surface Proteins to Fitness and Virulence of a Classical Group A Streptococcal Skin Strain. Freitag NE, editor. Infect Immun. 2017 Nov;85(11):e00374-17.

83. Medina E, Goldmann O, Toppel AW, Chhatwal GS. Survival of *Streptococcus pyogenes* within Host Phagocytic Cells: A Pathogenic Mechanism for Persistence and Systemic Invasion. J Infect Dis. 2003 Feb 15;187(4):597–603.

84. Pastural É, McNeil SA, MacKinnon-Cameron D, Ye L, Langley JM, Stewart R, et al. Safety and immunogenicity of a 30-valent M protein-based group a streptococcal vaccine in healthy adult volunteers: A randomized, controlled phase I study. Vaccine. 2020 Feb 5;38(6):1384–92.

85. Steer AC, Law I, Matatolu L, Beall BW, Carapetis JR. Global emm type distribution of group A streptococci: systematic review and implications for vaccine development. Lancet Infect Dis. 2009;

86. Reglinski M, Lynskey NN, Choi YJ, Edwards RJ, Sriskandan S. Development of a multicomponent vaccine for Streptococcus pyogenes based on the antigenic targets of IVIG. J Infect. 2016 Apr;72(4):450–9.

87. Henningham A, Gillen CM, Walker MJ. Group A Streptococcal Vaccine Candidates: Potential for the Development of a Human Vaccine. In Springer, Berlin, Heidelberg; 2012 [cited 2019 Mar 15]. p. 207–42. Available from: http://link.springer.com/10.1007/82_2012_284

88. Azuar, Jin, Mukaida, Hussein, Toth, Skwarczynski. Recent Advances in the Development of Peptide Vaccines and Their Delivery Systems Against Group A Streptococcus. Vaccines. 2019;7(3):58.

89. Kuo CF, Tsao N, Hsieh IC, Lin YS, Wu JJ, Hung YT. Immunization with a streptococcal multiple-epitope recombinant protein protects mice against invasive group A streptococcal infection. PLoS ONE [Internet]. 2017 Mar 29 [cited 2020 Oct 13];12(3). Available from: https://www.ncbi.nlm.nih.gov/pmc/articles/PMC5371370/

90. Pandey M, Langshaw E, Hartas J, Lam A, Batzloff MR, Good MF. A synthetic M protein peptide synergizes with a CXC chemokine protease to induce vaccine-mediated protection against virulent streptococcal pyoderma and bacteremia. J Immunol Baltim Md 1950. 2015 Jun 15;194(12):5915–25.

91. Rivera-Hernandez T, Carnathan DG, Jones S, Cork AJ, Davies MR, Moyle PM, et al. An Experimental Group A Streptococcus Vaccine That Reduces Pharyngitis and Tonsillitis in a Nonhuman Primate Model. mBio [Internet]. 2019 Apr 30 [cited 2020 Oct 22];10(2). Available from: https://mbio.asm.org/content/10/2/e00693-19

92. Ozberk V, Pandey M, Good MF. Contribution of cryptic epitopes in designing a group A streptococcal vaccine. Hum Vaccines Immunother. 2018 Jun 14;14(8):2034–52.

93. Raynes JM, Young PG, Proft T, Williamson DA, Baker EN, Moreland NJ. Protein adhesins as vaccine antigens for Group A Streptococcus. Pathog Dis [Internet]. 2018 Mar 1 [cited 2020 Sep 29];76(2). Available from: https://academic.oup.com/femspd/article/76/2/fty016/4919728

94. Steemson JD, Moreland NJ, Williamson D, Morgan J, Carter PE, Proft T. Survey of the bp/tee genes from clinical group A streptococcus isolates in New Zealand – implications for vaccine development. J Med Microbiol. 2014;63(12):1670–8.

95. Buccato S, Maione D, Rinaudo CD, Volpini G, Taddei AR, Rosini R, et al. Use of Lactococcus lactis Expressing Pili from Group B Streptococcus as a Broad-Coverage Vaccine against Streptococcal Disease. J Infect Dis. 2006 Aug 1;194(3):331–40.

96. Clow F, Peterken K, Pearson V, Proft T, Radcliff FJ. PilVax, a novel Lactococcus lactis-based mucosal vaccine platform, stimulates systemic and mucosal immune responses to Staphylococcus aureus. Immunol Cell Biol. 2020 May;98(5):369–81.

97. Blanchett S, Tsai CJ, Sandford S, Loh JM, Huang L, Kirman JR, et al. Intranasal immunization with Ag85B peptide 25 displayed on Lactococcus lactis using the PilVax platform induces antigen-specific B- and T-cell responses. Immunol Cell Biol. 2021 Aug;99(7):767–81.

98. Medzhitov R. Recognition of microorganisms and activation of the immune response. Nature. 2007 Oct;449(7164):819–26.

99. Basset C, Holton J, O'Mahony R, Roitt I. Innate immunity and pathogen–host interaction. Vaccine. 2003 Jun;21:S12–23.

100. Mogensen TH. Pathogen Recognition and Inflammatory Signaling in Innate Immune Defenses. Clin Microbiol Rev. 2009 Apr;22(2):240–73.

101. Takeuchi O, Akira S. Pattern Recognition Receptors and Inflammation. Cell. 2010 Mar 19;140(6):805–20.

102. Lubbers R, Van Essen MF, Van Kooten C, Trouw LA. Production of complement components by cells of the immune system. Clin Exp Immunol. 2017 Apr 6;188(2):183–94.

103. Dempsey PW, Vaidya SA, Cheng G. The Art of War: Innate and adaptive immune responses. Cell Mol Life Sci CMLS. 2003 Dec;60(12):2604–21.

104. Gal P, Ambrus G. Structure and Function of Complement Activating Enzyme Complexes C1 and MBL-MASPs. Curr Protein Pept Sci. 2001 Mar 1;2(1):43–59.

105. Boero E, Gorham RD, Francis EA, Brand J, Teng LH, Doorduijn DJ, et al. Purified complement C3b triggers phagocytosis and activation of human neutrophils via complement receptor 1. Sci Rep. 2023 Jan 6;13(1):274.

106. Menny A, Serna M, Boyd CM, Gardner S, Joseph AP, Morgan BP, et al. CryoEM reveals how the complement membrane attack complex ruptures lipid bilayers. Nat Commun. 2018 Dec 14;9(1):5316.

107. Du Clos TW. Pentraxins: Structure, Function, and Role in Inflammation. ISRN Inflamm. 2013 Sep 14;2013:1–22.

108. Kawai T, Akira S. The role of pattern-recognition receptors in innate immunity: update on Toll-like receptors. Nat Immunol. 2010 May;11(5):373–84.

109. Iwasaki A, Medzhitov R. Control of adaptive immunity by the innate immune system. Nat Immunol. 2015 Apr;16(4):343–53.

110. Albiger B, Dahlberg S, Henriques-Normark B, Normark S. Role of the innate immune system in host defence against bacterial infections: focus on the Toll-like receptors. J Intern Med. 2007 Jun;261(6):511–28.

111. Geijtenbeek TBH, Gringhuis SI. Signalling through C-type lectin receptors: shaping immune responses. Nat Rev Immunol. 2009 Jul;9(7):465–79.

112. Sancho D, Reis E Sousa C. Signaling by Myeloid C-Type Lectin Receptors in Immunity and Homeostasis. Annu Rev Immunol. 2012 Apr 23;30(1):491–529.

113. Li K, Underhill DM. C-Type Lectin Receptors in Phagocytosis. In: Yamasaki S, editor. C-Type Lectins in Immune Homeostasis [Internet]. Cham: Springer International Publishing; 2020 [cited 2023 Nov 13]. p. 1–18. (Current Topics in Microbiology and Immunology; vol. 429). Available from: http://link.springer.com/10.1007/82_2020_198

114. Akira S, Uematsu S, Takeuchi O. Pathogen Recognition and Innate Immunity. Cell. 2006 Feb;124(4):783–801.

115. Kanneganti TD, Lamkanfi M, Núñez G. Intracellular NOD-like Receptors in Host Defense and Disease. Immunity. 2007 Oct;27(4):549–59.

116. Tsutsumi-Ishii Y, Nagaoka I. NF-kappa B-mediated transcriptional regulation of human beta-defensin-2 gene following lipopolysaccharide stimulation. J Leukoc Biol. 2002 Jan;71(1):154–62.

117. Farlik M, Reutterer B, Schindler C, Greten F, Vogl C, Müller M, et al. Nonconventional Initiation Complex Assembly by STAT and NF-κB Transcription Factors Regulates Nitric Oxide Synthase Expression. Immunity. 2010 Jul;33(1):25–34.

118. Liu T, Zhang L, Joo D, Sun SC. NF-κB signaling in inflammation. Signal Transduct Target Ther. 2017 Jul 14;2(1):17023.

119. Dorrington MG, Fraser IDC. NF-κB Signaling in Macrophages: Dynamics, Crosstalk, and Signal Integration. Front Immunol. 2019 Apr 9;10:705.

120. Gaudino SJ, Kumar P. Cross-Talk Between Antigen Presenting Cells and T Cells Impacts Intestinal Homeostasis, Bacterial Infections, and Tumorigenesis. Front Immunol. 2019 Mar 6;10:360.

121. Heath WR, Kato Y, Steiner TM, Caminschi I. Antigen presentation by dendritic cells for B cell activation. Curr Opin Immunol. 2019 Jun;58:44–52.

122. Milstone DS, Ilyama M, Chen M, O'Donnell P, Davis VM, Plutzky J, et al. Differential Role of an NF-κB Transcriptional Response Element in Endothelial Versus Intimal Cell VCAM-1 Expression. Circ Res. 2015 Jul 3;117(2):166–77.

123. Druszczyńska M, Godkowicz M, Kulesza J, Wawrocki S, Fol M. Cytokine Receptors— Regulators of Antimycobacterial Immune Response. Int J Mol Sci. 2022 Jan 20;23(3):1112.

124. Clark R, Kupper T. Old Meets New: The Interaction Between Innate and Adaptive Immunity. J Invest Dermatol. 2005 Oct 1;125(4):629–37.

125. Caamaño J, Hunter CA. NF-κB Family of Transcription Factors: Central Regulators of Innate and Adaptive Immune Functions. Clin Microbiol Rev. 2002 Jul;15(3):414–29.

126. Wicherska-Pawłowska K, Wróbel T, Rybka J. Toll-Like Receptors (TLRs), NOD-Like Receptors (NLRs), and RIG-I-Like Receptors (RLRs) in Innate Immunity. TLRs, NLRs, and RLRs Ligands as Immunotherapeutic Agents for Hematopoietic Diseases. Int J Mol Sci. 2021 Dec 13;22(24):13397.

127. Van Vliet SJ, García-Vallejo JJ, Van Kooyk Y. Dendritic cells and C-type lectin receptors: coupling innate to adaptive immune responses. Immunol Cell Biol. 2008 Oct;86(7):580–7.

128. Krishnaswamy JK, Chu T, Eisenbarth SC. Beyond pattern recognition: NOD-like receptors in dendritic cells. Trends Immunol. 2013 May;34(5):224–33.

129. Browne EP. Regulation of B-cell responses by Toll-like receptors. Immunology. 2012 Aug;136(4):370–9.

130. Nouri Y, Weinkove R, Perret R. T-cell intrinsic Toll-like receptor signaling: implications for cancer immunotherapy and CAR T-cells. J Immunother Cancer. 2021 Nov;9(11):e003065.

131. Blander JM. Regulation of Phagosome Maturation by Signals from Toll-Like Receptors. Science. 2004 May 14;304(5673):1014–8.

132. Akira S, Takeda K, Kaisho T. Toll-like receptors: Critical proteins linking innate and acquired immunity. Nat Immunol. 2001;

133. Fujii S ichiro, Liu K, Smith C, Bonito AJ, Steinman RM. The Linkage of Innate to Adaptive Immunity via Maturing Dendritic Cells In Vivo Requires CD40 Ligation in Addition to Antigen Presentation and CD80/86 Costimulation. J Exp Med. 2004 Jun 21;199(12):1607–18.

134. Wykes M, Macpherson G. Dendritic cell-B-cell interaction: dendritic cells provide B cells with CD40-independent proliferation signals and CD40-dependent survival signals: *DC mediate B-cell proliferation and survival*. Immunology. 2000 May;100(1):1–3.

135. Awate S, Babiuk LA, Mutwiri G. Mechanisms of Action of Adjuvants. Front Immunol [Internet]. 2013 [cited 2021 Jul 4];4. Available from: http://journal.frontiersin.org/article/10.3389/fimmu.2013.00114/abstract

136. Didierlaurent AM, Morel S, Lockman L, Giannini SL, Bisteau M, Carlsen H, et al. AS04, an Aluminum Salt- and TLR4 Agonist-Based Adjuvant System, Induces a Transient Localized Innate Immune Response Leading to Enhanced Adaptive Immunity. J Immunol. 2009 Nov 15;183(10):6186–97.

137. Korsholm KS, Petersen RV, Agger EM, Andersen P. T-helper 1 and T-helper 2 adjuvants induce distinct differences in the magnitude, quality and kinetics of the early inflammatory response at the site of injection. Immunology. 2010 Jan;129(1):75–86.

138. Rosenthal KL. Tweaking innate immunity: The promise of innate immunologicals as anti-infectives. Can J Infect Dis Med Microbiol. 2006;17(5):307–14.

139. Zhu X, Zhu J. CD4 T Helper Cell Subsets and Related Human Immunological Disorders. Int J Mol Sci. 2020 Oct 28;21(21):8011.

140. Lee SK, Rigby RJ, Zotos D, Tsai LM, Kawamoto S, Marshall JL, et al. B cell priming for extrafollicular antibody responses requires Bcl-6 expression by T cells. J Exp Med. 2011 Jul 4;208(7):1377–88.

141. Olatunde AC, Hale JS, Lamb TJ. Cytokine-skewed Tfh cells: functional consequences for B cell help. Trends Immunol. 2021 Jun;42(6):536–50.

142. Crotty S. T Follicular Helper Cell Biology: A Decade of Discovery and Diseases. Immunity. 2019 May;50(5):1132–48.

143. Sheikh AA, Groom JR. Transcription tipping points for T follicular helper cell and T-helper 1 cell fate commitment. Cell Mol Immunol. 2021 Mar;18(3):528–38.

144. Redecke V, Häcker H, Datta SK, Fermin A, Pitha PM, Broide DH, et al. Cutting Edge: Activation of Toll-Like Receptor 2 Induces a Th2 Immune Response and Promotes Experimental Asthma. J Immunol. 2004 Mar 1;172(5):2739–43.

145. Jain S, Chodisetti SB, Agrewala JN. CD40 Signaling Synergizes with TLR-2 in the BCR Independent Activation of Resting B Cells. Sechi LA, editor. PLoS ONE. 2011 Jun 2;6(6):e20651.

146. Pasare C, Medzhitov R. Toll-like receptors: Linking innate and adaptive immunity. Microbes Infect. 2004;

147. Meyer-Bahlburg A, Khim S, Rawlings DJ. B cell–intrinsic TLR signals amplify but are not required for humoral immunity. J Exp Med. 2007 Dec 24;204(13):3095–101.

148. Coffman RL, Sher A, Seder RA. Vaccine Adjuvants: Putting Innate Immunity to Work. Immunity. 2010 Oct;33(4):492–503.

149. Beran J. Safety and immunogenicity of a new hepatitis B vaccine for the protection of patients with renal insufficiency including pre-haemodialysis and haemodialysis patients. Expert Opin Biol Ther. 2008 Feb;8(2):235–47.

150. Podda A. The adjuvanted influenza vaccines with novel adjuvants: experience with the MF59-adjuvanted vaccine. Vaccine. 2001 Mar;19(17–19):2673–80.

151. Banzhoff A, Gasparini R, Laghi-Pasini F, Staniscia T, Durando P, Montomoli E, et al. MF59®-Adjuvanted H5N1 Vaccine Induces Immunologic Memory and Heterotypic Antibody Responses in Non-Elderly and Elderly Adults. Sandberg JK, editor. PLoS ONE. 2009 Feb 6;4(2):e4384.

152. Schwarz TF, Horacek T, Knuf M, Damman HG, Roman F, Dramé M, et al. Single dose vaccination with AS03-adjuvanted H5N1 vaccines in a randomized trial induces strong and broad immune responsiveness to booster vaccination in adults. Vaccine. 2009 Oct;27(45):6284–90.

153. Phipps JP, Haas KM. An Adjuvant That Increases Protective Antibody Responses to Polysaccharide Antigens and Enables Recall Responses. J Infect Dis. 2019 Jan 7;219(2):323–34.

154. Duthie MS, Windish HP, Fox CB, Reed SG. Use of defined TLR ligands as adjuvants within human vaccines. Immunol Rev. 2011;

155. Galli G, Medini D, Borgogni E, Zedda L, Bardelli M, Malzone C, et al. Adjuvanted H5N1 vaccine induces early CD4 [+] T cell response that predicts long-term persistence of protective antibody levels. Proc Natl Acad Sci. 2009 Mar 10;106(10):3877–82.

156. Caskey M, Lefebvre F, Filali-Mouhim A, Cameron MJ, Goulet JP, Haddad EK, et al. Synthetic double-stranded RNA induces innate immune responses similar to a live viral vaccine in humans. J Exp Med. 2011 Nov 21;208(12):2357–66.

157. Kolumam GA, Thomas S, Thompson LJ, Sprent J, Murali-Krishna K. Type I interferons act directly on CD8 T cells to allow clonal expansion and memory formation in response to viral infection. J Exp Med. 2005 Sep 5;202(5):637–50.

158. Spadaro F, Lapenta C, Donati S, Abalsamo L, Barnaba V, Belardelli F, et al. IFN-α enhances cross-presentation in human dendritic cells by modulating antigen survival, endocytic routing, and processing. Blood. 2012 Feb 9;119(6):1407–17.

159. Tewari K, Flynn BJ, Boscardin SB, Kastenmueller K, Salazar AM, Anderson CA, et al. Poly(I:C) is an effective adjuvant for antibody and multi-functional CD4+ T cell responses to Plasmodium falciparum circumsporozoite protein (CSP) and αDEC-CSP in non human primates. Vaccine. 2010 Oct;28(45):7256–66.

160. Kovalcsik E, Lowe K, Fischer M, Dalgleish A, Bodman-Smith MD. Poly(I:C)-induced tumour cell death leads to DC maturation and Th1 activation. Cancer Immunol Immunother. 2011 Nov;60(11):1609–24.

161. Facciolà A, Visalli G, Laganà A, Di Pietro A. An Overview of Vaccine Adjuvants: Current Evidence and Future Perspectives. Vaccines. 2022 May 22;10(5):819.

162. Hopkins M, Lees BG, Richardson DG, Woroniecki SR, Wheeler AW. Standardisation of Glutaraldehyde-modified Tyrosine-adsorbed Tree Pollen Vaccines Containing the Th1-inducing Adjuvant, Monophosphoryl Lipid A (MPLÆÊ). Allergol Immunopathol (Madr). 2001 Jan;29(6):245–54.

163. Otsuka T, Nishida S, Shibahara T, Temizoz B, Hamaguchi M, Shiroyama T, et al. CpG ODN (K3)—toll-like receptor 9 agonist—induces Th1-type immune response and enhances cytotoxic activity in advanced lung cancer patients: a phase I study. BMC Cancer. 2022 Dec;22(1):744.

164. Tada R, Muto S, Iwata T, Hidaka A, Kiyono H, Kunisawa J, et al. Attachment of class B CpG ODN onto DOTAP/DC-chol liposome in nasal vaccine formulations augments antigen-specific immune responses in mice. BMC Res Notes. 2017 Dec;10(1):68.

165. Treanor JJ, Taylor DN, Tussey L, Hay C, Nolan C, Fitzgerald T, et al. Safety and immunogenicity of a recombinant hemagglutinin influenza–flagellin fusion vaccine (VAX125) in healthy young adults. Vaccine. 2010 Dec;28(52):8268–74.

166. Huleatt JW, Jacobs AR, Tang J, Desai P, Kopp EB, Huang Y, et al. Vaccination with recombinant fusion proteins incorporating Toll-like receptor ligands induces rapid cellular and humoral immunity. Vaccine. 2007 Jan;25(4):763–75.

167. Yang JX, Tseng JC, Yu GY, Luo Y, Huang CYF, Hong YR, et al. Recent Advances in the Development of Toll-like Receptor Agonist-Based Vaccine Adjuvants for Infectious Diseases. Pharmaceutics. 2022 Feb 16;14(2):423.

168. Loof TG, Rohde M, Chhatwal GS, Jung S, Medina E. The Contribution of Dendritic Cells to Host Defenses against Streptococcus pyogenes. J Infect Dis. 2007 Dec 15;196(12):1794–803.

169. Mishalian I, Ordan M, Peled A, Maly A, Eichenbaum MB, Ravins M, et al. Recruited Macrophages Control Dissemination of Group A Streptococcus from Infected Soft Tissues. J Immunol. 2011 Dec 1;187(11):6022–31.

170. Valderrama JA, Nizet V. Group A *Streptococcus* encounters with host macrophages. Future Microbiol. 2018 Jan;13(1):119–34.

171. Ermert D, Shaughnessy J, Joeris T, Kaplan J, Pang CJ, Kurt-Jones EA, et al. Virulence of Group A Streptococci Is Enhanced by Human Complement Inhibitors. Wessels MR, editor. PLOS Pathog. 2015 Jul 22;11(7):e1005043.

172. Syed S, Viazmina L, Mager R, Meri S, Haapasalo K. Streptococci and the complement system: interplay during infection, inflammation and autoimmunity. FEBS Lett. 2020 Aug;594(16):2570–85.

173. Nordstrand A, McShan WM, Ferretti JJ, Holm SE, Norgren M. Allele Substitution of the Streptokinase Gene Reduces the Nephritogenic Capacity of Group A Streptococcal Strain NZ131. Fischetti VA, editor. Infect Immun. 2000 Mar;68(3):1019–25.

174. Wyatt RJ, Forristal J, West CD, Sugimoto S, Curd JG. Complement profiles in acute post-streptococcal glomerulonephritis. Pediatr Nephrol. 1988;2(2):219–23.

175. Chung AW, Ho TK, Hanson-Manful P, Tritscheller S, Raynes JM, Whitcombe AL, et al. Systems immunology reveals a linked IgG3–C4 response in patients with acute rheumatic fever. Immunol Cell Biol. 2020 Jan;98(1):12–21.

176. Gorton D, Sikder S, Williams NL, Chilton L, Rush CM, Govan BL, et al. Repeat exposure to group A streptococcal M protein exacerbates cardiac damage in a rat model of rheumatic heart disease. Autoimmunity. 2016 Nov 16;49(8):563–70.

177. Soderholm AT, Barnett TC, Sweet MJ, Walker MJ. Group A streptococcal pharyngitis: Immune responses involved in bacterial clearance and GAS-associated immunopathologies. J Leukoc Biol. 2018;103(2):193–213.

178. Castiglia V, Piersigilli A, Ebner F, Janos M, Goldmann O, Damböck U, et al. Type I Interferon Signaling Prevents IL-1β-Driven Lethal Systemic Hyperinflammation during Invasive Bacterial Infection of Soft Tissue. Cell Host Microbe. 2016 Mar 9;19(3):375–87.

179. Hsu LC, Enzler T, Seita J, Timmer AM, Lee CY, Lai TY, et al. IL-1β-driven neutrophilia preserves antibacterial defense in the absence of the kinase IKKβ. Nat Immunol. 2011 Feb;12(2):144–50.

180. Gratz N, Siller M, Schaljo B, Pirzada ZA, Gattermeier I, Vojtek I, et al. Group A streptococcus activates type I interferon production and MyD88-dependent signaling without involvement of TLR2, TLR4, and TLR9. J Biol Chem. 2008;

181. Di Nardo A, Yamasaki K, Dorschner RA, Lai Y, Gallo RL. Mast Cell Cathelicidin Antimicrobial Peptide Prevents Invasive Group A Streptococcus Infection of the Skin. J Immunol Baltim Md 1950. 2008 Jun 1;180(11):7565–73.

182. Loof TG, Goldmann O, Medina E. Immune recognition of Streptococcus pyogenes by dendritic cells. Infect Immun. 2008;76(6):2785–92.

183. Elgueta R, Benson M, De Vries V, Wasiuk A, Guo Y, Noelle R. Molecular mechanism and function of CD40/CD40L engagement in the immune system [Internet]. [cited 2021 Jun 2]. Available from: https://onlinelibrary.wiley.com/doi/full/10.1111/j.1600-065X.2009.00782.x

184. Kaisho T, Akira S. Dendritic-cell function in Toll-like receptor- and MyD88-knockout mice. Trends Immunol. 2001 Feb 1;22(2):78–83.

185. Gratz N, Hartweger H, Matt U, Kratochvill F, Janos M, Sigel S, et al. Type I Interferon Production Induced by Streptococcus pyogenes-Derived Nucleic Acids Is Required for Host Protection. Cheung A, editor. PLoS Pathog. 2011 May 19;7(5):e1001345.

186. Zinkernagel AS, Hruz P, Uchiyama S, von Köckritz-Blickwede M, Schuepbach RA, Hayashi T, et al. Importance of Toll-Like Receptor 9 in Host Defense against M1T1 Group A Streptococcus Infections. J Innate Immun. 2012 Feb;4(2):213–8.

187. Goldmann O, von Köckritz-Blickwede M, Höltje C, Chhatwal GS, Geffers R, Medina E. Transcriptome Analysis of Murine Macrophages in Response to Infection with Streptococcus pyogenes Reveals an Unusual Activation Program. Infect Immun. 2007 Aug;75(8):4148–57.

188. Areschoug T, Waldemarsson J, Gordon S. Evasion of macrophage scavenger receptor A-mediated recognition by pathogenic streptococci. Eur J Immunol. 2008;38(11):3068–79.

189. Påhlman LI, Mörgelin M, Eckert J, Johansson L, Russell W, Riesbeck K, et al. Streptococcal M Protein: A Multipotent and Powerful Inducer of Inflammation. J Immunol. 2006 Jul 15;177(2):1221–8.

190. Richter J, Monteleone MM, Cork AJ, Barnett TC, Nizet V, Brouwer S, et al. Streptolysins are the primary inflammasome activators in macrophages during *Streptococcus pyogenes* infection. Immunol Cell Biol. 2021 Nov;99(10):1040–52.

191. Nozawa T, Aikawa C, Minowa-Nozawa A, Nakagawa I. The intracellular microbial sensor NLRP4 directs Rho-actin signaling to facilitate Group A *Streptococcus*-containing autophagosome-like vacuole formation. Autophagy. 2017 Nov 2;13(11):1841–54.

192. Aikawa C, Nakajima S, Karimine M, Nozawa T, Minowa-Nozawa A, Toh H, et al. NLRX1 Negatively Regulates Group A Streptococcus Invasion and Autophagy Induction by Interacting With the Beclin 1–UVRAG Complex. Front Cell Infect Microbiol. 2018 Nov 14;8:403.

193. Midiri A, Mancuso G, Beninati C, Gerace E, Biondo C. The Relevance of IL-1-Signaling in the Protection against Gram-Positive Bacteria. Pathogens. 2021 Jan 28;10(2):132.

194. Imai T, Matsumura T, Mayer-Lambertz S, Wells CA, Ishikawa E, Butcher SK, et al. Lipoteichoic acid anchor triggers Mincle to drive protective immunity against invasive group A *Streptococcus* infection. Proc Natl Acad Sci [Internet]. 2018 Nov 6 [cited 2023 Nov 14];115(45). Available from: https://pnas.org/doi/full/10.1073/pnas.1809100115

195. Moudgil KD, Choubey D. Cytokines in autoimmunity: role in induction, regulation, and treatment. J Interferon Cytokine Res. 2011;31(10):695–703.

196. Ellis NMJ, Li Y, Hildebrand W, Fischetti VA, Cunningham MW. T Cell Mimicry and Epitope Specificity of Cross-Reactive T Cell Clones from Rheumatic Heart Disease. J Immunol. 2005 Oct 15;175(8):5448–56.

197. Guilherme L, Cury P, Demarchi LMF, Coelho V, Abel L, Lopez AP, et al. Rheumatic Heart Disease. Am J Pathol. 2004 Nov;165(5):1583–91.

198. Carapetis JR, Beaton A, Cunningham MW, Guilherme L, Karthikeyan G, Mayosi BM, et al. Acute rheumatic fever and rheumatic heart disease. Nat Rev Dis Primer. 2016 Jan 14;2(1):15084.

199. Becher B, Tugues S, Greter M. GM-CSF: From Growth Factor to Central Mediator of Tissue Inflammation. Immunity. 2016 Nov;45(5):963–73.

200. Azevedo PM, Bauer R, Caparbo VDF, Silva CAA, Bonfá E, Pereira RMR. Interleukin-1 receptor antagonist gene (IL1RN) polymorphism possibly associated to severity of rheumatic carditis in a Brazilian cohort. Cytokine. 2010 Jan;49(1):109–13.

201. Barocchi MA, Ries J, Zogaj X, Hemsley C, Albiger B, Kanth A, et al. A pneumococcal pilus influences virulence and host inflammatory responses. Proc Natl Acad Sci. 2006;103(8):2857–62.

202. Banerjee A, Kim BJ, Carmona EM, Cutting AS, Gurney MA, Carlos C, et al. Bacterial Pili exploit integrin machinery to promote immune activation and efficient blood-brain barrier penetration. Nat Commun. 2011;2(462).

203. Chattopadhyay D, Carey AJ, Caliot E, Webb RI, Layton JR, Wang Y, et al. Phylogenetic lineage and pilus protein Spb1/SAN1518 affect opsonin-independent phagocytosis and intracellular survival of Group B Streptococcus. Microbes Infect. 2011 Apr 1;13(4):369–82.

204. Thomas CJ, Schroder K. Pattern recognition receptor function in neutrophils. Trends Immunol. 2013;

205. Gupta A, Singh K, Fatima S, Ambreen S, Zimmermann S, Younis R, et al. Neutrophil Extracellular Traps Promote NLRP3 Inflammasome Activation and Glomerular Endothelial Dysfunction in Diabetic Kidney Disease. Nutrients. 2022 Jul 20;14(14):2965.

206. Takahashi R, Radcliff FJ, Proft T, Tsai CJ. Pilus proteins from *Streptococcus pyogenes* stimulate innate immune responses through Toll-like receptor 2. Immunol Cell Biol. 2022 Mar;100(3):174–85.

207. Wigerblad G, Kaplan MJ. Neutrophil extracellular traps in systemic autoimmune and autoinflammatory diseases. Nat Rev Immunol. 2023 May;23(5):274–88.

208. Han SH, Kim JH, Martin M, Michalek SM, Nahm MH. Pneumococcal Lipoteichoic Acid (LTA) Is Not as Potent as Staphylococcal LTA in Stimulating Toll-Like Receptor 2. Infect Immun. 2003 Oct;71(10):5541–8.

209. Malley R, Henneke P, Morse SC, Cieslewicz MJ, Lipsitch M, Thompson CM, et al. Recognition of pneumolysin by Toll-like receptor 4 confers resistance to pneumococcal infection. Proc Natl Acad Sci U S A. 2003 Feb 18;100(4):1966–71.

210. Basset A, Zhang F, Benes C, Sayeed S, Herd M, Thompson C, et al. Toll-like receptor (TLR) 2 mediates inflammatory responses to oligomerized RrgA pneumococcal pilus type 1 protein. J Biol Chem. 2013 Jan 25;288(4):2665–75.

211. Hilleringmann M, Giusti F, Baudner BC, Masignani V, Covacci A, Rappuoli R, et al. Pneumococcal pili are composed of protofilaments exposing adhesive clusters of Rrg A. PLoS Pathog. 2008;

212. Izoré T, Contreras-Martel C, El Mortaji L, Manzano C, Terrasse R, Vernet T, et al. Structural Basis of Host Cell Recognition by the Pilus Adhesin from Streptococcus pneumoniae. Structure. 2010 Jan 13;18(1):106–15.

213. Loh JMS, Adenwalla N, Wiles S, Proft T. Galleria mellonella larvae as an infection model for group A streptococcus. Virulence. 2013;4(5):419–28.

214. Tsai CJY, Loh JMS, Proft T. Galleria mellonella infection models for the study of bacterial diseases and for antimicrobial drug testing. Virulence. 2016;

215. Bisno AL, Brito MO, Collins CM. Molecular basis of group A streptococcal virulence. Lancet Infect Dis. 2003;3(4):191–200.

216. Anderson J, Imran S, Frost HR, Azzopardi KI, Jalali S, Novakovic B, et al. Immune signature of acute pharyngitis in a Streptococcus pyogenes human challenge trial. Nat Commun. 2022;13(1).

217. Moudgil KD. Interplay among cytokines and T cell subsets in the progression and control of immune-mediated diseases. Cytokine. 2015;74(1):1–4.

218. Raphael I, Nalawade S, Eagar TN, Forsthuber TG. T cell subsets and their signature cytokines in autoimmune and inflammatory diseases. Cytokine. 2015;74(1):5–17.

219. Middleton FM, McGregor R, Webb RH, Wilson NJ, Moreland NJ. Cytokine imbalance in acute rheumatic fever and rheumatic heart disease: Mechanisms and therapeutic implications. Autoimmun Rev. 2022;21(12).

220. Liu YH, Wu PH, Kang CC, Tsai YS, Chou CK, Liang CT, et al. Group A Streptococcus Subcutaneous Infection-Induced Central Nervous System Inflammation Is Attenuated by Blocking Peripheral TNF. Front Microbiol. 2019 Feb 19;10:265.

221. Wilde S, Johnson AF, LaRock CN. Playing With Fire: Proinflammatory Virulence Mechanisms of Group A Streptococcus. Front Cell Infect Microbiol. 2021 Jul 6;11:704099.

222. Dieye Y, Oxaran V, Ledue-Clier F, Alkhalaf W, Buist G, Juillard V, et al. Functionality of sortase A in Lactococcus lactis. Appl Environ Microbiol. 2010 Nov;76(21):7332–7.

223. J-Khemlani AH, Pilapitiya D, Tsai CJ, Proft T, Loh JMS. Expanding strain coverage of a group A *Streptococcus* pilus–expressing *Lactococcus lactis* mucosal vaccine. Immunol Cell Biol. 2023 Apr 24;imcb.12643.

224. Cunningham MW. Pathogenesis of Group A Streptococcal Infections. Clin Microbiol Rev. 2000 Jul;13(3):470–511.

225. Ménard G, Rouillon A, Cattoir V, Donnio PY. Galleria mellonella as a Suitable Model of Bacterial Infection: Past, Present and Future. Front Cell Infect Microbiol. 2021 Dec 22;11:782733.

226. Ramarao N, Nielsen-Leroux C, Lereclus D. The Insect Galleria mellonella as a Powerful Infection Model to Investigate Bacterial Pathogenesis. J Vis Exp. 2012 Dec 11;(70):4392.

227. Serrano I, Verdial C, Tavares L, Oliveira M. The Virtuous Galleria mellonella Model for Scientific Experimentation. Antibiotics. 2023 Mar 3;12(3):505.

228. Fuchs BB, O'Brien E, Khoury JB, Mylonakis E. Methods for using Galleria mellonella as a model host to study fungal pathogenesis. Virulence. 2010;1(6):475–82.

229. Bidla G, Lindgren M, Theopold U, Dushay M. Hemolymph coagulation and phenoloxidase in larvae. Dev Comp Immunol. 2005;29(8):669–79.

230. Sheehan G, Kavanagh K. Analysis of the early cellular and humoral responses of *Galleria mellonella* larvae to infection by *Candida albicans*. Virulence. 2018 Dec 31;9(1):163–72.

231. Loh JMS, Adenwalla N, Wiles S, Proft T. Galleria mellonella larvae as an infection model for group A streptococcus. Virulence. 2013;4(5):419–28.

232. Aspell T, Khemlani AHJ, Tsai CJY, Loh JMS, Proft T. The Cell Wall Deacetylases Spy1094 and Spy1370 Contribute to Streptococcus pyogenes Virulence. Microorganisms. 2023 Jan 24;11(2):305.

233. Desalermos A, Fuchs BB, Mylonakis E. Selecting an Invertebrate Model Host for the Study of Fungal Pathogenesis. Heitman J, editor. PLoS Pathog. 2012 Feb 2;8(2):e1002451.

234. Smoot LM, Smoot JC, Graham MR, Somerville GA, Sturdevant DE, Migliaccio CAL, et al. Global differential gene expression in response to growth temperature alteration in group A *Streptococcus*. Proc Natl Acad Sci. 2001 Aug 28;98(18):10416–21.

235. Sheehan G, Dixon A, Kavanagh K. Utilization of Galleria mellonella larvae to characterize the development of Staphylococcus aureus infection. Microbiol Read. 2019;165(8):863–75.

236. Chen GY, Nuñez G. Sterile inflammation: sensing and reacting to damage. Nat Rev Immunol. 2010 Dec;10(12):826–37.

237. Woolley VC, Teakle GR, Prince G, De Moor CH, Chandler D. Cordycepin, a metabolite of Cordyceps militaris, reduces immune-related gene expression in insects. J Invertebr Pathol. 2020 Nov;177:107480.

238. Smith DFQ, Dragotakes Q, Kulkarni M, Hardwick JM, Casadevall A. Melanization is an important antifungal defense mechanism in *Galleria mellonella* hosts [Internet]. Microbiology; 2022 Apr [cited 2023 Jun 26]. Available from: http://biorxiv.org/lookup/doi/10.1101/2022.04.02.486843

239. Senior NJ, Titball RW. Isolation and primary culture of Galleria mellonella hemocytes for infection studies. F1000Research. 2021 Feb 16;9:1392.

240. Nakata M, Kreikemeyer B. Genetics, Structure, and Function of Group A Streptococcal Pili. Front Microbiol. 2021 Feb 9;12:616508.

241. Schneewind O, Mihaylova-Petkov D, Model P. Cell wall sorting signals in surface proteins of gram-positive bacteria. EMBO J. 1993 Dec;12(12):4803–11.

242. Tsai C, Loh JMS, Blanchett S, Proft T. Using Lactococcus lactis as Surrogate Organism to Study Group A Streptococcus Surface Proteins. In: Proft T, Loh JMS, editors. Group A Streptococcus [Internet]. New York, NY: Springer US; 2020 [cited 2023 Jun 21]. p. 155–62. (Methods in Molecular Biology; vol. 2136). Available from: http://link.springer.com/10.1007/978-1-0716-0467-0_11

243. Acebo P, Herranz C, Espenberger LB, Gómez-Sanz A, Terrón MC, Luque D, et al. A Small Non-Coding RNA Modulates Expression of Pilus-1 Type in Streptococcus pneumoniae. Microorganisms. 2021 Sep 5;9(9):1883.

244. Pereira T, De Barros P, Fugisaki L, Rossoni R, Ribeiro F, De Menezes R, et al. Recent Advances in the Use of Galleria mellonella Model to Study Immune Responses against Human Pathogens. J Fungi. 2018 Nov 27;4(4):128.

245. Zdybicka-Barabas A, Mak P, Jakubowicz T, Cytryńska M. LYSOZYME AND DEFENSE PEPTIDES AS SUPPRESSORS OF PHENOLOXIDASE ACTIVITY IN *Galleria mellonella*: *Phenoloxidase Control in* Galleria mellonella. Arch Insect Biochem Physiol. 2014 Sep;87(1):1–12.

246. Hillyer JF. Insect immunology and hematopoiesis. Dev Comp Immunol. 2016 May;58:102–18.

247. Arteaga Blanco LA, Crispim JS, Fernandes KM, De Oliveira LL, Pereira MF, Bazzolli DMS, et al. Differential cellular immune response of Galleria mellonella to Actinobacillus pleuropneumoniae. Cell Tissue Res. 2017 Oct;370(1):153–68.

248. Bergin D, Brennan M, Kavanagh K. Fluctuations in haemocyte density and microbial load may be used as indicators of fungal pathogenicity in larvae of Galleria mellonella. Microbes Infect. 2003 Dec;5(15):1389–95.

249. F. Q. Smith D, Casadevall A. Fungal immunity and pathogenesis in mammals versus the invertebrate model organism *Galleria mellonella*. Pathog Dis. 2021 Mar 20;79(3):ftab013.

250. Ishii K, Adachi T, Hamamoto H, Oonishi T, Kamimura M, Imamura K, et al. Insect cytokine paralytic peptide activates innate immunity via nitric oxide production in the silkworm Bombyx mori. Dev Comp Immunol. 2013 Mar;39(3):147–53.

251. Nazario-Toole AE, Wu LP. Phagocytosis in Insect Immunity. In: Advances in Insect Physiology [Internet]. Elsevier; 2017 [cited 2023 Jun 26]. p. 35–82. Available from: https://linkinghub.elsevier.com/retrieve/pii/S0065280616300480

252. Takahashi R, J-Khemlani AH, Loh JMS, Radcliff FJ, Proft T, Tsai CJ. Different Group A Streptococcus pili lead to varying proinflammatory cytokine responses and virulence. Immunol Cell Biol. 2023 Oct 5;imcb.12692.

253. Loh JMS, Rivera-Hernandez T, McGregor R, Khemlani AHJ, Tay ML, Cork AJ, et al. A multivalent T-antigen-based vaccine for Group A Streptococcus. Sci Rep. 2021 Dec;11(1):4353.

254. Guilherme L, Kalil J, Cunningham M. Molecular mimicry in the autoimmune pathogenesis of rheumatic heart disease. Autoimmunity. 2006 Jan;39(1):31–9.

255. Asturias EJ, Excler JL, Ackland J, Cavaleri M, Fulurija A, Long R, et al. Safety of *Streptococcus pyogenes* Vaccines: Anticipating and Overcoming Challenges for Clinical Trials and Post-Marketing Monitoring. Clin Infect Dis. 2023 May 26;ciad311.

256. Netea MG, Van Der Meer JWM, Sutmuller RP, Adema GJ, Kullberg BJ. From the Th1/Th2 Paradigm towards a Toll-Like Receptor/T-Helper Bias. Antimicrob Agents Chemother. 2005 Oct;49(10):3991–6.

257. Massari P, Henneke P, Ho Y, Latz E, Golenbock DT, Wetzler LM. Cutting Edge: Immune Stimulation by Neisserial Porins Is Toll-Like Receptor 2 and MyD88 Dependent. J Immunol. 2002 Feb 15;168(4):1533–7.

258. Gopinath SCB. Biosensing applications of surface plasmon resonance-based Biacore technology. Sens Actuators B Chem. 2010 Oct;150(2):722–33.

259. Koymans KJ, Feitsma LJ, Brondijk THC, Aerts PC, Lukkien E, Lössl P, et al. Structural basis for inhibition of TLR2 by staphylococcal superantigen-like protein 3 (SSL3). Proc Natl Acad Sci U S A. 2015;

260. Ozinsky A, Underhill DM, Fontenot JD, Hajjar AM, Smith KD, Wilson CB, et al. The repertoire for pattern recognition of pathogens by the innate immune system is defined by cooperation between Toll-like receptors. Proc Natl Acad Sci. 2000 Dec 5;97(25):13766–71.

261. Jin MS, Kim SE, Heo JY, Lee ME, Kim HM, Paik SG, et al. Crystal Structure of the TLR1-TLR2 Heterodimer Induced by Binding of a Tri-Acylated Lipopeptide. Cell. 2007;130(6):1071–82.

262. Kang JY, Nan X, Jin MS, Youn SJ, Ryu YH, Mah S, et al. Recognition of Lipopeptide Patterns by Toll-like Receptor 2-Toll-like Receptor 6 Heterodimer. Immunity. 2009;31(6):873–84.

263. Young KA, Mancera RL. Review: Investigating the aggregation of amyloid beta with surface plasmon resonance: Do different approaches yield different results? Anal Biochem. 2022 Oct;654:114828.

264. Sundberg EJ, Andersen PS, Gorshkova II, Schuck P. Surface Plasmon Resonance Biosensing in the Study of Ternary Systems of Interacting Proteins. In: Schuck P, editor. Protein Interactions [Internet]. Boston, MA: Springer US; 2007 [cited 2023 Jul 3]. p. 97–141. Available from: http://link.springer.com/10.1007/978-0-387-35966-3_4

265. Andersen PS, Schuck P, Sundberg EJ, Geisler C, Karjalainen K, Mariuzza RA. Quantifying the Energetics of Cooperativity in a Ternary Protein Complex. Biochemistry. 2002 Apr 1;41(16):5177–84.

266. Garrido-Jareño M, Puchades-Carrasco L, Orti-Pérez L, Sahuquillo-Arce JM, Del Carmen Meyer-García M, Mollar-Maseres J, et al. A surface plasmon resonance based approach for measuring response to pneumococcal vaccine. Sci Rep. 2021 Mar 22;11(1):6502.

267. Oliveira-Nascimento L, Massari P, Wetzler LM. The role of TLR2 ininfection and immunity. Front Immunol. 2012;3:1–17.

268. Massari P, Visintin A, Gunawardana J, Halmen KA, King CA, Golenbock DT, et al. Meningococcal porin PorB binds to TLR2 and requires TLR1 for signaling. J Immunol Baltim Md 1950. 2006 Feb 15;176(4):2373–80.

269. Wang Y, Liu L, Davies DR, Segal DM. Dimerization of Toll-like Receptor 3 (TLR3) Is Required for Ligand Binding. J Biol Chem. 2010 Nov;285(47):36836–41.

270. Boettiger D, Lynch L, Blystone S, Huber F. Distinct Ligand-binding Modes for Integrin $\alpha v\beta 3$-Mediated Adhesion to Fibronectinversus Vitronectin. J Biol Chem. 2001 Aug;276(34):31684–90.

271. Berry SM, Chin EN, Jackson SS, Strotman LN, Goel M, Thompson NE, et al. Weak protein–protein interactions revealed by immiscible filtration assisted by surface tension. Anal Biochem. 2014 Feb;447:133–40.

272. Nimma S, Gu W, Maruta N, Li Y, Pan M, Saikot FK, et al. Structural Evolution of TIR-Domain Signalosomes. Front Immunol. 2021 Nov 17;12:784484.

273. Im J, Baik JE, Lee D, Park OJ, Park DH, Yun CH, et al. Bacterial Lipoproteins Induce BAFF Production via TLR2/MyD88/JNK Signaling Pathways in Dendritic Cells. Front Immunol. 2020 Oct 2;11:564699.

274. Yokoyama R, Itoh S, Kamoshida G, Takii T, Fujii S, Tsuji T, et al. Staphylococcal Superantigen-Like Protein 3 Binds to the Toll-Like Receptor 2 Extracellular Domain and Inhibits Cytokine Production Induced by Staphylococcus aureus, Cell Wall Component, or Lipopeptides in Murine Macrophages. Bäumler AJ, editor. Infect Immun. 2012 Aug;80(8):2816–25.

275. von Ossowski I, Pietilä TE, Rintahaka J, Nummenmaa E, Mäkinen VM, Reunanen J, et al. Using Recombinant Lactococci as an Approach to Dissect the Immunomodulating Capacity of Surface Piliation in Probiotic Lactobacillus rhamnosus GG. PLoS ONE. 2013;8(5):e64416.

276. Farhat K, Riekenberg S, Heine H, Debarry J, Lang R, Mages J, et al. Heterodimerization of TLR2 with TLR1 or TLR6 expands the ligand spectrum but does not lead to differential signaling. J Leukoc Biol. 2008 Mar 1;83(3):692–701.

277. Travassos LH, Girardin SE, Philpott DJ, Blanot D, Nahori MA, Werts C, et al. Toll-like receptor 2-dependent bacterial sensing does not occur via peptidoglycan recognition. EMBO Rep. 2004;

278. Xie Y, Zheng Y, Li H, Luo X, He Z, Cao S, et al. GPS-Lipid: A robust tool for the prediction of multiple lipid modification sites. Sci Rep. 2016;

279. Fuchs K, Cardona Gloria Y, Wolz O, Herster F, Sharma L, Dillen CA, et al. The fungal ligand chitin directly binds TLR 2 and triggers inflammation dependent on oligomer size. EMBO Rep. 2018 Dec;19(12):e46065.

280. Kattner C, Toussi DN, Zaucha J, Wetzler LM, Rüppel N, Zachariae U, et al. Crystallographic analysis of Neisseria meningitidis PorB extracellular loops potentially implicated in TLR2 recognition. J Struct Biol. 2014 Mar;185(3):440–7.

281. Schaub B, Bellou A, Gibbons FK, Velasco G, Campo M, He H, et al. TLR2 and TLR4 Stimulation Differentially Induce Cytokine Secretion in Human Neonatal, Adult, and Murine Mononuclear Cells. J Interferon Cytokine Res. 2004 Sep;24(9):543–52.

282. Caproni E, Tritto E, Cortese M, Muzzi A, Mosca F, Monaci E, et al. MF59 and Pam3CSK4 Boost Adaptive Responses to Influenza Subunit Vaccine through an IFN Type I-Independent Mechanism of Action. J Immunol. 2012 Apr 1;188(7):3088–98.

283. West MA, Prescott AR, Chan KM, Zhou Z, Rose-John S, Scheller J, et al. TLR ligand–induced podosome disassembly in dendritic cells is ADAM17 dependent. J Cell Biol. 2008 Sep 8;182(5):993–1005.

284. Agrawal S, Agrawal A, Doughty B, Gerwitz A, Blenis J, Van Dyke T, et al. Cutting Edge: Different Toll-Like Receptor Agonists Instruct Dendritic Cells to Induce Distinct Th Responses via Differential Modulation of Extracellular Signal-Regulated Kinase-Mitogen-Activated Protein Kinase and c-Fos. J Immunol. 2014;

285. Ashhurst AS, Johansen MD, Maxwell JWC, Stockdale S, Ashley CL, Aggarwal A, et al. Mucosal TLR2-activating protein-based vaccination induces potent pulmonary immunity and protection against SARS-CoV-2 in mice. Nat Commun. 2022 Nov 15;13(1):6972.

286. Choi YS, Kageyama R, Eto D, Escobar TC, Johnston RJ, Monticelli L, et al. ICOS Receptor Instructs T Follicular Helper Cell versus Effector Cell Differentiation via Induction of the Transcriptional Repressor Bcl6. Immunity. 2011 Jun;34(6):932–46.

287. Boeglin E, Smulski CR, Brun S, Milosevic S, Schneider P, Fournel S. Toll-Like Receptor Agonists Synergize with CD40L to Induce Either Proliferation or Plasma Cell Differentiation of Mouse B Cells. Allen RL, editor. PLoS ONE. 2011 Oct 3;6(10):e25542.

288. Kaur A, Baldwin J, Brar D, Salunke DB, Petrovsky N. Toll-like receptor (TLR) agonists as a driving force behind next-generation vaccine adjuvants and cancer therapeutics. Curr Opin Chem Biol. 2022 Oct;70:102172.

289. Azmi F, Ahmad Fuaad AAH, Skwarczynski M, Toth I. Recent progress in adjuvant discovery for peptide-based subunit vaccines. Hum Vaccines Immunother. 2014 Mar;10(3):778–96.

290. Kumar S, Sunagar R, Gosselin E. Bacterial Protein Toll-Like-Receptor Agonists: A Novel Perspective on Vaccine Adjuvants. Front Immunol. 2019 May 29;10:1144.

291. Manicassamy S, Pulendran B. Modulation of adaptive immunity with Toll-like receptors. Semin Immunol. 2009 Aug;21(4):185–93.

292. Łęga T, Weiher P, Obuchowski M, Nidzworski D. Presenting Influenza A M2e Antigen on Recombinant Spores of Bacillus subtilis. Turner SJ, editor. PLOS ONE. 2016 Nov 30;11(11):e0167225.

293. Sei CJ, Rao M, Schuman RF, Daum LT, Matyas GR, Rikhi N, et al. Conserved Influenza Hemagglutinin, Neuraminidase and Matrix Peptides Adjuvanted with ALFQ Induce Broadly Neutralizing Antibodies. Vaccines. 2021 Jun 25;9(7):698.

294. Tan MP, Tan WS, Mohamed Alitheen NB, Yap WB. M2e-Based Influenza Vaccines with Nucleoprotein: A Review. Vaccines. 2021 Jul 4;9(7):739.

295. Lamb RA, Zebedee SL, Richardson CD. Influenza virus M2 protein is an integral membrane protein expressed on the infected-cell surface. Cell. 1985 Mar;40(3):627–33.

296. Stepanova LA, Kotlyarov RY, Kovaleva AA, Potapchuk MV, Korotkov AV, Sergeeva MV, et al. Protection against Multiple Influenza A Virus Strains Induced by Candidate

Recombinant Vaccine Based on Heterologous M2e Peptides Linked to Flagellin. Kang SM, editor. PLOS ONE. 2015 Mar 23;10(3):e0119520.

297. Kavishna R, Kang TY, Vacca M, Chua BYL, Park HY, Tan PS, et al. A single-shot vaccine approach for the universal influenza A vaccine candidate M2e. Proc Natl Acad Sci. 2022 Mar 29;119(13):e2025607119.

298. Petrie JG, Malosh RE, Cheng CK, Ohmit SE, Martin ET, Johnson E, et al. The Household Influenza Vaccine Effectiveness Study: Lack of Antibody Response and Protection Following Receipt of 2014–2015 Influenza Vaccine. Clin Infect Dis. 2017 Oct 30;65(10):1644–51.

299. Mezhenskaya D, Isakova-Sivak I, Rudenko L. M2e-based universal influenza vaccines: a historical overview and new approaches to development. J Biomed Sci. 2019 Dec;26(1):76.

300. Blanco-Pérez F, Papp G, Goretzki A, Möller T, Anzaghe M, Schülke S. Adjuvant Allergen Fusion Proteins as Novel Tools for the Treatment of Type I Allergies. Arch Immunol Ther Exp (Warsz). 2019 Oct;67(5):273–93.

301. Shirota H, Sano K, Hirasawa N, Terui T, Ohuchi K, Hattori T, et al. Novel Roles of CpG Oligodeoxynucleotides as a Leader for the Sampling and Presentation of CpG-Tagged Antigen by Dendritic Cells. J Immunol. 2001 Jul 1;167(1):66–74.

302. Schülke S, Wolfheimer S, Gadermaier G, Wangorsch A, Siebeneicher S, Briza P, et al. Prevention of Intestinal Allergy in Mice by rflaA:Ova Is Associated with Enforced Antigen Processing and TLR5-Dependent IL-10 Secretion by mDC. Giambartolomei GH, editor. PLoS ONE. 2014 Feb 7;9(2):e87822.

303. Krupka M, Zachova K, Cahlikova R, Vrbkova J, Novak Z, Sebela M, et al. Endotoxin-minimized HIV-1 p24 fused to murine hsp70 activates dendritic cells, facilitates endocytosis and p24-specific Th1 response in mice. Immunol Lett. 2015 Jul;166(1):36–44.

304. Bates JT, Uematsu S, Akira S, Mizel SB. Direct Stimulation of *tlr5* +/+ CD11c+ Cells Is Necessary for the Adjuvant Activity of Flagellin. J Immunol. 2009 Jun 15;182(12):7539–47.

305. Wortham C, Grinberg L, Kaslow DC, Briles DE, McDaniel LS, Lees A, et al. Enhanced Protective Antibody Responses to PspA after Intranasal or Subcutaneous Injections of PspA Genetically Fused to Granulocyte-Macrophage Colony-Stimulating Factor or Interleukin-2. Infect Immun. 1998 Apr;66(4):1513–20.

306. Zhang H xin, Qiu Y yu, Zhao Y hui, Liu X ting, Liu M, Yu A lian. Immunogenicity of oral vaccination with Lactococcus lactis derived vaccine candidate antigen (UreB) of Helicobacter pylori fused with the human interleukin 2 as adjuvant. Mol Cell Probes. 2014 Feb;28(1):25–30.

307. Schülke S, Burggraf M, Waibler Z, Wangorsch A, Wolfheimer S, Kalinke U, et al. A fusion protein of flagellin and ovalbumin suppresses the TH2 response and prevents murine intestinal allergy. J Allergy Clin Immunol. 2011 Dec;128(6):1340-1348.e12.

308. Ignacio BJ, Albin TJ, Esser-Kahn AP, Verdoes M. Toll-like Receptor Agonist Conjugation: A Chemical Perspective. Bioconjug Chem. 2018 Mar 21;29(3):587–603.

309. Luchner M, Reinke S, Milicic A. TLR Agonists as Vaccine Adjuvants Targeting Cancer and Infectious Diseases. Pharmaceutics. 2021 Jan 22;13(2):142.

310. Park J, Pho T, Champion JA. Chemical and biological conjugation strategies for the development of multivalent protein vaccine nanoparticles. Biopolymers. 2023 Aug;114(8):e23563.

311. Lees A, Sen G, LopezAcosta A. Versatile and efficient synthesis of protein–polysaccharide conjugate vaccines using aminooxy reagents and oxime chemistry. Vaccine. 2006 Feb;24(6):716–29.

312. Chen S, Ozberk V, Sam G, Gonzaga ZJC, Calcutt A, Pandey M, et al. Polymeric epitope-based vaccine induces protective immunity against group A Streptococcus. Npj Vaccines. 2023 Jul 14;8(1):102.

313. Medrano G, Dolan MC, Condori J, Radin DN, Cramer CL. Quality Assessment of Recombinant Proteins Produced in Plants. In: Lorence A, editor. Recombinant Gene Expression [Internet]. Totowa, NJ: Humana Press; 2012 [cited 2023 Aug 18]. p. 535–64. (Methods in Molecular Biology; vol. 824). Available from: https://link.springer.com/10.1007/978-1-61779-433-9_29

314. Raynal B, Lenormand P, Baron B, Hoos S, England P. Quality assessment and optimization of purified protein samples: why and how? Microb Cell Factories. 2014 Dec;13(1):180.

315. Gabbard J, Velappan N, Di Niro R, Schmidt J, Jones CA, Tompkins SM, et al. A humanized anti-M2 scFv shows protective in vitro activity against influenza. Protein Eng Des Sel. 2008 Oct 16;22(3):189–98.

316. Taylor RJ, Geeson MB, Journeaux T, Bernardes GJL. Chemical and Enzymatic Methods for Post-Translational Protein–Protein Conjugation. J Am Chem Soc. 2022 Aug 17;144(32):14404–19.

317. Yu K, Liu C, Kim BG, Lee DY. Synthetic fusion protein design and applications. Biotechnol Adv. 2015 Jan;33(1):155–64.

318. Talbot HK, Rock MT, Johnson C, Tussey L, Kavita U, Shanker A, et al. Immunopotentiation of Trivalent Influenza Vaccine When Given with VAX102, a Recombinant Influenza M2e Vaccine Fused to the TLR5 Ligand Flagellin. Montgomery JM, editor. PLoS ONE. 2010 Dec 28;5(12):e14442.

319. Christensen T, Amiram M, Dagher S, Trabbic-Carlson K, Shamji MF, Setton LA, et al. Fusion order controls expression level and activity of elastin-like polypeptide fusion proteins: Effect of Fusion Order. Protein Sci. 2009 Jul;18(7):1377–87.

320. Sachdev D, Chirgwin JM. Order of Fusions between Bacterial and Mammalian Proteins Can Determine Solubility inEscherichia coli. Biochem Biophys Res Commun. 1998 Mar;244(3):933–7.

321. Kang HJ, Baker EN. Intramolecular Isopeptide Bonds Give Thermodynamic and Proteolytic Stability to the Major Pilin Protein of Streptococcus pyogenes. J Biol Chem. 2009 Jul;284(31):20729–37.

322. Wang B, Xiao S, Edwards SA, Gräter F. Isopeptide Bonds Mechanically Stabilize Spy0128 in Bacterial Pili. Biophys J. 2013 May;104(9):2051–7.

323. Smoot JC, Barbian KD, Van Gompel JJ, Smoot LM, Chaussee MS, Sylva GL, et al. Genome sequence and comparative microarray analysis of serotype M18 group A *Streptococcus* strains associated with acute rheumatic fever outbreaks. Proc Natl Acad Sci. 2002 Apr 2;99(7):4668–73.

324. Holden MTG, Scott A, Cherevach I, Chillingworth T, Churcher C, Cronin A, et al. Complete Genome of Acute Rheumatic Fever-Associated Serotype M5 *Streptococcus pyogenes* Strain Manfredo. J Bacteriol. 2007 Feb 15;189(4):1473–7.

325. Pointon JA, Smith WD, Saalbach G, Crow A, Kehoe MA, Banfield MJ. A Highly Unusual Thioester Bond in a Pilus Adhesin Is Required for Efficient Host Cell Interaction*. J Biol Chem. 2010 Oct;285(44):33858–66.

326. Hendrickx APA, Budzik JM, Oh SY, Schneewind O. Architects at the bacterial surface — sortases and the assembly of pili with isopeptide bonds. Nat Rev Microbiol. 2011 Mar;9(3):166–76.

327. Cheung CY, Dubey S, Hadrovic M, Ball CR, Ramage W, McDonald JU, et al. Development of an ELISA-Based Potency Assay for Inactivated Influenza Vaccines Using Cross-Reactive Nanobodies. Vaccines. 2022 Sep 5;10(9):1473.

328. Gairola S, Gautam M, Waghmare S. A novel ELISA for quantification of glycoprotein in human rabies vaccines using a clinically proven virus neutralizing human monoclonal antibody. Hum Vaccines Immunother. 2020 Aug 2;16(8):1857–65.

329. Singh B, Fleury C, Jalalvand F, Riesbeck K. Human pathogens utilize host extracellular matrix proteins laminin and collagen for adhesion and invasion of the host. FEMS Microbiol Rev. 2012 Nov;36(6):1122–80.

330. Hsu SH, Lo YY, Tung JY, Ko YC, Sun YJ, Hung CC, et al. Leptospiral Outer Membrane Lipoprotein LipL32 Binding on Toll-like Receptor 2 of Renal Cells As Determined with an Atomic Force Microscope. Biochemistry. 2010 Jul 6;49(26):5408–17.

331. Hauk P, Macedo F, Romero EC, Vasconcellos SA, De Morais ZM, Barbosa AS, et al. In LipL32, the Major Leptospiral Lipoprotein, the C Terminus Is the Primary Immunogenic Domain and Mediates Interaction with Collagen IV and Plasma Fibronectin. Infect Immun. 2008 Jun;76(6):2642–50.

332. Chen X, Zaro JL, Shen WC. Fusion protein linkers: Property, design and functionality. Adv Drug Deliv Rev. 2013 Oct;65(10):1357–69.

333. Bai Y, Ann DK, Shen WC. Recombinant granulocyte colony-stimulating factor-transferrin fusion protein as an oral myelopoietic agent. Proc Natl Acad Sci. 2005 May 17;102(20):7292–6.

334. Fitzgerald KA, Kagan JC. Toll-like Receptors and the Control of Immunity. Cell. 2020 Mar;180(6):1044–66.

335. Banchereau J, Steinman RM. Dendritic cells and the control of immunity. Nature. 1998 Mar;392(6673):245–52.

336. Duan T, Du Y, Xing C, Wang HY, Wang RF. Toll-Like Receptor Signaling and Its Role in Cell-Mediated Immunity. Front Immunol. 2022 Mar 3;13:812774.

337. Parameswaran N, Patial S. Tumor necrosis factor-a signaling in macrophages. Crit Rev Eukaryot Gene Expr. 2010;

338. Trevejo JM, Marino MW, Philpott N, Josien R, Richards EC, Elkon KB, et al. TNF-α-dependent maturation of local dendritic cells is critical for activating the adaptive immune response to virus infection. Proc Natl Acad Sci. 2001 Oct 9;98(21):12162–7.

339. Traini G, Ruiz-de-Angulo A, Blanco-Canosa JB, Zamacola Bascarán K, Molinaro A, Silipo A, et al. Cancer Immunotherapy of TLR4 Agonist–Antigen Constructs Enhanced with Pathogen-Mimicking Magnetite Nanoparticles and Checkpoint Blockade of PD-L1. Small. 2019 Jan;15(4):1803993.

340. Duverger A, Carré JM, Jee J, Leppla SH, Cormet-Boyaka E, Tang WJ, et al. Contributions of Edema Factor and Protective Antigen to the Induction of Protective Immunity by *Bacillus anthracis* Edema Toxin as an Intranasal Adjuvant. J Immunol. 2010 Nov 15;185(10):5943–52.

341. Yüksel S, Pekcan M, Puralı N, Esendağlı G, Tavukçuoğlu E, Rivero-Arredondo V, et al. Development and in vitro evaluation of a new adjuvant system containing Salmonella Typhi porins and chitosan. Int J Pharm. 2020 Mar;578:119129.

342. Krishnan L, Sad S, Patel GB, Sprott GD. The potent adjuvant activity of archaeosomes correlates to the recruitment and activation of macrophages and dendritic cells in vivo. J Immunol Baltim Md 1950. 2001 Feb 1;166(3):1885–93.

343. Goldmann O, von Köckritz-Blickwede M, Höltje C, Chhatwal GS, Geffers R, Medina E. Transcriptome analysis of murine macrophages in response to infection with Streptococcus pyogenes reveals an unusual activation program. Infect Immun. 2007 Aug;75(8):4148–57.

344. Berridge MV, Herst PM, Tan AS. Tetrazolium dyes as tools in cell biology: new insights into their cellular reduction. Biotechnol Annu Rev. 2005;11:127–52.

345. Ghasemi M, Turnbull T, Sebastian S, Kempson I. The MTT Assay: Utility, Limitations, Pitfalls, and Interpretation in Bulk and Single-Cell Analysis. Int J Mol Sci. 2021 Nov 26;22(23):12827.

346. Präbst K, Engelhardt H, Ringgeler S, Hübner H. Basic Colorimetric Proliferation Assays: MTT, WST, and Resazurin. In: Gilbert DF, Friedrich O, editors. Cell Viability Assays [Internet]. New York, NY: Springer New York; 2017 [cited 2023 Oct 6]. p. 1–17. (Methods in Molecular Biology; vol. 1601). Available from: http://link.springer.com/10.1007/978-1-4939-6960-9_1

347. Pang S, Smith J, Onley D, Reeve J, Walker M, Foy C. A comparability study of the emerging protein array platforms with established ELISA procedures. J Immunol Methods. 2005 Jul;302(1–2):1–12.

348. Mountjoy KG. ELISA versus LUMINEX assay for measuring mouse metabolic hormones and cytokines: sharing the lessons I have learned. J Immunoassay Immunochem. 2021 Mar 4;42(2):154–73.

349. Martins KA, Bavari S, Salazar AM. Vaccine adjuvant uses of poly-IC and derivatives. Expert Rev Vaccines. 2015 Mar 4;14(3):447–59.

350. De Filette M, Fiers W, Martens W, Birkett A, Ramne A, Löwenadler B, et al. Improved design and intranasal delivery of an M2e-based human influenza A vaccine. Vaccine. 2006 Nov;24(44–46):6597–601.

351. Eliasson DG, Bakkouri KE, Schön K, Ramne A, Festjens E, Löwenadler B, et al. CTA1-M2e-DD: A novel mucosal adjuvant targeted influenza vaccine. Vaccine. 2008 Feb;26(9):1243–52.

352. De Filette M, Ramne A, Birkett A, Lycke N, Löwenadler B, Min Jou W, et al. The universal influenza vaccine M2e-HBc administered intranasally in combination with the adjuvant CTA1-DD provides complete protection. Vaccine. 2006 Jan;24(5):544–51.

353. Price GE, Lo CY, Misplon JA, Epstein SL. Mucosal Immunization with a Candidate Universal Influenza Vaccine Reduces Virus Transmission in a Mouse Model. García-Sastre A, editor. J Virol. 2014 Jun;88(11):6019–30.

354. Tumpey TM, Renshaw M, Clements JD, Katz JM. Mucosal Delivery of Inactivated Influenza Vaccine Induces B-Cell-Dependent Heterosubtypic Cross-Protection against Lethal Influenza A H5N1 Virus Infection. J Virol. 2001 Jun;75(11):5141–50.

355. Neutra MR, Kozlowski PA. Mucosal vaccines: the promise and the challenge. Nat Rev Immunol. 2006 Feb;6(2):148–58.

356. Mozdzanowska K, Zharikova D, Cudic M, Otvos L, Gerhard W. Roles of adjuvant and route of vaccination in antibody response and protection engendered by a synthetic

matrix protein 2-based influenza A virus vaccine in the mouse. Virol J. 2007 Dec;4(1):118.

357. Deng L, Cho K, Fiers W, Saelens X. M2e-Based Universal Influenza A Vaccines. Vaccines. 2015 Feb 13;3(1):105–36.

358. Freytag LC, Clements JD. Mucosal Adjuvants. In: Mucosal Immunology [Internet]. Elsevier; 2015 [cited 2023 Oct 31]. p. 1183–99. Available from: https://linkinghub.elsevier.com/retrieve/pii/B9780124158474000616

359. Guerrini G, Vivi A, Gioria S, Ponti J, Magrì D, Hoeveler A, et al. Physicochemical Characterization Cascade of Nanoadjuvant–Antigen Systems for Improving Vaccines. Vaccines. 2021 May 21;9(6):544.

360. Ou B, Yang Y, Lv H, Lin X, Zhang M. Current Progress and Challenges in the Study of Adjuvants for Oral Vaccines. BioDrugs. 2023 Mar;37(2):143–80.

361. Ohlsson L, Exley C, Darabi A, Sandén E, Siesjö P, Eriksson H. Aluminium based adjuvants and their effects on mitochondria and lysosomes of phagocytosing cells. J Inorg Biochem. 2013 Nov;128:229–36.

362. Mosmann T. Rapid colorimetric assay for cellular growth and survival: Application to proliferation and cytotoxicity assays. J Immunol Methods. 1983 Dec;65(1–2):55–63.

363. Chou YJ, Lin CC, Dzhagalov I, Chen NJ, Lin CH, Lin CC, et al. Vaccine adjuvant activity of a TLR4-activating synthetic glycolipid by promoting autophagy. Sci Rep. 2020 May 21;10(1):8422.

364. Wang Y qi, Mao J bo, Zhou M qian, Jin Y wei, Lou C hua, Dong Y, et al. Polysaccharide from Phellinus Igniarius activates TLR4-mediated signaling pathways in macrophages and shows immune adjuvant activity in mice. Int J Biol Macromol. 2019 Feb;123:157–66.

365. Chen CH, Campbell PA, Newman LS. MTT Colorimetric Assay Detects Mitogen Responses of Spleen but not Blood Lymphocytes. Int Arch Allergy Immunol. 1990;93(2–3):249–55.

366. Van Tonder A, Joubert AM, Cromarty AD. Limitations of the 3-(4,5-dimethylthiazol-2-yl)-2,5-diphenyl-2H-tetrazolium bromide (MTT) assay when compared to three commonly used cell enumeration assays. BMC Res Notes. 2015 Dec;8(1):47.

367. Aguiar MPD, Vieira JH. Entrance to the multifaceted world of CD4+ T cell subsets. Explor Immunol. 2024 Mar 5;4(2):152–68.

368. Zhu J, Paul WE. CD4 T cells: fates, functions, and faults. Blood. 2008 Sep 1;112(5):1557–69.

369. Kaiko GE, Horvat JC, Beagley KW, Hansbro PM. Immunological decision-making: how does the immune system decide to mount a helper T-cell response? Immunology. 2008 Mar;123(3):326–38.

370. Spellberg B, Edwards JE. Type 1/Type 2 Immunity in Infectious Diseases. Clin Infect Dis. 2001 Jan 1;32(1):76–102.

371. Choi J -P., Kim Y -S., Kim OY, Kim Y -M., Jeon SG, Roh T -Y., et al. TNF -alpha is a key mediator in the development of T h2 cell response to inhaled allergens induced by a viral PAMP double-stranded RNA. Allergy. 2012 Sep;67(9):1138–48.

372. Zhu J, Yamane H, Paul WE. Differentiation of Effector CD4 T Cell Populations. Annu Rev Immunol. 2010 Mar 1;28(1):445–89.

373. Davignon JL, Rauwel B, Degboé Y, Constantin A, Boyer JF, Kruglov A, et al. Modulation of T-cell responses by anti-tumor necrosis factor treatments in rheumatoid arthritis: a review. Arthritis Res Ther. 2018 Dec;20(1):229.

374. Zhang W, Chen Z, Li F, Kamencic H, Juurlink B, Gordon JR, et al. Tumour necrosis factor-α (TNF-α) transgene-expressing dendritic cells (DCs) undergo augmented cellular maturation and induce more robust T-cell activation and anti-tumour immunity than DCs generated in recombinant TNF-α. Immunology. 2003 Feb;108(2):177–88.

375. Mehta AK, Gracias DT, Croft M. TNF activity and T cells. Cytokine. 2018 Jan;101:14–8.

376. Yokota S, Geppert TD, Lipsky PE. Enhancement of antigen- and mitogen-induced human T lymphocyte proliferation by tumor necrosis factor-alpha. J Immunol Baltim Md 1950. 1988 Jan 15;140(2):531–6.

377. Brunner C, Seiderer J, Schlamp A, Bidlingmaier M, Eigler A, Haimerl W, et al. Enhanced Dendritic Cell Maturation by TNF-α or Cytidine-Phosphate-Guanosine DNA Drives T Cell Activation In Vitro and Therapeutic Anti-Tumor Immune Responses In Vivo. J Immunol. 2000 Dec 1;165(11):6278–86.

378. Unutmaz D, Pileri P, Abrignani S. Antigen-independent activation of naive and memory resting T cells by a cytokine combination. J Exp Med. 1994 Sep 1;180(3):1159–64.

379. Tsuji M, Suzuki K, Kitamura H, Maruya M, Kinoshita K, Ivanov II, et al. Requirement for Lymphoid Tissue-Inducer Cells in Isolated Follicle Formation and T Cell-Independent Immunoglobulin A Generation in the Gut. Immunity. 2008 Aug;29(2):261–71.

380. Craxton A, Magaletti D, Ryan EJ, Clark EA. Macrophage- and dendritic cell—dependent regulation of human B-cell proliferation requires the TNF family ligand BAFF. Blood. 2003 Jun 1;101(11):4464–71.

381. Jaczewska J, Abdulreda MH, Yau CY, Schmitt MM, Schubert I, Berggren PO, et al. TNF-α and IFN-γ promote lymphocyte adhesion to endothelial junctional regions facilitating transendothelial migration. J Leukoc Biol. 2013 Sep 26;95(2):265–74.

382. Franitza S, Hershkoviz R, Kam N, Lichtenstein N, Vaday GG, Alon R, et al. TNF-α Associated with Extracellular Matrix Fibronectin Provides a Stop Signal for Chemotactically Migrating T Cells. J Immunol. 2000 Sep 1;165(5):2738–47.

383. Song L, Dong G, Guo L, Graves DT. The function of dendritic cells in modulating the host response. Mol Oral Microbiol. 2018 Feb;33(1):13–21.

384. Rosales C. Neutrophils at the crossroads of innate and adaptive immunity. J Leukoc Biol. 2020 Jul 1;108(1):377–96.

385. Kaplanski G. IL-6: a regulator of the transition from neutrophil to monocyte recruitment during inflammation. Trends Immunol. 2003 Jan;24(1):25–9.

386. McLoughlin RM, Jenkins BJ, Grail D, Williams AS, Fielding CA, Parker CR, et al. IL-6 trans-signaling via STAT3 directs T cell infiltration in acute inflammation. Proc Natl Acad Sci. 2005 Jul 5;102(27):9589–94.

387. Diehl S, Chow CW, Weiss L, Palmetshofer A, Twardzik T, Rounds L, et al. Induction of NFATc2 Expression by Interleukin 6 Promotes T Helper Type 2 Differentiation. J Exp Med. 2002 Jul 1;196(1):39–49.

388. Diehl S, Anguita J, Hoffmeyer A, Zapton T, Ihle JN, Fikrig E, et al. Inhibition of Th1 Differentiation by IL-6 Is Mediated by SOCS1. Immunity. 2000 Dec;13(6):805–15.

389. Suematsu S, Matsuda T, Aozasa K, Akira S, Nakano N, Ohno S, et al. IgG1 plasmacytosis in interleukin 6 transgenic mice. Proc Natl Acad Sci. 1989 Oct;86(19):7547–51.

390. Ballesteros-Tato A, León B, Graf BA, Moquin A, Adams PS, Lund FE, et al. Interleukin-2 Inhibits Germinal Center Formation by Limiting T Follicular Helper Cell Differentiation. Immunity. 2012 May;36(5):847–56.

391. Boyman O, Sprent J. The role of interleukin-2 during homeostasis and activation of the immune system. Nat Rev Immunol. 2012 Mar;12(3):180–90.

392. Chabot V, Martin L, Meley D, Sensebé L, Baron C, Lebranchu Y, et al. Unexpected impairment of TNF-α-induced maturation of human dendritic cells in vitro by IL-4. J Transl Med. 2016 Dec;14(1):93.

393. Nguyen BN, Chávez-Arroyo A, Cheng MI, Krasilnikov M, Louie A, Portnoy DA. TLR2 and endosomal TLR-mediated secretion of IL-10 and immune suppression in response to phagosome-confined Listeria monocytogenes. Brodsky IE, editor. PLOS Pathog. 2020 Jul 7;16(7):e1008622.

394. Armstrong L, Jordan N, Millar A. Interleukin 10 (IL-10) regulation of tumour necrosis factor alpha (TNF-alpha) from human alveolar macrophages and peripheral blood monocytes. Thorax. 1996 Feb 1;51(2):143–9.

395. Subbarayal B, Chauhan SK, Di Zazzo A, Dana R. IL-17 Augments B Cell Activation in Ocular Surface Autoimmunity. J Immunol. 2016 Nov 1;197(9):3464–70.

396. Ye P, Rodriguez FH, Kanaly S, Stocking KL, Schurr J, Schwarzenberger P, et al. Requirement of Interleukin 17 Receptor Signaling for Lung Cxc Chemokine and

Granulocyte Colony-Stimulating Factor Expression, Neutrophil Recruitment, and Host Defense. J Exp Med. 2001 Aug 20;194(4):519–28.

397. Plater-Zyberk C, Joosten LAB, Helsen MMA, Koenders MI, Baeuerle PA, Van Den Berg WB. Combined blockade of granulocyte-macrophage colony stimulating factor and interleukin 17 pathways potently suppresses chronic destructive arthritis in a tumour necrosis factor α-independent mouse model. Ann Rheum Dis. 2009 May;68(5):721–8.

398. Kolls JK, Lindén A. Interleukin-17 Family Members and Inflammation. Immunity. 2004 Oct;21(4):467–76.

399. Alspach E, Lussier DM, Schreiber RD. Interferon γ and Its Important Roles in Promoting and Inhibiting Spontaneous and Therapeutic Cancer Immunity. Cold Spring Harb Perspect Biol. 2019 Mar;11(3):a028480.

400. Silva-Filho JL, Caruso-Neves C, Pinheiro AAS. IL-4: an important cytokine in determining the fate of T cells. Biophys Rev. 2014 Mar;6(1):111–8.

401. Linterman MA, Hill DL. Can follicular helper T cells be targeted to improve vaccine efficacy? F1000Research. 2016 Jan 20;5:88.

402. Nurieva RI, Chung Y, Hwang D, Yang XO, Kang HS, Ma L, et al. Generation of T Follicular Helper Cells Is Mediated by Interleukin-21 but Independent of T Helper 1, 2, or 17 Cell Lineages. Immunity. 2008 Jul;29(1):138–49.

403. Dalgėdienė I, Lučiūnaitė A, Žvirblienė A. Activation of Macrophages by Oligomeric Proteins of Different Size and Origin. Mediators Inflamm. 2018 Nov 18;2018:1–13.

404. Carreno BM, Collins M. The B7 Family of Ligands and Its Receptors: New Pathways for Costimulation and Inhibition of Immune Responses. Annu Rev Immunol. 2002 Apr;20(1):29–53.

405. Lim TS, Goh JKH, Mortellaro A, Lim CT, Hämmerling GJ, Ricciardi-Castagnoli P. CD80 and CD86 Differentially Regulate Mechanical Interactions of T-Cells with Antigen-Presenting Dendritic Cells and B-Cells. Agrewala JN, editor. PLoS ONE. 2012 Sep 14;7(9):e45185.

406. Fulton SA, Reba SM, Pai RK, Pennini M, Torres M, Harding CV, et al. Inhibition of Major Histocompatibility Complex II Expression and Antigen Processing in Murine Alveolar Macrophages by *Mycobacterium bovis* BCG and the 19-Kilodalton Mycobacterial Lipoprotein. Infect Immun. 2004 Apr;72(4):2101–10.

407. Zhao Y, Xiong J, Chen HX, Zhang M, Zhou LN, Wu YF, et al. A Spontaneous H2-Aa Point Mutation Impairs MHC II Synthesis and CD4+ T-Cell Development in Mice. Front Immunol. 2022 Mar 4;13:810824.

408. Li JG, Du YM, Yan ZD, Yan J, Zhuansun YX, Chen R, et al. CD80 and CD86 knockdown in dendritic cells regulates Th1/Th2 cytokine production in asthmatic mice. Exp Ther Med. 2016 Mar;11(3):878–84.

409. Fuse S, Obar JJ, Bellfy S, Leung EK, Zhang W, Usherwood EJ. CD80 and CD86 Control Antiviral CD8 [+] T-Cell Function and Immune Surveillance of Murine Gammaherpesvirus 68. J Virol. 2006 Sep 15;80(18):9159–70.

410. Hoebe K, Janssen EM, Kim SO, Alexopoulou L, Flavell RA, Han J, et al. Upregulation of costimulatory molecules induced by lipopolysaccharide and double-stranded RNA occurs by Trif-dependent and Trif-independent pathways. Nat Immunol. 2003 Dec;4(12):1223–9.

411. Pasare C, Medzhitov R. Toll-Dependent Control Mechanisms of CD4 T Cell Activation. Immunity. 2004 Nov;21(5):733–41.

412. Chow A, Toomre D, Garrett W, Mellman I. Dendritic cell maturation triggers retrograde MHC class II transport from lysosomes to the plasma membrane. Nature. 2002 Aug;418(6901):988–94.

413. Blander JM, Medzhitov R. Toll-dependent selection of microbial antigens for presentation by dendritic cells. Nature. 2006 Apr;440(7085):808–12.

414. Wilson NS, El-Sukkari D, Villadangos JA. Dendritic cells constitutively present self antigens in their immature state in vivo and regulate antigen presentation by controlling the rates of MHC class II synthesis and endocytosis. Blood. 2004 Mar 15;103(6):2187–95.

415. Cella M, Engering A, Pinet V, Pieters J, Lanzavecchia A. Inflammatory stimuli induce accumulation of MHC class II complexes on dendritic cells. Nature. 1997 Aug;388(6644):782–7.

416. Wijdeven RH, Van Luijn MM, Wierenga-Wolf AF, Akkermans JJ, Van Den Elsen PJ, Hintzen RQ, et al. Chemical and genetic control of IFN γ-induced MHCII expression. EMBO Rep. 2018 Sep;19(9):e45553.

417. Buxadé M, Huerga Encabo H, Riera-Borrull M, Quintana-Gallardo L, López-Cotarelo P, Tellechea M, et al. Macrophage-specific MHCII expression is regulated by a remote *Ciita* enhancer controlled by NFAT5. J Exp Med. 2018 Nov 5;215(11):2901–18.

418. Maroof A, Yorgensen YM, Li Y, Evans JT. Intranasal Vaccination Promotes Detrimental Th17-Mediated Immunity against Influenza Infection. Subbarao K, editor. PLoS Pathog. 2014 Jan 23;10(1):e1003875.

419. Yin L, Chen X, Tiwari A, Vicini P, Hickling TP. The Role of Aggregates of Therapeutic Protein Products in Immunogenicity: An Evaluation by Mathematical Modeling. J Immunol Res. 2015;2015:1–14.

420. Maru Y, Afar DE, Witte ON, Shibuya M. The Dimerization Property of Glutathione - Transferase Partially Reactivates Bcr-Abl Lacking the Oligomerization Domain. J Biol Chem. 1996 Jun;271(26):15353–7.

421. Brayden DJ, Hill TA, Fairlie DP, Maher S, Mrsny RJ. Systemic delivery of peptides by the oral route: Formulation and medicinal chemistry approaches. Adv Drug Deliv Rev. 2020;157:2–36.

422. Barnowski C, Kadzioch N, Damm D, Yan H, Temchura V. Advantages and Limitations of Integrated Flagellin Adjuvants for HIV-Based Nanoparticle B-Cell Vaccines. Pharmaceutics. 2019 May 1;11(5):204.

423. Nempont C, Cayet D, Rumbo M, Bompard C, Villeret V, Sirard JC. Deletion of Flagellin's Hypervariable Region Abrogates Antibody-Mediated Neutralization and Systemic Activation of TLR5-Dependent Immunity. J Immunol. 2008 Aug 1;181(3):2036–43.

424. Yang J, Zhong M, Zhang Y, Zhang E, Sun Y, Cao Y, et al. Antigen replacement of domains D2 and D3 in flagellin promotes mucosal IgA production and attenuates flagellin-induced inflammatory response after intranasal immunization. Hum Vaccines Immunother. 2013 May 14;9(5):1084–92.

425. Khim K, Bang YJ, Puth S, Choi Y, Lee YS, Jeong K, et al. Deimmunization of flagellin for repeated administration as a vaccine adjuvant. Npj Vaccines. 2021 Sep 13;6(1):116.

426. Liu F, Yang J, Zhang Y, Zhou D, Chen Y, Gai W, et al. Recombinant flagellins with partial deletions of the hypervariable domain lose antigenicity but not mucosal adjuvancy. Biochem Biophys Res Commun. 2010 Feb;392(4):582–7.

427. Pires A, Fortuna A, Alves G, Falcão A. Intranasal Drug Delivery: How, Why and What for? J Pharm Pharm Sci. 2009 Oct 12;12(3):288.

428. Riese P, Sakthivel P, Trittel S, Guzmán CA. Intranasal formulations: promising strategy to deliver vaccines. Expert Opin Drug Deliv. 2014 Oct;11(10):1619–34.

429. Kunkel EJ, Butcher EC. Plasma-cell homing. Nat Rev Immunol. 2003 Oct;3(10):822–9.

430. MacPherson GG, Liu LM. Dendritic Cells and Langerhans Cells in the Uptake of Mucosal Antigens. In: Kraehenbuhl JP, Neutra MR, editors. Defense of Mucosal Surfaces: Pathogenesis, Immunity and Vaccines [Internet]. Berlin, Heidelberg: Springer Berlin Heidelberg; 1999 [cited 2023 Oct 24]. p. 33–53. (Compans RW, Cooper M, Hogle JM, Ito Y, Koprowski H, Melchers F, et al., editors. Current Topics in Microbiology and Immunology; vol. 236). Available from: http://link.springer.com/10.1007/978-3-642-59951-4_3

431. Pavot V, Rochereau N, Genin C, Verrier B, Paul S. New insights in mucosal vaccine development. Vaccine. 2012 Jan;30(2):142–54.

432. Lee SF, Halperin SA, Wang H, MacArthur A. Oral colonization and immune responses to *Streptococcus gordonii* expressing a pertussis toxin S1 fragment in mice. FEMS Microbiol Lett. 2002 Mar;208(2):175–8.

433. Tomar J, Tonnis WF, Patil HP, De Boer AH, Hagedoorn P, Vanbever R, et al. Pulmonary immunization: deposition site is of minor relevance for influenza vaccination

but deep lung deposition is crucial for hepatitis B vaccination. Acta Pharm Sin B. 2019 Nov;9(6):1231–40.

434. Minne A, Louahed J, Mehauden S, Baras B, Renauld J, Vanbever R. The delivery site of a monovalent influenza vaccine within the respiratory tract impacts on the immune response. Immunology. 2007 Nov;122(3):316–25.

435. Lever AR, Park H, Mulhern TJ, Jackson GR, Comolli JC, Borenstein JT, et al. Comprehensive evaluation of poly(I:C) induced inflammatory response in an airway epithelial model. Physiol Rep. 2015 Apr;3(4):e12334.

436. Vila A, Sánchez A, Janes K, Behrens I, Kissel T, Jato JLV, et al. Low molecular weight chitosan nanoparticles as new carriers for nasal vaccine delivery in mice. Eur J Pharm Biopharm. 2004 Jan;57(1):123–31.

437. Zhou Z, Barrett J, He X. Immune Imprinting and Implications for COVID-19. Vaccines. 2023 Apr 20;11(4):875.

438. Renegar KB, Small PA. Immunoglobulin A mediation of murine nasal anti-influenza virus immunity. J Virol. 1991 Apr;65(4):2146–8.

439. Renegar KB, Small PA, Boykins LG, Wright PF. Role of IgA versus IgG in the Control of Influenza Viral Infection in the Murine Respiratory Tract. J Immunol. 2004 Aug 1;173(3):1978–86.

440. Gould VMW, Francis JN, Anderson KJ, Georges B, Cope AV, Tregoning JS. Nasal IgA Provides Protection against Human Influenza Challenge in Volunteers with Low Serum Influenza Antibody Titre. Front Microbiol. 2017 May 17;8:900.

441. Giri PK, Sable SB, Verma I, Khuller GK. Comparative evaluation of intranasal and subcutaneous route of immunization for development of mucosal vaccine against experimental tuberculosis. FEMS Immunol Med Microbiol. 2005 Jul;45(1):87–93.

442. Schmidt ST, Khadke S, Korsholm KS, Perrie Y, Rades T, Andersen P, et al. The administration route is decisive for the ability of the vaccine adjuvant CAF09 to induce antigen-specific CD8 + T-cell responses: The immunological consequences of the biodistribution profile. J Controlled Release. 2016 Oct;239:107–17.

443. Wojda I. Immunity of the greater wax moth *Galleria mellonella*. Insect Sci. 2017 Jun;24(3):342–57.

444. Nascimento IP, Leite LCC. Recombinant vaccines and the development of new vaccine strategies. Braz J Med Biol Res. 2012 Dec;45(12):1102–11.

445. Vetter V, Denizer G, Friedland LR, Krishnan J, Shapiro M. Understanding modern-day vaccines: what you need to know. Ann Med. 2018 Feb 17;50(2):110–20.

446. Toussi DN, Liu X, Massari P. The FomA Porin from Fusobacterium nucleatum Is a Toll-Like Receptor 2 Agonist with Immune Adjuvant Activity. Clin Vaccine Immunol. 2012 Jul;19(7):1093–101.

447. Foster WS, Lee JL, Thakur N, Newman J, Spencer AJ, Davies S, et al. Tfh cells and the germinal center are required for memory B cell formation & humoral immunity after ChAdOx1 nCoV-19 vaccination. Cell Rep Med. 2022 Dec;3(12):100845.

448. Li J, Lee DSW, Madrenas J. Evolving Bacterial Envelopes and Plasticity of TLR2-Dependent Responses: Basic Research and Translational Opportunities. Front Immunol [Internet]. 2013 [cited 2023 Nov 18];4. Available from: http://journal.frontiersin.org/article/10.3389/fimmu.2013.00347/abstract

449. Zheng SY, Dong JZ. Role of Toll-Like Receptors and Th Responses in Viral Myocarditis. Front Immunol. 2022 Apr 19;13:843891.

450. Jin J, Samuvel DJ, Zhang X, Li Y, Lu Z, Lopes-Virella MF, et al. Coactivation of TLR4 and TLR2/6 coordinates an additive augmentation on IL-6 gene transcription via p38MAPK pathway in U937 mononuclear cells. Mol Immunol. 2011 Dec;49(3):423–32.

451. Shirakawa T, Enomoto T, Shimazu S ichiro, Hopkin JM. The Inverse Association Between Tuberculin Responses and Atopic Disorder. Science. 1997 Jan 3;275(5296):77–9.

452. Dannemann A, Van Ree R, Kulig M, Bergmann RL, Bauer P, Forster J, et al. Specific IgE and lgG4 Immune Responses to Tetanus and Diphtheria Toxoid in Atopic and Nonatopic Children during the First Two Years of Life. Int Arch Allergy Immunol. 1996;111(3):262–7.

453. Lavelle EC, Ward RW. Mucosal vaccines — fortifying the frontiers. Nat Rev Immunol. 2022 Apr;22(4):236–50.

454. Baker JR, Farazuddin M, Wong PT, O'Konek JJ. The unfulfilled potential of mucosal immunization. J Allergy Clin Immunol. 2022 Jul;150(1):1–11.

455. Newsted D, Fallahi F, Golshani A, Azizi A. Advances and challenges in mucosal adjuvant technology. Vaccine. 2015 May;33(21):2399–405.

456. Van Ginkel FW, Jackson RJ, Yoshino N, Hagiwara Y, Metzger DJ, Connell TD, et al. Enterotoxin-Based Mucosal Adjuvants Alter Antigen Trafficking and Induce Inflammatory Responses in the Nasal Tract. Infect Immun. 2005 Oct;73(10):6892–902.

457. Gagliardi MC, Sallusto F, Marinaro M, Langenkamp A, Lanzavecchia A, De Magistris MT. Cholera toxin induces maturation of human dendritic cells and licences them for Th2 priming. Eur J Immunol. 2000;30(8):2394–403.

458. Terrinoni M, Holmgren J, Lebens M, Larena M. Proteomic analysis of cholera toxin adjuvant-stimulated human monocytes identifies Thrombospondin-1 and Integrin-β1 as strongly upregulated molecules involved in adjuvant activity. Sci Rep. 2019 Feb 26;9(1):2812.

459. Moschos S, Bramwell V, Somavarapu S, Alpar H. Adjuvant synergy: The effects of nasal coadministration of adjuvants. Immunol Cell Biol. 2004 Dec;82(6):628–37.

460. Malik A, Gupta M, Gupta V, Gogoi H, Bhatnagar R. Novel application of trimethyl chitosan as an adjuvant in vaccine delivery. Int J Nanomedicine. 2018;13:7959–70.

461. Scherließ R, Buske S, Young K, Weber B, Rades T, Hook S. In vivo evaluation of chitosan as an adjuvant in subcutaneous vaccine formulations. Vaccine. 2013 Oct;31(42):4812–9.

462. Andersen JM, Al-Khairy D, Ingalls RR. Innate Immunity at the Mucosal Surface: Role of Toll-Like Receptor 3 and Toll-Like Receptor 9 in Cervical Epithelial Cell Responses to Microbial Pathogens1. Biol Reprod. 2006 May 1;74(5):824–31.

463. Xu M, Li N, Fan X, Zhou Y, Bi S, Shen A, et al. Differential Effects of Toll-Like Receptor Signaling on the Activation of Immune Responses in the Upper Respiratory Tract. Iyer SS, editor. Microbiol Spectr. 2022 Feb 23;10(1):e01144-21.

464. McClure R, Massari P. TLR-Dependent Human Mucosal Epithelial Cell Responses to Microbial Pathogens. Front Immunol [Internet]. 2014 Aug 12 [cited 2023 Nov 7];5. Available from: http://journal.frontiersin.org/article/10.3389/fimmu.2014.00386/abstract

465. Dekkerová-Chupáčová J, Borghi E, Morace G, Bujdáková H. Up-Regulation of Antimicrobial Peptides Gallerimycin and Galiomicin in Galleria mellonella Infected with Candida Yeasts Displaying Different Virulence Traits. Mycopathologia. 2018 Dec;183(6):935–40.

466. Oyler-Yaniv J, Oyler-Yaniv A, Shakiba M, Min NK, Chen YH, Cheng S yann, et al. Catch and Release of Cytokines Mediated by Tumor Phosphatidylserine Converts Transient Exposure into Long-Lived Inflammation. Mol Cell. 2017 Jun;66(5):635-647.e7.

467. El-Ghrably IA, Dua HS, Orr GM, Fischer D, Tighe PJ. Detection of cytokine mRNA production in infiltrating cells in proliferative vitreoretinopathy using reverse transcription polymerase chain reaction. Br J Ophthalmol. 1999 Nov 1;83(11):1296–9.

468. Jiang P, Zhang Y, Ru B, Yang Y, Vu T, Paul R, et al. Systematic investigation of cytokine signaling activity at the tissue and single-cell levels. Nat Methods. 2021 Oct;18(10):1181–91.

469. Jang YH, Choi JK, Jin M, Choi YA, Ryoo ZY, Lee HS, et al. House Dust Mite Increases pro-Th2 Cytokines IL-25 and IL-33 via the Activation of TLR1/6 Signaling. J Invest Dermatol. 2017 Nov;137(11):2354–61.